VIBRATION-INDUCED SHEAR RESISTANCE REDUCTION IN GRANULAR SOILS: EXPERIMENT, MODEL, AND MECHANISM

Vibration-induced shear resistance reduction in granular soils: experiment, model, and mechanism

By

Tao Xie, B.Sc.

A THESIS

SUBMITTED TO THE DEPARTMENT OF CIVIL ENGINEERING AND THE SCHOOL OF GRADUATE STUDIES OF MCMASTER UNIVERSITY IN PARTIAL FULFILMENT TO THE REQUIREMENTS FOR THE DEGREE OF

DOCTOR OF PHILOSOPHY

Descriptive Note

DOCTOR OF PHILOSOPHY (2023) McMaster University

(Civil Engineering) Hamilton, Ontario

TITLE: Vibration-induced shear resistance reduction in granular soils: experiment, model, and mechanism

AUTHOR: Tao Xie

B. Sc. (Wuhan Institute of Technology, China)

SUPERVISOR: Dr. Peijun Guo & Dr. Dieter Stolle

NUMBER OF PAGES: xiii, 216

To my dearest daughter,

courageous wife,

and selfless parents

Abstract

The phenomenon of vibration-induced shear resistance reduction (ViSRR) in granular soil is characterized by the loss of shear resistance without significant excess pore pressure generation. It has diverse potential applications in various industries such as mining, pharmaceuticals, and civil engineering, including the installation of vibratory-driven piles. Despite limited research on this topic, both experimentally and theoretically, the mechanism associated with ViSRR remains challenging to explain. There is currently no established constitutive model to properly describe it. This dissertation investigates the fundamental features of ViSRR and develops a model to describe the process that leads ViSRR.

To achieve these objectives, three main areas of investigation were undertaken. First, a series of laboratory tests were conducted using a modified triaxial apparatus that allowed for vibrations superimposed on the monotonic shearing of granular soil samples. Second, by correlating macroscopic plastic strains with the transition, creation, and destruction of mesoscopic shear-transformation-zones (STZs), which can be considered as weak particle loops in granular assemblies, the conventional thermodynamic-based STZ model was extended to soil mechanics. Third, the concept of "vibration-induced shear resistance relaxation" was proposed, which refers to the loss of shear resistance in granular material subjected to restricted deformations in response to plastic strains induced by vibrations. In other words, ViSRR occurs when the total deformation rate of the granular material is constrained and does not keep up with the rate of plastic deformation induced by vibrations.

By conducting laboratory tests, developing the extended STZ model, and proposing the concept of "vibration-induced shear resistance relaxation", this dissertation contributes to a better understanding of ViSRR in granular soil and provides insights into the mechanisms governing this phenomenon. The results of this research can be used to improve the design and construction of geotechnical structures.

Acknowledgments

I would like to extend my heartfelt thanks to the following individuals who have played a significant role in the completion of my research. First and foremost, my deepest appreciation goes to my primary supervisor, Dr. Peijun Guo, for his unwavering guidance, invaluable advice, constant support, and words of encouragement, especially during my challenging times. I consider myself incredibly fortunate to have had such a knowledgeable and professional supervisor who possesses meticulousness, humility, energy, and creativity. I am also immensely grateful to my co-supervisor, Dr. Dieter Stolle, for his constructive feedback, suggestions, and prompt responses to my queries throughout the duration of my research work. I would like to express my gratitude to my supervisory committee members, Dr. SeonHong Na and Dr. Cancan Yang, for their valuable comments and inputs during the course of my research.

I am indebted to the laboratory technician, Peter Koudys, for providing me with technical support in setting up the modified triaxial shear apparatus. His expertise has been instrumental in the successful execution of my experiments. Furthermore, I am grateful to Prof. Qiang Luo at Southwest Jiaotong University for his assistance in my academic pursuits. His support has been instrumental in shaping my career.

I would like to convey my deepest appreciation to my wife, Jie Liu, for her unwavering companionship, understanding, support, and encouragement throughout this journey. I also express my heartfelt gratitude to my lovely daughter, Lexi Xie, whose smile has been my biggest motivation to keep moving forward. Last but not least, my utmost gratitude goes to my parents for their unwavering sacrifices, unconditional love, and unwavering support. They have been the pillars of my life, and without them, I would have been lost.

Preface (Co-Authorship and Declaration of Academic Achievement)

This dissertation, which contains the original works of the author, is prepared in accordance with McMaster University's regulations for a "sandwich" thesis format. It includes six previously published papers. Since collaboration is common in modern education and research, these papers that are presented in Chapters 3~7 have multiple authors. The contributions of each author to the papers are outlined below:

Paper 1: Xie, T., & Guo, P. (2022). A modified triaxial apparatus for soils under high-frequency, low-amplitude vibrations. *Geotechnical Testing Journal*, 45(1), 1-19.

T. Xie conducted the construction, calibration of the testing system, and all the experiments. P. Guo designed the testing system. The original manuscript was written by T. Xie and edited by P. Guo.

Paper 2: Xie, T., Guo, P., & Stolle, D. (2022). Experimental investigation of vibration-induced shear resistance reduction in sheared granular soils. *Canadian Geotechnical Journal*, 60(1), 44-59.

T. Xie performed all the tests, analysis of experimental data, and writing of the manuscript that was edited by P. Guo and D. Stolle. P. Guo designed the experiment and proposed the concept of "vibro-critical state". D. Stolle provided valuable suggestions to improve the paper.

Paper 3: Xie, T., Guo, P., & Stolle, D. (2022). Development of extended STZ model for granular soils subjected to combined static loading and vibration. *Géotechnique*, 1-9.

T. Xie developed the extended STZ model, including hypotheses, formulation, and validation of the model. P. Guo proposed the use of the STZ theory to model vibration-induced shear resistance reduction and supervised the development of the model. D.

Stolle provided editorial and technical comments during the preparation of the manuscript. The manuscript was written by T. Xie and edited by D. Stolle.

Paper 4: Xie, T., Guo, P., & Stolle, D. (2023). Thermodynamic basis of granular STZ model and its application in revealing shear resistance reduction mechanisms of granular soils under vibration. *Continuum Mechanics and Thermodynamics*, 1-15.

T. Xie developed the thermodynamic model and formulation. P. Guo and D. Stolle provided insightful comments during the development of the model. The manuscript was written by T. Xie under the supervision of P. Guo and edited by D. Stolle.

Paper 5: Xie, T., Guo, P., & Stolle, D. (2023). Shear resistance relaxation of granular materials under vibration and restricted deforming conditions. *Géotechnique*, 1-13.

T. Xie originally proposed the concept of "vibration-induced shear resistance relaxation" as the mechanism of shear resistance reduction, analyzed the modelling results, and organized the manuscript. P. Guo and D. Stolle provided helpful suggestions and comments during the preparation of the manuscript and performed full review of the manuscript.

Paper 6: Xie, T., Guo, P., & Stolle, D. (2023). Experimental and modelling investigation of vibration-induced fluidization in sheared granular soils. *International Journal for Numerical and Analytical Methods in Geomechanics*, 47(8), 1399-1415.

T. Xie performed all laboratory tests and the simulations. The manuscript was written by T. Xie under the supervision of P. Guo. D. Stolle provided constructive comments on the writing and organization of the manuscript.

Table of Contents

List of Figures

Chapter 1 Introduction

1.1 Background and literature review

Owing to its discrete nature, a granular material that is subjected to vibration trends to accumulate deformation, and undergo volume change, or shear resistance reduction, which depends on the initial density and boundary conditions. For instance, vibratory compaction provides an effective means of soil improvement that has been widely applied and extensively investigated in engineering practice (Barkan, 1962; Ayer and Soppet, 1965 & 1966; Chen and Fang, 2008). However, the vibration-induced shear resistance reduction (ViSRR) of granular soils has not attracted as much attention as the vibration-induced compaction in geotechnical engineering, in spite of the ViSRR having been observed in a broad spectrum of natural processes (Hosoi & Goldman, 2015; Sharpe et al., 2015) and geophysical (Griffa et al., 2013; Ferdowsi et al., 2015), and has wide applications in the mining and pharmaceutical industries (Ringer & Mujumdar, 1983; Rosato et al., 2002; Hsiau et al., 2011) as well as in civil engineering (O'Neill et al., 1990; Viking & Bodare, 1999; Bingham et al., 2000).

ViSRR is believed to be the primary reason for some long-runout landslides of dry soil on the moon and Mars (Melosh, 1987). Melosh and Sornette (Melosh, 1979 & 1983; Sornette & Sornette, 2000) suggested that ViSRR is the mechanism that is responsible for dry rock debris behaving like a fluid in some earthquakes. In geophysics, the weakening of granular “fault gouge” is considered as a potential triggering mechanism of earthquakes (Van Der Elst & Brodsky, 2010; Marsan & Lengline, 2008). That is, a fault gouge accumulates energy associated with the seismic waves that is finally transferred from the ‘stick’ phase to the ‘slip’ phase (Brace & Byerlee, 1966; Johnson et al., 1973 & 2008). ViSRR is also observed in civil engineering. For example, vibratory-driven piles take advantage of ViSRR during pile installation. The local shear resistance reduction of a granular soils around a pile accelerates the penetration rate of

vibratory-driven piles, when compared with jacked pile installation (O'Neill et al., 1990; Viking & Bodare, 1999; Bingham et al., 2000). In some cases, vibration even allows a pile to be driven into a soil under its own weight.

(1) *Experimental studies*

There is a long history of investigating ViSRR in granular soils. Krey (1932) is one of the first researchers to explore the influence of vibration on soil strength via a vibrational platform. He observed a decline in the angle of repose of dry sand due to the decreased friction during vibration. Using a direct shear device mounted on a vibrator, Barkan (1962) studied the effect of frequency (up to 50 Hz) and amplitude of vibration on the friction angle of sand. In his study, the vertical normal stress was kept constant during vibration and the direction of vibration was the same as the applied shear stress in the horizontal direction. The test results showed that the decrease in friction angle is controlled by the acceleration of horizontal vibration. The experimental results obtained by Mogami and Kubo (1953) revealed that, as the horizontal acceleration increases, the shear strength drops continuously until the specimen completely collapses. They found that the horizontal acceleration, rather than the frequency or the amplitude of vibration, dominates the shear strength reduction induced by vibration. This conclusion was confirmed by Youd (1967). Recently, Taslagyan et al. (2015, 2016) investigated ViSRR using a modified direct shear apparatus. In their study, horizontal vibration is applied by a voice coil actuator connecting with the loading rod. As such, the horizontal vibration is superimposed on the static shear force in the horizontal direction thereby avoiding the vibration of the whole testing device. They observed that the direct shear friction angle of sand decreases with an increase of acceleration. That is, a transition of the material from a solid-like state to a fluid-like state is expected to occur under an

intensive vibration.

ViSRR was also investigated by using the a "sphere/intruder penetration test" (Barkan, 1962; Denies et al., 2010; Darbois Texier et al., 2017; Omidvar et al., 2019). In these tests, a sphere or intruder is pushed into a granular media by vibration. Even at a very low amplitude, vibration can significantly reduce the penetration resistance of granular soils. For example, at a very small amplitude (10 μm) and high frequency (50~100 Hz) vibration, the penetration resistance when pushing a vibrating cylindric intruder into a dry granular material can be reduced by 90% (Denies et al., 2010). However, the complex stress state in the granular material around the intruder makes it difficult to judge which factor dominates the process of strength degradation. It is also difficult to construct a theoretical model based on the penetration and the corresponding penetration resistance. Moreover, owing to the unknown stress and loading conditions, as well as non-uniform deformation within the granular material, the result of penetration tests is improper for establishing constitutive models.

(2) *Mechanisms*

Regarding the mechanisms behind the decreased shear strength in vibrated granular soils, several conceptual or physical hypotheses have been proposed. Barkan (1962) attributed it to the vanishing of "dry" friction when intense vibrations are imposed. He assumed that the velocity-dependent "viscous" friction dominates the behavior of cohesionless soil during vibration. Blekhman (2000) further proposed the concept of "vibrational force" that reflects the "nature of the viscous friction" for vibrated granular materials. However, there is a lack of evidence, on the physical side, to support the existence of the "viscous" friction. L'Hermite and Tournon (as reported by Denies & Holeyman, 2017) proposed a concept of "shaking pressure" to interpret the shear

strength reduction of dry sand induced by vibration, that reduces the normal pressure similar to excess pore pressure. However, this "shaking pressure" was introduced based on the measured shear resistance of the sand without a clear physical interpretation. For saturated sands, vibration-induced excess pore pressure, or local liquefaction is another frequently mentioned mechanism of shear resistance reduction (Vanden Berghe et al., 2001; Hwang et al., 2001; Pestana et al., 2002; Osinov, 2013). Nonetheless, the shear resistance reduction in dry sand cannot be explained by excess pore pressure (O'Neill, et al., 1990; Viking, & Bodare, 1999). Additionally, for vibro-driven piles, the concept of "horizontal soil arch" (Heerema, 1978; White & Lehane, 2004; Moriyasu et al., 2018) has been proposed to explain the reduced shaft resistance during installation. It is believed that the irregular movements of the pile form temporary horizontal soil arches surrounding the pile (Heerema, 1978). The soil arch tends to reduce the normal pressure acting on the pile and hence causes a decline in the shaft resistance. It should be noted that the concept of soil arch cannot explain the toe resistance reduction. In other words, the existence of a soil arch has not been confirmed.

Recently, in view of the advances in testing technology and numerical analysis, e.g., Discrete element method (DEM), more information regarding the behavior of granular media under vibrations can be traced on the microscopic level. For example, Denies (2010) argues that a decrease in both contact forces and contact lifetimes in a vibrated granular soil does not allow the shear stress to be transmitted effectively through the interrupted force chains. From the results of DEM simulation, Ferdowsi et al. (Ferdowsi et al, 2014) realized the importance of energy change within granular media during the transition process from the stick phase to the slip phase when vibration is applied. Even though this phenomenon has been observed from DEM simulations, it is difficult to quantify the energy change and the transition from stick to slip at particle contacts

mathematically and to verify the mathematical model experimentally. As a result, it is challenging to correlate the energy change with the shear resistance reduction explicitly.

(3) *Theoretical analysis*

A constitutive model for soils can be either based on continuum mechanics or granular mechanics. Based on continuum mechanics, a large number of phenomenological models have been formulated to describe the different observed phenomena, including hypoplastic theories (Kolymbas, 1991 & 1993), elasto-plasticity models (Roscoe et al., 1963; Roscoe & Burland, 1968; Duncan & Chang, 1970), generalized plasticity (Zienkiewicz and Mroz, 1984; Pastor, 1990), incrementally nonlinear models (Darve, 1990; Darve et al., 1995), as well as visco-elasticity and visco-plasticity models (Truesdell, 1955; Perzyna, 1963). A major limitation of the aforementioned models is the inability to consider the physics of observed material behaviors in terms of the interaction among the particles.

Models based on the micromechanics of granular materials account for the particle-scale interaction between particles at contact, as well as the internal structure of the material. These models can be grouped into one of two categories, either the computer-simulation approach or the micromechanics approach. The former deals with the granular material responses based on the governing equations for the interaction of particles, e.g., the Discrete Element Method (DEM) established by Cundall and Strack (Cundall & Strack, 1979; Chang et al., 1992; Potyondy & Cundall, 2004; Zhou et al., 2020). Although a significant progress has been achieved in this area with an obvious increase in the computing power and the improved algorithms, the number of particles that can be handled by computer-simulations is still very limited when compared with the huge number of particles that must be considered, even for a handful of sand.

The constitutive behavior of granular materials in the micromechanics approach can be presented at the contact level and the representative element volume (REV) level (Chang et al., 1992). At the contact level, the continuum concepts such as strain and

stress are not applicable, but rather the constitutive law handles the relation between relative movement and contact force of two particles. At the REV level, the continuum concepts of stress and strain are used for constitutive law development at the REV level. Volume averaging is applied to establish the relation between strain and relative particle displacements as well as stress and interparticle contact forces. The internal structure or particle connectivity is taken into account in this process. Nevertheless, it is still challenging for the micromechanics approach to transfer the microscale interaction of particles into the macroscale strain and stress of an ensemble.

In short, the complexity of constitutive behavior of granular assembly stems both from the local properties at particle level, and from the disordered packing and the interaction of particles. Regarding ViSRR, the combined static and dynamic loading makes this issue more complicated. There is no constitutive model at this point that properly accommodates ViSRR especially when a granular material is subjected to high-frequency vibrations, although such a model spans a wide variety of phenomena and has many potential applications.

The Shear Transformation Zone (STZ) model can be viewed as an extension of the rate process theory, which is grounded in statistical mechanics. Rate process theory finds its origins in physical chemistry, where it was employed to analyze chemical reaction rates (Eyring, 1936; Glasstone et al., 1941). It was later adapted for use in soil mechanics to explore the rheology of clays (Mitchell, 1964; Mitchell & Soga, 2005). The central premise of the theory revolves around atomic-scale entities, termed "flow units," participating in a time-dependent deformation process. The motion of these "flow units" is constrained by their neighboring units. This constraint is characterized by the concept of an "energy barrier." Surmounting this energy barrier allows a "flow unit" in one equilibrium state to transform to another state, resulting in plastic deformation.

In contrast to the classical rate process theory, the STZ theory (Falk & Langer, 1998; Bouchbinder & Langer, 2009b; Pechenik, 2005; Lieou et al., 2015; Kothari & Elbanna,

2017) can address plastic deformations of flow units significantly larger than individual atoms and can operate on much longer timescales. The STZ theory examines a local STZ, which represents a defect or a weak domain within the material. The evolution of an STZ and its impact on material deformation are investigated using principles akin to those found in rate process theory.

The STZ theory has found applications in diverse fields, including the plastic deformation of metallic glasses and amorphous solids (Falk & Langer, 1998; Bouchbinder & Langer, 2009a; Langer & Pechenik, 2003; Urata & Li, 2018), weakening of faults in dynamic earthquake triggering (Langer & Pechenik, 2003; Daub & Carlson, 2010; Di Toro et al., 2006), the flow of granular materials in mining and power industries (Lieou et al., 2015; Kothari & Elbanna, 2017), and the development of grain breakage (Lieou et al., 2014). Essentially, for granular materials, a STZ represents a cluster of particles at a local scale that undergoes inelastic shear distortion, and transformation from a relatively lower energy state to another, more activated one of higher energy. This transition leads to a redistribution of stress and strain in the vicinity of STZ regions, analogous to the activated process of "flow units" in rate process theory, in which a STZ corresponds a "flow unit".

1.2 Scope and objectives

The primary objective of this research is to investigate the shear resistance reduction of granular soils induced by high-frequency vibrations. Three aspects are addressed: (1) an experimental investigation; (2) model development for simulating the process of ViSRR; and (3) exploration of the mechanism responsible for ViSRR. The specific objectives are summarized as follows:

(1) Basic characteristics of ViSRR in granular soils

A modified triaxial apparatus is employed to investigate the potential influencing factors of ViSRR, including the soil's initial density, effective confining pressure, deviatoric stress level at which a vibration is applied, as well as vibration frequency,

intensity, and duration. The key parameters that dominate the ViSRR are expected to be revealed through the experimental study.

(2) Development of a theoretical model to simulate ViSRR in granular materials

The microscopic physical theory of the shear-transformation-zone (STZ) model is extended to soil mechanics to describe the process of ViSRR. Based on the proposed model, the ViSRR is further investigated and some features that are not obtained through the tests are explored via the model.

(3) Mechanism of ViSRR

Based on the experimental investigation and the extended STZ model, the mechanism behind the ViSRR is clarified.

1.3 Dissertation organization

The dissertation is organized into three parts with 8 chapters of which 6 are published papers. Owing to the "sandwich" format adopted, there is some overlap among chapters, especially in the introduction and literature review, as well as descriptions of the experiments and model. A brief outline of the dissertation is provided as follows:

- **Part I** consists of Chapter 2 and Chapter 3 that addresses the experimental studies. Chapter 2 introduces the modified triaxial apparatus by which static loading and vibration can be applied to the soil specimen synchronously. Chapter 3 describes experimental results obtained via the modified triaxial apparatus.
- **Part II** develops extended STZ model in Chapter 4 and Chapter 5. Chapter 4 focuses on the thermodynamic fundamentals of the extended STZ model. Chapter 5 formulates the framework of the extended STZ model, including the basic assumptions and governing functions.
- **Part III** concentrates on the mechanism and modelling analysis of ViSRR in Chapter 6 and Chapter 7. The emphasis of Chapter 6 is placed on addressing the mechanism of ViSRR and model validation. Chapter 7 investigates the vibration-induced fluidization as a special case of ViSRR, i.e., when granular soil completely

loses its shear resistance and behaves like a fluid.

Finally, Chapter 8 summarizes the main contributions of this research and highlights the future work.

1.4 References

Ayer, J. E., and Soppet, F. E. (1965). Vibratory compaction: I, compaction of spherical shapes. J. Am. Ceram. Soc. 48(4), 180–183.

Ayer, J. E., and Soppet, F. E. (1966). Vibratory compaction: II, compaction of angular shapes. J. Am. Ceram. Soc., 49(4), 207–210.

Barkan, D. D. (1962). Dynamics of bases and foundations, Trans. L. Drashevska, McGraw-Hill, New York, 207–210.

Bingham, C. M., Stone, D. A., Schofield, N., Howe, D., & Peel, D. (2000). Amplitude and frequency control of a vibratory pile driver. IEEE Transactions on Industrial Electronics, 47(3), 623-631.

Blekhman, I.I. (2000). Vibrational mechanics. World Scientific, Singapore. 509 p.

Brace, W. F., & Byerlee, J. D. (1966). Stick-slip as a mechanism for earthquakes. Science, 153(3739), 990-992.

Bouchbinder, E., & Langer, J. S. (2009a). Nonequilibrium thermodynamics of driven amorphous materials. I. Internal degrees of freedom and volume deformation. Physical Review E, 80(3), 031131.

Bouchbinder, E., & Langer, J. S. (2009b). Nonequilibrium thermodynamics of driven amorphous materials. III. Shear-transformation-zone plasticity. Physical Review E, 80(3), 031133.

Chang, C. S., Chang, Y., & Kabir, M. G. (1992). Micromechanics modeling for stress-strain behavior of granular soils. I: Theory. Journal of geotechnical engineering, 118(12), 1959-1974.

Chen, T.J., and Fang, Y.-S. (2008). Earth pressure due to vibratory compaction. J. Geotech. Geoenviron. Eng, 134(4), 437-444.

Cundall, P. A., & Strack, O. D. (1979). A discrete numerical model for granular assemblies. geotechnique, 29(1), 47-65.

Darbois Texier, B., Ibarra, A., & Melo, F. (2017). Low-resistive vibratory penetration in granular media. PloS one, 12(4), e0175412.

Darve, F. (1990). The expression of rheological laws in incremental form and the main classes of constitutive equations. Geomaterials: Constitutive Equations and Modelling, 123-148.

Darve, F., Flavigny, E., & Meghachou, M. (1995). Yield surfaces and principle of superposition: revisit through incrementally non-linear constitutive relations. International Journal of Plasticity, 11(8), 927-948.

Daub, E. G., & Carlson, J. M. (2010). Friction, fracture, and earthquakes. Annu. Rev.

Condens. Matter Phys., 1(1), 397-418.

Denies, N. (2010). Dynamic behavior of vibrated dry sand: sphere penetration experiments and discrete element modeling of vibrofluidization (Doctoral dissertation, UCL-Université Catholique de Louvain).

Denies, N., Canou, J., Roux, J. N., & Holeyman, A. (2010). Sphere penetration experiments in vertically vibrated sand. In Proceedings of the Fifth International Conference on Recent Advances in Geotechnical Earthquake Engineering and Soil Dynamics, San Diego, Calif. [CD-ROM]

Denies, N., & Holeyman, A. (2017). Shear strength degradation of vibrated dry sand. Soil Dynamics and Earthquake Engineering, 95, 106-117.

Di Toro, G., Hirose, T., Nielsen, S., Pennacchioni, G., & Shimamoto, T. (2006). Natural and experimental evidence of melt lubrication of faults during earthquakes. science, 311(5761), 647-649.

Duncan, J. M., & Chang, C. Y. (1970). Nonlinear analysis of stress and strain in soils. Journal of the soil mechanics and foundations division, 96(5), 1629-1653.

Eyring, H. (1936). Viscosity, plasticity, and diffusion as examples of absolute reaction rates.

Falk, M. L., & Langer, J. S. (1998). Dynamics of viscoplastic deformation in amorphous solids. Physical Review E, 57(6), 7192.

Ferdowsi, B., Griffa, M., Guyer, R. A., Johnson, P. A., Marone, C., & Carmeliet, J. (2014). Three-dimensional discrete element modeling of triggered slip in sheared granular media. Physical Review E, 89(4), 042204.

Ferdowsi, B., Griffa, M., Guyer, R. A., Johnson, P. A., Marone, C., & Carmeliet, J. (2015). Acoustically induced slip in sheared granular layers: Application to dynamic earthquake triggering. Geophysical Research Letters, 42(22), 9750-9757.

Glasstone, S., Laidler, K. J., & Eyring, H. (1941). The theory of rate processes; the kinetics of chemical reactions, viscosity, diffusion and electrochemical phenomena (No. 541.39). McGraw-Hill Book Company.

Griffa, M., Ferdowsi, B., Guyer, R. A., Daub, E. G., Johnson, P. A., Marone, C., & Carmeliet, J. (2013). Influence of vibration amplitude on dynamic triggering of slip in sheared granular layers. Physical Review E, 87(1), 012205.

Heerema, E. P. (1978). Predicting pile driveability: Heather as an illustration of the "friction fatigue" theory. In SPE European Petroleum Conference. Society of Petroleum Engineers. (pp. SPE-8084).

Hosoi, A. E., & Goldman, D. I. (2015). Beneath our feet: strategies for locomotion in granular media. Annual review of fluid mechanics, 47, 431-453.

Hsiau, S. S., Liao, C. C., Sheng, P. Y., & Tai, S. C. (2011). Experimental study on the influence of bed height on convection cell formation. Experiments in fluids, 51(3), 795.

Hwang, J. H., Liang, N., & Chen, C. H. (2001). Ground response during pile driving. Journal of Geotechnical and Geoenvironmental Engineering, 127(11), 939-949.

Johnson, T., Wu, F. T., & Scholz, C. H. (1973). Source parameters for stick-slip and for earthquakes. Science, 179(4070), 278-280.

Johnson, P. A., Savage, H., Knuth, M., Gomberg, J., & Marone, C. (2008). Effects of acoustic waves on stick–slip in granular media and implications for earthquakes. Nature, 451(7174), 57-60.

Kolymbas, D. I. H. D. (1991). An outline of hypoplasticity. Archive of applied mechanics, 61(3), 143-151.

Kolymbas, D., & Wu, W. (1993). Introduction to hypoplasticity. Modern approaches to plasticity, 213-223.

Kothari, K. R., & Elbanna, A. E. (2017). Localization and instability in sheared granular materials: Role of friction and vibration. Physical Review E, 95(2), 022901.The Journal of chemical physics, 4(4), 283-291.

Krey, H. (1932). Erddruck, Erdwiderstand und Tragfähigkeit des Baugrundes Berlin, Deutschland, Wilhelm Ernst ahd Sohn.

Langer, J. S., & Pechenik, L. (2003). Dynamics of shear-transformation zones in amorphous plasticity: Energetic constraints in a minimal theory. Physical Review E, 68(6), 061507.

Lieou, C. K., Elbanna, A. E., & Carlson, J. M. (2014). Grain fragmentation in sheared granular flow: Weakening effects, energy dissipation, and strain localization. Physical Review E, 89(2), 022203.

Lieou, C. K., Elbanna, A. E., Langer, J. S., & Carlson, J. M. (2015). Stick-slip instabilities in sheared granular flow: The role of friction and acoustic vibrations. Physical Review E, 92(2), 022209.

Marsan, D., & Lengline, O. (2008). Extending earthquakes' reach through cascading. Science, 319(5866), 1076-1079.

Melosh, H. J. (1979). Acoustic fluidization: A new geologic process?. Journal of Geophysical Research: Solid Earth, 84(B13), 7513-7520.

Melosh, H. J. (1983). Acoustic fluidization: can sound waves explain why dry rock debris appears to flow like a fluid in some energetic geologic events?. American Scientist, 71(2), 158-165.

Melosh, H. J. (1987). The mechanics of large rock avalanches: Geological Society of America Review in Engineering Geology, v. 7.

Mitchell, J. K. (1964). Shearing resistance of soils as a rate process. Journal of Soil Mechanics & Foundations Div, 90(Proc. Paper 3773).

Mitchell, J. K., & Soga, K. (2005). Fundamentals of soil behavior (Vol. 3). New York: John Wiley & Sons.

Mogami, T. and Kubo, K. (1953). The behavior of soil during vibration. Proc. 3rd Int. Conf. on Soil Mech. and Found. Eng., Switzerland, Vol. 1, 152-155.

Moriyasu, S., Kobayashi, S. I., & Matsumoto, T. (2018). Experimental study on friction fatigue of vibratory driven piles by in situ model tests. Soils and foundations, 58(4), 853-865.

Omidvar, M., Bless, S., & Iskander, M. (2019). Recent insights into penetration of sand and similar granular materials. In Shock Phenomena in Granular and Porous Materials (pp. 137-163). Springer, Cham.

O'Neill, M. W., Vipulanadan, C., & Wong, D. O. (1990). Evaluation of bearing capacity of vibro-driven piles from laboratory experiments. Transportation Research Record, (1277).

Osinov, V. A. (2013). Application of a high-cycle accumulation model to the analysis of soil liquefaction around a vibrating pile toe. Acta Geotechnica, 8(6), 675-684.

Pechenik, L. (2005). Dynamics of shear-transformation zones in amorphous plasticity: Nonlinear theory at low temperatures. Physical Review E, 72(2), 021507.

Perzyna, P. (1963). The constitutive equation for work-hardening and rate sensitive plastic materials. In Proc. Vibrational Problems (Vol. 4, No. 3, pp. 281-290).

Pestana, J. M., Hunt, C. E., & Bray, J. D. (2002). Soil deformation and excess pore pressure field around a closed-ended pile. Journal of geotechnical and geoenvironmental engineering, 128(1), 1-12.

Potyondy, D. O., & Cundall, P. A. (2004). A bonded-particle model for rock. International journal of rock mechanics and mining sciences, 41(8), 1329-1364.

Ringer, D. U., & Mujumdar, A. S. (1983). Analysis of aerodynamics and heat transfer in vibro-fluidized beds. Drying Technology, 2(4), 449-470.

Roscoe, K. H., Schofield, A., & Thurairajah, A. (1963). Yielding of clays in states wetter than critical. Geotechnique, 13(3), 211-240.

Roscoe, K., & Burland, J. B. (1968). On the generalized stress-strain behaviour of wet clay.

Rosato, A. D., Blackmore, D. L., Zhang, N., & Lan, Y. (2002). A perspective on vibration-induced size segregation of granular materials. Chemical Engineering Science, 57(2), 265-275.

Sharpe, S. S., Kuckuk, R., & Goldman, D. I. (2015). Controlled preparation of wet granular media reveals limits to lizard burial ability. Physical biology, 12(4), 046009.

Sornette, D., & Sornette, A. (2000). Acoustic fluidization for earthquakes?. Bulletin of the Seismological Society of America, 90(3), 781-785.

Taslagyan, K. A., Chan, D. H., & Morgenstern, N. R. (2015). Effect of vibration on the critical state of dry granular soils. Granular Matter, 17(6), 687-702.

Taslagyan, K. A., Chan, D. H., & Morgenstern, N. R. (2016). Vibrational fluidization of granular media. International Journal of Geomechanics, 16(3), 04015080.

Truesdell, C. (1955). Hypo-elasticity. Journal of Rational Mechanics and Analysis, 4, 83-1020.

Urata, S., & Li, S. (2018). A multiscale shear-transformation-zone (STZ) model and simulation of plasticity in amorphous solids. Acta Materialia, 155, 153-165.

Vanden Berghe, J. F., Holeyman, A., Juaristi, E., & Schmitt, A. (2001). Interlock friction in a sheet pile wall: laboratory tests. In International Conference on soil mechanics

and geotechnical engineering (pp. 1273-1276).

Van Der Elst, N. J., & Brodsky, E. E. (2010). Connecting near‐field and far‐field earthquake triggering to dynamic strain. Journal of Geophysical Research: Solid Earth, 115(B7).

Viking, K., & Bodare, A. (1999). Laboratory studies of dynamic shaft resistance response of a vibro-driven model pile in granular soil by varying the relative density. In Twelfth European Conference on Soil Mechanics and Geotechnical Engineering (Proceedings) The Netherlands Society of Soil Mechanics and Geotechnical Engineering; Ministry of Transport, Public Works and Water Management; AP van den Berg Machinefabriek; Fugro NV; GeoDelft; Holland Railconsult (No. Volume 2, pp. 863-869).

White, D. J., & Lehane, B. M. (2004). Friction fatigue on displacement piles in sand. Géotechnique, 54(10), 645-658.

Youd, T. L. (1967). The engineering properties of cohesionless materials during vibration. PhD dissertation, Iowa State University.

Zhou, G. G., Du, J., Song, D., Choi, C. E., Hu, H. S., & Jiang, C. (2020). Numerical study of granular debris flow run-up against slit dams by discrete element method. Landslides, 17(3), 585-595.

Part I: Experimental Studies

Chapter 2 Introduction of the testing system

(Paper 1)

A modified triaxial apparatus for soils under high-frequency low-amplitude vibrations

Geotechnical Testing Journal, 45(1), 1-19.

Tao Xie[1] (xiet20@mcmaster.ca), Peijun Guo[1*] (guop@mcmaster.ca)

[1]Department of Civil Engineering, McMaster University, Hamilton, ON, Canada L8S 4L7

Abstract: A modified triaxial apparatus was developed to explore the behaviour of cohesionless soil subjected to high-frequency low-amplitude vibrations, such as that induced by high-speed trains. It was based on a conventional Bishop-type triaxial apparatus to utilize its existing static loading module. The major modification was an added dynamic loading module with a low-inertia linear voice coil actuator (VCA) mounted coaxially with the vertical loading rod. Through a signal generator and an amplifier connected to the VCA, a vibration input with wide range of frequencies and amplitudes could be superimposed to a monotonic loading process. A series of tests under different conditions were performed to demonstrate the effectiveness and performance of the modified triaxial apparatus, with the focus being placed on the reduction of shear resistance and accumulative deformation of sand induced by high-frequency low-amplitude vibrations.

Keywords: modified triaxial apparatus; high-frequency low-amplitude vibration; strength reduction; accumulative deformation

1. Introduction

In engineering practice, different types of vibrations may be imposed on soils, such as those induced by moving vehicle, earthquake, machinery vibration and blasting. Various phenomena related to soil vibration and cyclic loading have been observed, which include seismic wave propagation (P-, S- and surface waves) (Pak and Behringer, 1993; Mujica and Melo,1998), densification and size segregation (Barkan, 1962; Ayer and Soppet, 1965, 1966; Alexeev et al., 2000), arching (Wassgren et al., 1996; Hsiau and Pan, 1998), convection flow (Laroche et al., 1989; Huan, 2008; Denies and Holeyman, 2017), accumulative settlement (Bian et al., 2010), increase of excess pore pressure and related strength reduction even liquefaction of saturated soil under intense vibration (Ishihara and Yasuda, 1975; Ishihara and Yamazaki, 1980; Ishihara, 1996; Wang et al., 2019). Depending on the nature of the engineering problems and the corresponding soil behaviours, various laboratory testing devices have been developed for different purposes; as summarized in Table 1.

Table 1: Laboratory tests for the investigation of dynamic soil behaviour

Laboratory tests	Purpose of research	Frequency	Strain level	References	Limitations
Cyclic triaxial test	Liquefaction, shear strength, shear modulus, damping ratio	< 5 Hz	10^{-4}~10^{-1}	Toki et al. (1995); Ishihara (1996)	Complex stress conditions such as non-symmetric stress state, principal stress rotation, etc.
Cyclic torsional shear test					
Cyclic simple shear test				Ishihara & Yamazaki (1980); Finn & Vaid (1977)	
Cyclic Direct shear test	Shear strength and internal friction angle	< 1 Hz (or controlled by rate of displacement)	--	Al-Douri & Poulos (1991); Vieira et al. (2013); Pra-ai & Boulon (2017)	Non-uniform and implicit states of stresses and strains
Direct shear apparatus on vibrator	Internal friction angle of sand under vibration	Up to 50 Hz		Barkan (1962); Youd (1967)	
Modified direct shear apparatus with vibration actuator	Strength loss of granular soils under horizontal vibration	Up to 140 Hz		Taslagyan et al. (2015b)	
Shaking table test	Repose angle of sand under vibration	< 5 Hz		Krey (1932)	Non-element test
Resonant column test	Shear modulus, damping ratio	5 to 6×10^{5} Hz	10^{-6}~10^{-3}	Hall & Richart (1963); Hardin (1965)	Low strain level
Wave propagation/ Bender element	Shear modulus	--	~10^{-6}	Dyvik & Madshus (1985); Ishihara (1996)	Low strain level with elastic responses

The influence of vibration of the shear strength of sand was first investigated using shake table and direct shear apparatus. Krey (1932) studied the effect of vibration on the repose angle of dry sand. Barkan (1962) and Youd (1967) investigated the influence of vibrations on the internal frictional angle using a direct shear device mounted on a vibrator, and they both observed vibration-induced loss of soil shear strength. More recently, Taslagyan et al. (2015a, 2016) performed an experimental study to investigate the variation of shear resistance of sand subjected to vibration of different intensities and frequencies using a modified direct shear apparatus. In this apparatus (Taslagyan et al., 2015b), an actuator was mounted horizontally between the load cell and the top half of the shear box. During a standard direct shear test at a constant rate of shear displacement, a horizontal vibration with selected acceleration was superimposed to the monotonic loading for a short period of time. Owing to the non-uniform stress state related to the boundary conditions, this modified direct shear box can only provide

information about the influence of vibration on the shear strength of soil.

Due to the inherent limitations of direct shear apparatus, other devices have been developed to investigate the dynamic soil properties under improved stress and strain conditions. These devices include cyclic triaxial apparatus, cyclic simple shear apparatus, and cyclic hollow cylinder apparatus. Comparing with the direct shear apparatus, the stresses and strains in the soil specimen in these devices are relatively uniform. In particular, triaxial tests have been widely used to investigate the behaviors of soils subjected to either monotonic loading or cyclic loading, depending on the function of the load control module. In a conventional triaxial compression test, the confining pressure is generally kept constant and the axial load can be applied in different ways. In a monotonic loading test under strain control, the specimen is sheared at a constant rate of axial displacement. The test may be performed by direct control of the axial load. In cyclic triaxial tests, cyclic axial stress could be superimposed on selected static stress states, with the focus being placed on the behavior of soil under cyclic loading. The frequency of cyclic loading is generally limited within the range of 1 to 5 Hz (Khan et al., 2011; Ishihara, 1996). Comparing with the axisymmetric stress conditions in cyclic triaxial tests, the dynamic hollow cylinder apparatus (Ishihara and Yasuda, 1975; Cai et al., 2018) can reproduce most of the complex stress conditions encountered in engineering practice, including non-symmetric stress state, principal stress rotation, etc. However, the cyclic loading frequency used in these devices is generally lower than 5 Hz.

Tests with cyclic loading frequency up to 5 to 10 Hz are appropriate for experimental studies of soil behavior in geotechnical earthquake engineering and pavement engineering. For high-speed railways, the characteristic frequency of train-induced dynamic load on soil increases with train speed. Zhai et al. (2015) observed that the significant frequencies of ground vibration due to high-speed train at speed over 300 km/h were mainly concentrated in the range of 20-60 Hz and the measured acceleration of ground vibration was up to (0.1~0.3)g. It has been reported that the high-frequency

dynamic train load may increase the accumulative settlement of earthen embankments, even at a very low amplitude of dynamic stress (Liu and Chen, 2008). There are also concerns about any complication of soil behavior when the train speed is approaching the shear or Rayleigh wave velocity of soil, i.e. the critical speed issue (Sheng et al., 1999; Madshus and Kaynia, 2000). Consequently, with the development of high-speed railways, there is an increasing demand for improved understanding of soil behavior and other phenomena in the ground induced by high-frequency loadings, such as the resonance effect (Milne et al., 2017; Shih et al., 2018) and critical speed issue (Sheng et al., 1999; Madshus and Kaynia, 2000).

In this paper, a new type of triaxial apparatus is described, which allows applying high-frequency low-amplitude cyclic loading in the process of a conventional triaxial compression test at constant confining pressure. The apparatus has the capability to apply monotonic loading either at constant strain rate or controlled axial stresses. To reduce the effect of friction, a ball bushing is used to guide the movement of the loading rod. A dynamic module is mounted on the loading rod and vibrations with different frequencies and intensities can be imposed vertically on the specimen. The influence of high-frequency low-amplitude (i.e., low displacement amplitude) vibration on the stress-strain behavior of soil can be determined. The effectiveness and the performance of the modified triaxial testing system are examined via a series of tests on specimens of Standard Ottawa sand C-109.

2. Modified triaxial apparatus and loading scheme

2.1 Modified triaxial apparatus

Figure 1 shows the major components of the modified triaxial testing system based on a conventional Bishop-type triaxial apparatus. The whole testing system is composed of three modules: a static loading module, a dynamic loading module, and a measurement/data acquisition module.

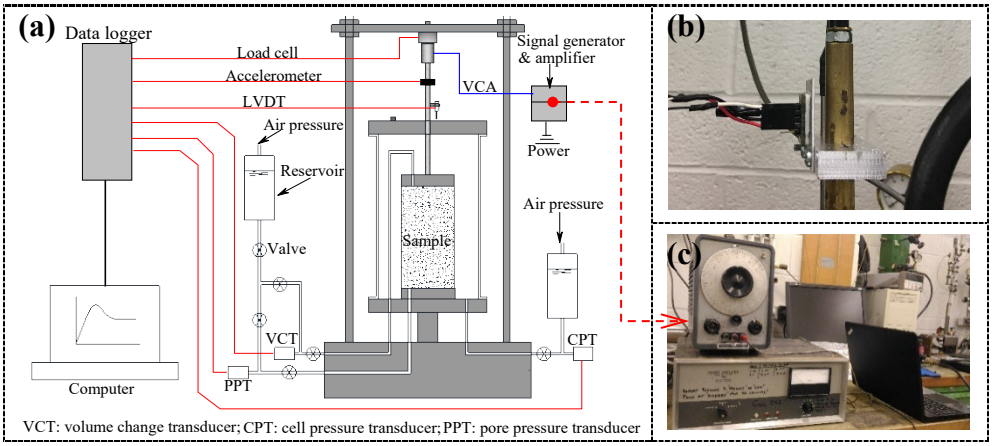

Figure 1: Modified triaxial testing system. (a) schematic layout of the modified triaxial apparatus; (b) accelerometer fixed on the loading rod; (c) signal generator and amplifier connected with the voice coil actuator (VCA) to control the frequency and intensity of vibration

(1) *Static loading module*

The static loading module is practically a conventional Bishop-type triaxial apparatus with a frictionless triaxial cell. A source of air pressure is used to apply back pressure and cell pressure via air-water pressure converters. All air pressures are controlled by precision regulators, with the accuracy of measurement being 0.1 kPa.

Under the mode of strain-control as shown in Figure 2, the specimen is sheared by imposing a constant rate of axial displacement. The modified triaxial apparatus can also work in a stress-controlled mode to investigate, for example, the accumulative deformation of soils induced by high-frequency low-amplitude vibrations under constant static stresses. To achieve the control of axial stress, a diaphragm air cylinder is mounted on the reaction beam of the loading frame and connect to the loading rod, as shown in Figure 3. The axial load is controlled by applying pressure to the top side of a Bellofram piston in the air cylinder through the regulated air pressure.

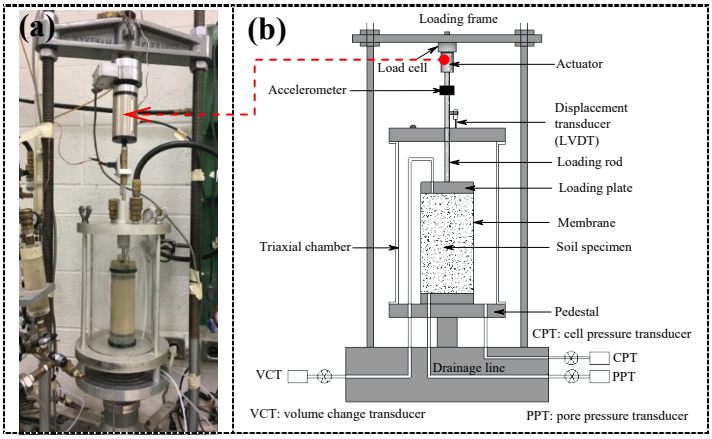

Figure 2: Modified triaxial apparatus in strain-controlled mode. (a) Photo, and (b) schematic illustration

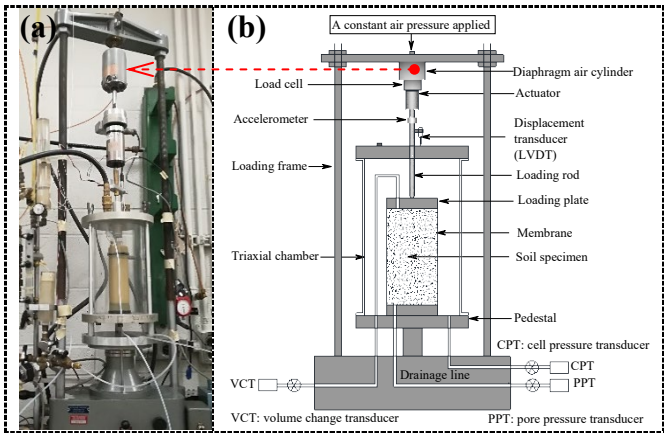

Figure 3: Modified triaxial apparatus in stress-controlled mode. (a) photo; (b) schematic illustration(2) *Measurement/data acquisition module*

The measurement module includes a load cell to measure the axial load, two pressure transducers (PT) to measure the pore pressure in the soil specimen and the cell pressure respectively, an accelerometer to measure the vibration acceleration of the loading rod, a linear variable differential transducer (LVDT) and a volume change transducer (VCT) to measure the axial displacement of the specimen and the volume change of the specimen, respectively. The data acquisition device can record data at a sampling rate of 1000 Hz, which is high enough for the frequency of vibration used in this research. The precisions in the measurements of the pore pressure and acceleration are 0.3kPa and 0.01g, respectively. The accuracy of the load cell was determined as 0.05% according to a calibration in the range of load used in this study. The VCT is made of a copper cylinder that is connected to a piston by means of a Bellofram. The movement

of the piston is guided in its vertical motion by a pair of high precision stainless steel linear Thompson Ball Bushings and its displacement is measured by a LVDT. The piston has an effective area equal to that of the specimen, with the precision of volumetric strain variation being 10^{-5}.

(3) *Dynamic loading module*

The major modification to the triaxial apparatus is the addition of a dynamic loading module, with the core part being a low-inertia linear voice coil actuator (VCA) mounted coaxially with the loading rod, as shown in Figure 2 and Figure 3. It is used to impose vertical vibrations on the specimen with a wide range of frequencies and intensities. Besides, a signal generator and an amplifier, as shown in Figure 1(c), are connected to the VCA to provide power and most importantly to control vibration frequency and intensity.

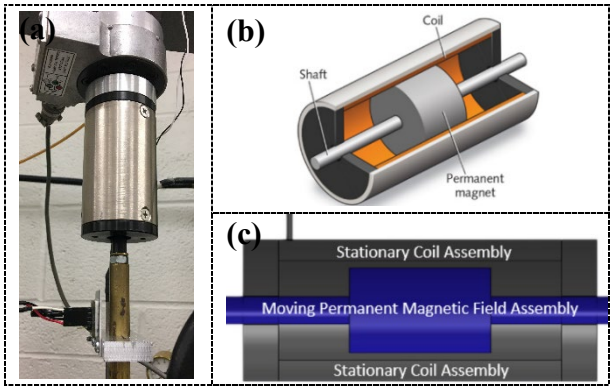

Figure 4: Moving-magnet type voice-coil actuator. (a) prototype; (b) internal structure; (c) operating principle diagram

The VCA, also known as a non-commutated DC linear actuator, is a type of direct-drive linear motor. There are two types of voice coil actuators: moving magnet actuator or moving coil actuator. In general, the operating principle of VCA is determined by the Lorentz force equation

$$\mathbf{F} = \mathbf{B} \times \mathbf{I} \tag{1}$$

where **F** is the force output, **B** and **I** denote the flux density of the magnetic field and the current in the coil, respectively. Specifically, a current-carrying conductor is put in

a magnetic field to generate a force and this force is proportional to the flux density and current, as shown in Figure 4. The direction of the force is determined by the polarity of the input current. Because the force output at any position is directly proportional to the current, a feedback device is unnecessary for controlling the force output of a VCA.

To minimize the inertial effect of the actuator, a moving magnet actuator is selected in this study. The moving mass of the VCA used in this study is 268 grams with the force constant being 20.5N/Amp, which corresponds to a theoretical acceleration constant of 7.80g/Amp or 0.008g/mA, which is consistent with the precision of the acceleration measurement of 0.01g in this study. With the maximum stroke of 6.4 mm and a force constant of 20.5 N/Amp, the peak force of the VCA is up to 119 N at the maximum power of 170 Watts. The frequency and the magnitude of current are controlled using a signal generator and an amplifier. Besides, the voltage of the input signal can also be adjusted so that the input energy for the voice coil actuator can be controlled to selected levels.

2.2 Calibration of testing system

As discussed previously, the function of the dynamic loading module was to produce a vibration with selected frequency and intensity (i.e. the amplitude of acceleration), there is no need to control the magnitude of the dynamic load generated by the VCA. To control the magnitude of the acceleration, trail tests were conducted using specimens of different relative density by adjusting the output energy level of the signal amplifier in the control module. This is because the actual acceleration or the magnitude of the dynamic load are affected by the properties of the specimen for an op-loop loading system without feedback control.

All transducers were calibrated prior to tests following proper procedures, which are summarized as follows:

- LVDT: The LVDT was calibrated using a precision LVDT calibrator (i.e. a micrometer) with 0.001 mm (0.000050 inch) resolution and 25 mm (1 inch) travel

range.

- Load cell: The load cell was calibrated using a certified proving ring, with the resolution of 0.1 N.
- Volume change transducer: The VCT was calibrated using graduated cylinders with the resolution of 0.2 ml, which corresponds to the resolution of volumetric strain measurement being approximately 10^{-5}.
- Accelerometer: The calibration of the accelerometer was performed using the acceleration due to gravity. The calibration procedure was described as follows
  - Position the accelerometer with the arrow pointing down for the first calibration point and define this as –1 g.
  - Rotate the accelerometer so the arrow points up and use the reading for the second calibration point and define this as +1 g.
  - The accelerometer will then read 0 with no acceleration when held horizontally.

In summary, the loading system was calibrated for reliable measurement of applied load, deformation of the specimen and the imposed acceleration by the VCA. The energy input to the VCA was used as the control parameter for the intensity of vibration. The dynamic load was not specifically controlled and it was measured as the specimen's response to the imposed vibration.

2.3 Loading scheme

As stated previously, the modified triaxial testing system was developed to investigate how the stress and deformation were affected by high-frequency low-amplitude vibration superimposed on a soil specimen subjected to static shearing. To achieve this goal, the test was performed according to the following two schemes:

Strain-controlled monotonic loading: In this loading scheme, after the specimen was consolidated under hydrostatic stresses, the deviatoric stress was applied by controlling a constant rate of axial displacement, as in a conventional triaxial compression test.

When the deviatoric stress (or the axial displacement) reached a pre-selected value, the VCA was turned on to apply a vertical vibration on the specimen with controlled frequency and acceleration amplitude for a period of T=10~30 seconds while the monotonic loading continued; as illustrated in Figure 5(a). The axial deformation and volume change of the specimen were continuously measured. Consequently, the influence of the superimposed vibration on soil behaviors could be obtained by separating the stress-strain curves under monotonic loading only from the measured stresses and strains. For the same specimen, the dynamic loading could be applied at different axial stress or strain levels.

Stress-controlled monotonic loading: In the mode of stress-controlled monotonic loading, the deviatoric stress was applied using an air cylinder that converted air pressure to axial load corresponding to selected stress level. The VCA was then turned on to apply a vertical vibration on the specimen for a relatively long period while the axial load was kept constant; as illustrated in Figure 5(b). Similar to the strain-controlled monotonic loading mode, the frequency and the amplitude of vertical vibration were controlled rather than the amplitude of the dynamic deviatoric stress. It should be noted that the intensity of vibration may also be controlled by energy input to the VCA instead of direct control of the acceleration amplitude.

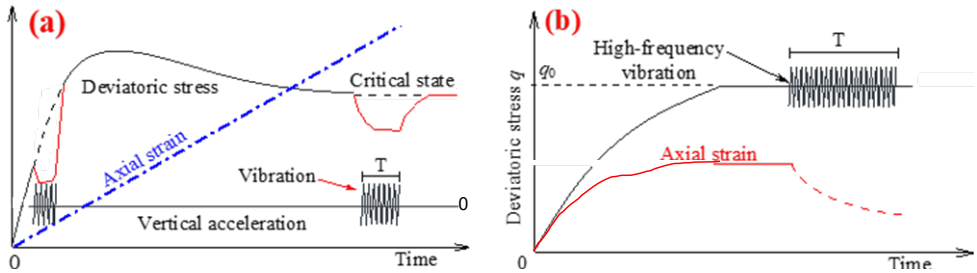

Figure 5: Loading schemes: (a) strain-controlled mode; and (b) stress-controlled mode

It should be noted that the mode of strain control can be used to investigate the influence of vibration on the stress-strain responses in both the pre-peak and post-peak stages; see Figure 5(a). The mode of stress-controlled monotonic loading, however, is close to the stress conditions encountered in engineering practice, for example, when

exploring the accumulative deformation of soil induced by high-frequency low-amplitude vibration generated by high-speed trains.

Comparing with ordinary cyclic triaxial apparatus, the modified device took advantage of the conventional triaxial apparatus with explicit stress states, uniform stress distribution and uniform deformation of the specimen. The adoption of a moving magnet voice coil actuator as the major component of the dynamic loading module allowed application of high frequency vibrations (up to 120 Hz) with minimal inertia effect. The dynamic loading module can control the frequency and the acceleration amplitude as well as the energy input to the VCA. The triaxial cell was built using a ball bushing to guide the movement of the loading rod to reduce the effect of friction, which might be significant otherwise under high-frequency excitation. In addition, the modified triaxial apparatus overcame the intrinsic shortcomings of the dynamic direct shear apparatus (Taslagyan et al., 2015b), such as the non-uniform distribution of stresses and strains.

3. Characteristics of the modified triaxial testing system

In order to examine the characteristics and the performance of the modified triaxial testing system, a series of tests were performed on specimens of Standard Ottawa sand C-109 under different conditions with both strain-controlled and stress-controlled monotonic loading modes. The performances of each module of the system were checked in detail to make sure all components functioned properly to produce reliable experimental results.

3.1 Testing material and sample preparations

Standard Ottawa sand C-109 is a uniform fine sand of rounded to sub-rounded grains with the specific gravity G_s=2.65, the mean particle size d_{50}=0.375 mm, the uniformity coefficient C_u=1.80 and the curvature coefficient C_z=1.20. The maximum and minimum void ratios are 0.81 and 0.50 following the ASTM test methods D4254-00 and D4253-

00, respectively.

To measure the volume changes of soil specimens in the triaxial tests, cylindrical specimens of 50mm in diameter and 100mm in height were fabricated by water pluviation (WP) method that can produce fully-saturated specimens (Chaney and Mulilis, 1978; Vaid and Negussey, 1984; Ishihara, 1996; Su, 2007). Prior to fabricating a specimen, the porous stones and predetermined amount of sand were boiled for about 20 minutes to remove any trapped air bubbles. A membrane was mounted on the base pedestal using two O-rings, and the split mold was put in position. Vacuum was used to make the membrane stick to the inner wall of the split mold. The mold was filled with de-aired water through the drainage line connected with the base pedestal. After that, the boiled sand was carefully poured into the mold using a spoon and, in this process, the sand grains should avoid exposure to air. The split mold was tapped gently from outside by using a hammer to control the density of the specimen. When the split mold was filled to a certain height, a porous stone and the top platen were mounted with care to make sure no air bubbles were trapped inside, and then the membrane was secured to the top platen with two O-rings. To keep the specimen standing after removing the split mold, a small suction (10 kPa and 5 kPa for dense and loose specimens respectively) was applied to the specimen. After mounting the triaxial cell, a cell pressure of 10 kPa was applied while the suction was removed at the same time. Then de-aired water was flushed through the specimen from the bottom to the top for at least 15 minutes to get rid of any residual air that might be trapped between the top platen and the specimen. To ensure fully-saturated sand specimens, a backpressure of 100 kPa was applied while keeping the effective confining stress as 10 kPa until a Skempton's B value reached 0.95. Following the saturation process, the specimen was consolidated under selected consolidation pressure. To keep the same initial condition of the specimens, the back pressure in all tests was kept at 100 kPa with B>0.95.

3.2 Strain-controlled monotonic loading mode

We first examine the performance of the modified triaxial apparatus via a series of tests following the strain-controlled monotonic loading scheme, with the test matrix being summarized in Table 2.

Table 2: Test matrix in strain-controlled monotonic loading mode

Factors	Range
Relative density (D_r)	35%, 75%
Degree of saturation (S_r)	Air-dried, fully saturated
Consolidation pressure (σ'_c)	50 kPa
Deviatoric stress level at which vibration was superimposed (q_0)	Pre-peak state: 45~150 kPa Near-critical state: about 150 kPa
Vibration Frequency (f)	60 Hz, 100 Hz
Duration of vibration (T)	10 s, 20 s

(1) *Vibration-induced loss of shear resistance*

Figure 6 illustrates the response of a fully-saturated loose sand specimen with relative density D_r=35% when a high-frequency vibration was superimposed during a strain-controlled loading. After being consolidated at an effective confining pressure of σ'_c=50kPa, the specimen was sheared under drained conditions at a constant axial strain rate $\dot{\varepsilon}_0$=0.1% per minute. When the deviatoric stress q was increased to q_0=45kPa, a vertical vibration with the acceleration amplitude a=0.21g at f=60 Hz was superimposed on the monotonic shearing for T=10 seconds. As shown in Figure 6(a), the deviatoric stress q experienced an immediate drop as the vibration was initiated. After terminating vibration, the deviatoric stress was gradually recovered as the monotonic shearing continued. The deviatoric stress q returned to its original trajectory in the absence of vibration, which implied that the influence of vibration on the specimen's shear resistance was erased at a large shear strain. Regarding the deformation of the specimen, the vibration caused additional volumetric compression, as indicated in Figure 6(b). In contrast to the full recovery of the deviatoric stress drop, the volumetric strain was permanent and irrecoverable in the process of continuous monotonic shearing after the vibration.

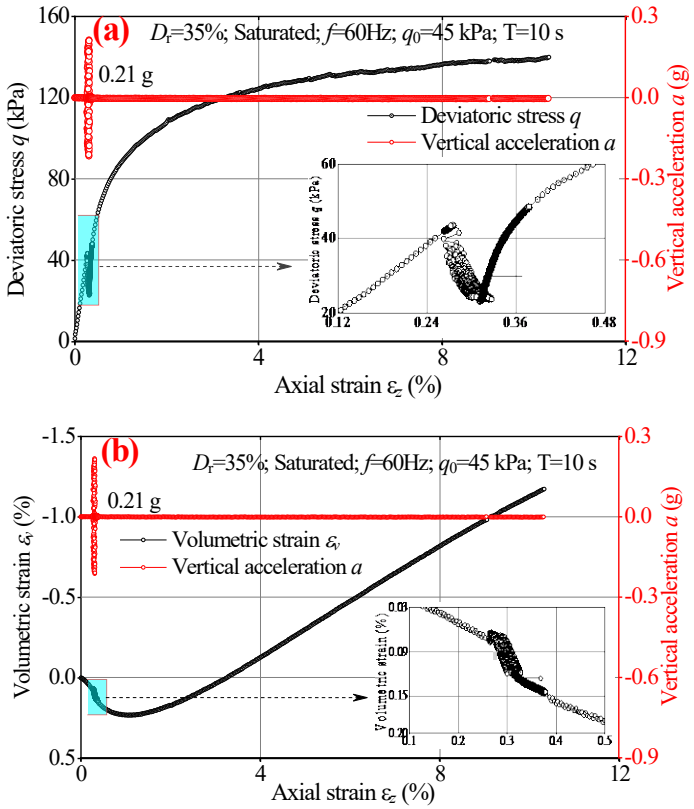

Figure 6: Measured soil responses when vibration was applied at pre-peak state. (a) deviatoric stress vs. axial strain; (b) volumetric strain vs. axial strain

The time history of the soil's responses during the application of vertical vibration are presented in Figure 7. As shown in Figure 7(a), immediately after the application of vibration, the average deviatoric stress decreased substantially. With the elapse of time, the rate of stress reduction gradually decreased, and the value of q tended to approach a stable level. Since the monotonic loading continued during vibration, the reduction in the axial stress implies that the superimposed vertical vibration tended to cause axial compression of the specimen, as an analogy to stress relaxation under static conditions. The axial stress gradually returned to its original trajectory in the absence of vibration, similar to that shown in Figure 6(a). The amplitude of stress oscillation was not significant, which meant that, for high-frequency vibrations, acceleration was a more significant indicator than cyclic stress to quantify the dynamic process.

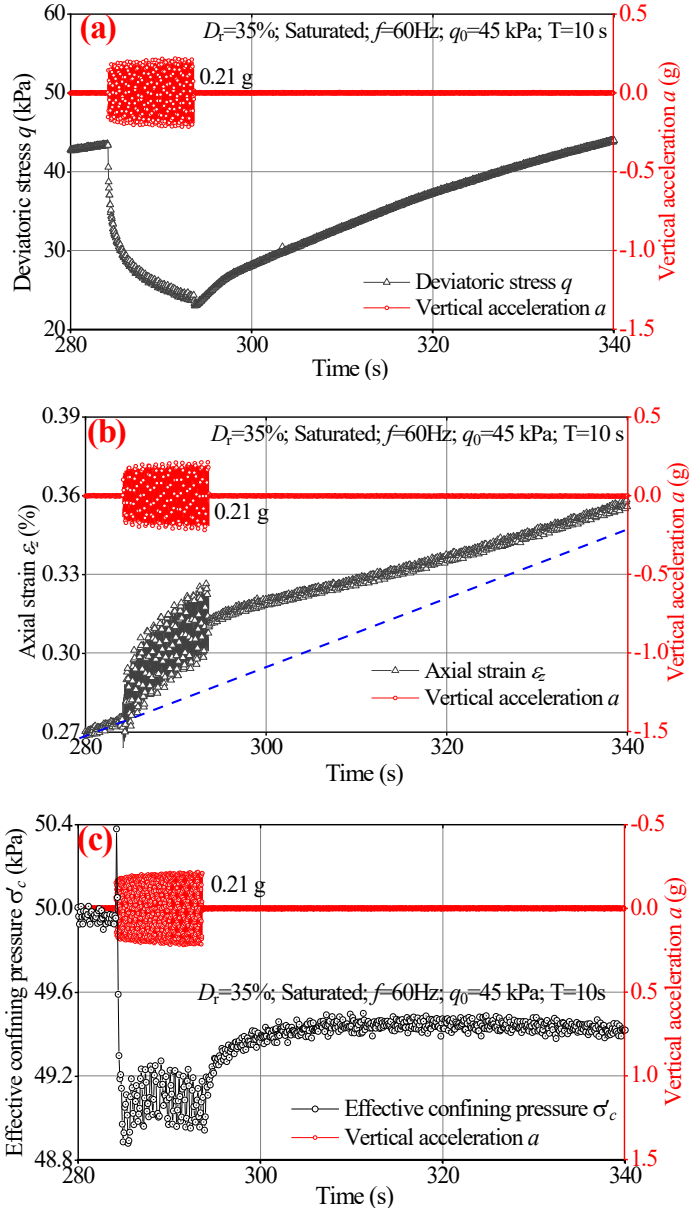

Figure 7: Time history of measured soil responses. (a) deviatoric stress; (b) axial strain; (c) effective confining pressure

Figure 7(b) shows the evolution of axial strain of the specimen during the vibration. Additional axial strain developed beyond the strain corresponding to the prescribed constant axial strain rate in monotonic loading. Like the variation of the deviatoric stress q, the rate of mean axial strain is decreased and it tends to approach a steady state if the duration of vibration was long enough. As the monotonic loading continued after the termination of vibration, the axial strain eventually approached the trajectory of prescribed axial deformation.

Since the test was conducted on a saturated specimen under drained conditions, the axial strain rate $\dot{\varepsilon}_0$=0.1% per minute was slow enough without inducing excess pore pressure during monotonic loading when drainage was allowed at both ends of the specimen (i.e., boundary of double drainage). During the application of high-frequency vibration, the possibility of excess pore pressure generation was examined. This was performed by keeping the drainage valve at the top of the specimen open while the water pressure was measured at the bottom of the specimen, as shown in Figure 1(a). An excess pore pressure of 0.5 to 1 kPa was measured during the application of vibration and it dissipated quickly after vibration. The resulting decrease in the effective confining stress was less than 2% of the target value 50 kPa. According to Terzaghi's 1D consolidation theory, the rate of excess pore pressure dissipation under double drainage conditions is four times faster than that measured under single drainage conditions. Consequently, the vibration-induced variation of the effective confining pressure in a fully saturated specimen under double drainage conditions was less than 0.5%, and its effect on the experimental results presented in Figure 6 and Figure 7 was negligible. It should be noted that the objective of the excess pore pressure measurement was to estimate its potential influence on the behaviour of soil when subjected to high-frequency vibration under drained conditions, rather than to determine the distribution of pore pressure in the specimen.

Figure 8 presents the responses of a dry specimen with D_r=70% subjected to three sequential vibrations of 60 Hz at near-critical state, with the acceleration amplitudes being 0.095g and 0.16g, respectively. An immediate shear resistance reduction was observed when vibration was applied in all three cases; as shown in Figure 8(a). Similar to the results of saturated specimen shown in Figure 6(a), the shear resistance decreased quickly at the onset of vibration and then gradually declined until approaching a stable value; as suggested in Figure 8(b). Moreover, higher intensity of vibration caused larger reduction of shear resistance. In particular, the shear strength reductions at a=0.095g

and 0.16g were about 35 kPa and 67 to 69 kPa, respectively. In all three case, vibration-induced shear resistance reduction was recovered in the continued monotonic shearing after the vibration was terminated. In other words, the critical state under monotonic loading was not affected by a short period of vibration imposed to the specimen at near-critical state, as clearly indicated in Figure 8(a).

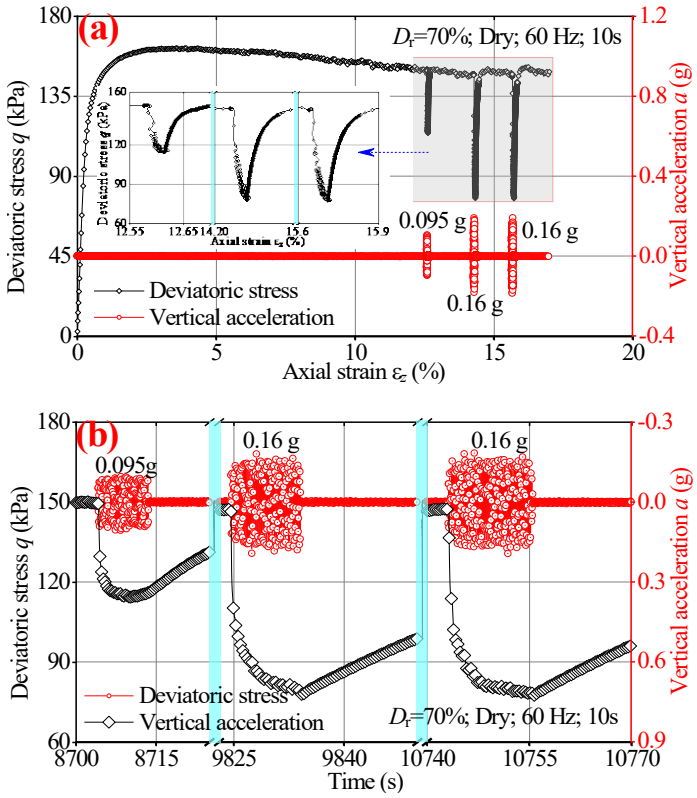

Figure 8: Responses of specimen subjected to vibrations of different accelerations at near-critical state. (a) deviatoric stress vs axial strain; and (b) time history of deviatoric stress

Figure 9 summarizes the vibration-induced shear resistance reduction measured in different tests with varying density of specimens, vibration frequency and intensity, as well as stress level q_0 at which vibration was superimposed. As shown in Figure 9(a), for specimens of a given relative density with vibrations applied at different pre-peak stress states, the relative shear resistance reduction $\Delta q/q_0$ increased linearly with the vibration acceleration a. The $\Delta q/q_0 \sim a/g$ relationship was independent of the stress level q_0 and vibration duration. Moreover, the results obtained from tests on dry specimens

and saturated one under drained conditions were practically identical in the range of acceleration used. However, the density of soil specimen had significant influence on the shear strength reduction induced by vibration at pre-peak states. Specifically, for a given acceleration, the shear resistance reduction of dense soils was smaller than that of loose specimens; as shown in Figure 9(a). For the near-critical state tests with vibration frequency f=60 Hz and $100\,\mathrm{Hz}$, a linear relationship between $\Delta q/q_0$ and a/g was obtained; as shown in Figure 9(b). The $\Delta q/q_0 \sim a/g$ relationship was not affected by the frequency of vibration and was independent of the initial density of the soil specimen, since the critical state of sand was independent of its initial density. The near critical state test results also revealed that the high frequency vibration did not induce significant excess pore pressure in the specimens, which is consistent with that observed in pre-peak vibration tests.

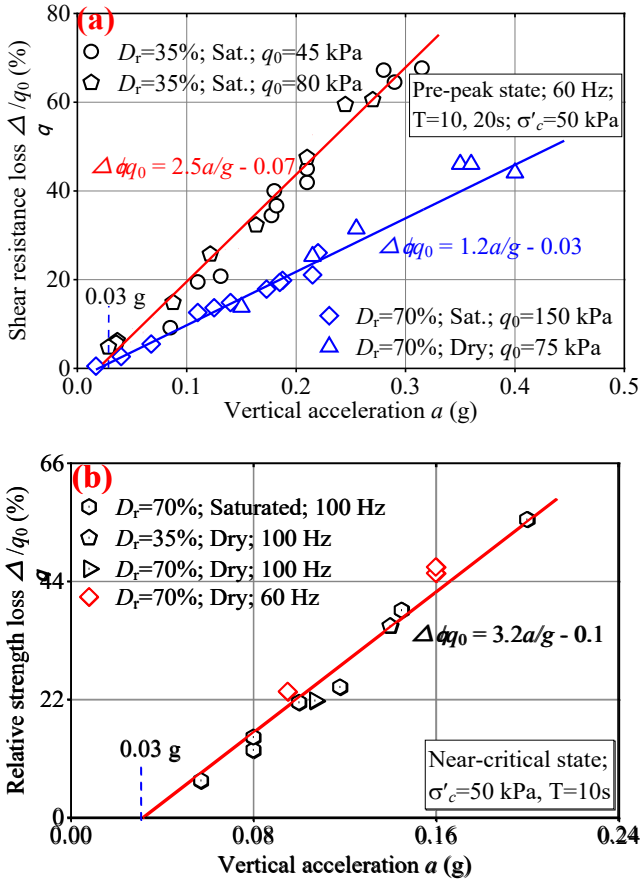

Figure 9: Influence of vibration intensity on shear resistance reduction of granular soils. (a) at pre-peak state; and (b) at near-critical state

(2) *Separation of vibration-induced responses from measured data*

In a test following the strain-controlled monotonic loading scheme, since the vibration was superimposed on the monotonic loading, the measured soil deformation and the corresponding deviatoric stress responses had components induced by both monotonic and dynamic loadings. For instance, the measured total axial strain (ε_z) consisted of a monotonic axial strain (ε_{zm}) increasing at a constant rate $\dot{\varepsilon}_0$, an instantaneous cyclic axial strain (ε_{zi}) as a response to cyclic loading, and an increment of axial strain ($\Delta\varepsilon_z$) induced by vibrations; i.e.,

$$\varepsilon_z(t) = \varepsilon_{zm}(t) + \varepsilon_{zi}(t) + \Delta\varepsilon_z(t), \quad \varepsilon_{zm}(t) = \dot{\varepsilon}_0 t \tag{2}$$

The instantaneous cyclic axial strain ε_{zi} can be used to verify the measured vertical acceleration a via

$$a = (2\pi f)^2 H \varepsilon_{zi} \tag{3}$$

where H is the height of the specimen and f the frequency of vibration. Figure 10 gives a typical example of separating the three strain components in the recorded axial strain. In this example, the density of specimen was D_r=70% with an effective confining pressure σ'_c=50kPa and acceleration amplitude a=0.3g with f = 60Hz. In Figure 10, 'A' and 'B' stand for the starting and ending points of vibration, respectively. The separated strain components presented in Figure 10(b) clearly show the changes in axial strain during and after the application of vibration.

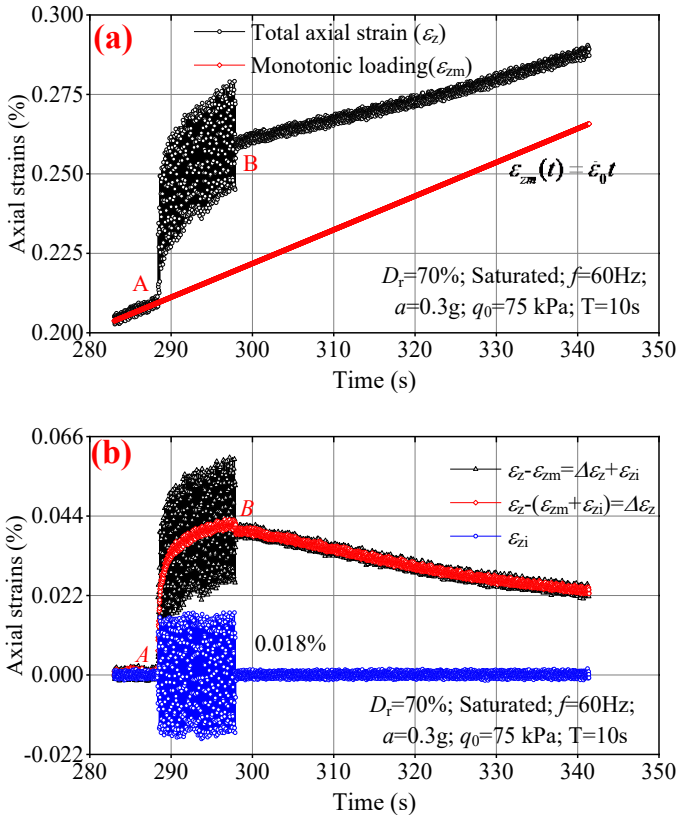

Figure 10: Separations of the measured axial strain. (a) ε_z and ε_{zm}; (b) $\Delta\varepsilon_z$ and ε_{zi}

Likewise, the recorded deviatoric stress q during the cyclic loading phase can be decomposed into three components:

$$q = q_m + \Delta q + \sigma_d, \qquad q_m = q_0 + \Delta q_m \tag{4}$$

in which σ_d is the instantaneous cyclic stress, Δq the vibration-induced decrease of deviator stress, and q_m the deviator stress corresponding to monotonic loading without vibration. To obtain Δq, as the first approximation, we assume that Δq_m increased

linearly with time during vibration. In other words, Δq_m varied linearly with $\Delta\varepsilon_{zm}(t)$. This assumption is reasonable since the duration of the vibration was less than 30 seconds (mostly 10 seconds) in this research. The procedure to separate the measured deviatoric stress is illustrated in Figure 11.

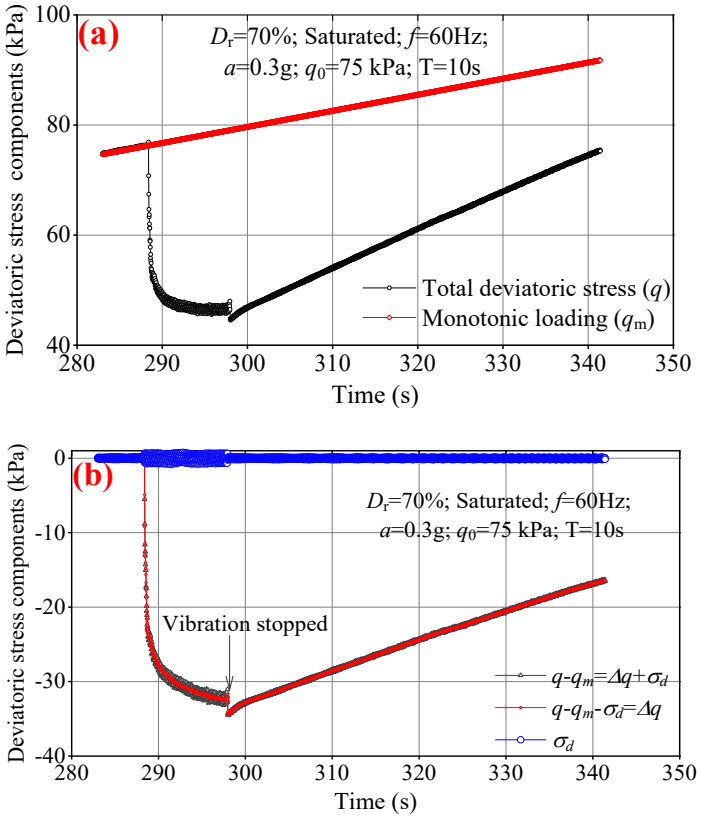

Figure 11: Separations of measured deviatoric stress. (a) q and q_m; (b) Δq and σ_d

After the determination of different components of the deviatoric stress and the axial strain (as shown in Figure 10 and Figure 11, respectively), the relation between the vibration-induced deviatoric stress variation Δq and the corresponding additional axial strain $\Delta\varepsilon_z$ can be established. As shown in Figure 12, during the vibration process, the value of $\Delta q/q_0$ increased nonlinearly with $\Delta\varepsilon_z$. In particular, the slope of the $\Delta q/q_0 \sim \Delta\varepsilon_z$ curve decreased with increasing axial strain. In the process of stress recovery during the continuous monotonic loading after vibration, an approximately linear relationship between $\Delta q/q_0$ and $\Delta\varepsilon_z$ was identified. The $\Delta q/q_0 \sim \Delta\varepsilon_z$ relationships during the vibration

process and the post-vibration recovery process were similar, at least qualitatively, to the stress-strain curves of soil during the monotonic loading and unloading processes in a conventional triaxial compression test, respectively.

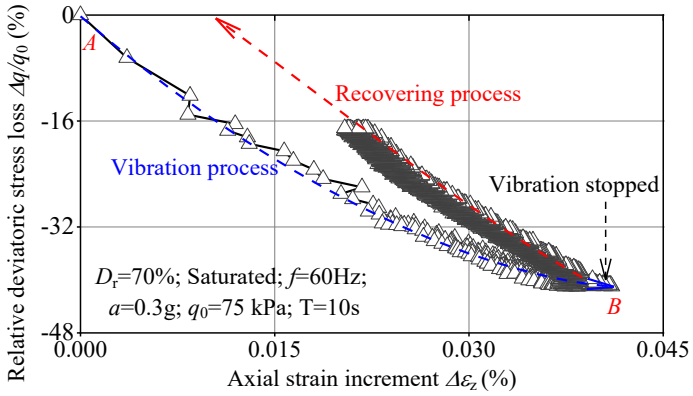

Figure 12: $\Delta q/q_0$~$\Delta\varepsilon_z$ curve during and after vibrations

The acceleration calculated from the instantaneous cyclic axial strain ε_{zi} by Eq. (3) can be used to verify the recorded acceleration from accelerometer, as illustrated in Figure 13. Obviously, the calculated accelerations are generally in accordance with the measured ones, which implies the data obtained from the measurement/data acquisition module is reliable.

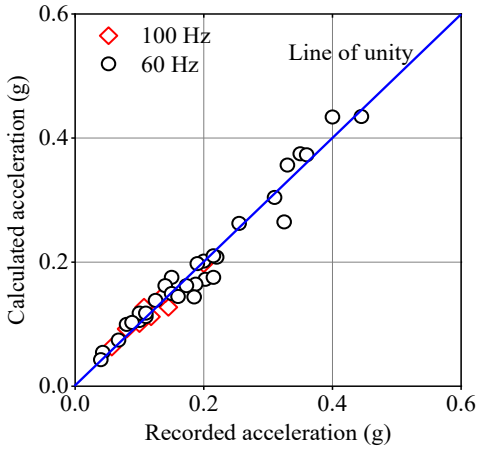

Figure 13: Comparison of calculated accelerations by ε_{zi} with the measured data by accelerometer

3.3 Stress-controlled monotonic loading mode

Figure 14 presents the time histories of axial strain, volumetric strain and excess pore

pressure of a dense sand specimen when a vibration of f = 60 Hz was superimposed to the specimen subjected to stress-controlled monotonic loading. During the test, a specimen with a relative density of D_r=70% was fully saturated in order to measure its volume change induced by vibration. Then, it was consolidated at an effective confining pressure of σ'_c=50kPa. After that, an axial load was applied gradually until reaching a deviatoric stress level q_0=20kPa. Finally, a vibration with f=60Hz and a=0.33g was superimposed for 1920 seconds. During the vibration period, the static deviatoric stress was kept constant at q_0=20kPa. Moreover, as shown in Figure 1(a), the excess pore pressure was recorded at the bottom of the specimen by a pore pressure transducer (PPT). At the same time, the drainage valve at the top of the specimen was open to allow the water drained out from the specimen into the volume change transducer (VCT).

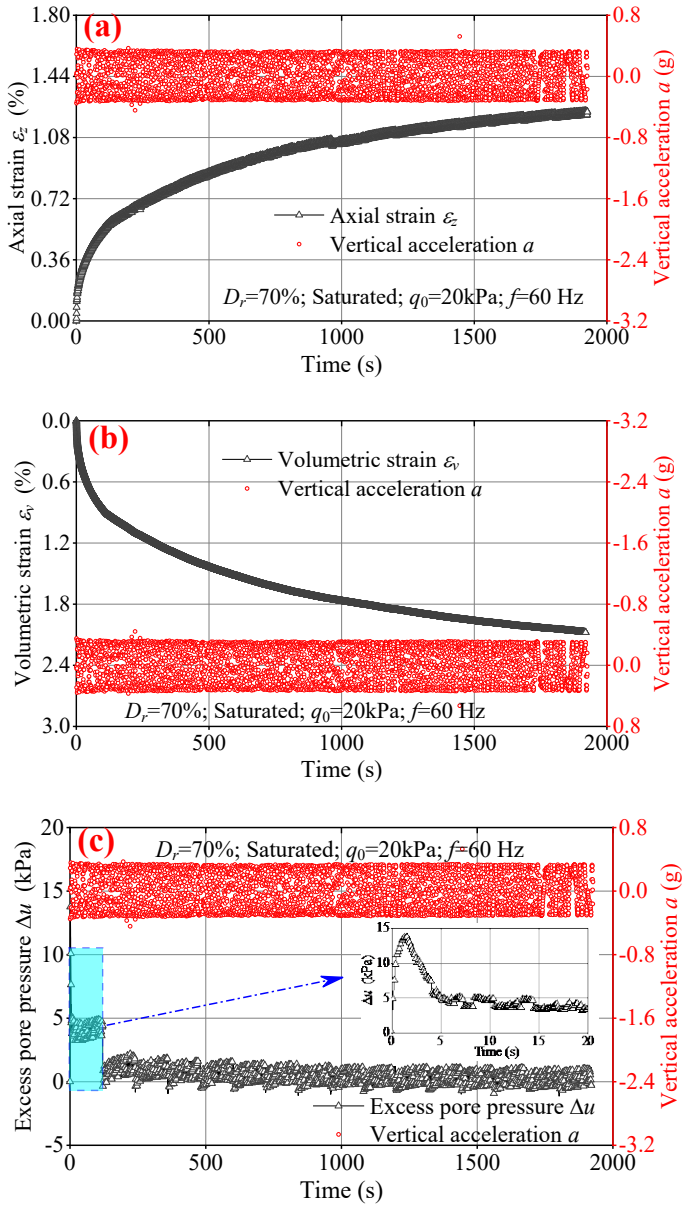

Figure 14: Responses of granular soil under high-frequency vibration at f=60Hz in stress-controlled monotonic loading mode: (a) axial strain; (b) volumetric strain; (c) excess pore pressure

Referring to results presented in Figure 14(a) and Figure 14(b), the superimposed vibration to a constant deviatoric stress induced continuous compressive axial and volumetric strains. At the beginning of vibration, the growth in the axial and volumetric strains was significant. With the continuation of vibration, the rates of axial and volumetric strains tended to decrease. Besides, even though drainage was allowed at the top of the specimen, excess pore pressure Δu was observed in a short period of time immediately after the application of vibration; as shown by the insert in Figure 14(c).

This may cause an underestimate of the volumetric strain in Figure 14(b) at the initial stage of vibration. The excess pore pressure was at a low level of 1 kPa in the majority time of vibration, which resulted in only 2% decline in the effective confining pressure, which is consistent with the results in Figure 7(c) for a test with strain-controlled monotonic loading mode. As discussed previously, when drainage was allowed at both ends of the specimen, the excess pore pressure at the mid-height of the specimen was at the level of 0.25 kPa, which had negligible influence on the measurement of volume change.

Summary and conclusions

A modified triaxial apparatus was developed to investigate the behavior of soil under high-frequency low-amplitude vibration such as that induced by high-speed trains. A dynamic module was added to a conventional triaxial testing system. The dynamic system consists of two components: (a) a low-inertia linear voice coil actuator (VCA) that is mounted coaxially with the vertical loading rod to generate vertical vibrations; and (b) a signal generator and an amplifier to provide signals of controlled frequency and amplitude to the VCA. The measurement/data acquisition module was also modified to accommodate the maximum frequency of vibration and the measurement of acceleration, dynamic displacement, and loading. The loading module was adapted so that static loading is applied under either strain or stress control. In addition, to capture the influence of high-frequency low-amplitude dynamic axial loading on soil behavior, a frictionless triaxial cell was fabricated to minimize any potential friction on the loading rod using ball bearings. A series of tests were performed to examine the effectiveness and the performance of the modified triaxial testing system under different loading conditions by focusing on the accumulative deformation and strength reduction of sand induced by high-frequency low-amplitude vibration.

Acknowledgments

Funding provided by the Natural Science and Engineering Research Council of Canada is gratefully acknowledged.

References

Alexeev, A., Royzen, V., Dudko, A., Goldshtein, A., and Shapiro, M., 2000, "Mixing and segregation in vertically vibrated granular layers," Solid Mechanics and Its Applications., Vol. 81, pp. 129–139, https://doi.org/10.1061/(ASCE)GM.1943-5622.0000568

Al-Douri, Y. and Poulos, H. G., 1991, "Static and cyclic direct shear tests on carbonate sands," Geotechnical Testing Journal., Vol. 15, No. 2, pp. 138-157, DOI:10.1520/GTJ10236J

Ayer, J. E., and Soppet, F. E., 1965, "Vibratory compaction: I, compaction of spherical shapes," J. Am. Ceram. Soc., Vol. 48, No. 4, pp. 180–183, https://doi.org/10.1111/j.1151-2916.1965.tb14708.x

Ayer, J. E., and Soppet, F. E., 1966, "Vibratory compaction: II, compaction of angular shapes." J. Am. Ceram. Soc., Vol. 49, No. 4, pp. 207–210, https://doi.org/10.1111/j.1151-2916.1966.tb13235.x

Barkan, D. D., 1962, Dynamics of bases and foundations, Trans. L. Drashevska, McGraw-Hill, New York, pp. 207–210

Bian, X., Jiang, H., & Chen, Y., 2010, "Accumulative deformation in railway track induced by high-speed traffic loading of the trains," Earthquake Engineering and Engineering Vibration, Vol. 9, No. 3, pp. 319-326, DOI: 10.1007/s11803-010-0016-2

Cai, Y., Wu, T., Guo, L., & Wang, J, 2018, "Stiffness degradation and plastic strain accumulation of clay under cyclic load with principal stress rotation and deviatoric stress variation," Journal of Geotechnical and Geoenvironmental Engineering, Vol. 144, No. 5, pp. 04018021, https://doi.org/10.1061/(ASCE)GT.1943-5606.0001854

Chaney, R. and Mulilis, J.P, 1978, "Suggested method for soil specimen remodeling by wet-raining," Geotechnical Testing Journal, ASTM, Vol. 1, No. 2, pp. 107-108, https://doi.org/10.1520/GTJ10378J

Denies, N. and Holeyman, A, 2017, "Shear strength degradation of vibrated dry sand," Soil Dynamics and Earthquake Engineering, Vol. 95, pp. 106–117, https://doi.org/10.1016/j.soildyn.2017.01.039

Dyvik, R. and Madshus, C., 1985, Lab Measurements of Gmax using Bender Elements, Advances in the Art of Testing Soils Under Cyclic Conditions, V. Khosla, Ed., ASCE, New York, pp. 186–196.

Finn, W. D. L., & Vaid, Y. P, 1977, Liquefaction potential from drained constant volume cyclic simple shear tests. In Proceedings of the 6th World Conference on Earthquake Engineering, New Delhi, India (pp. 10-14).

Hall, J.R. and Richart, F.E, 1963, "Dissipation of elastic wave energy in granular soils,"

Journal of Soil Mechanics and Foundations Division, ASCE, Vol. 89, No. SM6, pp. 27-56.

Hardin, B.O, 1965, "The nature of damping in sands," Journal of Soil Mechanics and Foundations Division, ASCE, Vol. 91, No. SM1, pp. 63-97, https://doi.org/10.1061/JSFEAQ.0002127

Hsiau, S. S. and Pan, S. J, 1998, "Motion state transition in a vibrated granular bed," Powder Technology, Vol. 96, pp. 219-226, https://doi.org/10.1016/S0032-5910(97)03377-9

Huan, C., 2008, "NMR experiments on vibrofluidized and gas fluidized granular systems," M.D. dissertation, Univ. of Massachusetts Amherst, Amherst, MA.

Ishihara, K., & Yasuda, S, 1975, "Sand liquefaction in hollow cylinder torsion under irregular excitation," Soils and Foundations, Vol. 15, No. 1, pp. 45-59, https://doi.org/10.3208/sandf1972.15.45

Ishihara, K., & Yamazaki, F, 1980, "Cyclic simple shear tests on saturated sand in multi-directional loading," Soils and Foundations, Vol. 20, No. 1, pp. 45-59, https://doi.org/10.3208/sandf1972.20.45

Ishihara, K.,1993, "Liquefaction and flow failure during earthquakes," Geotechnique, Vol. 43, No. 3, pp. 351-451, https://doi.org/10.1680/geot.1993.43.3.351

Ishihara, K.,1996, Soil Behaviour in Earthquake Geotechnics. Oxford University Press, New York, N.Y.

Khan, Z., El Naggar, M. H., & Cascante, G, 2011, "Frequency dependent dynamic properties from resonant column and cyclic triaxial tests," Journal of the Franklin Institute, Vol. 348, No. 7, pp. 1363-1376, https://doi.org/10.1016/j.jfranklin.2010.04.003

Krey, H., 1932, Erddruck, Erdwiderstand und Tragfähigkeit des Baugrundes Berlin, Deutschland, Wilhelm Ernst & Sohn.

Laroche, C., Douady, S., and Fauve, S, 1989, "Convective flow of granular masses under vertical vibration," J. Phys., Vol. 50, No. C7, pp. 699–706, https://doi.org/10.1051/jphys:01989005007069900

Liu, X. Z., & Chen, G. X., 2008, "Advances in Researches on Mechanical Behavior of Subgrade Soils under Repeated-load of High-speed Track Vehicles," Journal of Disaster Prevention and Mitigation Engineering, Vol. 2, doi:CNKI:SUN:DZXK.0.2008-02-024

Madshus, C. 5., & Kaynia, A. M, 2000, "High-speed railway lines on soft ground: dynamic behaviour at critical train speed," Journal of Sound and Vibration, Vol. 231, No. 3, pp. 689-701, https://doi.org/10.1006/jsvi.1999.2647

Milne, D. R. M., Le Pen, L. M., Thompson, D. J., & Powrie, W, 2017, "Properties of train load frequencies and their applications," Journal of Sound and Vibration, Vol. 397, pp. 123-140, https://doi.org/10.1016/j.jsv.2017.03.006

Mujica, N., and Melo, F., 1998, "Solid-liquid transition and hydrodynamic surface waves in vibrated granular layers," Phys. Rev. Lett., Vol. 80, No. 23, pp. 5121–

5124, https://doi.org/10.1103/PhysRevLett.80.5121

Pak, H. K., and Behringer, R. P., 1993, "Surface waves in vertically vibrated granular materials," Phys. Rev. Lett, Vol. 71, No. 12, pp. 1832–1835, https://doi.org/10.1103/PhysRevLett.71.1832

Pra-ai, S. and Boulon, M., 2017, "Soil–structure cyclic direct shear tests: a new interpretation of the direct shear experiment and its application to a series of cyclic tests," Acta Geotech., Vol. 12, pp. 107–127, https://doi.org/10.1007/s11440-016-0456-6

Sheng, X., Jones, C. J. C., & Petyt, M., 1999, "Ground vibration generated by a load moving along a railway track," Journal of Sound and Vibration, Vol. 228, No. 1, pp. 129-156, https://doi.org/10.1006/jsvi.1999.2406

Shih, J. Y., Thompson, D. J., & Ntotsios, E., 2018, "Analysis of resonance effect for a railway track on a layered ground," Transportation Geotechnics, Vol. 16, pp. 51-62, https://doi.org/10.1016/j.trgeo.2018.07.001

Su, X., 2007, Influence of Sample Preparation Methods and Interlocking on Sand Behaviour: An Experimental Investigation, M.D. dissertation, McMaster University, https://canadaresearch.mcmaster.ca/handle/11375/21796

Taslagyan, K. A., Chan, D. H., & Morgenstern, N. R., 2015a, "Effect of vibration on the critical state of dry granular soils," Granular Matter, Vol. 17, No. 6, pp. 687-702, DOI 10.1007/s10035-015-0589-6

Taslagyan, K. A., Chan, D. H., & Morgenstern, N. R., 2015b, "A direct shear apparatus with vibrational loading," Geotechnical Testing Journal, Vol. 38, No. 1, pp. 1-8, https://doi.org/10.1520/GTJ20140078

Taslagyan, K. A., Chan, D. H., & Morgenstern, N. R., 2016, "Vibrational fluidization of granular media," International Journal of Geomechanics, Vol. 16, No. 3, pp. 04015080, https://doi.org/10.1061/(ASCE)GM.1943-5622.0000568

Toki, S., Shibuya, S. and Yamashita, S., 1995, Standardization of laboratory test methods to determine the cyclic deformation properties of geomaterials in Japan, Keynote Papert, Pre-failure Deformation of Geomaterials, Shibuya, S., Mitacchi, T. and Miura, S. (eds.), Balkema, Vol. 2, pp. 741-784, http://worldcat.org/isbn/905410399X

Vaid, Y.P. and Negussey, D., 1984, "Relative density for air and water pluviated sand," Soils and Foundation, Vol. 24, No. 2, pp. 101-105, https://doi.org/10.3208/sandf1972.24.2_101

Vieira, C. S., Lopes, M. D. L., & Caldeira, L. M, 2013, "Sand-geotextile interface characterisation through monotonic and cyclic direct shear tests," Geosynthetics International, Vol. 20, No. 1, pp. 26-38, https://doi.org/10.1680/gein.12.00037

Wang, R., Fu, P., Zhang, J. M., & Dafalias, Y. F., 2019, "Fabric characteristics and processes influencing the liquefaction and re-liquefaction of sand," Soil Dynamics and Earthquake Engineering, Vol. 125, pp. 105720, https://doi.org/10.1016/j.soildyn.2019.105720

Wassgren, C. R., Brennen, C. E. and Hunt, M. L., 1996, "Vertical vibration of a deep bed of granular material in a container," Journal of Applied Mechanics, Vol. 63, pp. 712-719, https://doi.org/10.1115/1.2823354

Youd, T. L., 1967, The engineering properties of cohesionless materials during vibration, M.D. dissertataion, Iowa State University, https://doi.org/10.31274/rtd-180813-1106

Zhai, W., Kai Wei, K., Song, X. and Shao, M., 2015, "Experimental investigation into ground vibrations induced by very high-speed trains on a non-ballasted track," Soil Dynamics and Earthquake Engineering, Vol. 72, pp. 24–36, https://doi.org/10.1016/j.soildyn.2015.02.002

Chapter 3 Experimental results

(Paper 2)

Experimental investigation of vibration-induced shear resistance reduction in sheared granular soils

Canadian Geotechnical Journal, 60(1), 44-59

Tao Xie[1], Peijun Guo[1], Dieter Stolle[1]

[1]Department of Civil Engineering, McMaster University, 1280 Main St W, Hamilton, ON, L8S 4L7, Canada

Abstract: To investigate the characteristics of vibration-induced shear resistance reduction (ViSRR) in granular soils, laboratory tests were performed using a modified triaxial apparatus. Monotonic loading and vibration with controlled frequency and acceleration amplitude were superimposed to shear soil specimens under drained conditions. Tests were conducted for dry and saturated specimens at relative densities of D_r=35% and 70%. The tests revealed that superimposed vibration causes a reduction of shear resistance in addition to additional volume change of the specimen. After termination of vibration, the shear resistance was found to be recovered as the monotonic shearing continued. It was confirmed that the shear resistance reduction was not caused by vibration-induced variation of excess pore pressure in the specimen. For high-frequency vibration with frequency varying between 60 and 120 Hz, the relative shear resistance loss tended to increase linearly with the peak acceleration. Based on the test results, the concept of "vibro-critical state" is proposed to describe the ViSRR of granular soil subjected to monotonic shear and vibration simultaneously.

Keywords: shear resistance reduction; granular soil; vibration; vibro-critical state; experimental investigation

1. Introduction

Owing to its discrete feature, a granular material may behave as solid, liquid, or even gas depending on its density and loading conditions (Jaeger et al., 1996). Soils may be subject to different types of vibrations, including those induced by earthquakes, blasting, traffic loading, and machine vibration. Depending on the intensity and frequency of vibration as well as the boundary conditions, various vibration-induced phenomena have been observed; for example, densification (Barkan, 1962; Ayer and Soppet, 1965, 1966; Youd, 1967), convection flow (Laroche et al., 1989; Hsiau and Chen, 2000; Denies and Holeyman, 2017), size segregation (Alexeev et al., 2000), surface waves (Pak and Behringer, 1993; Mujica and Melo, 1998), and pattern formation in granular material (Ord and Hobbs, 2010). If sufficient vibration energy is transferred to a granular system, a transition from solid to liquid states (i.e., fluidization) can take place that results in a liquid-like behavior of granular soil (Jaeger et al., 1996).

Vibration induced compaction of loose cohesionless soils has been recognized for a long time (e.g., Barkan, 1962; Ayer and Soppet, 1965, 1966; Youd, 1967). Vibratory compaction has been widely applied in engineering practice as an effective mean for soil improvement to increase the density and shear strength of the soil. Under constraint conditions (e.g., deep vibratory compaction), vibration tends to increase the horizontal effective stresses in soil (Massarsch et al., 2020). As outlined in Canadian foundation engineering manual (Canadian Geotechnical Society, 2006), for cohesionless soil placed against rigid retaining walls or rigid foundation walls, vibratory compaction increases the lateral earth pressure, resulting in higher values of the coefficient of earth pressure at rest. Experimental evidences can be found in Chen and Fang (2008).

The effect of vibration on shear strength and shear-induced volume change characteristics of granular soils is another important aspect. In geotechnical engineering practice, the installation of piles by vibratory means in cohesionless soils is significantly affected by the properties of the soils under vibration. The penetration takes advantage of vibration-induced decrease of shear resistance at the interface between the pile and

surrounding soil (Bingham, et al., 2000; Viking, 2002; Felming, et al. 2008). Although the frequency of pile vibratory hammers is primarily lower than 50 Hz, it has been found that vibration at higher frequency can drive the pile more efficiently and reduce ground vibration at the same time. In particular, the resonant driver operates at frequencies in the ranges of 90 to 150 Hz (Felming, et al. 2008). The central principle of the resonant driver is to induce resonant response of the pile-soil system, which facilitates pile driving. However, the differences between vibratory pile driving via high frequency-low intensity vibration and low frequency–high intensity vibration are still not understood well (Rausche, 2002).

With the presence of underground water, the local liquefaction of sand around the pile is usually regarded as one of the mechanisms for vibration-induced penetration resistance reduction (Vanden Berghe et al., 2001; Hwang et al., 2001; Osinov, 2013). However, there is experimental evidence that the reduction in pile's shaft and toe resistance also occurs in air-dry sands (O'Neill and Vipulanandan, 1989; Viking and Bodare, 2001), suggesting that excess pore pressure generation may not be the primary influencing factor. An alternative explanation for the reduced penetration resistance of vibration plies is the introduction of a "soil arch" (Heerema, 1978; White and Lehane, 2004; Moriyasu, et al., 2018). Heerema (1978) argued that the irregular movements of the pile form a temporary horizontal soil arch around the pile, which decreases the normal pressure acting on the pile, thus causing a loss in shaft resistance. However, this argument cannot explain the loss of toe resistance and there is still a lack of evidence for the formation of vibration-induced soil arches. In the natural world, a few animals (Hosoi and Goldman, 2015) master the skill in using the decreased strength of vibrated granular soils to their advantage. Ocellated skinks, for example, know how to exploit head oscillation to reduce forward resistance during burial locomotion (Sharpe et al., 2015).

Vibration-induced soil resistance reduction has also been investigated using the "sphere/intruder penetration test" (Barkan, 1962; Denies et al., 2010; Darbois Texier et

al., 2017; Omidvar et al., 2019). When pushing a sphere or intruder into a granular media, vibration (even at a very low displacement amplitude) can significantly reduce the penetration resistance. For example, Darbois Texier et al. (2017) observed that the penetration resistance when pushing a vibrating cylindric intruder into a dry granular material is reduced by 90% at a very small amplitude (10 μm) high frequency (50~100Hz) vibration. However, the complex stress state in the granular material around the intruder makes it difficult to judge which factor dominates in the process of strength loss, and it is difficult to use the measured data to construct a theoretical model directly.

Krey (1932) is one of the first researchers to investigate the influence of vibration on soil strength as a material property. He observed a decline in the repose angle, thus internal friction of dry sand during vibration. Using a direct shear device mounted on a shake table vibrating in the horizontal direction, Barkan (1962) studied the effect of frequency (up to 50 Hz) and amplitude of vibration on the friction angle of sand. During the test, the vertical load applied on the specimen was kept constant. The test results showed that the shake table's horizontal acceleration amplitude dominated the decrease of the specimen's friction angle. The experimental results obtained by Mogami and Kubo (1953) revealed that, as the horizontal acceleration of the shaking table increased, the shear strength of soil decreased and finally approached zero. They also found that the acceleration rather than the frequency and the amplitude of vibration dominated the ViSRR. The experimental results reported by Youd (1967) confirm these observations. Meneses et al. (1998, 2000) investigated the undrained behaviour of saturated sand when a complementary cyclic shear stress was superimposed on strain-controlled monotonic loading. The complementary cyclic shear stress had a sine wave with constant amplitude and frequencies in the range of 0.01 to 1 Hz. It was observed that the superimposed cyclic shear stress caused reduction of shear resistance attained under monotonic loading application alone. Moreover, the shear strength reduction was affected by the cyclic shear stress amplitudes, density of the specimen and the number

of stress cycles resulting in 1% additional shear strain. Recently, Taslagyan et al. (2015, 2016) investigated the shear strength loss induced by vibration using a modified direct shear apparatus. In their tests, horizontal vibration was applied by an actuator connected to the rod that applied the shear force. In this way, the vibration could be superimposed to the static shear force and directly applied to the specimen, and the vibration of the whole testing device was avoided. The results revealed that the friction angle of sand decreased with an increase of acceleration. Furthermore, the shear resistance of sand tended to vanish and the transition from a solid-like state to a fluid-like state could occur during intense vibration (Taslagyan et al., 2015, 2016).

With the development of high-speed railways, there are increased interests and needs to explore the effect of low-displacement amplitude, high-frequency vibration induced by high-speed trains on the behavior of granular soils (Bian et al., 2015; Jiang et al., 2016; Milne et al., 2017). Passing wheels of high-speed trains tend to produce high-frequency vibration (including vibration of the track), which further causes low-displacement amplitude, high-frequency vibration of the foundation soil. For example, Zhai et al. (2015) observed that the important frequencies of ground vibration due to high-speed train at speed over 300km/h tended to be concentrated in the range of 20-60 Hz and the measured accelerations of ground vibration were as high as 0.3*g*. Even higher frequency vibrations but at smaller amplitudes could occur due to the unevenness of track and the out-of-roundness of wheels. With an increase of the velocity of future high-speed trains (e.g., the design speed of Moscow-Kazan-Ekaterinburg high-speed train is 400 km/h; see Shteyn et al., 2017), the frequency of induced ground vibration could be even higher.

The objective of this paper is to investigate the shear strength reduction of granular soil and the additional deformation induced by vibration using a modified triaxial apparatus that can apply vibration at frequencies up to 150 Hz. The focus is placed on vibrations with low-displacement amplitude and high-frequency (60~120 Hz), since this is the range of vibration frequency encountered in geotechnical engineering but the

behaviour soil in this frequency range has not been investigated systematically. This paper is organized as follows: We first present a brief description of the modified triaxial apparatus that can apply both monotonic loading and high-frequency cyclic loading to the specimen. Following the summary of the test procedure and the properties of testing materials, the results of tests completed under various combinations of static loading and vibration are presented. Thereafter, the test results are analyzed, and the concept of "vibro-critical state" is proposed. For conciseness, in the rest of this paper, low-amplitude, high-frequency vibration will be used to replace low displacement amplitude, high-frequency vibration.

2. A modified triaxial apparatus and experimental procedure

2.1 A modified triaxial apparatus

To investigate the influence of vibration on the behavior of soil originally subjected to monotonic loading, a conventional triaxial apparatus was modified so that a vibration could be superimposed to a monotonic loading process. Figure 1 shows the modified triaxial apparatus that consists of three modules: static loading module, dynamic loading and control module, measurement and data acquisition module. The loading system for the conventional triaxial apparatus was used as the static loading module. A frictionless triaxial cell was used to reduce the influence of friction between the loading rod and the top-plate of the triaxial cell. Referring to Figure 1, a vertical vibration is added to the static loading by a low-inertia linear voice coil actuator (VCA) that is mounted coaxially with the loading rod.

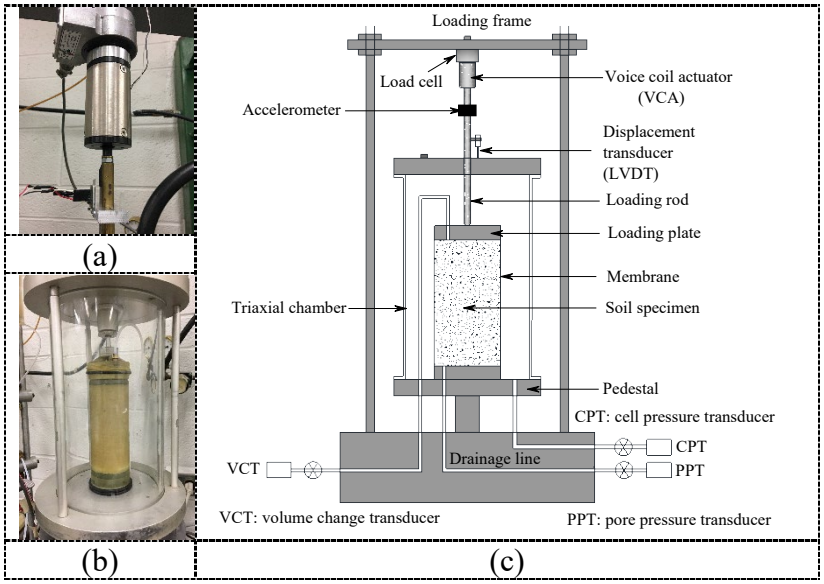

Figure 1. Modified triaxial apparatus: (a) VCA; (b) specimen in triaxial chamber; (c) schematic of the triaxial apparatus

To minimize the inertial effect of the actuator, a moving magnet VCA was selected. The moving mass is only 268 grams, which means the inertial force is less than 1 N that corresponds to 0.5 kPa axial stress in the specimen when the acceleration amplitude A<0.3 *g*. The magnetic field produced by the coil generated a force on the moving mass in its moving direction. Such a force was directly proportional to the magnitude of the input current and the flux density of the magnetic field. The VCA had low inertia with zero friction between the moving mass and the coil. The frequency and the magnitude of current were both controlled by a signal generator and an amplifier. It should be noted that the load rod is made of light-weighted material to minimize the inertia effect, particularly for high-frequency vibrations.

Various transducers were used to measure the forces applied to the specimen, the acceleration generated by the VCA and the resulting deformation of the specimen. Specifically, a load cell was used to measure the axial load (including both the static and vibrational components). A linear variable differential transducer (LVDT) with dynamic response up to 300 Hz measured the specimen's axial deformation. Figure 1 shows an accelerometer mounted on the loading rod to measure the acceleration of vibration generated by the VCA. The sampling frequency was set to higher than 5 times

the vibration frequency to capture the detailed dynamic response of the specimen. The errors in the measurements of the strain, pore pressure, and acceleration were 0.001%, 0.3kPa, and 0.01*g*, respectively. More details about this testing system can be found in Xie and Guo (2021).

2.2 Test material and method

Figure 2 illustrates the loading scheme adopted in this study. Similar to conventional triaxial compression test produces, a specimen under drained conditions was first sheared under monotonic loading with a fixed axial strain rate of $\dot{\varepsilon}_1$=0.1% per minute and constant effective confining pressure. At a selected deviatoric stress q_0, the vibration with constant acceleration amplitude (0.02~0.26 g) and frequency (60~120 Hz) was superimposed to the monotonic loading for a period T (typically 10~35 seconds) without interruption in monotonic shearing. The duration of vibration T is determined by how fast the deviatoric stress q stabilizes, and T should be long enough to allow q reach its stable value during vibration. In some tests, several individual vibrations with various vibration intensities and frequencies were applied to the same specimen at different deformation states, both at pre-peak and near-critical states. The interval between two adjacent vibrations was long enough so that the "memory" of the specimen associated with previous experimental vibration could be considered erased. In particular, the shear resistance reduction the specimen experienced during the previous vibration is recovered in the continuous monotonic shearing before the subsequent vibration, as if the proceeding vibration were not applied.

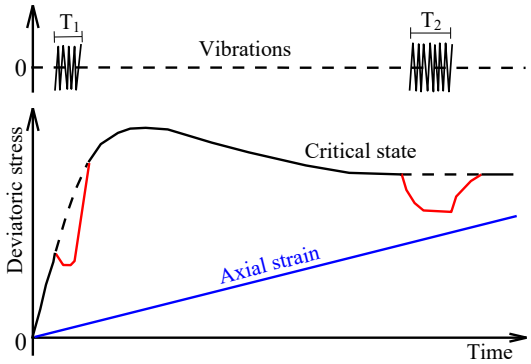

Figure 2. Loading scheme adopted in tests

It is generally understood that the behavior of cohesionless soil is affected by its density, stress level and stress state. When subjected to cyclic loading, soil dynamics research related to geotechnical earthquake engineering reveals the importance of the amplitude of cyclic stress and the number of stress cycles (or equivalently the duration of vibration for a fixed frequency). Consequently, it is expected that these factors will also have certain influence on the responses of granular soil under combined monotonic loading and high-frequency, low-amplitude vibration.

Standard Ottawa sand C-109 was used in this study. It is a uniform quartz sand of sub-rounded particles with the mean grain size d_{50}=0.375 mm, uniformity coefficient C_u=1.80, and coefficient of curvature C_c=1.20. The maximum and minimum void ratios are 0.811 and 0.503 according to ASTM test methods D4254-16 and D4253-16e1, respectively. To explore the mechanism of vibration-induced shear resistance reduction (ViSRR), both air-dry and fully saturated specimens were used in the experimental study, as summarized in Table 1. To examine any potential effect of density, specimens of two typical relative densities, D_r=70% and 35% corresponding to the void ratio of e=0.59 and 0.69 respectively, were tested under various loading conditions. For convenience of description, the specimens are referred to as “loose” and “dense” in the rest of the paper, without referring to whether they are contractive or dilative when sheared. Drained tests were mostly conducted at relatively low effective confining pressures of σ_c=50 kPa due to the capacity of the VCA, with few tests being carried out at σ_c = 75 and 100 kPa to examine the influence of σ_c on ViSRR when the vibration

was applied at pre-peak state. For saturated specimens, the volume change (including that induced by vibration) was obtained by measuring the volume of water flowing out of the specimen.

Table 1: Test matrix

Factors	Range
Moisture	Air-dried, fully saturated
Relative density (D_r)	35%, 75%
Effective confining pressure (σ_c)	50 kPa (mostly), 75 kPa, 100 kPa
Vibration frequency (f)	60~120 Hz
Duration of vibration (T)	10~35 s
Amplitude of acceleration (A)	(0.02~0.26) g

Cylindrical specimens of 50 mm diameter and 100 mm height were fabricated by water pluviation method for saturated specimens and dry tamping method for dry specimens. Specifically, to obtain a fully saturated specimen, a membrane was firstly mounted to the base pedestal and secured by two O-rings. Then, a split mold was put in position and filled with de-aired water. After that, boiled sand sample was poured into the mold carefully by a spoon and deposited by pluviation. In this process, the exposure of sand to air must be avoided. Finally, a porous stone and top platen was mounted when the split mold was filled to an expected height. To control the density of the specimen, a rubber hammer was used to tap the split model gently in the horizontal direction. When preparing a dry specimen, dry sand was placed in the mold by five layers and each layer was tamped to a desirable height. Details about these methods can be found in Ishihara (1996), Su (2007) and Xie and Guo (2021).

3. Typical experimental results

This section separately investigates the influence of superimposed high-frequency low-amplitude vibration on the performance of sand in the pre-peak and near-critical regimes, with the focus being placed on the additional deformation and shear resistance reduction induced by vibration.

3.1 ViSRR and addifitonal deformation at near-critical state

In the context of classical soil mechanics (Wood, 1990; Schofield and Wroth, 1968) with the soil being considered isotropic and homogeneous, for a specimen subjected to monotonic shearing under drained conditions, the critical state is reached when the material keeps deforming in shear at constant stress and volume such that $\dot{\varepsilon}_v$=0, $\dot{q}$ = $\dot{p}$=0, and $\dot{\varepsilon}_q \neq 0$. Herein p is the mean effective stress, q the stress deviator, ε_v and ε_q the volumetric strain and deviatoric strain, respectively. Under a triaxial stress condition, these quantities are defined as $p=(\sigma_1+2\sigma_3)/3$ and $q=(\sigma_1-\sigma_3)$, $\varepsilon_v = \varepsilon_1+2\varepsilon_3$ and $\varepsilon_q=2(\varepsilon_1-\varepsilon_3)/3$. The subscripts 1 and 3 stand for quantities in the axial and radial directions, respectively. At the critical state, the friction angle reaches a constant φ_{cr}, with a constant stress ratio $M=(q/p)_{cr}=6\sin\varphi_{cr}/(3-\sin\varphi_{cr})$. The critical state void ratio $e_{cr}=e_{cr}(p_{cr})$ is a function of the mean effective stress at critical state but independent of the initial density of the specimen. For conciseness, the stresses are referred to as effective unless otherwise stated.

When accounting for the influence of internal structure of granular materials, the critical values for the stress and void ratio need to be enhanced by appropriate measure of fabric-anisotropy; as described by the Anisotropic Critical State Theory in Li and Dafalias (2012). However, the effect of fabric is not taken into account in the current study.

In this study, the stresses and strains at the near-critical state where a vibration is superimposed which satisfies (a) $\varepsilon_1 > 10\%$, $-d\varepsilon_v / d\varepsilon_1 < 0.1$, $q / p < 1.1M$ and $dq / d\varepsilon_1 < 0$ for dilatant specimens; and (b) $\varepsilon_1 > 10\%$, $d\varepsilon_v / d\varepsilon_1 < 0.1$, $q / p > 0.9M$ and $dq / d\varepsilon_1 > 0$ for contractive specimens under triaxial stress conditions with constant effective confining pressure. These conditions ensure that the stress and deformation state is at the vicinity of critical state. Continuous strain-

controlled monotonic shearing will bring the specimen to critical state with limited increase of axial strain.

(1) *Effect of vibration intensity*

Figure 2 illustrates the loading scheme applied to a specimen at the near-critical state when a vibration is added to the monotonic shearing. Figure 3 shows the test results corresponding to a dense specimen of D_r=70% when a 60 Hz low-amplitude vibration with peak acceleration A/g=0.17 was superimposed at a near-critical state (Point *N* on the stress-strain curve). The deviatoric stress and volumetric strain curves of the specimen are observed to be typical for dense, dilatant sand under monotonic shearing. At the beginning of deformation, shear-induced volume contraction occurs, followed by significant dilation (see Figure 3(b)). Referring to the figure, a peak-stress state is attained on the deviatoric stress-strain curve before strain-softening develops as shear continues until the critical state is approached (see Figure 3(a)). No shear bands were observed in the specimen during this test.

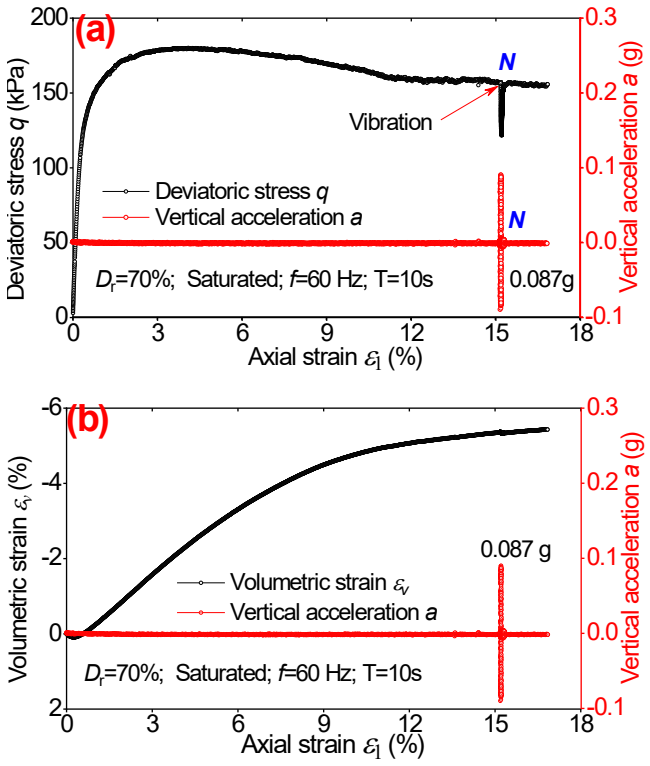

Figure 3. Responses of a dense specimen under vibration superimposed at near-critical state: (a) q~ε_1 curve; (b) ε_v~ε_1 curve

We first examine the time history of the deviatoric stress q and the specimen deformation after vibration is introduced at Point N for a duration of T=26 sec. As shown in Figure 4(a), the value of q decreases immediately after the vibration is imposed. At the onset of vibration, q declines rapidly and then reaches a stable state as the vibration continues. At the same time, the imposed vibration causes additional volumetric contraction of the specimen. Similar to the variation of q, the rate of volumetric contraction $\dot{\varepsilon}_v$ is high at the onset of the vibration but decreases quickly. The resulting volumetric strain ε_v is observed to approach a stable level in Figure 4(b) as vibration continues. Even though the volumetric strain does not reach a stable value at T=26 sec, it is likely that such a value would have been attained at longer T.

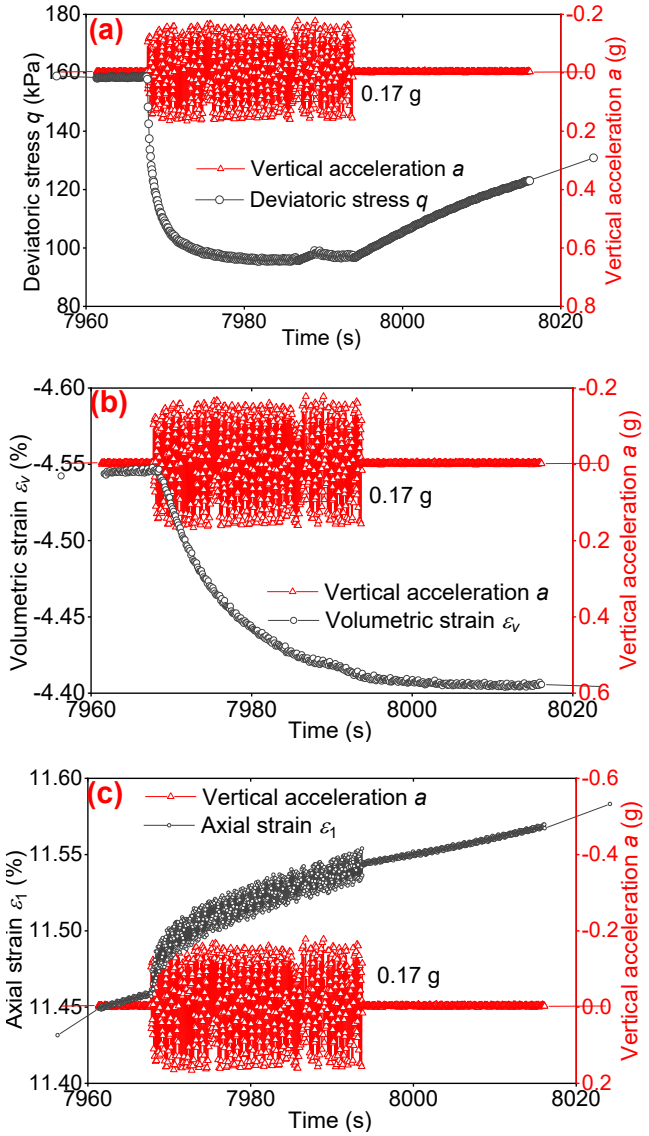

Figure 4. Time history of responses of a dense specimen during and after vibration at near-critical state: (a) deviatoric stress; (b) volumetric strain; (c) axial strain

We observed that once the vibration was terminated, the deviatoric stress and volumetric strain began to recover as the monotonic shearing continued. Eventually, they approached the deviatoric and volumetric strain levels corresponding to the original monotonic shearing without vibration (i.e., the critical state under monotonic shearing), respectively. The time required for the recovery of vibration-induced shear resistance reduction (ViSRR) was much longer than the duration of vibration, particularly for the volumetric strains. Similar phenomena were observed by Taslagyan et al. (2015, 2016) in direct shear tests on sand.

In addition to the reduction of shear resistance and additional volumetric compression, the superimposed vibration also results in additional axial compression of the specimen, as shown in Figure 4(c). Analogous to the variation of shear resistance and volumetric strain, the axial strain rate increases quickly at the onset of vibration, with gradually decreasing rate to approach the original monotonic axial strain rate. When the vibration stops, the axial strain rate further decreases, and the axial strain returns to its axial strain trajectory in monotonic shearing.

Figure 5 and Figure 6 show the influence of vibration intensity on the reduction of the shear resistance and volumetric contraction of a dense specimen (D_r=70%) at near-critical states. In this test, two series of vibrations (f=60 Hz) with peak acceleration A/g=0.18 and 0.22 were applied for T=20sec at a time interval of 21 minutes, which was long enough to minimize a potential interaction of the first and second vibrations. Referring to Figure 6(a), as the vibration intensity increases from A/g=0.18 to 0.22, the ViSRR increases from 68 kPa to 83 kPa. The additional volumetric compression also increases with the intensity of vibration. After the termination of vibration, the volumetric compression induced by the vibration does not recover as quickly as the deviatoric stress; as shown in Figure 6(b). However, the dilation owing to continuous monotonic shearing appears to offset the volumetric contraction induced by vibrations, until the critical void ratio is reached, which can be observed clearly from Figures 5(b) and (c). In other words, the continuous monotonic shearing after an imposed vibration is bound to bring the soil back to the critical state. The superimposed vibration, after being terminated, does not affect the critical state under monotonic shearing. This confirms the observation in classical geotechnical earthquake engineering that the stress ratio and void ratio at critical state are unique and independent of loading history including superimposed vibrations. It should be emphasized that the focus of this work is primarily put on the ViSRR and additional deformation induced by low-amplitude, high-frequency vibrations.

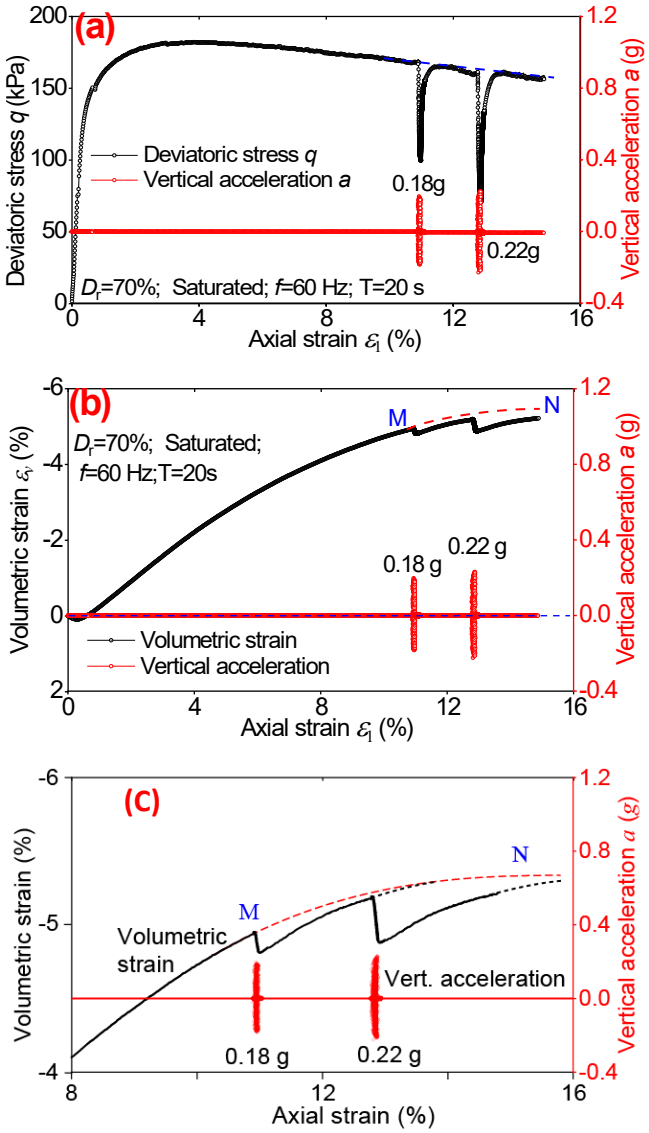

Figure 5. Responses of a dense specimen with vibration (A/g=0.18 and 0.22) superimposed at near-critical state: (a) q~ε_1 curve; (b) ε_v~ε_1 curve; (c) details of ε_v~ε_1 curve before and after termination of vibration

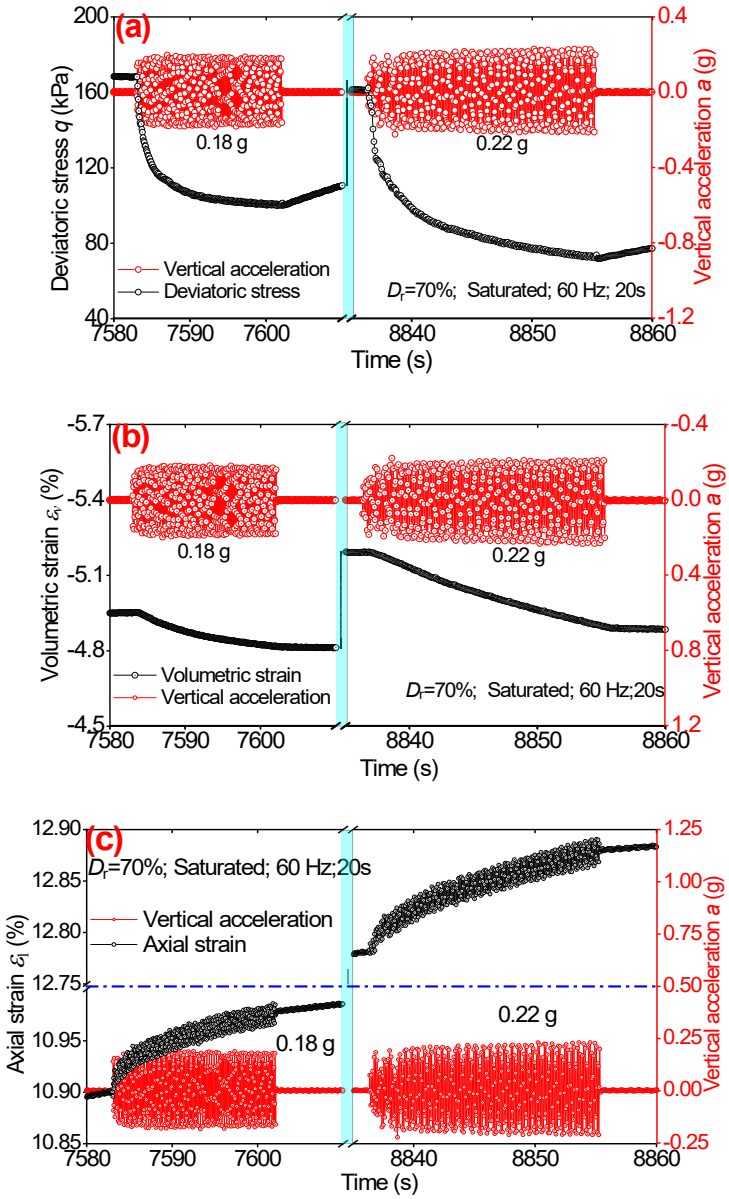

Figure 6. Time history of soil responses of a dense specimen with vibration (A/*g*=0.18 and 0.22) applied at near-critical state: (a) deviatoric stress; (b) volumetric strain; (c) axial strain

(2) *Influence of vibration on specimens of different densities*

To examine the ViSRR and additional volume change for specimens of different densities at near-critical state, a test on a loose specimen of D_r=35% was peformed at a superimposed vibration of A/*g*=0.16 and *f*=60 Hz. The duration of vibration was T=15s and the test results are summarized in Figure 7.

Regarding the deviatoric and volumetric strain responses under monotonic shearing,

a comparison of the q~ε_1 and ε_v~ε_1 curves in Figure 3 or Figure 5 for the dense specimen of D_r=70% with those in Figures 7(a) and (b) for the loose specimen shows that the denser specimen has higher dilation, higher peak deviatoric stress and strain-softening of stress-strain response, which is consistent with the general understanding of sand behavior.

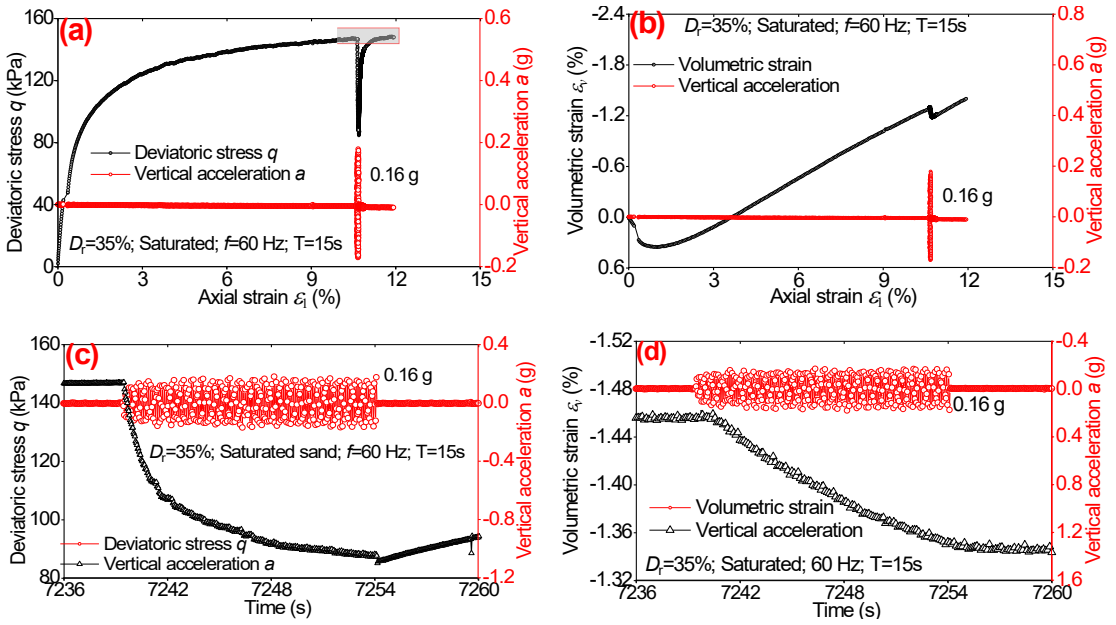

Figure 7. Responses of a loose specimen (D_r=35%) with vibration superimposed at near-critical state: (a) q~ε_1 curve; (b) ε_v~ε_1 curve; (c) time history of q during vibration; and (d) time history of ε_v during vibration

When the vibration is superimposed to the monotonic shearing at a near-critical state, the responses of the loose specimen (Dr=35%) are observed to be similar to those of dense specimens (Dr=70%). The time histories of ViSRR and volume change of the loose specimen are presented in Figure 7(c). In general, the vibration-induced variations in q and ε_v of the loose specimen have the same trend as those of the dense specimen shown in Figures 4(a) and (b). Since the vibration lasted only 15 seconds, at the end of vibration, both the deviatoric stress and the volumetric strain tended to approach but did not reach their stable values. However, it is observed that the ViSSR and the additional volumetric contraction of the looser specimen was larger than those of the denser specimens. More test results with detailed analyses regarding the influence of density

are presented in later sections.

3.2 ViSRR and additional deformation at pre-peak states

Since the critical state of soil is reached only when the shear resistance is fully mobilized at large deformation, the critical state can be considered as a failure state in critical state soil mechanics (Wood, 1990). For a geotechnical system under normal working conditions, the stress and deformation states are generally in the pre-peak regime. Consequently, it is necessary to examine the influence of vibration on the behavior of sand at pre-peak stress states regarding the serviceability of geotechnical structures.

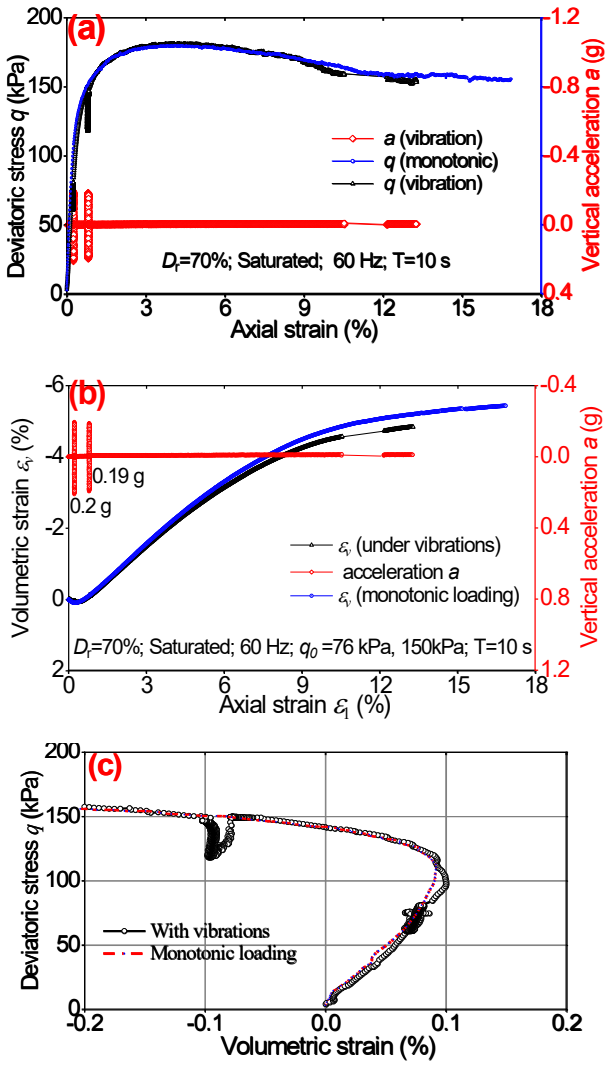

Figure 8. Response of a dense specimen with vibration superimposed to pre-peak state: (a) q~ε_1 curve; (b) ε_v~ε_1 curve (c) q~ε_1 curve

Figure 8 presents the complete stress and volumetric strain responses of a single dense specimen when 60 Hz vibration was superimposed for 10 seconds on monotonic loading at pre-peak stress state corresponding to q_0=76 kPa and 150 kPa. The peak accelerations of these two vibrations were almost identical, with A/g=0.20 and 0.19, respectively. Both the time and axial strain intervals between the two series of vibrations were large enough to ensure the specimen's memory regarding the first vibration was practically erased. The relation between the deviatoric stress and volumetric strain was presented in Figure 8(c), which clearly shows the simultaneous evolution of shear resistance reduction and volume contraction induced by vibration. For comparison purposes, the responses of the specimen under monotonic loading only are also presented in the figure.

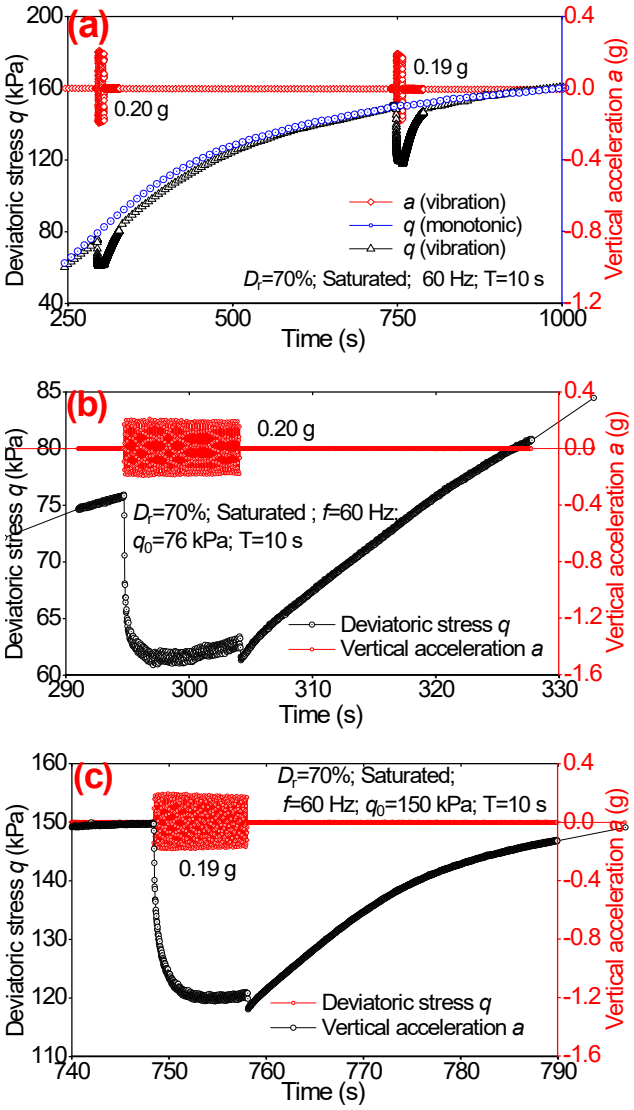

Figure 9. Time history of soil responses of a dense specimen during and after vibration at pre-peak stress states: (a) comparison of deviatoric stress histories with and without superimposed vibration; (b) ViSRR at q_0=76 kPa; (c) ViSRR at q_0=150 kPa

Figures 9(a) to (c) present the time histories of deviatoric stress variation induced by superimposed vibrations. The mobilized shear resistance (q_0=76 kPa or 150 kPa) due to monotonic shearing decreased sharply, immediately after the application of vibration; as shown in Figures 9 (b) and (c). Following the initial deviatoric stress reduction, the value of q tended to rise slightly as the vibration continues. When the vibration was terminated, the decreased shear resistance gradually return to the stress trajectory of monotonic shearing, as can be observed from Figure 9(a). In other words, the ViSRR was temporary and the influence of vibration on the mobilized shear resistance vanished

as monotonic shearing continued. These observations are similar to ViSRR at near critical state shown in Figure 4(a) and Figure 7(c).

As shown in Figures 9(b) and (c), for vibrations of the same intensity, frequency and duration, the ViSRR at pre-peak stress states was affected by the deviatoric stress q_0 at which the vibration was superimposed. When compared with the test results in Figure 5(a) for specimens of the same initial void ratio with almost identical vibrations, the ViSRR at near-critical state was much higher than that occurring at pre-peak stress states (approximately 70 kPa at near-critical state vs. 15 kPa and 30kPa at pre-peak stress states with q_0=76 kPa and q_0=150 kPa, respectively).

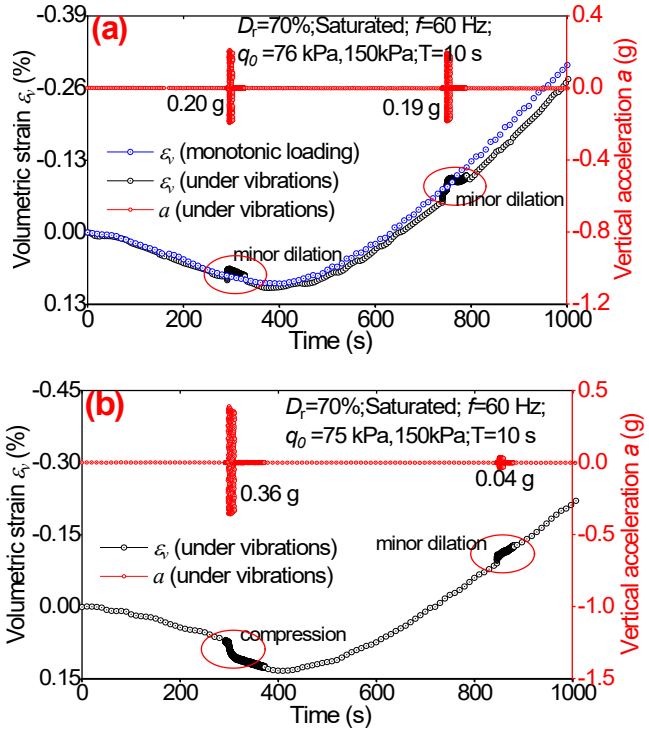

Figure 10. Time history of volume change of dense sand (D_r=70%) subjected to vibrations at pre-peak state: (a) A/g =0.19-0.20; (b) A/g =0.36 and 0.04 at different levels of q_0

Figure 10(a) presents the characteristics of additional volume change induced by vibration with A/g=0.2 and f=60 Hz at pre-peak stress states in the test shown in Figure 8. One observes that the superimposed vibration in the pre-peak regime also caused volume change of the specimen. With reference to the volumetric strain curve in

monotonic shearing, additional dilative volume change occurred upon the application of vibration, comparing with vibration induced volume contraction at near-critical state presented in Figure 5(b). After termination of vibration, the volume change induced by continuous monotonic shearing followed the same trend as the original monotonic shear, however, with minor contraction. It should be noted that ViSSR and additional volume change occurred simultaneously, as shown in Figure 8(c). It is likely that the additional volumetric contraction would be permanent if there is no continuous monotonic shearing after vibration. Figure 10(b) shows the volume change of a dense specimen, induced by 60 Hz vibrations of A/g=0.36 and 0.04 at the same q_0 as those in Figure 10(a). One observes that the vibration of the increased intensity tended to cause larger volumetric contraction.

Figure 11 presents the influence of density on vibration-induced volume change of a loose soil specimen with D_r=35%, in which volumetric contraction is induced by vibrations of A/g=0.20 and A/g=0.14 at q_0=60kPa and 115kPa, respectively. Compared to the results in Figure 10(a), the looser specimen was more likely to generate a contractive volumetric deformation under more intensive vibration than the denser specimen under a less intensive vibration. In other words, different from that at near-critical states, the characteristics of volume change induced by vibration at pre-peak states were affected by the specimen's density, the intensity of vibration and the deviatoric stress q_0 at which the vibration was superimposed. Depending on the values of these quantities, the additional volume change induced by vibration can be either contractive or dilative.

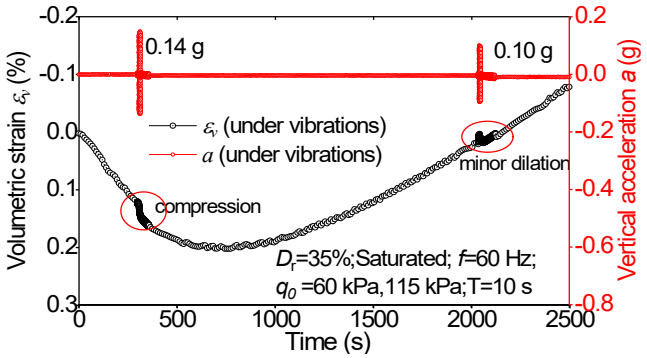

Figure 11. Influence of soil's initial density on vibration-induced volume change at pre-peak state: D_r=35%, A/g =0.14 at q_0=60 kPa, and A/g=0.10 at q_0=115 kPa

3.3 Vibration-induced excess pore pressure in saturated specimens under drained conditions

As stated previously, tests of saturated specimens were performed under drained conditions to facilitate the measurement of their volume change characteristics. When a specimen is sheared at slow rate, no excess pore pressure is expected to develop. However, excess pore pressure Δu can develop during the application of high-frequency vibration even if the drainage valves are open at both ends of the specimen, owing to short period of vibration that does not provide sufficient time for the excess pore pressure to dissipate completely. To examine the magnitude of vibration-induced excess pore pressure $|\Delta u|$ as well as its influence on the measurement of volume change and the reduction of shear resistance, additional tests were carried out by allowing drainage only at the bottom of the specimen, while the drainage valve at the specimen top was close to measure the potential excess pore pressure. Under such boundary conditions, the measured $|\Delta u|$ is expected to be higher than that generated at the mid-height of the specimen when drainage is allowed at both ends of the specimen.

Figure 12(a) shows the excess pore pressure measured in the test presented in Figure 5 corresponding to f = 60Hz superimposed vibration on a dense specimen at near-critical state. The high-frequency vibration caused, as expected, excess pore pressure Δu that dissipated slowly after the termination of vibration. It is observed that the magnitude of Δu tended to increase with the peak acceleration. The values of $|\Delta u_{max}|$ were 3 kPa and

5 kPa for A/g=0.18 and 0.22, respectively. At A/g=0.22, $|\Delta u_{max}|$ accounted for less than 10% of the effective confining pressure σ_c=50 kPa, with the deviatoric stress decreasing from 161 kPa to 72 kPa that corresponds to $\Delta q/q_0$=55%. When drainage was allowed at both ends of the specimen, $|\Delta u_{max}|$ developed at the mid-height of the specimen was expected to be one-quarter of that in the specimen with single drainage owing to the different drainage lengths (Terzaghi, et al., 1996). In other words, the values of $|\Delta u_{max}|$ was expected to be approximately 1 kPa (or 2% of the effective confining pressure) in the test presented in Figure 5. As a result, vibration-induced excess pore pressure is not the primary reason for ViSRR in granular soils. This conclusion is further confirmed by tests on dry specimens, which is discussed in the later section. The influence of the minor excess pore pressure on the measured volume change of soil specimen is expected to be insignificant, at either the near-critical state or pre-peak stress states.

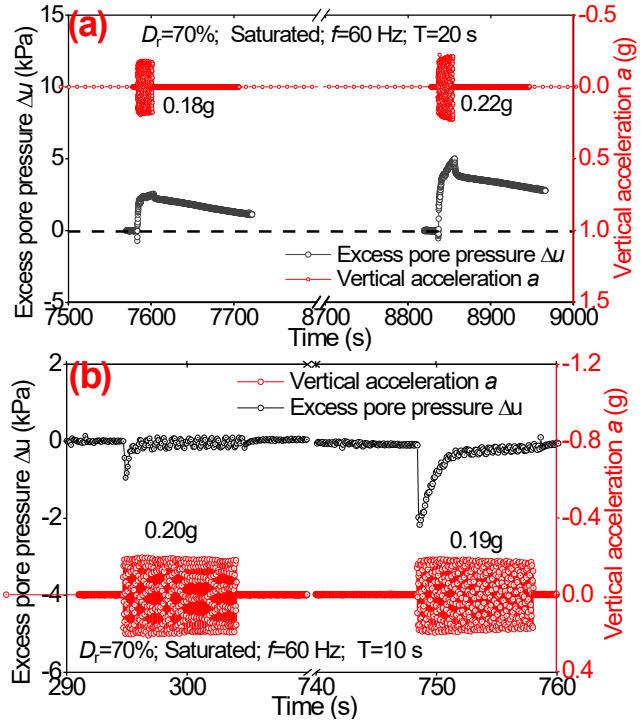

Figure 12. Excess pore pressure induced by superimposed vibration in saturated specimens under drained condition: (a) vibration imposed at near-critical state; (b) vibration imposed at pre-peak stress states

Negative excess pore pressures were measured in tests presented in Figure 8 when

vibration was applied at pre-peak stress states, as shown in Figure 12(b). This low level of negative pore pressure (approximately 2 kPa) at the onset of vibration was related to vibration-induced dilation of the specimen, similar to the occurrence of negative pore pressure in conventional undrained triaxial tests. Intuitively, this observation seems to contradict the observed shear resistance reduction if the variation of effective confining pressure σ_c is thought as the main reason of ViSRR. In fact, the increase in σ_c was only 4% while the decrease in deviatoric stress was about 20%; as observed in Figure 9. It should be noted that the excess pore pressure, either negative or positive, in the soil specimen was non-uniform along the specimen during vibration, although it only accounts for less than 5% of effective confining pressure. In addition, the non-uniform distribution excess pore pressure implies that pore water was at transient flow state. According to the theory of perturbation, if the state of the specimen is not at the vicinity of a certain threshold (such as the onset of shear band or the peak on the stress-strain curve), this small fluctuation of effective stress would not result in dramatic variation of material responses.

According to the test results of dry and saturated specimens under different conditions, we conclude that minor excess pore pressure induced by low-amplitude, high-frequency vibration in the specimens is not the primary factor resulting in ViSRR. Phenomenally, the occurrence of ViSRR can be attributed to the coupling between the tendency of vibration-induced soil deformation and the restrained rate of monotonic shearing. Physically, the mechanism of ViSRR is related to the internal structure variation of granular soil induced by vibration. Additional study is necessary for the identification of the mechanisms, particularly in terms of the micromechanics of granular materials.

4. Analyses of experimental results

The previous section presented typical test results for 60 Hz vibrations superimposed to sand specimens at near-critical and pre-peak states. This section provides detailed

analyses and interpretation of the test results. The focus is placed on the influence of various factors on ViSSR and the additional deformation of the specimen. These factors include the relative density D_r of specimen, the effective confining pressure σ_c, the intensity of vibration quantified by the normalized magnitude of acceleration A/g, the vibration frequency f, and the static deviatoric stress level q_0 at which vibration is introduced. In the following, we examine the test results obtained at pre-peak stress states and near-critical states separately.

4.1 Vibration superimposed at near-critical state

We first address the dependency of the near-critical state responses on the vibration intensity in drained triaxial tests on loose (D_r=35%) and dense (D_r=70%) specimens. The vibration frequencies were in the range of 60 to 120 Hz, with vibration intensities of A/g=0.02 to 0.26. The tests were carried out at nominal effective confining stress of σ_c=50 kPa, using both saturated and dry specimens.

Figure 13 summarizes the variation of ViSRR with vibration intensity A/g at near-critical state under various conditions. For convenience, the relative shear resistance reduction (RSRR) $\Delta q/q_0$ is used to characterize the reduction of shear resistance. A threshold value of A_0/g=0.04 is identified, below which the ViSRR is negligible. When the applied acceleration amplitude A is higher than A_0, $\Delta q/q_0$ increases with the peak acceleration following a linear relation $\Delta q/q_0$=3(A/g–0.04). The relation between $\Delta q/q_0$ and A/g appears to be independent of the relative density of the specimens and the frequency of vibration. Moreover, the RSRR $\Delta q/q_0$ is practically not affected by the duration of vibration in the range of T = 10s to 35s, which implies that ViSRR occurred in about 10s with a stable stress state being attained. An important finding from Figure 13 is that, at a selected peak acceleration, the ViSRR obtained from saturated and dry specimens are practically identical, at least when A/g < 0.26. This observation confirms

that the ViSRR of sand at near-critical state is not induced by the minor excess pore pressure that results from the vibration.

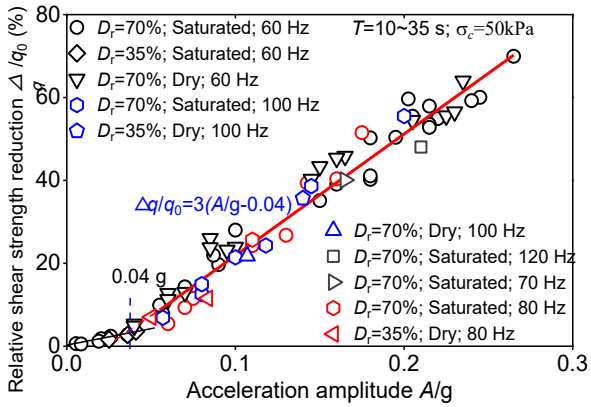

Figure 13. Summaries of ViSRR at near-critical state under different conditions

Figure 14 presents the influence of vibration intensity A/g on the additional volume contraction $\Delta\varepsilon_v$ induced by vibration at near-critical state. The results confirm the existence of a vibration intensity threshold $A_0/g = 0.04$, with $\Delta\varepsilon_v$ being negligible when $A < A_0$. When $A > A_0$, a nonlinear relation $\Delta\varepsilon_v(\%) = 0.235(A/g - 0.04)^{2.836}$ is defined, even though the data are slightly scattered when $A/g > 0.15$. Since $\Delta\varepsilon_v$ reflects the additional volume change measured at the end of vibration, the data scatteredness in Figure 14 may be partially attributed to the differences in the duration of vibration, the peak velocity of specimen deformation, and the minor residual excess pore pressure in the specimen.

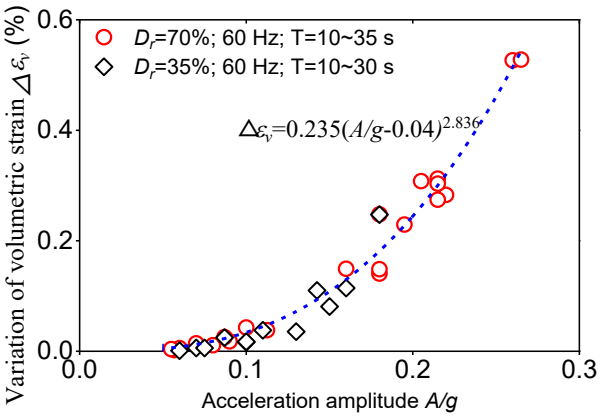

Figure 14. Effect of acceleration amplitude on the additional volumetric strain induced by vibration at near-critical state

It should be emphasized that the additional volume contraction of the specimens was induced by the superimposed vibration, even though they were almost at their critical states under monotonic shearing prior to vibration. For a given effective confining stress in a triaxial compression test, the critical state void ratio is a constant independent of the initial void ratio of the material. For a selected vibration intensity, the additional volume change induced by vibration tended to approach a stable value as the duration of vibration increased, which corresponds to a new constant void ratio e_{vcr} of the specimen. Herein e_{vcr} is termed as the vibro-critical state void ratio, which is a nonlinear function of A/g according to the data presented in Figure 14 since $e_{vcr} = e_{cr} - \left(1 + e_{cr}\right)\Delta\varepsilon_v$ in which e_{cr} is the critical state void ratio without vibration.

4.2 Vibration superimposed at pre-peak state

Figure 15 presents a summary of ViSRR corresponding to f=60 Hz when vibrations of different intensities were superimposed at pre-peak stress states. Most of these tests were performed at σ_c=50 kPa, with other tests being conducted at σ_c=75 and 100 kPa. Both saturated and dry specimens were considered. Similar to the results at near-critical states presented in Figure 13, we observe a threshold peak acceleration below which the influence of vibration is negligible, regardless of the specimens' initial density and the value of q_0 at which the vibration was superimposed. According to Figure 15, the pre-peak threshold acceleration amplitude is $A_{0,pre\text{-}peak} \approx 0.02g$, which is lower than that of $A_{0,cr}$=0.04g at near-critical states in Figure 13.

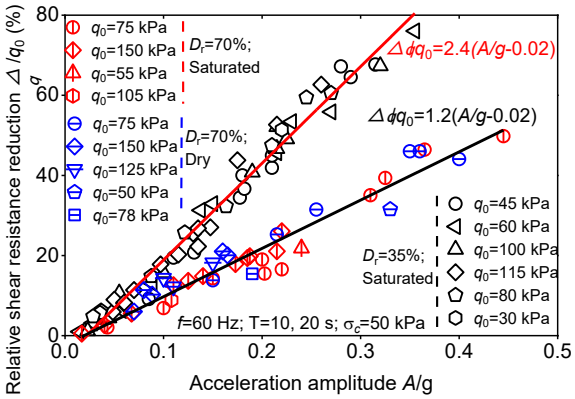

Figure 15. Summaries of vibration-induced shear resistance reduction at pre-peak state

When the intensity of vibration is higher than $A_{0,pre\text{-}peak}/g$, the RSRR $\Delta q/q_0$ tended to increase linearly with A/g for specimens of a given initial density, with

$$\Delta q/q_0 = k(A/g - A_{0,pre\text{-}peak}/g) \quad (1)$$

As shown in Figure 15, the relation between $\Delta q/q_0$ and A/g is independent of q_0 at which a vibration is superimposed. Different from the observations for the near-critical states, the slope of the $\Delta q/q_0$~A/g relationship at pre-peak states depends on the initial density of specimens. For the same vibration intensity, a looser specimen tended to have a higher RSRR $\Delta q/q_0$. In particular, the values of k in Eq. (1) are 1.2 and 2.4 for specimens of D_r=70% and 35% respectively, which are both smaller than that (k = 3.0) at near-critical states (Figure 13). This is attributed to the differences in the density (or void ratio) at critical state and pre-peak stress states. Referring to the volumetric strain curves in Figure 5(a) and Figure 7(b), we observe that the near-critical state void ratio was higher than that at the pre-peak stress states for both dense and loose specimens. In other words, the value of k in Eq. (1) tended to increase with initial void ratio of the specimens. It should be pointed out that the results for both dry and saturated specimens in Figure 15 provide solid evidence that the ViSRR does not appear to be associated with the minor variation of excess pore pressure induced by vibration.

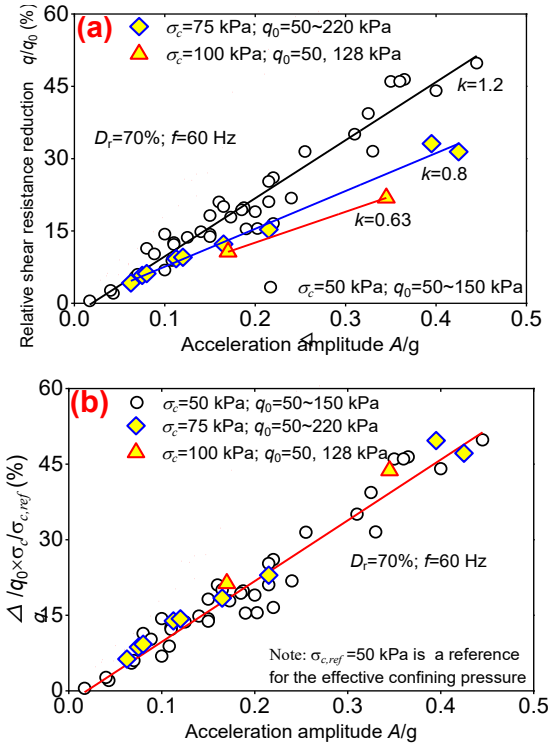

Figure 16. Influence of effective confining pressure on ViSRR at pre-peak states

To investigate the influence of effective confining pressure σ_c on the ViSRR at pre-peak stress states, additional tests were conducted on dense specimens at σ_c=75 kPa and 100 kPa. The results are summarized in Figure 16. Similar to the results at σ_c=50 kPa in Figure 15, for a given effective confining pressure, the variation of the relative shear resistance reduction (RSRR) $\Delta q/q_0$ with A/g can be approximated by Eq. (1), as shown in Figure 16(a). The value of slope k in Eq. (1) decreases with an increase of σ_c following k=60.4/σ_c approximately. In other words, $\Delta q/q_0$ can be considered inversely proportional to the effective confining pressure σ_c. By introducing a reference effective confining pressure $\sigma_{c,ref}$ to normalize $\Delta q/q_0$, all the points at various effective confining pressures fall on the same line, which can be expressed as when choosing $\sigma_{c,ref}$=50 kPa:

$$\frac{\Delta q}{q_0}\frac{\sigma_c}{\sigma_{c,ref}} = 1.2\left(A/g - 0.02\right) \tag{2}$$

as shown in Figure 16(b).

4.3 Relation between ViSRR and additional deformation

Similar to a stress-strain relation under monotonic loading, the ViSRR can be related to the additional deformation of the specimen during vibration. To obtain this relation, the measured axial strain and deviatoric stress need to be decomposed to separate the components associated with monotonic and vibration loadings. At any time during vibration, the total axial strain $\varepsilon_1(t)$ consists of three components: (1) monotonic strain component $\varepsilon_{1m}(t)$ that increases with time at a constant rate $\dot{\varepsilon}_1$, (2) the additional axial strain $\Delta\varepsilon_1(t)$ induced by superimposed vibration, which represents the equilibrium position from the location corresponding to monotonic constant strain rate, and (3) an instantaneous strain component as the axial strain oscillating with the amplitude $\varepsilon_{1i}(t)$, which reflects the instantaneous position from the equilibrium position during vibration; as shown in Figure 17(a). Similarly, the total deviatoric stress can be decomposed into three parts corresponding to the three axial strain components: (1) the monotonic deviatoric stress q_m corresponding to $\varepsilon_{1m}(t)$, (2) the instantaneous cyclic stress σ_d corresponding to axial strain oscillation $\varepsilon_{1i}(t)$ during vibration, and (3) the shear resistance reduction Δq associated with $\Delta\varepsilon_1(t)$ induced by vibration. Figures 17(b) and (c) present the time histories of the decomposed stress and strain components. More details about the stress and strain decomposition can be found in Xie and Guo (2021).

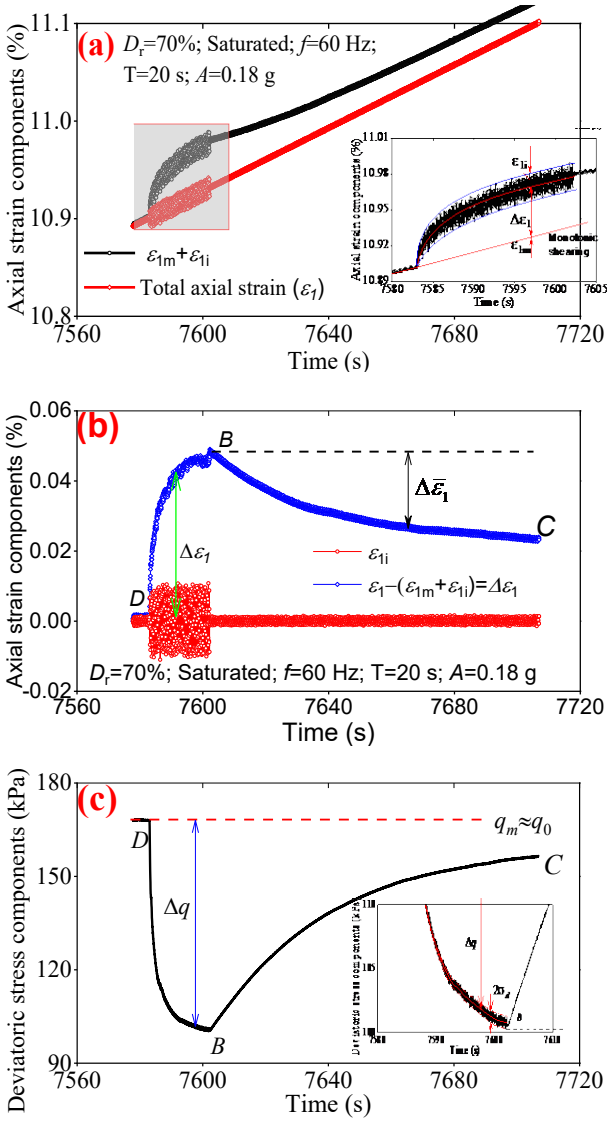

Figure 17. Separations of deviatoric stress and axial strain: (a) ε_1 and ε_{1m}; (b) $\Delta\varepsilon_1$ and ε_{1i}; (c) separation of stress

Following the decomposition of stresses and strains presented in Figure 17, the $\Delta q \sim \Delta\varepsilon_1$ relation during vibration (from "*D*" to "*B*" in Figure 17(b) and (c)) can be established. Figure 18 summarizes the $\Delta q/q_0 \sim \Delta\varepsilon_1$ relations obtained from tests on specimens of different densities under various conditions at pre-peak and near critical states. The experimental data for $\Delta q/q_0 \sim \Delta\varepsilon_1$ relations are observed to be distributed in a narrow zone that can be described by a hyperbolic function

$$\frac{\Delta q(t)}{q_0} = \frac{K_0(\Delta q / q_0)_\infty \Delta\varepsilon_1(t)}{(\Delta q / q_0)_\infty + K_0\Delta\varepsilon_1(t)} \tag{3}$$

where K_0 is the initial slope of the $\Delta q/q_0 \sim \Delta\varepsilon_1$ curve with $K_0 = 1875$ to 2000,

$(\Delta q / q_0)_\infty$ is the nominal maximum ViSRR when $\Delta\varepsilon_1(t) \to \infty$. The value of $(\Delta q / q_0)_\infty$ is different with the measured ViSRR given in Eq. (1) or (2) that corresponds to the small $\Delta\varepsilon_1$ induced by vibration. The data in Figure 18 show that K_0 is independent of the intensity and frequency of vibration, the deviatoric stress level q_0 at which the vibration was superimposed, as well as the density of the specimens. Physically, the $\Delta q(t)/q_0 \sim \Delta\varepsilon_1(t)$ relation during vibration implies that the ViSRR and the corresponding deformation (both axial deformation and volume change) are not independent. Instead, they are closely related with the relation in Eq. (3) that reflects the material properties.

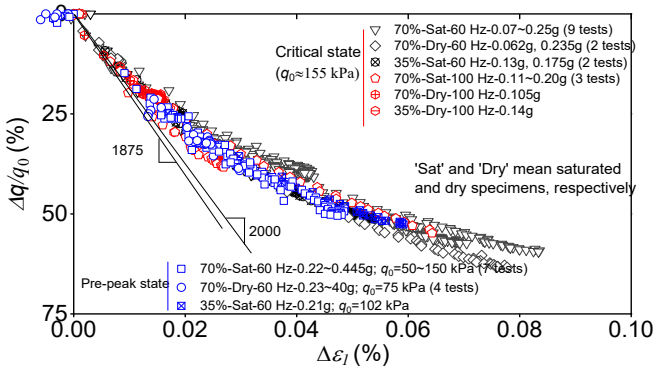

Figure 18. Summaries of $\Delta q/q_0$~$\Delta\varepsilon_1$ curve during vibration

5. Concept of vibro-critical state

According to the test results presented in Figures 4 to 7 and Figures 13 to 15, a new steady state is reached when a high-frequency low-(displacement) amplitude vibration is superimposed to the specimen at a near-critical state for a certain time. This new steady state is similar to the critical state of soil under monotonic shearing, with the following characteristics:

$$\begin{aligned} &\ddot{u}(t) = \ddot{\hat{u}} + \ddot{u}_d(t),\ \ddot{u}_d(t) = A\sin\left(2\pi ft\right), \\ &\frac{d\hat{\varepsilon}_q}{dt} \neq 0,\ \frac{d\hat{q}}{dt} = 0,\ \frac{d\hat{p}}{dt} = 0,\ \frac{d\hat{\varepsilon}_v}{dt} = 0 \end{aligned} \tag{4}$$

and

$$e_{vcr} = e_{vcr}\left(e_{cr},\ f,\ \frac{A}{g}\right);\ \hat{M} = \frac{\hat{q}}{\hat{p}} = \hat{M}\left(M,\ f,\ \frac{A}{g}\right)\ \text{or}\ \varphi_{vcr} = \varphi_{vcr}\left(\varphi_{cr},\ f,\ \frac{A}{g}\right) \quad (5)$$

where ($\hat{\xi}$) stands for the average of quantity $\xi(t)$ during vibration, $M = \frac{q_{cr}}{p_{cr}} = \frac{6\sin\varphi_{cr}}{3-\sin\varphi_{cr}}$ is the stress ratio at critical state under monotonic shearing, e_{vcr} and φ_{vcr} are the void ratio and friction angle at this new steady state. Since this new steady state only exists during vibration, it is terms as the vibro-critical state.

Figure 19 illustrates the concept of vibro-critical state. In this figure, the solid curves represent the stress-strain curve and the volumetric strain response of sand subjected to monotonic shearing in a conventional triaxial compression test. The dashed curve denotes the deviatoric stress-strain response $\hat{q} \sim \varepsilon_z$ after considering the ViSRR when a vibration is superimposed on monotonic shearing. Similar to the critical state under monotonic loading conditions, the shear resistance at the vibro-critical state is independent of the initial void ratio and the mean effective stress. Moreover, the vibro-critical state is not affected by the duration of vibration, as shown by the results summarized in Figure 13.

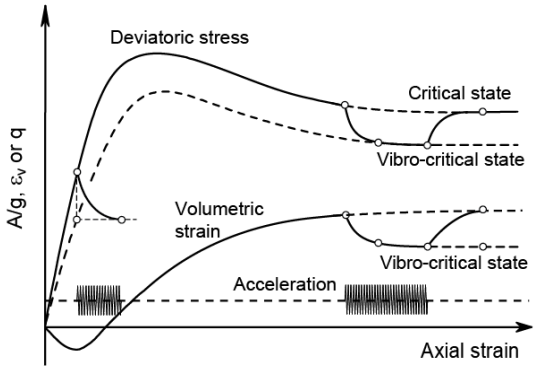

Figure 19. Concept of vibro-critical state

The deviatoric stress ratio $\hat{M}$ can be related to the critical stress ratio M at monotonic loading via

$$\hat{M} = \frac{\hat{q}_{vcr}}{\hat{p}_{vcr}} = \frac{q_{cr} - \Delta q}{p_{cr} - \frac{1}{3}\Delta q} = M\frac{1 - (\Delta q / q_{cr})}{1 - \frac{1}{3}M(\Delta q / q_{cr})} \quad (6)$$

The friction angle φ_{vcr} at vibro-critical state is determined as $\sin\varphi_{vcr} = 3\hat{M} / \left(6 + \hat{M}\right)$. For vibration with frequency in the range of f=60~120Hz, by applying Eq. (1) with k = 3, $\hat{M}$ in Eq. (6) can be directly related to the peak acceleration as

$$\hat{M} = M\frac{1.12 - 3A / g}{1 - M(A / g - 0.04)}, \quad A / g > 0.04 \quad (7)$$

It should be emphasized that the vibro-critical friction angle φ_{vcr} and the vibro-critical void ratio e_{vcr} depend on the intensity of superimposed vibration, which are different from those at the ordinary critical state. Moreover, the vibro-critical state is reached only during a vibration that is superimposed on a specimen at its critical state under monotonic shearing. As soon as the vibration stops, continued monotonic shearing is bounded to bring the soil back to the critical state with unique stress ratio M and void ratio e_{cr}, as suggested by the results shown in Figures 3, 5 and 7.

Conclusions

This paper adopted a new experimental technique and apparatus are adopted to investigate the effect of high-frequency vibration (f=60~120Hz) on the behavior of a granular material subjected to monotonic shearing. Based on the test results of Ottawa sand C109, the following conclusions are obtained:

(1) During a monotonic shearing at constant strain rate, a superimposed vibration causes a loss of mobilized shear resistance, accompanied by the additional volume change of the specimen. Both the loss of shear resistance and volume change can be recovered after vibration as monotonic shearing continues. The recovery of volume change is not as quick as that of shear resistance.

(2) The peak acceleration, as an indicator of vibration intensity at high frequency, plays an important role in the relative loss of shear resistance $\Delta q/q_0$. The reduction of shear resistance and additional volume compaction tend to increase with the peak vibration acceleration.

(3) In the pre-peak regime, the relative loss of shear resistance $\Delta q/q_0$ is independent of the deviatoric stress at which vibration is imposed, but $\Delta q/q_0$ varies with the initial void ratio of the material.

(4) The reduction of shear resistance during the vibration occurs in both dry and saturated material under drained conditions. This confirms that it is not induced by potential excess pore pressure in a saturated material.

(5) The relative loss of shear strength at critical state is independent of the initial void ratio of the soil specimen. A vibro-critical state is reached during a vibration that is superimposed on a specimen that reaches its critical state under monotonic shearing. After vibration, the stresses and void ratio can return to the critical state as the monotonic shearing continues.

Acknowledgments

Funding from the Natural Sciences and Engineering Research Council of Canada is greatly appreciated.

References

Alexeev, A., Royzen, V., Dudko, A., Goldshtein, A., and Shapiro, M. (2000). “Mixing and segregation in vertically vibrated granular layers.” Solid mechanics and its applications, Vol. 81, A. D. Rosato and D. L. Blackmore, eds., Springer, New York, 129–139.

Ayer, J. E., and Soppet, F. E. (1965). Vibratory compaction: I, compaction of spherical shapes. J. Am. Ceram. Soc. 48(4), 180–183.

Ayer, J. E., and Soppet, F. E. (1966). Vibratory compaction: II, compaction of angular shapes. J. Am. Ceram. Soc., 49(4), 207–210.

Barkan, D. D. (1962). Dynamics of bases and foundations, Trans. L. Drashevska, McGraw-Hill, New York, 207–210.

Bian, X., Jiang, H., Chang, C., Hu, J., & Chen, Y. (2015). Track and ground vibrations generated by high-speed train running on ballastless railway with excitation of vertical track irregularities. Soil Dynamics and Earthquake Engineering, 76, 29-43.

Bingham, C. M., Stone, D. A., Schofield, N., Howe, D., & Peel, D. (2000). Amplitude and frequency control of a vibratory pile driver. IEEE Transactions on Industrial Electronics, 47(3), 623-631.

Chen, T.J., and Fang, Y.-S. (2008). Earth pressure due to vibratory compaction. J. Geotech. Geoenviron. Eng, 134(4), 437-444.

Canadian Geotechnical Society (2006). Canadian Foundation Engineering Manual (4th edition) , BiTech Publishers, Richmond, B.C.

Darbois Texier, B., Ibarra, A., & Melo, F. (2017). Low-resistive vibratory penetration in granular media. PloS One, 12(4), e0175412.

Denies, N. and Holeyman, A. (2017). Shear strength degradation of vibrated dry sand. Soil Dynamics and Earthquake Engineering 95, 106–117.

Denies, N., Canou, J., Roux, J. N., & Holeyman, A. (2010). Sphere penetration experiments in vertically vibrated sand.

Felming, K., Weltman, A., Randolph, M. and Elson, K. (2008) Piling engineering, 3rd ed., Taylor & Francis, London.

Heerema, E. P. (1978). Predicting pile driveability: Heather as an illustration of the" friction fatigue" theory. In SPE European Petroleum Conference. Society of Petroleum Engineers.

Hosoi, A. E., & Goldman, D. I. (2015). Beneath our feet: strategies for locomotion in granular media. Annual review of fluid mechanics, 47.

Hsiau, S. S. and Chen, C.H. (2000). Granular convection cells in a vertical shaker. Powder Technology 111, 210–217.

Hwang, J. H., Liang, N., & Chen, C. H. (2001). Ground response during pile driving. Journal of Geotechnical and Geoenvironmental Engineering, 127(11), 939-949.

Jaeger, H. M., Nagel, S. R., & Behringer, R. P. (1996). Granular solids, liquids, and gases. Reviews of modern physics, 68(4), 1259.

Jiang, H., Bian, X., Cheng, C., Chen, Y., & Chen, R. (2016). Simulating train moving loads in physical model testing of railway infrastructure and its numerical calibration. Acta Geotechnica, 11(2), 231-242.

Krey, H. (1932). Erddruck, Erdwiderstand und Tragfähigkeit des Baugrundes Berlin, Deutschland, Wilhelm Ernst and Sohn.

Laroche, C., Douady, S., and Fauve, S. (1989). Convective flow of granular masses under vertical vibration. J. Phys., 50(C7), 699–706.

Massarsch, K. R., Wersäll, C., and Fellenius, B. H. (2020) Horizontal stress increase induced by deep vibratory compaction. Geotechnical Engineering, 173(3), 228-253.

Meneses, J., Ishihara, K., & Towhata, I. (1998). Effects of superimposing cyclic shear stress on the undrained behavior of saturated sand under monotonic loading. Soils

and foundations, 38(4), 115-127.

Meneses-Loja, J., Ishihara, K., & Towhata, I. (2000). Flow failure of saturated sand under simultaneous monotonic and cyclic stresses. Journal of geotechnical and geoenvironmental engineering, 126(2), 131-138.

Milne, D. R. M., Le Pen, L. M., Thompson, D. J., & Powrie, W. (2017). Properties of train load frequencies and their applications. Journal of sound and vibration, 397, 123-140.

Mogami, T. and Kubo, K. (1953). The behavior of soil during vibration. Proc. 3rd Int. Conf. on Soil Mech. and Found. Eng., Switzerland, Vol. 1, 152-155.

Moriyasu, S., Kobayashi, S. I., & Matsumoto, T. (2018). Experimental study on friction fatigue of vibratory driven piles by in situ model tests. Soils and foundations, 58(4), 853-865.

Mujica, N., and Melo, F. (1998). Solid-liquid transition and hydrodynamic surface waves in vibrated granular layers. Phys. Rev. Lett., 80(23), 5121–5124.

Omidvar, M., Bless, S., & Iskander, M. (2019). Recent insights into penetration of sand and similar granular materials. In Shock Phenomena in Granular and Porous Materials (pp. 137-163). Springer, Cham.

Ord, A., & Hobbs, B. E. (2010). Fracture pattern formation in frictional, cohesive, granular material. Philosophical Transactions of the Royal Society A: Mathematical, Physical and Engineering Sciences, 368(1910), 95-118.

Osinov, V. A. (2013). Application of a high-cycle accumulation model to the analysis of soil liquefaction around a vibrating pile toe. Acta Geotechnica, 8(6), 675-684.

O'Neill, M. W., and Vipulanandan, C. (1989). Laboratory evaluation of piles installed with vibratory drivers (No. 316).

Pak, H. K., and Behringer, R. P. (1993). Surface waves in vertically vibrated granular materials. Phys. Rev. Lett, 71(12), 1832–1835.

Rausche F. (2002). Modeling of vibratory pile driving. Eds. A Holeyman and J-F Vanden Berghe, Transvib2002, Proc. Int. Conf. on Vibratory Pile Driving and Deep Soil Compaction, Louvain-la-Neuve, Belgium, 9-10 September 2002, p.21-32.

Schofield, A. N., and Wroth, P. (1968). Critical state soil mechanics. London: McGraw-Hill.

Sharpe, S. S., Kuckuk, R., & Goldman, D. I. (2015). Controlled preparation of wet granular media reveals limits to lizard burial ability. Physical biology, 12(4), 046009.

Shteyn, A. I., Orlov, G. G., Pereselenkov, G. S., & Cherkasov, A. M. (2017). Problems of planning and quality management in the design and construction of the Moscow-Kazan-Ekaterinburg High-Speed Railway. In: International Conference, Quality Management, Transport and Information Security, Information Technologies (IT&QM&IS), pp. 447-450, IEEE.

Sun, L., Xie, W., He, X., & Hayashikawa, T. (2016). Prediction and mitigation analysis of ground vibration caused by running high-speed trains on rigid-frame viaducts.

Earthquake Engineering and Engineering Vibration, 15(1), 31-47.

Taslagyan, K. A., Chan, D. H., & Morgenstern, N. R. (2015). Effect of vibration on the critical state of dry granular soils. Granular Matter, 17(6), 687-702.

Taslagyan, K. A., Chan, D. H., & Morgenstern, N. R. (2016). Vibrational fluidization of granular media. International Journal of Geomechanics, 16(3), 04015080.

Terzaghi, K., Peck, R.B., Mesri, G. (1996) Soil mechanics in Engineering Practice, Third Edition, John Wiley & Sons, Inc.,ISBN 0-471-08658-4.

Vanden Berghe, J. F., Holeyman, A., Juaristi, E., & Schmitt, A. (2001). Interlock friction in a sheet pile wall: laboratory tests. In International Conference on soil mechanics and geotechnical engineering (pp. 1273-1276).

Viking, K. (2002). Vibro-driveability-a field study of vibratory driven sheet piles in non-cohesive soils (Doctoral dissertation, Byggvetenskap).

White, D. J., & Lehane, B. M. (2004). Friction fatigue on displacement piles in sand. Géotechnique, 54(10), 645-658.

Wood, M. D. (1990) Soil behaviour and critical state soil mechanics. Cambridge, UK: Cambridge University Press.

Xie, T., & Guo, P. (2021). A Modified Triaxial Apparatus for Soils under High-Frequency, Low-Amplitude Vibrations. Geotechnical Testing Journal, 45(1).

Youd, T. L. (1967). The engineering properties of cohesionless materials during vibration. PhD dissertation, Iowa State University.

Zhai, W., Kai Wei, K., Song, X. and Shao, M. (2015). Experimental investigation into ground vibrations induced by very high-speed trains on a non-ballasted track. Soil Dynamics and Earthquake Engineering 72, 24–36.

Part II: Model Development

Chapter 4 Framework of the extended STZ model

(Paper 3)

Development of extended STZ model for granular soils subjected to combined static loading and vibration

Géotechnique, *1-9*

Tao Xie[1], Peijun Guo[1], Dieter Stolle[1]

[1]Department of Civil Engineering, McMaster University, 1280 Main St W, Hamilton, ON, L8S 4L7, Canada

Abstract: The "shear-transformation zone" (STZ), which may be referred to as a weak domain in granular material, is the main source of plastic deformations in non-cohesive soils such as sand or gravel. To theoretically investigate the vibration-induced shear resistance reduction (ViSRR) of granular materials, this paper proposes an extended STZ model that considers the coupling effect between vibration and quasi-static loadings. The framework of the model consists of three components: (1) the motion of STZs including the transition, creation and destruction of STZs; (2) the relation between the motion of small-scale STZs and the observable, macroscopic plastic strain; and (3) the evolution law of a "configurational temperature" that reflects the energy that drives the motion of STZs. The conventional STZ model developed for amorphous materials is enhanced to accommodate both volumetric and shear deformations in the spatial stress state. Specifically, in addition to considering plastic shear strains induced by the change in STZ orientation as the result of the transition, as in conventional STZ models, the extended STZ model correlates plastic volumetric strains with the change in STZ amount resulted from creation and destruction.

Keywords: extended STZ model; granular soil; combined static loading and vibration; shear resistance reduction; motion of STZ

1. Introduction

Different from the liquefaction of sand that is attributed to a decrease of effective stresses induced by excess pore pressure increase of saturated sand under undrained conditions or dry sand subjected to a constraint of constant volume, vibration-induced shear resistance reduction (ViSRR) is related to the internal structural change in the vibrating granular media. In extreme cases, it may lead to natural hazards, such as the triggering of landslides during earthquakes (Uzuoka et al., 2005), the initiation of avalanches (Melosh, 1996), and long-runout landslides of dry soil on the moon and Mars (Melosh, 1987). Furthermore, ViSRR in granular "fault gauges" is believed to be a potential mechanism for the dynamic triggering of earthquakes in geophysics (Griffa et al., 2013). On the positive side, a few animals such as Ocellated skinks take advantage of head oscillations to reduce the resistance when boring in granular soils (Hosoi & Goldman, 2015; Sharpe et al., 2015). Vibrational techniques are also used in geotechnical engineering when installing piles in sandy soils (O'Neill et al., 1990; Bingham et al., 2000; Viking, 2002; Moriyasu, 2018) given that the vibration of a pile significantly reduces both shaft and toe resistance. Several experimental and numerical studies have been carried out to study ViSRR; see, for example, Barkan (1962), Taslagyan et al. (2016), and Ferdowsi et al. (2014). Nevertheless, the lack of a fundamental understanding makes it difficult to design and optimize vibratory pile installation qualitatively and reliably. Recently, an explanation for the mechanism behind ViSRR was presented based on energy considerations (Xie et al., 2022). Similar to stress relaxation of any engineering materials, it is found that a restricted deformation rate of granular material (*e.g.*, the strain rate of material in the vibration direction is fixed to be constant) at the onset of vibration is a basic requirement for the occurrence of ViSRR. Furthermore, the ViSRR can be expressed as a function of vibrational and plastic strain energies. Nevertheless, the calculation of plastic strain, thus the plastic strain energy, is still a challenge, especially for frictional granular soils subjected to simultaneous vibration and quasi-static loadings.

To explore the reduced shear resistance in granular soil subjected to simultaneous quasi-static and dynamic loadings, this paper is the first of two papers devoted to extending the conventional micromechanics-based framework of "shear-transformation-zone (STZ) theory" to soil mechanics, particularly for granular soils. Section 2 of this paper provides the background and a brief review of the conventional STZ model. The relation between the motion of STZ and the associated plastic strain is elucidated in Section 3, along with the consideration for vibration-induced compression and shear-induced dilation. The configurational temperature is introduced as an indicator of energy and the driving power for the motion of STZ. Thereafter, the parameters of the extended STZ model and the evolution function of configurational temperature are determined based on the previous work (Xie et al., 2022).

2. Introduction of STZ theory

2.1 Background of STZ theory

The STZ theory has been used in various fields to analyze different types of problems, such as plastic deformations of metallic glasses and amorphous solids (Falk & Langer, 1998; Bouchbinder & Langer, 2009a; Langer & Pechenik, 2003; Pechenik, 2005), weakening of faults in dynamic earthquake triggering (Daub & Carlson, 2010; Di Toro et al., 2016), the flow of granular materials in mining and power industries (Lieoue et al., 2015; Kothari & Elbanna, 2017), and particle fragmentation in sheared granular flow (Lieoue et al., 2014). Essentially, the STZ model can be considered as an extension of the rate process theory, which is based on statistical mechanics. It was mainly applied in physical chemistry to cope with chemical reaction rate (Eyring, 1936; Glasstone et al., 1941) and was later introduced to soil mechanics to describe the rheology of clays (Mitchell, 1964; Mitchell & Soga, 2005). The rate process theory originally focused on "flow units" on the atomic or molecule scale, which participates in time-dependent deformation processes. The relative movement of a "flow unit" is constrained by its

neighbors, and this constraint is termed "energy barrier" e_z. Upon overcoming the energy barrier, a "flow unit" at one equilibrium state jumps to an adjacent one, thereby yielding viscous or plastic deformation.

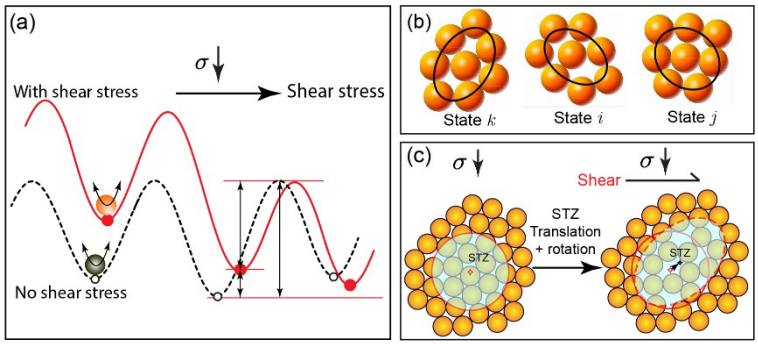

Figure 1. Schematic illustration of energy barrier in rate process theory and a potential energy landscape (a) that arises from the disordered nature of the force network in granular materials (b), and that arises from the motion of STZs in amorphous materials (c)

When applying rate process theory to soils (Mitchell, 1964), as shown in Figure 1, the rate process of deformation involves several important concepts: energy of flow unit, energy barrier, effective temperature, and the shear force applied to the flow unit. To better understand these concepts and their roles in a flipping process, we examine a cube that flips on a tilting table. The cube at an equilibrium state must overcome its gravitational potential energy to overturn to another equilibrium state. In this process, the gravitational potential energy of the cube is equivalent to the energy barrier in the rate process theory. The tilting table plays a role of shear stress which makes the cube easier to overturn down than to overturn up. The energy distribution for the flow units in a system is not uniform but rather follows a certain kind of distribution, *e.g.*, Boltzmann's distribution. In the probability density function of energy distribution, a system with a higher temperature means a larger proportion of flow units are at a high enough energy to overcome the energy barrier and thus allow movement from one stable state to another equilibrium state. Instead of the thermal energy of atomic-scale particles and the corresponding ordinary thermal temperature, the internal energy of solid

materials (including granular soil and amorphous materials) is much more important for the deformation process of granular material at room temperature (Jaeger et al., 1996; Bouchbinder & Langer, 2009b; Karmin & Bouchbinder, 2014). Consequently, these materials are treated as an athermal material (Jiang & Liu, 2017), with an energy-based "effective temperature" being used to describe the rate process in the STZ theory for amorphous materials and granular materials. Herein, the temperature in the original rate process theory or the "effective temperature" in the STZ model is essentially a macroscopic indicator reflecting the internal energy distribution of flow units in a system.

The definition of effective temperature depends on the interaction of the particles. In a kinetic-governed subsystem (Haff, 1986) composed of sufficiently dispersed constituent grains *e.g.*, a granular gas, the transition of energy, momentum, and other relevant quantities is mainly through particle collisions. In this case, the velocity fluctuation of particles is used to define the effective temperature (Ogawa, 1978; Jaeger et al., 1989), or called kinetic temperature to be exactly; Nevertheless, in a configuration-governed system (Haff, 1986), *e.g.*, a granular soil, the transition of the involved quantities is mostly through particle contact, specifically the sliding at particle contacts as well as particle overriding and rotation, which can be driven by either increase of quasi-static shear force or low-amplitude vibration. In this case, the free volume or compactivity (Mehta & Edwards, 1989; Falk & Langer, 1998) is used to define the effective temperature or called configurational temperature to be exactly. Herein the free volume is referred to the effective volume accessible to the moving particles (Falk & Langer, 1998). For a granular soil subjected to combined static loadings and low-amplitude vibrations as investigated in this paper, it still belongs to the configuration-governed system before doesn't completely lose shear resistance. Hence, the free volume is adopted as the configurational temperature in this paper.

In addition to the use of different temperatures, the sizes of flow units also vary for different materials in different theories. Whereas the original rate process theory mainly

deals with the phenomenon on the atomic or molecule scale on which thermal energy dominates the whole process, the analogous STZ theory (Argon, 1979; Falk & Langer, 1998; Pechenik, 2005; Bouchbinder & Langer, 2009c; Lieou et al., 2015; Kothari & Elbanna, 2017) developed primarily for amorphous materials can handle plastic deformations of flow units much larger than the atom. The STZ theory focuses on the motion of defects or weak domains within the shear transformation zone of a material rather than the motion of "excited particles" on the atom- or molecular-scale. Essentially, a STZ is a cluster of randomly close-packed particles at a local scale that undergoes an inelastic shear distortion from one configuration to another, thus leading to a redistribution of stress and strain around the STZs. This process is similar to the process of motion for a "flow unit" in rate process theory, with the "flow unit" being "STZ" in the STZ theory.

2.2 Review of conventional STZ model

We now briefly introduce the conventional STZ model based on the framework established by Langer and coworkers (Bouchbinder & Langer, 2009a & 2009c; Falk & Langer, 1998; Lieou et al., 2015) for amorphous materials that are spatially uniform and undergo only volume conserving pure-shear deformations. It should be noted that the simple shear deformation process can be handled mathematically as a one-dimensional problem since it can be uniquely characterized by the shear strain macroscopically. Consequently, the STZs occur only with orientations either along "+" or opposite "–" to the shear direction. The extensive numbers of STZs (*i.e.*, number in a volume) oriented in the "+" direction N_+ and "–" direction N_- are internal state variables of the material. The switch of STZ orientation from "+" or "–" directions is called STZ flipping. During a deformation process, the STZs at one state flip into another with the development of plastic deformation,

$$\tau_0 \dot{\gamma}^{pl} = \frac{v_v}{V}\left(R_+ N_- - R_- N_+\right) \tag{1}$$

where v_v is the volume of the plastic core of an STZ, and V is a representative element volume of the material; $R_{\pm}$ are flipping rates reflecting the proportion of STZ taking part in flipping in the corresponding directions, and they are a function of the shear stress $\pm s_c$ and configurational temperature χ; γ^{pl} is plastic shear strain in '+' direction, and it becomes $-\gamma^{pl}$ in '–' direction. The first term in the right-hand side of Eq. (1) describes the amount of STZs successfully flipped from '–' to '+' directions and the second one is that from '+' to '–' directions. It should be noted that τ_0 is the inertial time scale for STZ flipping, and it is determined as $\tau_0 = d(\rho_g / \sigma_c)^{0.5}$ with d, ρ_g, and σ_c referring to particle size, material density, and confining pressure, respectively (Jop, et al., 2006).

In addition to the variation of STZ orientations by flipping, STZs can also be created and annihilated to accommodate plastic strain within the materials. The variation of $N_{\pm}$ in each direction is described by the following equation:

$$\tau_0 \dot{N}_{\pm} = R_{\pm} N_{\mp} - R_{\mp} N_{\pm} + \tilde{\Gamma}\left(\frac{N^{eq}}{2} - N_{\pm}\right) \tag{2}$$

where $\tilde{\Gamma} N^{eq}/2$ and $\tilde{\Gamma} N_{\pm}$ refer to the amount of STZ created and annihilated in the deformation process, respectively; N^{eq} is the total number of STZ in steady equilibrium; and $\tilde{\Gamma}$ is the attempt frequency or equivalently a noise strength reflecting the activity of STZ creation and annihilation; To determine the rate factor, it is assumed that $\tilde{\Gamma}$ is proportional to the rate of plastic strain energy and thus is converted into the disordered configurational fluctuations (Langer, 2008). To address the coupling effect of quasi-static deformation and vibration, $\tilde{\Gamma}$ is expressed as $\tilde{\Gamma} = \Gamma + \lambda$, in which Γ and λ denote the mechanical and vibrational noise strengths characterizing the fluctuations in the energy of mechanical deformation and vibration that are termed as the mechanical

and vibrational noise strengths, respectively.

For convenience, four dimensionless quantities are introduced:

$$\Lambda=\frac{N_+ + N_-}{N_g},\quad m=\frac{N_+ - N_-}{N_+ + N_-},\quad R=\frac{R_+ + R_-}{2},\quad T=\frac{R_+ - R_-}{R_+ + R_-} \tag{3}$$

in which N_g is the total number of granular grains. Substituting Eq. (3) into Eqs. (1) and (2) yields,

$$\tau_0\dot{\gamma}^{pl}=\frac{N_g v_v}{V}\Lambda R\left(T-m\right) \tag{4}$$

$$\tau_0\dot{m}=2R\left(T-m\right)-\tilde{\Gamma}m-\frac{\dot{\Lambda}}{\Lambda}m\tau_0,\quad \tau_0\dot{\Lambda}=\tilde{\Gamma}\left(\Lambda^{eq}-\Lambda\right) \tag{5}$$

where $\Lambda^{eq}=N^{eq}/N_g$ is the value of Λ at steady equilibrium. Eqs. (4) and (5) are the governing equations in the conventional STZ model proposed by Falk & Langer (1998).

It should be noted that the conventional STZ model is primarily used for amorphous materials to deal with material's responses under vibration. The focus is placed on the influence of vibration on the material behavior at steady equilibrium (analogous to the critical state in soil mechanics), instead of on the stress-strain relationship. Hence, to extend the conventional STZ model to accommodate granular soil to investigate the shear resistance reduction induced by vibration, the following challenges must be addressed:

(1) A constitutive model in soil mechanics must be able to deal with general stress conditions in 3D (dimensions) rather than only simple shear conditions in 2D as that for the conventional STZ model.

(2) In addition to shear strains considered in the original STZ model, the plastic volumetric strain due to shear- and vibration-induced compression or dilation should be considered.

(3) The conventional STZ model characterizes vibration in terms of energy that is a scalar. For granular materials under 3D stress conditions, the strains induced by vibration cannot be described as a scalar. In addition, the effect of vibration also depends on the direction of vibration motion.

(4) Under static loading, the stress-strain relationship in the conventional STZ model is considered as perfect elastic-plastic. For granular soils, however, the stress-strain relation is generally affected by the plastic deformation, stress state and the internal variables of the material.

The following section presents an "extended STZ model" for granular materials. In this model, the four challenges mentioned above are addressed by taking into account the discrete nature of granular materials.

3. Development of an extended STZ model for granular materials

The goal of this section is to establish a framework of the extended STZ model for granular soils, by which the motion of STZs including the transition, creation, and destruction of STZs under quasi-static and vibrational loadings can be expressed in terms of the rates of plastic deviatoric and volumetric strains of granular soil.

2.3 STZ in a granular material

For a granular material under external loadings, its behavior is mainly governed by two distinct, interacting phases (Nicot et al., 2016 & 2017): a strong phase constituted of force chains is responsible for the strength of the medium, with the contacting grains transmitting substantial contact forces; and a weak phase constituted of particle loops is responsible for deformability of the granular assembly. As we all know that the plastic deformation of granular assembly is primarily from the rearrangement of particles, of which the weak "particle loops" (more than three sides) play a crucial role (Kuhn, 1999; Zhu et al., 2016b), especially those adjacent strong force chains (Tordesillas et al., 2010a & 2010b; Zhu et al., 2016a). Under external disturbances, these particle loops can deform, rotate, collapse, and rebuild as shown in Figure 2, with global volumetric variation (dilatancy or contraction) being accompanied (Kuhn, 1999; Zhu et al., 2016b). It is found from discrete element method (DEM) simulation (Zhu et al., 2016b; Nicot et al., 2016) that particle loops with more number sides, especially those with at least six

sides L_{6+}, have a greater ability of transformation, due to shape fine-tuning or completely breaking to other loop categories with fewer number sides (L_3, L_4, L_5). Herein, L_i represents the particle loop with i sides.

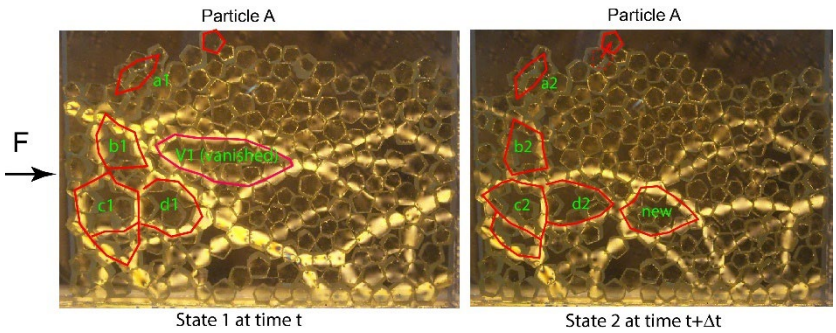

Figure 2. Different types of particle loop motion in a strong force chain network in a biaxial compression using pentagonal disks of photo-elastic material: deformation, rotation (a to d), collapse (V1), and generation (new)

The STZs, as the weak zones in material, are the major source of inelastic deformation in materials. Hence, similar to sheared glasses in which a STZ is visualized as a dislocation loop (Argon, 1979), the weak particle loop (or the particle clusters in 3D) with at least four sides is regarded as the STZ in the granular assembly. It should be noted that the collapse and creation of STZs in granular materials have different mechanisms from the annihilation and creation of STZs in the conventional STZ model for amorphous solids. Owing to its discrete feature, the behavior of a granular material is different from that of amorphous materials. Particularly, the shear and mean stresses induced volume changes as the result of collapse and formation of STZs must be considered in the extended STZ model for granular soils.

3.1 Basic assumptions

(1) *Characterization of STZs*

A STZ is a group of particles that forms a local weak domain. It is not necessarily spherical with principal directions oriented randomly in space. To quantify the spatial

distribution of the STZs in a representative element volume of the material, a STZ tensor H_{ij} is defined as

$$H_{ij} = \frac{1}{N_g}\sum_{\alpha=1}^{N} h_i^{\alpha} h_j^{\alpha} \tag{6}$$

where H_{ij} is a second-order tensor with three eigenvalues; h_i^{α} is the unit orientation vector of the α^{th} STZ in the granular material; N and N_g respectively refer to the total numbers of STZs and particles in a representative element volume V. This definition of STZ tensor H_{ij} is similar to the fabric tensor $F_{ij} = \sum_{\alpha=1}^{N} b_i^{\alpha} b_j^{\alpha}$ for granular materials with b_i^{α} being the unit vector of contact normal.

(2) *Transition of STZ*

The STZ oriented along one direction can transit to any other arbitrary direction, *i.e.*, change in STZ orientation. It is assumed that this transition process can be described by

$$\tau_0 \dot{H}_{ij}^{tra} = \Lambda R_{ij} - R^* H_{ij} \tag{7}$$

where $\dot{H}_{ij}^{tra}$ is the change of H_{ij} with respect to time as the result of transition; R_{ij} is transition rate tensor, which is a function of deviatoric stress tensor s_{ij}; $R^*=R_{ii}$; $\Lambda=H_{ii}$ is STZ density. In this paper, Einstein's summation convention is adopted. The first term on the right-hand side of Eq. (7) is the increased number of STZs oriented in one direction owing to the transition of STZs originally not in this direction, and the second term is the number of STZs transited away from this direction. During the transition process, as illustrated in Figure 3, the plastic strain rate is assumed to be related to $\dot{H}_{ij}^{tra}$ via

$$\dot{\varepsilon}_{ij}^{pl\_tra} = \omega_s \dot{H}_{ij}^{tra} \tag{8}$$

where ω_s is "elementary increment" of plastic strain in transition. From Eqs. (7) and (8) we know $\dot{\varepsilon}_{ii}^{pl\_tra}=0$, which implies that the transition of STZs only yields plastic

deviatoric strain without inducing any volume change.

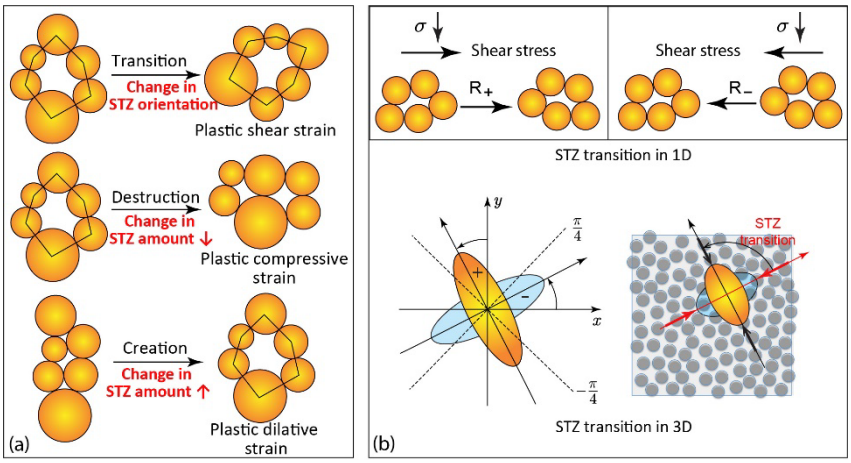

Figure 3. Extended STZ model for granular soils: (a) motion of STZ including transition, creation, and destruction; (b) illustration of STZ transition in cases of 1D and 3D deformation states

(3) *Creation and destruction of STZs*

Under external disturbances such as quasi-static shearing and vibration, the STZs can be created and destructed. It is further assumed that the creation and destruction of STZs can be respectively expressed as

$$\tau_0 \dot{H}_{ij}^{cre} = \frac{\Lambda^{eq}}{\Lambda} \tilde{\Gamma}_{im} H_{mj} \tag{9}$$

$$\tau_0 \dot{H}_{ij}^{des} = -\tilde{\Gamma}_{im} H_{mj} \tag{10}$$

where $\dot{H}_{ij}^{cre}$ and $\dot{H}_{ij}^{des}$ are change of H_{ij} induced by creation and destruction, respectively; Λ^{eq} is the value of Λ at steady equilibrium (*i.e.*, critical state in soil mechanics). It is noted that the scalar "attempt frequency" $\tilde{\Gamma} = \Gamma + \lambda$ is used in the conventional STZ model to quantify the rate of change in STZ amount, as shown in Eq. (2). In the extended STZ model, a tensor called "loading strength" $\tilde{\Gamma}_{ij}$ is adopted in order to consider the impact of vibration direction on the creation and destruction of STZs (change in STZ amount), *i.e.*,

$$\tilde{\Gamma}_{ij} = \Gamma \delta_{ij} + \lambda d_{ij} \tag{11}$$

with Γ and λ referring to mechanical and vibrational noise strengths, respectively; d_{ij} is a unit-magnitude deviatoric tensor with major principal direction in the direction of vibration.

As illustrated in Figure 3, the plastic strain is accompanied by the creation and destruction of STZs. Specifically, the destruction of STZ, like the breakage of weak particle loops, yields compressive plastic strain, whereas the creation of STZs (rebuilding of weak particle loop) yields dilative plastic strain, *i.e.*,

$$\dot{\varepsilon}_{ij}^{pl\_cre\&des} = -\omega_v \left(\dot{H}_{ij}^{cre} + \dot{H}_{ij}^{des} \right), \quad \text{with } \omega_v = \frac{N_g v_v}{V} \tag{12}$$

with ω_v being "elementary increment" of plastic strain during creation or destruction; v_v being the volume change when an STZ is created or destructed. It is found that $\dot{\varepsilon}_{ii}^{pl\_cre\&des} \neq 0$ from Eqs. (9)~(12) and $\dot{\varepsilon}_{ii}^{pl\_tra} = 0$ from Eqs. (7), (8). Hence, the creation and destruction of STZs are the only sources of plastic volumetric strain in this model. In the conventional STZ model mainly focusing on continuous materials, the plastic volumetric deformation induced by the creation and destruction of STZs is not considered. This is one of the main differences between the extended and conventional STZ models.

3.2 Motion of STZ and the corresponding plastic strains

The evolution of STZ consists of three parts: transition, creation, and destruction, which are collectively called the "motion of STZ". Based on the above assumptions Eqs. (7), (9) and (10), the motion of STZ is written as

$$\tau_0 \dot{H}_{ij} = \tau_0 \left(\dot{H}_{ij}^{tra} + \dot{H}_{ij}^{cre} + \dot{H}_{ij}^{des} \right) = \Lambda R_{ij} - R^* H_{ij} + \left(\frac{\Lambda^{eq}}{\Lambda} - 1 \right) \tilde{\Gamma}_{im} H_{mj} \tag{13}$$

with the corresponding plastic strain rate $\dot{\varepsilon}_{ij}^{pl}$ being derived from Eqs. (8) and (12), *i.e.*,

$$\tau_0 \dot{\varepsilon}_{ij}^{pl} = \tau_0 \left(\dot{\varepsilon}_{ij}^{pl\_tra} + \dot{\varepsilon}_{ij}^{pl\_cre\&des} \right) = \omega_s \left(\Lambda R_{ij} - R^* H_{ij} \right) - \omega_v \left(\frac{\Lambda^{eq}}{\Lambda} - 1 \right) \tilde{\Gamma}_{im} H_{mj} \tag{14}$$

Moreover, the plastic volumetric strain rate $\dot{\varepsilon}_v^{pl}$ is obtained from Eq. (14) as

$$\dot{\varepsilon}_v^{pl} = \dot{\varepsilon}_{ii}^{pl} = -\omega_v \dot{\Lambda}, \quad \text{with } \tau_0 \dot{\Lambda} = \tau_0 \dot{H}_{ii} = \left(\frac{\Lambda^{eq}}{\Lambda} - 1 \right) \tilde{\Gamma}_{im} H_{mi} \tag{15}$$

This indicates that the rate of plastic volumetric strain is proportional to the rate of STZ density, *i.e.*, change in the amount of STZs.

For an initially isotropic material, H_{ij} is co-directional with the stress tensor or strain tensors, particularly when there is no principal stress rotation during the deformation process. Hence, the formulation of the model can be established in the principal space of H_{ij} for an isotropic granular material under triaxial stress conditions.

4. Model parameters and evolution of configurational temperature

4.1 Parameters in the extended STZ model

(1) *Noise strengths* Γ *and* λ

The loading strength $\tilde{\Gamma}_{ij}$ reflects the probability of STZ creation and destruction, which in turn controls the rate of plastic deformation of the system. For a granular system subjected to coupled quasi-static shearing and vibration, $\tilde{\Gamma}_{ij}$ consists of two individual components: mechanical noise strength Γ and vibrational noise strength λ as indicated in Eq. (11), which characterize the fluctuations in the energy of mechanical deformation and vibration, respectively. When the transition of a STZ does not induce any volume change, based on Pechenik hypothesis (Langer & Pechenik, 2003), Γ is proportional to the plastic strain energy associated with plastic shear strain in the conventional STZ model.

For granular soils under quasi-static loading, two mechanisms are considered to contribute to the total plastic volumetric strain: one is the mean-stress-induced compression (or consolidation), and another is the deviatoric-stress-induced dilation or compression. To incorporate these two mechanisms into the extended STZ model, the mechanical noise strength Γ is decomposed into two components, *i.e.*,

$$\Gamma=\Gamma_v+\Gamma_d \tag{16}$$

where Γ_v and Γ_d determine the plastic volumetric strain induced by mean stress (consolidation) and deviatoric stress, respectively. The amplitudes of Γ_v and Γ_d are proportional to the plastic volumetric energy $\tau_0\dot{W}_{vol}^{pl}$ and plastic deviatoric strain energy $\tau_0\dot{W}_{dev}^{pl}$, respectively. Combined with Eq. (14), the definitions of Γ_v and Γ_d are given as

$$\Gamma_v=\frac{\alpha V\tau_0\dot{W}_{vol}^{pl}}{N_g\Lambda v_v p_0}=-\frac{\xi_v p}{p_0}\left(\frac{\Lambda^{eq}}{\Lambda}-1\right),\ \text{with}\ \xi_v=\alpha\frac{\tilde{\Gamma}_{im}H_{mi}}{\Lambda} \tag{17}$$

$$\Gamma_d=\frac{\xi_d V\tau_0\dot{W}_{dev}^{pl}}{N_g\Lambda v_0 p_0}=\frac{\xi_d s_{ij}}{\Lambda p_0}\left(\Lambda R_{ij}-R^* H_{ij}\right) \tag{18}$$

In the above,

$$\tau_0\dot{W}_{dev}^{pl}=\tau_0 s_{ij}\dot{\varepsilon}_{ij}^{pl}=\omega_s s_{ij}\left(\Lambda R_{ij}-R^* H_{ij}\right),\quad \dot{W}_{vol}^{pl}=p\dot{\varepsilon}_v^{pl}=-\omega_v p\dot{\Lambda} \tag{19}$$

with ξ_v and ξ_d being regarded as constant coefficients, α representing an intermediate coefficient, p_0=1 kPa denoting unit pressure and p being the mean stress. From Eqs. (16), (17) and (18), the mechanical noise strength Γ becomes

$$\Gamma=\frac{\xi_d s_{ij}}{\Lambda p_0}\left(\Lambda R_{ij}-R^* H_{ij}\right)-\frac{\xi_v p}{p_0}\left(\frac{\Lambda^{eq}}{\Lambda}-1\right) \tag{20}$$

The vibrational noise strength λ, which controls the plastic volume change induced by vibration, is related to the vibrational energy. Based on our previous work (Xie, et al., 2022), the definition of λ can be given as:

$$\dot{E}_V-\dot{E}_F=\lambda A_0 \tag{21}$$

where E_V is the density of vibrational energy acting on the soil, E_F denotes the energy dissipation per unit volume due to inelastic contacts and inelastic collisions of particles (when vibration is applied) that have a negligible contribution to the plastic strain; and A_0 is a constant coefficient. It has been known that the inelastic deformation of granular soils is mainly due to the rearrangement and rotation of particles, with the contribution

of particle deformation being negligible. Consequently, E_F has no contribution to soil's plastic deformation and is not included in the density of plastic strain energy W^{pl} of the material. Since vibrational energy E_V depends on the frequency and amplitude of vibration, these two factors also affect the vibrational noise strength λ. It is noted that there is no clear definition of λ in the conventional STZ model (Edwards & Grinev, 1998; Daniels & Behringer, 2005 & 2006). From our previous investigation (Xie, et al., 2022), we know that the vibration-induced shear resistance reduction $\Delta q/q_0$ at critical state can be related to the vibrational and mechanical noise strength, which leads to

$$\frac{\Delta q}{q_0} = \frac{\dot{E}_V - \dot{E}_F}{\dot{W}^{pl}} \tag{22}$$

Examination of Eq. (22), we observe that the energy dissipation E_F offsets the effect of vibration on the shear resistance reduction of granular materials, which supports the form of definition of λ in Eq. (21). In other words, a part of the vibration energy imported to the material is dissipated via inelastic particle deformation and particle collisions. In the extended STZ model, the influence of $\dot{E}_F$ on soil's behavior is incorporated into the vibrational noise strength λ, as shown in Eq. (21).

In summary, the three components Γ_v, Γ_d and λ of the loading strength $\tilde{\Gamma}_{ij}$ respectively describe the plastic volumetric deformations caused by deviatoric stress (shearing), mean stress (consolidation), and vibration.

(2) *Transition rate and STZ density at steady state*

The tensor of transition rate R_{ij} depends on the energy barrier of the STZ transformation and energy fluctuations. For 1D problems, different functional forms have been adopted to describe the transition rate factor including an Eyring-like activation factor at small stresses and a smooth transition from Eyring to power-law (Langer, 2008; Langer & Manning, 2007). In particular, Bouchbinder & Langer (2009c)

proposed $R(s_c) = R_c \exp(v_v s_c / \chi)$ for an 1D problem at a shear stress s_c. In this study, we assume the same functional form for the tensor of transition rate R_{ij}, such that

$$R_{ij} = \frac{R_0}{3} \exp(\omega_s v_g s_{ij} / \chi) \tag{23}$$

in which χ is the configurational temperature, and R_0 is regarded as a constant coefficient. The value of $\omega_s v_g s_{ij} / \chi$ is small considering that the transition rate in granular materials could not be high as pointed out by Bouchbinder & Langer (2009b). Herein, $v_g = V/N_g$ is the occupied particle volume. Thus, the parameter $R^* = R_{ii} \approx R_0$ holds and R^* can be replaced by R_0 in the involved expressions.

The density of STZs at their steady equilibrium Λ^{eq} is related to configurational temperature in steady equilibrium and the formation energy e_z of STZs (Bouchbinder & Langer, 2009b),

$$\Lambda^{eq} = \begin{cases} \exp(-e_z / \chi^{eq}), & \lambda=0 \\ \exp(-e_z \chi^{eq} / (\chi \cdot \chi_v^{eq})), & \lambda>0 \end{cases} \tag{24}$$

where e_z is equivalent to the energy barrier in the rate process theory; χ^{eq} is the value of χ in steady equilibrium without vibration; χ_v^{eq} corresponds to the value of χ in steady equilibrium when only vibration is applied without plastic strain energy being developed.

(3) *Time scale*

A basic feature of granular materials is that, upon application of stresses, particles move and rearrange themselves through reconfiguration of force chain networks and particles with plastic irreversible deformation concentrated in localized regions (or STZs). The STZs undergo slow configurational rearrangement, which results in the variation of H_{ij} and occurs on longer time scales than the scale of kinetic vibrations of the particles. The extended STZ model is required to handle these two processes with

different time scales. It should be noted that, depending on the nature of a problem, different processes may be selected. In this study, the time scale τ_0 reflects the time required for the transition, creation and destruction of STZs. During the quasi-static deformation process of a granular soil, this time scale is supposed to be governed by the rate of particle rearrangement that occurs on longer time scales than the scale of kinetic vibrations of the particles. In monotonic shearing with a constant strain rate $\dot{\gamma}$, the process of STZ transitions becomes faster as $\dot{\gamma}$ increases. This time scale can be chosen as the inverse of the strain rate. For a traditional triaxial compression test with a constant axial strain rate $\dot{\varepsilon}_a$, the inverse of time scale τ_0^{-1} is assumed to be proportional to $\dot{\varepsilon}_a$, *i.e.*,

$$\tau_0 \dot{\varepsilon}_a = \kappa \tag{25}$$

where κ is a constant. Taking

$$\tau_0 \frac{\mathrm{d}\sim}{\mathrm{d}t} = \tau_0 \dot{\varepsilon}_a \frac{\mathrm{d}\sim}{\mathrm{d}\varepsilon_a} = \kappa \frac{\mathrm{d}\sim}{\mathrm{d}\varepsilon_a} \tag{26}$$

into Eqs. (13)~(15) to eliminate τ_0, the governing functions of the model can be presented in terms of axial strain, *i.e.*, $\mathrm{d}\sim/\mathrm{d}\varepsilon_a$.

4.2 Evolution law of configurational temperature

The basic principle of the extended STZ model presented above provides us with the fundamental relationships between the rate of plastic strain tensor $\dot{\varepsilon}_{ij}^{pl}$ and the motion of STZ tensor $\dot{H}_{ij}$. From Eqs. (23) and (24), we can find that the intermediate quantities R_{ij} and Λ^{eq} in the governing equations all depend on the configurational temperature χ, which determines the proportion of STZ that can overcome the energy barrier and hence the rate of plastic strains.

This study focuses on the responses of granular soil subjected to simultaneous static

and vibration, it belongs to the configuration-govern system (Haff, 1986). Hence, the free volume (*i.e.*, the volume in excess of close packing that the particles have available for motion) is chosen as the configurational temperature χ, which is only related to the system configuration based on the particle positions. In the conventional STZ model, various evolution equations of χ have been proposed depending on the nature of the problem investigated (Bouchbinder & Langer, 2009b; Lieou et al., 2015). In this research, the combined effect of static and dynamic loadings with different time scales makes the analysis more complicated than if one were to treat them independently. From the thermodynamic fundamentals of STZ model for a granular soil system, as presented in our previous research (Xie et al., 2022), the evolution of χ can be expressed as

$$C_0\dot{\chi}=\left(1-\frac{\chi}{\chi^{eq}}\right)\dot{W}^{pl}+\left(1-\eta\frac{\chi}{\chi_v^{eq}}\right)\left(\dot{E}_V-\dot{E}_F\right) \tag{27}$$

where C_0 is the energy capacity coefficient of the system, η>1 is a constant parameter. The evolution equation of χ similar to Eq. (27) can be found in Kothari & Elbanna (2017), Bouchbinder & Langer (2009b) and Lieou, et al. (2015). It should be noted that $\dot{W}^{pl}$ in Eq. (27) includes plastic strain energy induced by deviatoric strain and volumetric strain such that $\dot{W}^{pl}=\dot{W}_{dev}^{pl}+\dot{W}_{vol}^{pl}$. Combined with Eqs. (19) and (21), the evolution law of χ can be rewritten as

$$\tau_0 C_0\dot{\chi}=\left[\omega_s s_{ij}\left(\Lambda R_{ij}-R_0 H_{ij}\right)-p\omega_v\tau_0\dot{\Lambda}\right]\left(1-\frac{\chi}{\chi^{eq}}\right)+\lambda A_0\left(1-\eta\frac{\chi}{\chi_v^{eq}}\right) \tag{28}$$

4.3 Summary of extended STZ model

(1) *In time rate form*

The structure of the extended STZ model can be summarized as follows: the evolution of configurational temperature χ, as the indicator of energy, drives the motion of STZ and the motion of STZ gives rise to the plastic strains in granular soil,

which in turn promotes the further evolution of χ. Hence, the model contains three groups of governing equations: the evolution law of χ, the motion of STZ, and the relationship between the motion of STZ and plastic strains.

Specifically, the plastic strain rate $\dot{\varepsilon}_{ij}^{pl}$ is decomposed into (1) the rate of plastic deviatoric strain induced by the transition of STZs, and (2) the rate of plastic volumetric strain resulted from the creation and destruction of STZs, *i.e.*,

$$\tau_0 \dot{\varepsilon}_{ij}^{pl} = \omega_s \left(\Lambda R_{ij} - R_0 H_{ij} \right) - \omega_v \left(\frac{\Lambda^{eq}}{\Lambda} - 1 \right) \tilde{\Gamma}_{im} H_{mj} \tag{29}$$

The motion of STZ, as shown in

$$\tau_0 \dot{H}_{ij} = \Lambda R_{ij} - R_0 H_{ij} + \left(\frac{\Lambda^{eq}}{\Lambda} - 1 \right) \tilde{\Gamma}_{im} H_{mj}, \quad \tau_0 \dot{\Lambda} = \left(\frac{\Lambda^{eq}}{\Lambda} - 1 \right) \tilde{\Gamma}_{im} H_{mi} \tag{30}$$

is driven by the evolution of χ as

$$\tau_0 C_0 \dot{\chi} = \left[\omega_s s_{ij} \left(\Lambda R_{ij} - R_0 H_{ij} \right) - p \omega_v \tau_0 \dot{\Lambda} \right] \left(1 - \frac{\chi}{\chi^{eq}} \right) + \lambda A_0 \left(1 - \eta \frac{\chi}{\chi_v^{eq}} \right) \tag{31}$$

(2) *In strain rate form for traditional triaxial tests*

The above governing equations can be also presented in terms of the axial strain rate $\dot{\varepsilon}_a$ using Eq. (26); *i.e.*,

$$\kappa \frac{\mathrm{d}\varepsilon_{ij}^{pl}}{\mathrm{d}\varepsilon_a} = \omega_s \left(\Lambda R_{ij} - R_0 H_{ij} \right) - \omega_v \left(\frac{\Lambda^{eq}}{\Lambda} - 1 \right) \tilde{\Gamma}_{im} H_{mj} \tag{32}$$

$$\kappa \frac{\mathrm{d}H_{ij}}{\mathrm{d}\varepsilon_a} = \Lambda R_{ij} - R_0 H_{ij} + \left(\frac{\Lambda^{eq}}{\Lambda} - 1 \right) \tilde{\Gamma}_{im} H_{mj}, \quad \kappa \frac{\mathrm{d}\Lambda}{\mathrm{d}\varepsilon_a} = \left(\frac{\Lambda^{eq}}{\Lambda} - 1 \right) \tilde{\Gamma}_{im} H_{mi} \tag{33}$$

$$C_0 \kappa \frac{\mathrm{d}\chi}{\mathrm{d}\varepsilon_a} = \left[\omega_s s_{ij} \left(\Lambda R_{ij} - R_0 H_{ij} \right) - \omega_v p \kappa \frac{\mathrm{d}\Lambda}{\mathrm{d}\varepsilon_a} \right] \left(1 - \frac{\chi}{\chi^{eq}} \right) + \lambda A_0 \left(1 - \eta \frac{\chi}{\chi_v^{eq}} \right) \tag{34}$$

Concluding Remarks

In essence, the mechanism of decreased shear resistance in granular soils under vibration is dominated by the evolution of energy within these soils. The framework of the extended STZ model established in this paper provides the bridge crossing the gap between the energy evolution law and the stress-strain relationship

In short, the configurational temperature χ, as the indicator of energy, pushes the motion of STZs and the motion of STZ gives rise to the plastic strains in granular soil, which in turn promotes the evolution of χ. Hence, the model contains three groups of governing equations: the evolution equation of χ, the motion equation of STZ, and the relationship between the STZ motion and plastic strain.

(1) The motion of STZ includes transition, creation, and destruction of STZs: the transition of STZ describes the change in the orientation of STZ, whereas the creation and destruction of STZs describe the change in the number of STZ.

(2) The relationship between the STZ motion and plastic strains. The transition of STZ, as the change in STZ orientation, only generates plastic deviatoric strain; While the creation and destruction of STZs, as the change in STZ amount, is the only source of plastic volumetric strain. The consideration of plastic volumetric strain as the result of the creation and destruction of STZs is one of the most striking differences between the conventional STZ models and the extended STZ model in this work.

(3) The energy, which includes vibrational energy, strain energy and energy dissipation, is the driving power for the motion of STZ, whose influence is embodied in the evolution law of configurational temperature.

Acknowledgments

Funding from the Natural Sciences and Engineering Research Council of Canada is greatly appreciated.

Notation:

The following symbols are used in this paper:

N number of STZ

N_+, N_- numbers of STZ oriented along and opposite shear directions in 2D, respectively

N^{eq} number of STZ in steady equilibrium

N_g number of particles

Λ STZ density

Λ^{eq} STZ density in steady equilibrium

m STZ orientation bias

T STZ flipping bias

R average flipping rate in 2D

R_0 transition rate coefficient

R_+, R_- flipping rates of STZ along and opposite shear directions in 2D, respectively

L_i particle loop with i sides

H_{ij} STZ tensor

$\dot{H}_{ij}^{tra}$, $\dot{H}_{ij}^{cre}$, $\dot{H}_{ij}^{des}$ changes of H_{ij} in transition, creation and destruction of STZs, respectively

h_i^{α} is the unit orientation vector of the α^{th} STZ

F_{ij} fabric tensor

b_i^{α} unit vector of contact normal.

R_{ij} transition rate tensor

s_{ij} deviatoric stress tensor

$R^*=R_{ii}$ total flipping rate

ε_{ij}^{pl} plastic strain tensor

$\varepsilon_{ij}^{pl\_tra}$ plastic strain induced by STZ transition

$\varepsilon_{ii}^{pl\_cre\&des}$ plastic strain induced by STZ creation and destruction

ε_v^{pl} plastic volumetric strain

ω_s elementary increment of plastic strain in STZ transition

ω_v elementary increment of plastic strain in STZ creation or destruction

$\tilde{\Gamma}_{ij}$ loading strength tensor

d_{ij} unit deviatoric tensor with major principal direction in the direction of vibration

Γ_v, Γ_d mechanical noise strength components

$W_{vol}^{pl}, W_{dev}^{pl}, W^{pl}$ volumetric, deviatoric, and total plastic strain energies, respectively

ξ_v, ξ_d coefficients of mechanical noise strength

p_0 unit pressure

p mean stress

Δq shear resistance reduction

q_0 initial deviatoric stress level

E_V density of vibrational energy

E_F density of energy dissipateon

A_0 coefficient of vibrational noise strength

e_z formation energy

$\dot{\varepsilon}_a$ loading rate

χ configurational temperature

χ^{eq} value of χ in steady equilibrium without vibration

χ_v^{eq} value of χ in steady equilibrium when only vibration is applied

C_0 energy capacity coefficient of granular system

τ_0 inertial time scale

κ coefficient of time scale

s_c shear stress in 2D

γ, γ^{pl} total and plastic shear strains in 2D, respectively

d particle size

ρ_g material density

σ_c confining pressure

$\tilde{\Gamma}$ attempt frequency in 2D

Γ mechanical strength

λ vibrational noise strength

V volume of the material

η coefficient of configuration temperature

v_v volume of the plastic core of STZ

v_g occupied particle volume

References

Argon, A. S. (1979). Plastic deformation in metallic glasses. Acta metall., 27(1), 47-58.

Barkan, D. D. (1962). Dynamics of bases and foundations, Trans. L. Drashevska, McGraw-Hill, New York, 207–210.

Bingham, C. M., Stone, D. A., Schofield, N., Howe, D., & Peel, D. (2000). Amplitude and frequency control of a vibratory pile driver. IEEE Transactions on Industrial Electronics, 47(3), 623-631.

Bouchbinder, E., & Langer, J. S. (2009a). Nonequilibrium thermodynamics of driven amorphous materials. I. Internal degrees of freedom and volume deformation. Physical Review E, 80(3), 031131.

Bouchbinder, E., & Langer, J. S. (2009b). Nonequilibrium thermodynamics of driven amorphous materials. II. Effective-temperature theory. Physical Review E, 80(3), 031132.

Bouchbinder, E., & Langer, J. S. (2009c). Nonequilibrium thermodynamics of driven amorphous materials. III. Shear-transformation-zone plasticity. Physical Review E, 80(3), 031133.

Daniels, K. E., & Behringer, R. P. (2005). Hysteresis and competition between disorder and crystallization in sheared and vibrated granular flow. Physical review letters, 94(16), 168001.

Daniels, K. E., & Behringer, R. P. (2006). Characterization of a freezing/melting transition in a vibrated and sheared granular medium. Journal of Statistical Mechanics: Theory and Experiment, 2006(07), P07018.

Daub, E. G., & Carlson, J. M. (2010). Friction, fracture, and earthquakes. Annu. Rev. Condense Matter Phys., 1(1), 397-418.

Di Toro, G., Hirose, T., Nielsen, S., Pennacchioni, G., & Shimamoto, T. (2006). Natural and experimental evidence of melt lubrication of faults during earthquakes. science, 311(5761), 647-649.

Edwards, S. F., & Grinev, D. V. (1998). Statistical mechanics of vibration-induced compaction of powders. Physical Review E, 58(4), 4758.

Eyring, H. (1936). Viscosity, plasticity, and diffusion as examples of absolute reaction rates.

Falk, M. L., & Langer, J. S. (1998). Dynamics of viscoplastic deformation in amorphous solids. Physical Review E, 57(6), 7192.

Ferdowsi, B., Griffa, M., Guyer, R. A., Johnson, P. A., Marone, C., & Carmeliet, J. (2014). Three-dimensional discrete element modeling of triggered slip in sheared granular media. Physical Review E, 89(4), 042204.

Glasstone, S., Laidler, K. J., & Eyring, H. (1941). The theory of rate processes; the kinetics of chemical reactions, viscosity, diffusion and electrochemical phenomena (No. 541.39). McGraw-Hill Book Company.

Griffa, M., Ferdowsi, B., Guyer, R. A., Daub, E. G., Johnson, P. A., Marone, C., & Carmeliet, J. (2013). Influence of vibration amplitude on dynamic triggering of slip in sheared granular layers. Physical Review E, 87(1), 012205.

Haff, P. K. (1986). A physical picture of kinetic granular fluids. Journal of Rheology, 30(5), 931-948.

Hosoi, A. E., & Goldman, D. I. (2015). Beneath our feet: strategies for locomotion in granular media. Annu. Rev. Fluid Mech, 47(1), 431-453.

Jaeger, H. M., Liu, C. H., & Nagel, S. R. (1989). Relaxation at the angle of repose. Physical Review Letters, 62(1), 40.

Jaeger, H. M., Nagel, S. R., & Behringer, R. P. (1996). Granular solids, liquids, and gases. Reviews of modern physics, 68(4), 1259.

Jiang, Y., & Liu, M. (2017). Why granular media are thermal, and quite normal, after all. The European Physical Journal E, 40(1), 1-16.

Jop, P., Forterre, Y., & Pouliquen, O. (2006). A constitutive law for dense granular flows. Nature, 441(7094), 727-730.

Kamrin, K. & Bouchbinder, E. (2014) Two-temperature continuum thermomechanics of deforming amorphous solids. Journal of the Mechanics and Physics of Solids, 73, 269–288.

Kothari, K. R., & Elbanna, A. E. (2017). Localization and instability in sheared granular materials: Role of friction and vibration. Physical Review E, 95(2), 022901.

Kuhn, M. R. (1999). Structured deformation in granular materials. Mechanics of materials, 31(6), 407-429.

Langer, J. S. (2008). Shear-transformation-zone theory of plastic deformation near the glass transition. Physical Review E, 77(2), 021502.

Langer, J. S., & Manning, M. L. (2007). Steady-state, effective-temperature dynamics in a glassy material. Physical Review E, 76(5), 056107.

Langer, J. S., & Pechenik, L. (2003). Dynamics of shear-transformation zones in amorphous plasticity: Energetic constraints in a minimal theory. Physical Review E, 68(6), 061507.

Lieou, C. K., Elbanna, A. E., & Carlson, J. M. (2014). Grain fragmentation in sheared granular flow: Weakening effects, energy dissipation, and strain localization. Physical Review E, 89(2), 022203.

Lieou, C. K., Elbanna, A. E., Langer, J. S., & Carlson, J. M. (2015). Stick-slip instabilities in sheared granular flow: The role of friction and acoustic vibrations. Physical Review E, 92(2), 022209.

Mehta, A., & Edwards, S. F. (1989). Statistical mechanics of powder mixtures. Physica A: Statistical Mechanics and its Applications, 157(3), 1091-1100.

Melosh, H. J. (1987). The mechanics of large rock avalanches: Geological Society of America Review in Engineering Geology, v. 7.

Melosh, H. J. (1996). Dynamical weakening of faults by acoustic fluidization. Nature,

379(6566), 601-606.

Mitchell, J. K. (1964). Shearing resistance of soils as a rate process. Journal of Soil Mechanics & Foundations Div, 90(Proc. Paper 3773).

Mitchell, J. K., & Soga, K. (2005). Fundamentals of soil behavior (Vol. 3). New York: John Wiley & Sons.

Moriyasu, S., Kobayashi, S. I., & Matsumoto, T. (2018). Experimental study on friction fatigue of vibratory driven piles by in situ model tests. Soils and foundations, 58(4), 853-865.

Nicot, F., Veylon, G., Zhu, H., Lerbet, J., & Darve, F. (2016). Mesoscopic scale instability in particulate materials. Journal of Engineering Mechanics-ASCE, 142(8), 1-12.

Nicot, F., Xiong, H., Wautier, A., Lerbet, J., & Darve, F. (2017). Force chain collapse as grain column buckling in granular materials. Granular Matter, 19(2), 1-12.

Ogawa, S. (1978). Multitemperature theory of granular materials. In Proc. of the US-Japan Seminar on Continuum Mechanical and Statistical Approaches in the Mechanics of Granular Materials, 1978 (pp. 208-217). Gakajutsu Bunken Fukyu-Kai.

O'Neill, M. W., Vipulanadan, C., & Wong, D. O. (1990). Evaluation of bearing capacity of vibro-driven piles from laboratory experiments. Transportation Research Record, (1277).

Pechenik, L. (2005). Dynamics of shear-transformation zones in amorphous plasticity: Nonlinear theory at low temperatures. Physical Review E, 72(2), 021507.

Sharpe, S. S., Kuckuk, R., & Goldman, D. I. (2015). Controlled preparation of wet granular media reveals limits to lizard burial ability. Physical Biology, 12(4), 046009.

Taslagyan, K. A., Chan, D. H., & Morgenstern, N. R. (2016). Vibrational fluidization of granular media. International Journal of Geomechanics, 16(3), 04015080

Tordesillas, A., O'Sullivan, P., & Walker, D. M. (2010a). Evolution of functional connectivity in contact and force chain networks: Feature vectors, k-cores and minimal cycles. Comptes Rendus Mécanique, 338(10-11), 556-569.

Tordesillas, A., Walker, D. M., & Lin, Q. (2010b). Force cycles and force chains. Physical Review E, 81(1), 011302.

Uzuoka, R., Sento, N., Kazama, M., & Unno, T. (2005). Landslides during the earthquakes on May 26 and July 26, 2003 in Miyagi, Japan. Soils and Foundations, 45(4), 149-163.

Viking, K. (2002). Vibro-driveability-a field study of vibratory driven sheet piles in non-cohesive soils (Doctoral dissertation, Byggvetenskap).

Xie, T., Guo, P., & Stolle, D., (2022). Mechanism of vibration-induced shear resistance reduction of granular soils: theoretical aspects. Continuum Mechanics and Thermodynamics. (Under review)

Zhu, H., Nicot, F., & Darve, F. (2016a). Meso-structure organization in two-dimensional granular materials along biaxial loading path. International Journal of Solids and Structures, 96, 25-37.

Zhu, H., Nicot, F., & Darve, F. (2016b). Meso-structure evolution in a 2D granular material during biaxial loading. *Granular Matter*, 18(1), 1-12.

Chapter 5 Thermodynamic basis of the extended STZ model (Paper 4)

Thermodynamic basis of granular STZ model and its application in exploring shear resistance reduction mechanisms in vibrated granular soils

Continuum Mechanics and Thermodynamics, *1-15*

Tao Xie[1], Peijun Guo[1], Dieter Stolle[1]

[1]Department of Civil Engineering, McMaster University, 1280 Main St W, Hamilton, ON, L8S 4L7, Canada

Abstract: The granular shear-transformation-zone (STZ) model is an energy-based constitutive model for studying granular materials subjected to vibration. This paper provides a detailed analysis of the thermodynamic foundation of the granular STZ model and applies it to investigate the mechanism of vibration-induced shear resistance reduction (ViSRR) in granular soils. Firstly, using the principles of thermodynamics, an energy conversion equation for a mechanical-energy-governed granular soil system is derived, accounting for vibration energy, configurational energy, strain energy, and contact energy dissipation. Then, by incorporating the critical state concept from soil mechanics, the energy conversion function is used to develop the evolution law of configurational temperature, one of the three governing functions of the granular STZ model. The analysis shows that ViSRR is influenced by the rate of strain energy development and the input rate of vibration energy, and that a limitation in soil deformation during vibration is necessary for ViSRR to occur. Furthermore, the contact energy dissipation arising from inelastic contact deformation and particle collisions

contributes to enhancing a granular soil's shear resistance by absorbing part of the external energy applied to the soil.

Keywords: thermodynamic basis; mechanism; shear resistance reduction; granular STZ model; vibration; granular materials

1. Introduction

Vibration-induced shear resistance reduction (ViSRR) of granular material refers to a granular material under vibration that loses shear resistance without invoking obvious excessive pore pressure. It is different from the liquefaction of saturated sands, for which the decline in the effective stress as the result of excess pore pressure is recognized as the dominant mechanism (Vanden Berghe et al., 2001; Hwang, et al., 2001; Pestana et al., 2002; Osinov, 2013). The ViSRR has been observed in various engineering disciplines, including geotechnical engineering (Taslagyan et al., 2015 & 2016), rock engineering and mining (Melosh, 1987), bulk material transport (Ringer & Mujumdar, 1983), and earthquake engineering (Griffa et al., 2013). Although such shear strength reduction can be of benefit to engineering practice, it also has detrimental consequences. It is often regarded as the main source of some long-runout landslides of dry soil on the moon and Mars (Melosh, 1987), as well as on the Earth (Uzuoka, et al., 2005). For example, ViSRR can cause fault weakening of rocks during earthquake initiation (Griffa et al., 2013) and triggering of avalanches (Melosh, 1996). Vibratory driving is a common method in geotechnical engineering for installing or extracting piles. Compared with jacked piles, vibro-driven piles can penetrate sandy soils more easily given that vibration significantly reduces shaft and toe resistance during installation (O'Neill et al., 1990; Bingham et al., 2000; Viking, 2002; Moriyasu et al., 2018). Vibratory compaction of loose sandy soil also takes advantage of ViSRR, since soil particles can move more easily. Interestingly, during the long course of evolution, some animals also mastered the skill of taking advantage of reducing the shear resistance of cohesionless soils via vibration. For example, ocellated skinks exploit head oscillation to minimize the resistance during boring (Hosoi & Goldman, 2015; Sharpe et al., 2015).

Experimental studies on the ViSRR of granular soils began more than half a century ago. The studies were first conducted using direct shear equipment mounted on a vibrational platform (Krey, 1932; Barkan, 1962; Youd, 1967). Taslagyan et al. (2015 &

2016) investigated the shear resistance reduction of sand by modifying a direct shear apparatus. To overcome the shortcomings of the direct shear apparatus, e.g., non-uniform stress distribution and localized shear deformation, Xie and Guo (2021) built a modified triaxial apparatus in which a coil voice actuator was added to superimpose high-frequency vibration in the vertical direction to the specimen in a conventional strain-controlled triaxial test. The test results obtained from this modified triaxial apparatus demonstrated that shear resistance reduction can be induced by vibration in addition to the compressive volumetric strain (Xie et al., 2022a). It was observed that strong vibration can cause granular soil at an air-dried condition to completely lose its shear resistance and behave like a fluid.

Several conceptual models have been proposed with various hypotheses based on experimental observations to explain ViSRR. Barkan (1962) suggested that ViSRR is caused by "dry" friction reduction induced by intense vibrations, and the behavior of cohesionless soil during vibration is dominated by velocity-dependent "viscous" friction. Blekhman (2000) proposed the concept of "vibrational force" having the "nature of viscous friction" for vibrated granular materials. However, there is still a lack of physical evidence supporting the occurrence of "viscous" friction. Denies and Holeyman (2007) proposed the concept of "shaking pressure" to interpret the ViSRR of dry sand. They assumed that the effect of "shaking pressure" was similar to that of excess pore pressure that reduces the "effective normal pressure". However, this "shaking pressure" is difficult to quantity since its physical meaning is not clear. Internal structure change has also been identified as a reason for ViSRR. In particular, it has been suggested that "horizontal soil arches" develop around a vibro-driven pile due to its irregular movements during installation (Heerema, 1978; White & Lehane, 2004; Moriyasu et al., 2018). Such soil arches could reduce the horizontal (normal) pressure acting on the pile and hence the shaft resistance. However, the existence of the horizontal soil arches surrounding the pipe has not been confirmed, and this hypothesis cannot explain the toe resistance reduction induced by vibration.

The behavior of granular materials subject to vibration has also been investigated numerically via the discrete element method (DEM) which can provide insight into the evolution of internal structure and the influence of the interaction between particles. In a series of DEM simulations on granular assemblies subjected to vibration, Denies (2010) observed that a decrease in both contact force and contact lifetime interrupted force chains of vibrated granular soil. This prevented the shear stress from no longer being transmitted effectively. Moreover, Ferdowsi et al. (2014) found that acceleration above a threshold caused early slip at particle contacts. With an increase in vibration intensity, more slip events and increased activity were observed to follow. In this process, a dramatic fall in coordination number was observed by Ferdowsi et al. (2015) during a transition from a "stick phase" to a "slip phase". Besides the weakening of the contact force network, which depended on the state of the assembly, the patterns of energy release owing to slipping at particles were observed to be different in the transition process between the phases. Even though this phenomenon was observed in DEM simulations, it is difficult to describe the transition at particle contacts mathematically. The details of the transitions have also been difficult to verify via physical tests directly. As a result, it has been challenging to correlate the internal energy change with the shear resistance reduction explicitly.

Another approach to studying ViSRR is to apply the basic principles of thermodynamics (Edwards & Oakeshott, 1989; Edwards & Grinev, 1998; Kremer, 2010; Bouchbinder & Langer, 2009a & 2019b) such has been done to investigate the behavior of various materials including metallic glasses and amorphous solids (Falk & Langer, 1998; Urata, 2018; Fierro et al., 2002), power materials (Jaeger et al., 1996; Kothari & Elbanna, 2017), and unsaturated soil (Zhao et al., 2019). In contrast to material behaviours on the molecular scale where thermal energy plays a dominant role, a granular material can be treated as an athermal granular system, with its behavior being primarily governed by kinetic energy and strain energy. For an athermal granular system, it is necessary to introduce some analogous intensive thermodynamic

parameters such as “effective temperature” to represent the internal disorder of the material, especially when the material is subjected to a combination of dynamic and quasi-static loadings. Mehta and Edwards (1989) constructed a formalism to substitute the conventional framework of thermodynamics. In their formalism, the concept of “compactivity χ” was adopted to play the same role as the temperature in classical thermodynamics, with $\chi = 0$ for the most compact powders and $\chi = \infty$ for the least compact.

Moreover, to deal with the collision of particles induced by dynamic loading together with the overriding of particles and sliding at particle contacts, which are mainly induced by quasi-static loading, a granular system can be decomposed into two subsystems (Haff, 1986): a kinetic subsystem and a configurational subsystem (or frictional subsystem). In a kinetic-governed system consisting of sufficiently dispersed grains, the transitions of quantities such as energy and momentum are mainly via the collisions of particles. On the other hand, in a configuration-governed system, the transitions of these quantities are mostly via sliding and overriding that depend on the shear force or low-amplitude vibration. By introducing an energy reservoir for more rigorous derivations in the framework of thermodynamics, Bouchbinder and Langer (2009b) extended the approach of Haff (1986) to the development of shear-transformation-zone (STZ) model (Falk & Langer, 1998), which is an energy-based physical model correlating the plastic macroscopic strain to the evolution of internal mesostructure of material. Recently, the conventional STZ model was further extended to soil mechanics to deal with shear resistance reduction of granular soils subjected to vibration and quasi-static shearing synchronously (Xie et al., 2022b & 2023).

This paper, which builds on the previous experimental research presented in the reference (Xie et al., 2022a), provides a theoretical foundation for the development of the granular STZ model (Xie et al., 2022b). It explores the mechanism of ViSRR in granular soils from the viewpoint of energy. The layout of this paper is as follows: Firstly, based on the work of Haff (Haff, 1986), and Bouchbinder and Langer (2009b),

a thermodynamic model of an athermal granular system is established. The evolution law of configurational temperature is then established as one of the three governing functions of the granular STZ model. The influence of vibration and contact energy dissipation resulting from inelastic deformation at particle contacts on the shear resistance of granular soils is discussed to examine the mechanism of ViSRR.

2. Thermodynamic model of a granular soil system

To explore the underlying mechanism of ViSRR from an energy aspect within a granular system that is subjected to vibration and quasi-static loading simultaneously, the energy conversion among different types of energy must be clarified, including vibration energy, work done by quasi-static forces, and contact energy dissipation induced by inelastic deformation at particle contact that plays a very important role in a granular soil's behavior.

2.1 Model assumptions

To construct a thermodynamic model for an athermal granular system subjected to combined static shearing and vibration, the following assumptions are adopted:

(1) Granular materials are compacted granular assemblies, in which the transitions of energy, momentum, and other relevant quantities are mainly through overriding and sliding among particles (Haff, 1986). Particle collisions and the corresponding kinetic energy are at a very low level.

(2) The granular system can be decomposed into two subsystems (Bouchbinder & Langer, 2009b; Haff, 1986): a configurational subsystem (CS) and a kinetic subsystem (KS). Each of these two subsystems has a "granular temperature" (in energy unit): configurational temperature χ and kinetic temperature (θ_K) that describe the internal disorder of the CS and KS subsystems, respectively. In addition, the kinetic and configurational subsystems are weakly coupled in that the KS can affect the internal variables $\{\Lambda_\alpha\}$ (α=1, 2, 3…) of CS via energy exchange; however, KS itself is

independent of the internal variables of CS.

Within the framework of thermodynamics, the configurational temperature χ reflects the energy involved in the potential capability of a granular configuration change, while the kinetic temperature θ_K reflects kinetic energy that is a function of the square of the particle's velocity fluctuation around the mean velocity (Haff, 1986; Jaeger et al., 1996). It is noted that χ and θ_K are analogous in concept but are different in scale with respect to the regular thermal temperature (θ_T). Specifically, χ and θ_K quantify the mechanical energy at the particle scale, while θ_T quantifies the thermal energy at the molecular scale. It is known that the mechanical energy is much larger than thermal energy for granular soils at room temperature (Jaeger et al., 1996), implying the configurational temperature χ and kinetic temperature θ_K are much higher than the thermal temperature θ_T.

(3) To maintain a kinetic temperature θ_K, the granular soil must transform some of the vibration energy to compensate for the energy dissipation. To account for the vibrational energy of the soil and the contact energy dissipation in the CS, we introduce a vibration container (VC) and a thermal reservoir (TR) into the granular system, as illustrated in Figure 1. The VC and the TR are used as a source of vibration energy and storage for the energy dissipated from the inelastic contact deformation of particles. Referring to Figure 1, the "External Work" corresponds to the strain energy performed by the external forces.

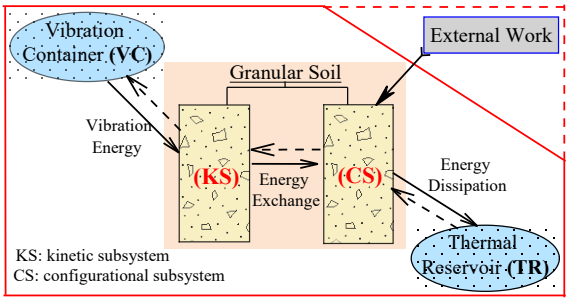

Figure 1. Thermodynamic model of an athermal granular system

(4) The total internal energy U_{tot} of the whole system including VC, KS, CS, and TR is

$$U_{tot} = U_C(S_C, \varepsilon_{ij}^{el}, \Lambda_\alpha) + U_K(S_K) + U_V(S_V) + U_T(S_T) \quad (1)$$

in which U_C, U_K, U_V, and U_T are the internal energies in CS, KS, VC, and TR, respectively; S_C, S_K, S_V, S_T are the respective entropies; ε_{ij}^{el} represents the elastic strain tensor; and Λ_α (α=1, 2, 3…) corresponds to a set of internal variables of the granular system. The variation of Λ_α is the only source of plastic strains in the system. It is noted that the CS, KS, and TR belong to a part of the granular system, while the VC is only used to provide vibration energy from outside of the granular system.

It is noted that we have two categories of energy dissipation in a granular soil system. One is "frictional energy dissipation", i.e., the plastic strain energy, which involves the plastic deformation process of a soil assembly (e.g., the change of voids within the assembly). Another is "contact energy dissipation" or called "contact dissipation" due to inelastic contact deformations in individual soil particles, which has no direct relation with the deformation of the granular soil assembly.

2.2 Energy conservation

The time rate of $U_C(S_C, \varepsilon_{ij}^{el}, \Lambda_\alpha)$ can be represented by

$$\dot{U}_C = \chi \dot{S}_C + \sigma_{ij} \dot{\varepsilon}_{ij}^{el} + \sum \frac{\partial U_C}{\partial \Lambda_\alpha} \dot{\Lambda}_\alpha \quad (2)$$

with

$$\chi = \frac{\partial U_C}{\partial S_C}, \ \sigma_{ij} = \frac{\partial U_C}{\partial \varepsilon_{ij}^{el}} \quad (3)$$

and the superposed dot implying rate and repeated indices denoting summation. The second term on the right-hand side of Eq. (2) is the time rate of elastic strain energy

with $\dot{\varepsilon}_{ij}^{el}$ and σ_{ij} denoting the rates of elastic strain and stress, respectively. Similarly, the time rates of U_K, U_V, U_T are expressed as

$$\dot{U}_K = \frac{\partial U_K}{\partial S_K}\dot{S}_K = \theta_K \dot{S}_K, \quad \dot{U}_V = \frac{\partial U_V}{\partial S_V}\dot{S}_V = \theta_V \dot{S}_V, \quad \dot{U}_T = \frac{\partial U_T}{\partial S_T}\dot{S}_T = \theta_T \dot{S}_T \tag{4}$$

where θ_K, θ_V, θ_T are temperatures in terms of energies of KS, VC, and TR, respectively. It is important to recognize that they are different from the granular thermal temperature.

According to the first law of thermodynamics (Bouchbinder & Langer, 2009b), the rate of total internal energy $\dot{U}_{tot}$ is equal to the rate of work $\dot{W} = \sigma_{ij}\dot{\varepsilon}_{ij}$ done by stresses induced by an applied external force. For small strain problems, $\dot{\varepsilon}_{ij} = \dot{\varepsilon}_{ij}^{pl} + \dot{\varepsilon}_{ij}^{el}$ with the superscripts "pl" and "el" standing for the elastic and plastic components respectively. As a result, the energy conservation equation without environmental temperature variation is expressed as

$$\dot{U}_{tot} = \sigma_{ij}\dot{\varepsilon}_{ij} = \sigma_{ij}\dot{\varepsilon}_{ij}^{pl} + \sigma_{ij}\dot{\varepsilon}_{ij}^{el} \tag{5}$$

Rewriting Eq. (5) with a combination of Eqs. (1), (2), and (4), the energy conservation law becomes

$$(\dot{U}_C - \sigma_{ij}\dot{\varepsilon}_{ij}) + \theta_K \dot{S}_K + \theta_V \dot{S}_V + \theta_T \dot{S}_T = 0 \tag{6}$$

By applying $\dot{\varepsilon}_{ij}^{el} = \dot{\varepsilon}_{ij} - \dot{\varepsilon}_{ij}^{pl}$ into Eq. (2), one has

$$\dot{U}_C - \sigma_{ij}\dot{\varepsilon}_{ij} = \chi \dot{S}_C + \sum \frac{\partial U_C}{\partial \Lambda_\alpha}\dot{\Lambda}_\alpha - \sigma_{ij}\dot{\varepsilon}_{ij}^{pl} \tag{7}$$

As a result, Eq. (6) becomes

$$\theta_K \dot{S}_K + \theta_V \dot{S}_V + \theta_T \dot{S}_T + \chi \dot{S}_C - \dot{W}_C = 0 \tag{8}$$

in which

$$\dot{W}_C = \sigma_{ij}\dot{\varepsilon}_{ij}^{pl} - \sum \frac{\partial U_C}{\partial \Lambda_\alpha}\dot{\Lambda}_\alpha \tag{9}$$

2.3 Increase of entropy

According to the second law of thermodynamics, the entropy variation of a system must be non-negative (Bouchbinder & Langer, 2009b), *i.e.*,

$$\dot{S}_{\mathrm{C}} + \dot{S}_K + \dot{S}_V + \dot{S}_T \geq 0 \tag{10}$$

Eliminating $\dot{S}_C$ in the Inequality (10) using Eq. (8) yields

$$\left(\frac{\chi}{\theta_K} - 1\right)\left(\theta_K \dot{S}_K + \frac{\theta_K}{\theta_V}\dot{U}_V\right) + \left(\frac{\chi}{\theta_T} - 1\right)\dot{U}_T + \left(\frac{\theta_K}{\theta_V} - 1\right)\dot{U}_V + \dot{W}_C \geq 0 \tag{11}$$

The left side of the Inequality (11) describes the energy exchange among subsystems. Eq. (10) is satisfied when

$$\left(\frac{\chi}{\theta_K} - 1\right)\left(\theta_K \dot{S}_K + \frac{\theta_K}{\theta_V}\dot{U}_V\right) \geq 0 \tag{12}$$

$$\left(\frac{\chi}{\theta_T} - 1\right)\dot{U}_T \geq 0 \tag{13}$$

$$\left(\frac{\theta_K}{\theta_V} - 1\right)\dot{U}_V \geq 0 \tag{14}$$

$$\dot{W}_C = \sigma_{ij}\dot{\varepsilon}_{ij}^{pl} - \sum \frac{\partial U_C}{\partial \Lambda_\alpha}\dot{\Lambda}_\alpha \geq 0 \tag{15}$$

It should be noted that Inequality (12) illustrates the energy flux between CS and KS; Inequality (13) illustrates the energy flux between CS and TR; and Inequality (14) illustrates the energy flux between KS and VC. The relations in (12)~ (14) provide sufficient but not necessary conditions for the second law of thermodynamics, which means tahr the energy transition among different subsystems is unique in this model, as shown in Figure 1. Following Bouchbinder & Langer (2009b), we write

$$\theta_K \dot{S}_K + \frac{\theta_K}{\theta_V}\dot{U}_V = -\mathrm{A}\left(1 - \frac{\chi}{\theta_K}\right) = -\dot{Q}_{KC} \tag{16}$$

$$\dot{U}_T = -\mathrm{D}\left(1 - \frac{\chi}{\theta_T}\right) = \dot{E}_F \tag{17}$$

$$\dot{U}_V = \mathrm{B}\frac{\theta_V}{\theta_K}\left(1 - \frac{\theta_K}{\theta_V}\right) \tag{18}$$

in which *A*, *B*, *D* are non-negative transport coefficients, Q_{KC} is the energy transferred from KS to CS, E_F is the energy flowing from CS to TR. Physically, E_F is the energy

dissipated due to the inelastic contact deformation of particles in this model. It is emphasized that the dissipation E_F has nothing to do with the arrangement of particles or plastic deformation of the granular soil. It is related to the inelasticity of particles and has been excluded from plastic strain energy W^{pl} and needs to be considered separately.

According to the definition of heat capacity in KS, the relation between $\dot{S}_K$ and $\dot{\theta}_K$ can be expressed as:

$$\theta_K \dot{S}_K = C_K \dot{\theta}_K \tag{19}$$

in which C_K is the coefficient of heat capacity per unit volume. Inserting Eq. (19) into Eq. (16) and eliminating $\dot{U}_V$ using Eq. (18), the equation in KS is determined as

$$C_K \dot{\theta}_K = \mathrm{B}\left(1 - \frac{\theta_K}{\theta_V}\right) + \mathrm{A}\left(1 - \frac{\chi}{\theta_K}\right) = \dot{E}_V - \dot{Q}_{KC}, \text{ with } \dot{E}_V = \mathrm{B}\left(1 - \frac{\theta_K}{\theta_V}\right) \tag{20}$$

where E_V is the vibration energy entering KS from VC. It is assumed (Bouchbinder & Langer, 2009b) that the VC is strong enough to provide vibration energy input for KS consistently and therefore maintain a stable kinetic temperature ($\dot{\theta}_K = 0$) in Eq. (20). This also implies that the magnitude of the transport coefficient 'B' is very large to ensure $\dot{E}_V > 0$ at $\theta_K \approx \theta_V$ (Bouchbinder & Langer, 2009b). Similar to Eq. (19), the heat capacity in CS is defined via

$$\chi \dot{S}_C = C_0 \dot{\chi} \tag{21}$$

with C_0 being the coefficient of heat capacity per unit volume. Using this definition with a combination of Eqs. (16), (17), (8), and $\theta_K \approx \theta_V$, the evolution of configurational temperature χ in the CS is expressed as

$$C_0 \dot{\chi} = \sigma_{ij} \dot{\varepsilon}_{ij}^{pl} - \sum \frac{\partial U_C}{\partial \Lambda_\alpha} \dot{\Lambda}_\alpha + \dot{Q}_{KC} - \dot{E}_F \tag{22}$$

Owing to $\dot{\theta}_K = 0$ in Eq. (20), we have $\dot{E}_V = \dot{Q}_{KC}$. Eq. (22) can now be rewritten as

$$C_0\dot{\chi}+\dot{H}_\alpha=\dot{W}^{pl}+\dot{E}_V-\dot{E}_F,\ \text{ with } \dot{H}_\alpha=\sum\frac{\partial U_C}{\partial\Lambda_\alpha}\dot{\Lambda}_\alpha,\quad \dot{W}^{pl}=\sigma_{ij}\dot{\varepsilon}_{ij}^{pl} \tag{23}$$

with $\dot{W}^{pl}$ denoting the rate of plastic strain energy. This relationship describes the energy transformation within the configurational subsystem. It should be emphasized that terms in Eq. (23) are not independent.

For granular soils, external disturbances (such as vibrations and rotations) tend to cause size segregation of particles (Jaeger et al., 1996; Asmaei et al., 2018). Intuitively, the segregation appears to violate the basic law of thermodynamics (the increase of entropy principle) since a system normally favours mixing (*i.e.*, increased disorder). Although the size segregation of the particles implies a decrease in the configurational entropy S_C (or configurational degree of freedom), the more significant increase in thermal entropy S_T due to the frictional energy dissipation during segregation, ensures the growth of the total entropy of the granular system, as implied in Inequality (10). Note that we attempted here to qualitatively explain the particle segregation of particles from perspectives of entropy increase. Further intensive research is still needed regarding the specific mechanism and details of particle segregation.

3. Mechanism of ViSRR at critical state

In the previous section, we explained the energy constituents and their transitions within a granular soil system based on thermodynamics. In this section, we will focus on the mechanism of ViSRR in granular soils from an energy perspective within the framework of critical state soil mechanics, with the combination of our previous experimental works. It should be noted that we use the soil mechanics sign convention where compression is considered positive in this paper.

3.1 Brief introduction of ViSRR in experiments

In this section, we provide a brief overview of the experimental investigation of ViSRR. More detailed information can be found in Xie et al., (2022a). The experiment

used a modified triaxial apparatus (Xie et al., 2021), which included a low-inertia linear voice coil actuator to apply vertical vibrations (in the direction of σ_1) to a uniform Standard Ottawa sand C-109 with a mean grain size of d_{50}=0.375 mm.

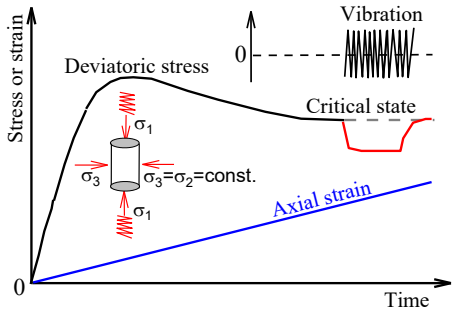

Figure 2. Loading scheme of the test under drained triaxial stress conditions

As shown in Figure 2, a specimen under drained conditions was subjected to monotonic loading with a fixed axial strain rate and constant effective confining pressure of 50 kPa (σ_2=σ_3=const.). A vibration was applied when the soil was approaching the critical state. This means that the soil specimen was subjected to both vibration and monotonic shearing simultaneously. In some tests, two or three individual vibrations with various intensities were applied to the same specimen with a certain period of interval.

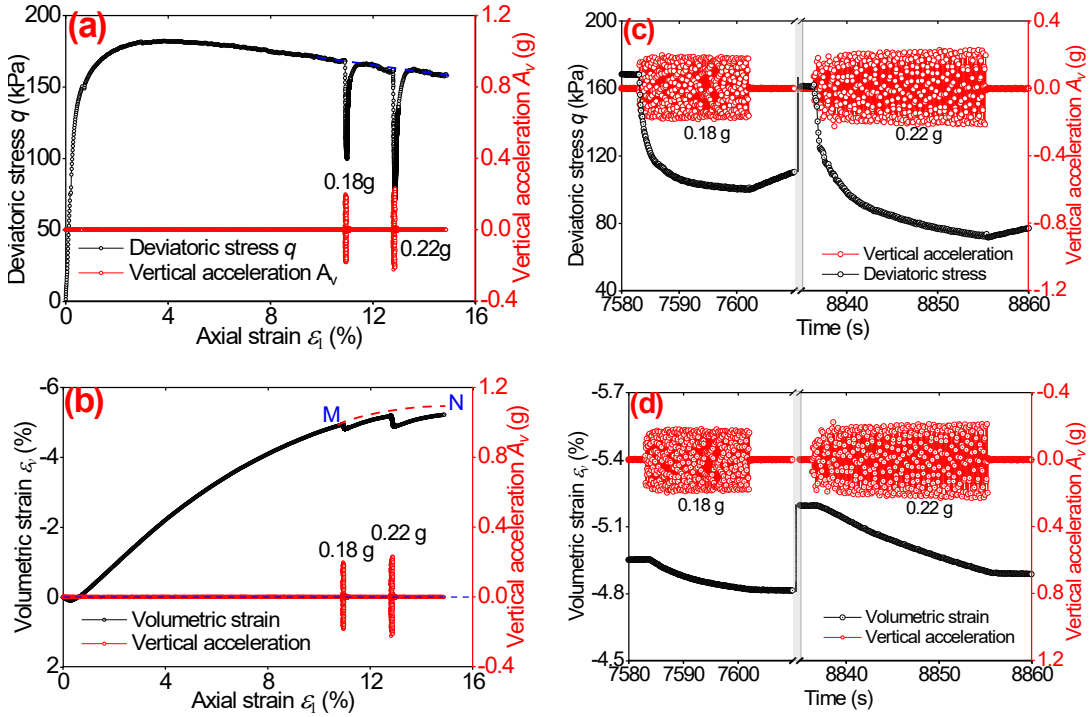

Figure 3. ViSRR of Ottawa sand in test with a vibration frequency of 60 Hz: (a) deviatoric stress; (b) volumetric strain; (c) time history of deviatoric stress during vibrations; (d) time history of volumetric strain during vibrations (Xie et al., 2022a)

Figure 3 illustrates the responses of dense soil with an initial void ratio of 0.59. Two individual vibrations with different intensities were applied to the specimen at the critical state, with a vibration frequency of 60 Hz. The vertical acceleration (A_v) was measured using an accelerometer attached to the loading rod and can be considered as an indicator of the vibration intensity at the same frequency. It can be observed that there is an immediate drop in the deviatoric stress (q=σ_1-σ_3) as soon as the vibration is applied, which reaches a plateau with the continuation of vibration, as shown in Figure 3(b). The deviatoric stress q returns to its original level under the monotonic shearing once the vibration is stopped. A comparison of the two vibrations in Figure 3(b) shows that the greater the vibration intensity (A_v), the greater the reduction in shear resistance (q). In addition, a compression in the volumetric strain (ε_v =ε_1+2ε_3) is observed during the process of shear resistance reduction, as shown in Figure 3(c) and Figure 3(d).

3.2 Critical state concept and its application in revealing ViSRR mechanism

In soil mechanics, the critical state (Roscoe et al., 1985; Schofield & Wroth, 1968) is defined as a unique state at which soil undergoes continuous shear deformation with no change in stress state at constant volume and fabric. It is independent of the soil's initial density and loading history. Under drained triaxial stress conditions as shown in Figure 2, the stresses and deformation of soil at critical state satisfy $\dot{p} = \dot{q} = \dot{\varepsilon}_v = 0$ and $\dot{\varepsilon}_q \neq 0$. Herein, $p = (\sigma_1+2\sigma_3)/3$, $\varepsilon_q = 2(\varepsilon_1\text{-}\varepsilon_3)/3$ are mean stress and deviatoric strain, respectively. More generally, the stresses and strains at critical state satisfy $\dot{\sigma}_{ij} = \dot{\varepsilon}_{ij}^{el} = \mathbf{0}$, $\dot{\varepsilon}_v = \dot{\varepsilon}_v^{pl} = 0$ and $\dot{e}_{ij}^{pl} = \dot{e}_{ij}$ with $\dot{e}_{ij}^{pl}$ and $\dot{e}_{ij}$ being the rate of plastic deviatoric strain and the rate of total deviatoric strain, respectively.

In a granular soil system, the configurational temperature χ can be defined in different ways depending on the selection of the measure for system disorder. Following the works done by Falk & Langer (1998), Lemaître (2002), Mehta & Edwards (1989), χ is coined as a function of "compactivity" or "free volume" of the system, *i.e.*, the volume in excess of close packing which the particles have available for motion. Therefore, one has

$$\dot{\chi}=0 \tag{24}$$

at critical state. In other words, the configurational subsystem at critical state is in steady equilibrium.

Moreover, the variation of microscopic internal variables, as the sole source of plastic deformation of granular soils, is highly dependent on the development of plastic deformation. In other words, the rate of the internal variables $\{\dot{\Lambda}_\alpha\}$ is only determined by the rate of plastic strain $\dot{\varepsilon}_{ij}^{pl}$. Consequently, for a given $\dot{\varepsilon}_{ij}$ at critical state, $\{\dot{\Lambda}_\alpha\}$ remains constant because $\dot{\varepsilon}_{ij}^{pl} = \dot{\varepsilon}_{ij} = const.$ From the definition in Eq. (23) we know that the parameter $\dot{H}_\alpha$, which is the energy involved in the variation of internal variables, also remains constant at critical state. In other words, the changes of external

vibration $\dot{E}_V$ and contact dissipation $\dot{E}_F$ do not alter the magnitude of $\dot{H}_\alpha$ for a fixed $\dot{\varepsilon}_{ij}$ at critical state**.**

To reveal the influence of the vibration energy and contact dissipation on a granular soil's shear resistance at critical state, the following discussion is limited to the conventional triaxial stress conditions in which $\sigma_2 = \sigma_3 = const$ during the deformation process. Under triaxial stress conditions, the rate of plastic strain energy $\dot{W}^{pl}$ is determined as

$$\dot{W}^{pl} = \sigma_{ij}\dot{\varepsilon}_{ij}^{pl} = p\dot{\varepsilon}_v^{pl} + \frac{2q_c}{3}\left[\dot{\varepsilon}_1^{pl} - \frac{1}{2}\left(\dot{\varepsilon}_v^{pl} - \dot{\varepsilon}_1^{pl}\right)\right] = q_c\dot{\varepsilon}_1^{pl}, \quad \text{with } \dot{\varepsilon}_v^{pl} = \dot{\varepsilon}_v = 0 \tag{25}$$

where $\dot{\varepsilon}_1^{pl}$ is the plastic component of the axial strain rate $\dot{\varepsilon}_1$ under triaxial stress conditions, and q_c is the deviatoric stress at the critical state. Substituting Eq. (25) into Eq. (23), the variation of H_α is expressed as

$$\dot{H}_\alpha = q_c\dot{\varepsilon}_1^{pl} + \dot{E}_V - \dot{E}_F \tag{26}$$

In a typical triaxial shear test, $\dot{\varepsilon}_1^{pl} = \dot{\varepsilon}_1$ is constant at critical state. The following discussions are conducted at a constant rate of axial strain $\dot{\varepsilon}_1$ in monotonic triaxial compression as the loading scheme shown in Figure 2, which implies that the magnitude of $\dot{H}_\alpha$ remains constant.

3.3 Roles of vibration and contact dissipation in soil's shear resistance

Case 1: Monotonic shearing without considering contact dissipation

We first discuss the simplest case without vibration in which the contact energy dissipation is negligible, i.e., $\dot{E}_V = \dot{E}_F = 0$. The energy function in Eq. (26) can be simplified as

$$\dot{H}_\alpha = q_s\dot{\varepsilon}_1^{pl} = \dot{W}_s^{pl} \tag{27}$$

Here q_s is used to denote the critical deviatoric stress in Case 1.

Case 2: Monotonic shearing with considering contact dissipation

In this case, a system only undergoes contact energy dissipation E_F without vibration, i.e., $\dot{E}_V = 0$ and $\dot{E}_F \neq 0$. Eq. (26) becomes

$$\dot{H}_\alpha = q_f \dot{\varepsilon}_1^{pl} - \dot{E}_F \tag{28}$$

Herein q_f is used to denote the critical deviatoric stress in *Case 2*. As discussed previously, the contact dissipation E_F does not affect the magnitude of $\dot{H}_\alpha$ at a fixed $\dot{\varepsilon}_1^{pl}$ that equals $\dot{\varepsilon}_1$ at critical state. Substitution of Eq. (27) into Eq. (28) yields

$$\dot{E}_F = \dot{\varepsilon}_1^{pl}\left(q_f - q_s\right) \tag{29}$$

Since the contact energy dissipation $\dot{E}_F > 0$ and $\dot{\varepsilon}_1^{pl} > 0$ always hold, we have

$$q_f > q_s \tag{30}$$

which reveals that the granular soil's shear resistance q_f with the presence of $\dot{E}_F$ is always larger than q_s in the absence of $\dot{E}_F$. Thus, the contact dissipation E_F induced by the inelastic contact deformation contributes to the increase of soil's shear resistance. Physically, the difference $q_f - q_s$ is attributed to the contact dissipation partially offsetting the external work done by the quasi-static shearing or vibration, thereby resulting in a higher shear resistance of the soil.

Furthermore, the relative significance of "contact dissipation" compared to that induced by plastic deformation depends on several factors, such as vibration amplitude, vibration frequency, degrees of compaction, the angularity of particles, and stress level (Pestana & Whittle, 1995; Einav, 2007; Forterre & Pouliquen, 2008). It should be noted that the significance of contact dissipation tends to increase with higher stress levels, especially when particle crushing is involved. However, in our experimental study, the stress level is relatively low, with an effective confining pressure of 50 kPa. Therefore,

it can be estimated that the significance of contact dissipation is relatively low compared to the energy dissipation induced by plastic deformations.

Case 3: Combined monotonic shearing and vibration without contact dissipation

For a granulr soil system subjected to vibration without contact energy dissipation E_F, we have $\dot{E}_V \neq 0$ and $\dot{E}_F = 0$ Thus the energy equation Eq. (26) becomes

$$\dot{H}_\alpha = q_v \dot{\varepsilon}_1^{pl} + \dot{E}_V \tag{31}$$

in which q_v denotes the critical deviatoric stress in Case 3. Inserting Eq. (27) into Eq. (31) by considering $\dot{H}_\alpha^{case(1)} = \dot{H}_\alpha^{case(3)}$ yields

$$\frac{q_s - q_v}{q_s} = \frac{\dot{E}_V}{q_s \dot{\varepsilon}_1^{pl}} = \frac{\dot{E}_V}{\dot{W}_s^{pl}} = \frac{\dot{E}_V}{\dot{W}_s} > 0, \quad \text{thus } q_v < q_s \tag{32}$$

This implies that the imposed vibration causes a shear resistance reduction $\Delta q = q_s - q_v$ of the granular soil with the magnitude of Δq depending on the ratio of $\dot{E}_V / \dot{W}_s$. As shown in Eq. (32), the more the vibration energy input $\dot{E}_V$, the larger the shear resistance reduction Δq. This trend is supported by the experimental results as shown in Figure 3(c). The shear resistance reduction Δq increased from 70 kPa at a low vibration intensity of A_v=0.18 g to 90 kPa at a relatively high vibration intensity of A_v=0.22 g. Herein, "g" is the gravitational acceleration.

Case 4: Combined monotonic shearing and vibration with contact dissipation

In a general case, in which $\dot{E}_V \neq 0$ and $\dot{E}_F' \neq 0$, the contact dissipation rate is denoted as $\dot{E}_F'$ to distinguish it from $\dot{E}_F$ in Case 2. The presence of vibration is expected to facilitate the rate of contact dissipation induced by inelastic particle contact deformation. Thus, $\dot{E}_F'$ is larger than $\dot{E}_F$ that corresponds to no vibration. The energy function Eq. (26) is expressed as

$$\dot{H}_{\alpha}=q_g\dot{\varepsilon}_1^{pl}+\dot{E}_V-\dot{E}_F'=q_g\dot{\varepsilon}_1^{pl}+\dot{E}_V-\dot{E}_F-\Delta\dot{E}_F,\ \text{with}\ \Delta\dot{E}_F=\dot{E}_F'-\dot{E}_F>0 \quad (33)$$

Here, a subscript 'g' is used to provide a distinction between Case 4 and the previous three cases. The last term $\Delta\dot{E}_F$ in Eq. (33) reflects the influence of vibration on the magnitude of contact dissipation and $\Delta\dot{E}_F$ must be smaller than the vibrational energy itself, *i.e.*,

$$0<\Delta\dot{E}_F<\dot{E}_V \quad (34)$$

After inserting Eq. (27) into Eq. (33), we have

$$q_s\dot{\varepsilon}_1^{pl}=q_g\dot{\varepsilon}_1^{pl}+\dot{E}_V-\dot{E}_F-\Delta\dot{E}_F \quad (35)$$

Using Eq. (29) to eliminate $\dot{E}_F$ in Eq. (35) results in

$$q_f\dot{\varepsilon}_1^{pl}=q_g\dot{\varepsilon}_1^{pl}+\dot{E}_V-\Delta\dot{E}_F \quad (36)$$

Thus, from Eqs. (34) and (36) we obtain

$$\frac{\Delta q}{q_f}=\frac{q_f-q_g}{q_f}=\frac{\dot{E}_V-\Delta\dot{E}_F}{q_f\dot{\varepsilon}_1^{pl}}=\frac{\dot{E}_V-\Delta\dot{E}_F}{\dot{W}_f^{pl}}=\frac{\dot{E}_V-\Delta\dot{E}_F}{\dot{W}_f}>0 \quad (37)$$

It follows that $q_g<q_f$. Herein, q_f is the deviatoric stress when only contact dissipation is considered, with $\dot{W}_f^{pl}$ and $\dot{W}_f$ being rates of total and plastic strain energies in the absence of vibration, respectively. The vibration can cause a shear resistance reduction in the presence of contact dissipation. Except for the added term $\Delta\dot{E}_F$, which is associated with the vibration frequency and amplitude, the relative shear resistance reduction $\Delta q/q_f$ in Eq. (37) has a similar structure as that of Eq. (32) in which the contact dissipation is excluded. The increased contact dissipation $\Delta\dot{E}_F$ during vibration consumes part of vibration energy, and hence partially offsets the impact of vibration as indicated in Eq. (37).

Based on Eq. (37), it can be inferred that an increase in shear resistance, indicated by a negative value of $\Delta q/q_f$, is likely to occur when the rate of plastic strain energy becomes negative. This suggests that the granular soil subjected to vibration

experiences significant plastic dilative deformation. It is noted that this phenomenon can only occur in very dense granular soils that are subjected to a minor vibration at a non-critical state, because only in this condition can the soil undergo significant plastic dilative deformation, resulting in a negative plastic energy rate. At the critical state, the soil always satisfies $\dot{W}_f^{pl} = \dot{W}_f$.

3.4 Discussion on ViSRR mechanism and its essential preconditions

Eq. (37) reveals the essential preconditions for the emergence of shear resistance reduction in vibrated granular soils. On one hand, a continuous vibration energy input is required so that the soil can continuously deform plastically, *i.e.*, $\dot{E}_V > 0$. As witnessed in the tests shown in Figure 3, continued monotonic shearing can bring the loss of shear resistance back to its original value after the termination of vibration ($\dot{E}_V = 0$); On the other hand, the rate of the soil's deformation at the onset of vibration must be restricted, as the loading scheme adopted in the tests (see Figure 2) in which the soil's deformation was restricted by a fixed strain rate ($\dot{\varepsilon}_1$ is constant). If a granular soil can deform freely, a dramatic surge in $\dot{\varepsilon}_1$ would be expected under vibration, which would offset the vibration-induced shear resistance change. An analogous requirement is found in the stress relaxation of concrete or metal, which takes place only when the deformation of the material is restricted and free of deforming.

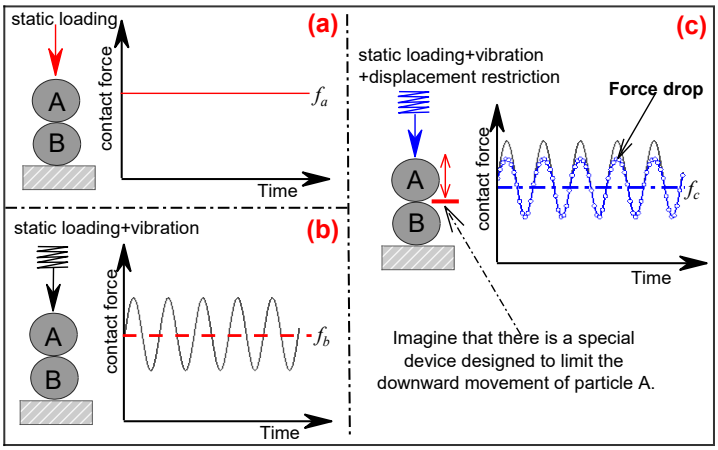

Figure 4. Mechanism of ViSRR at particle contact scale: (a) under static loading; (b) under combined static loading and vibration; (c) under combined static loading and vibration with the downward movement of particle A being restricted.

The shear resistance in granular materials originates from a combination of "static" and "dynamic" friction forces at the particle level. In densely packed granular materials subjected to slow (quasi-static) shearing or slight vibrations, as investigated in this research, the shear resistance is primarily due to mechanical interlocking and friction at the contact points between individual grains, known as static friction. On the other hand, in granular materials subjected to high shear rates or violent vibrations, the shear resistance primarily arises from particle collision and sliding during shear deformation, referred to as dynamic friction. Typically, dynamic friction is lower than static friction, as the relative motion between grains at higher velocities or under vibrations reduces mechanical interlocking and contact forces. Thus, a crossover from a dynamic friction-dominated regime to a static friction-dominated regime is considered to be the physical mechanism behind the vibro-fluidization of granular materials (Jaege et al., 1996; Melosh, 1996; Taslagyan et al., 2016). Herein, the vibro-fluidization where the shear resistance is reduced to zero can be treated as a special case of ViSRR.

Let's analyze how the contact force is diminished by studying a set of particle contacts, and explore the roles of the continuous vibration and deformation restriction in the reduction of contact force. Under static loading, as depicted in Figure 4(a), the contact force remains constant, represented by f_a. However, when a sine vibration is added to

the static loading, as shown in Figure 4(b), a fluctuating contact force around the mean value f_b is expected, where $f_b=f_a$. Additionally, if a particular device partially restricts the downward movement of the top particle "A," as depicted in Figure 4(c), the contact force would decrease compared to the case without displacement restriction when the particle moves downward, leading to a decrease in the mean contact force, i.e., $f_c<f_b=f_a$. It is evident from the variation in contact force between the two particles that deformation restriction and continuous vibration are essential conditions for the occurrence of ViSRR at the particle contact scale. Herein, we only briefly explained the mechanism of ViSRR from the perspective of a set of particle contacts. In reality, a granular soil is composed of thousands of particle contacts, and the overall response under vibrational conditions will be more complex. This requires further investigation using tools such as discrete element analysis in the future.

4. Thermodynamic basis of granular STZ model

Verifying the mechanism of ViSRR revealed in Section 3 is challenging, as the soil is subjected to high-frequency vibration and monotonic loading simultaneously during ViSRR. Therefore, we established a new theoretical constitutive model, namely, the energy-based granular STZ model (Xie et al., 2022b & 2023), to replicate the ViSRR process.

4.1 Introduction of granular STZ model

The shear-transformation-zone (STZ), which is the primary source of plastic deformation within materials, can be thought of as the "weak particle loop" in granular soils, as depicted in Figure 5. When subjected to external disturbances, such as static loading or vibration, STZs can be created, rotated, and destroyed, which together constitute the motion of STZs, leading to the corresponding plastic deformation (Xie et al., 2022b & 2023). Specifically, the rotation of STZs produces plastic shear strain, while the creation and destruction of STZs generate plastic dilative and compressive

strains, respectively. The fundamental principles of the granular STZ model, called the extended STZ model in Xie et al. (2022b), aim to convert the motion of STZs at the particle group scale into plastic strain at the representative elementary volume (REV) scale. Therefore, the granular STZ model has three sets of governing functions: the motion of STZs, the plastic strain resulting from the motion of STZs, and the evolution law of configurational temperature served as the driving energy for the motion of STZs.

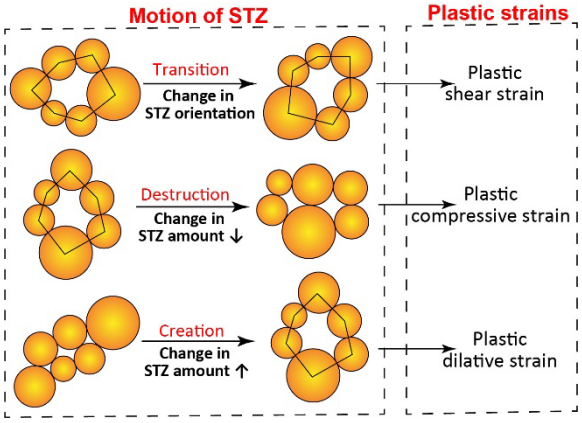

Figure 5. Basic principles of the granular STZ model (Xie et al., 2022b)

While the formula of the granular STZ model has been established (Xie et al., 2022b) and has been successfully applied to soil mechanics to study ViSRR (Xie et al., 2023), there is still a missing component in the thermodynamic fundamentals of the model, namely, the derivation of the third set of governing functions. The main goal of this section is to derive the evolution law of configurational temperature from the thermodynamics of the granular system discussed earlier.

4.2 Evolution function of configurational temperature for granular STZ model

(1) *Basic hypothesis*

The introduction of the critical state concept makes it possible to derive the evolution law of configurational temperature directly from the energy equation Eq. (23). At the non-critical state, necessary assumptions must be introduced due to variations in the stress tensor density and the fabric of the material. When choosing the compactivity or

free volume as the configurational temperature χ in a granular soil system (Falk & Langer, 1998; Lemaître, 2002; Mehta & Edwards, 1989), χ can be regarded as a function of granular material's void ratio and is supposed to be independent of contact dissipation E_F. The rationale is that the contact dissipation induced by the inelastic contact deformation and the inelastic collisions of the particles has nothing to do with the volume change of the voids in granular soils. In other words, E_F has negligible influence on soil's plastic deformation and thus does not affect the magnitude of χ. More specifically, the granular soil's deformation is mainly from the rearrangement of particles rather than the deformation of the particle itself as the result of inelastic particle contacts.

From Eqs. (23) and (24), one has

$$\dot{H}_\alpha = \dot{W}^{pl} + \dot{E}_V - \dot{E}_F, \quad @ \text{ critical state} \tag{38}$$

It is further assumed that $\dot{H}_\alpha$ in a general condition, which may be at critical state or non-critical state, can be expressed as

$$\dot{H}_\alpha = \frac{\chi}{\chi^{eq}}\left(\dot{W}^{pl} + \dot{E}_V - \dot{E}_F\right) \tag{39}$$

where χ^{eq} is the value of the configurational temperature at critical state with $\chi = \chi^{eq}$ at critical state to make sure that Eq. (39) can return to Eq. (38). A linear relationship is adopted between $\dot{H}_\alpha$ and $(\dot{W}^{pl} + \dot{E}_V - \dot{E}_F)$ in Eq. (39) with χ / χ^{eq} being used as the multiplier to ensure that χ has a fixed value of χ^{eq} at critical state, irrespective of the initial value of χ that corresponds to a soil's initial void ratio. This implies the existence of a critical void ratio in granular soils under a certain level of vibration that is independent of the soil's initial density. This assumption is in accordance with the concept of "critical state" or "vibro-critical state" (Xie et al., 2022a) for the case of vibrations. Moreover, following the discussion in Section 3, the magnitude of $\dot{H}_\alpha$ is determined by the plastic strain rate $\dot{\varepsilon}_{ij}^{pl}$. The presence or absence

of $\dot{E}_V$ and $\dot{E}_F$ only change the constituents of $\dot{H}_\alpha$ but cannot change the magnitude of $\dot{H}_\alpha$ for a given $\dot{\varepsilon}_{ij}^{pl}$. Given the above assumptions, the evolution law of χ can be derived directly from Eq. (23) instead of assuming the form of the evolution law as in the conventional STZ models (Falk & Langer, 1998).

(2) *Evolution function*

Like the strategy for exploring the mechanism of ViSRR at the critical state, the discussion here builds up from the simplest condition of $\dot{E}_V = \dot{E}_F = 0$. In this case, Eq. (23) becomes

$$C_0\dot{\chi}+\dot{H}_\alpha=\dot{W}_s^{pl} \tag{40}$$

where q_s and $\dot{W}_s^{pl}$ are the deviatoric stress and the rate of plastic strain energy at non-critical state, respectively. When combined with Eq. (39), we get

$$\dot{H}_\alpha=\frac{\chi}{\chi^{eq}}\dot{W}_s^{pl} \tag{41}$$

Consequently, the evolution of χ can be expressed as

$$C_0\dot{\chi}=\left(1-\frac{\chi}{\chi^{eq}}\right)\dot{W}_s^{pl} \tag{42}$$

In a general situation of $\dot{E}_F' \neq 0$, $\dot{E}_V \neq 0$, Eq. (23) becomes

$$C_0\dot{\chi}_v+\dot{H}_\alpha=\dot{W}_g^{pl}+\dot{E}_V-\left(\dot{E}_F+\Delta\dot{E}_F\right),\ \text{with}\ \dot{E}_F+\Delta\dot{E}_F=\dot{E}_F' \tag{43}$$

and

$$\dot{H}_\alpha=\frac{\chi_v}{\chi_v^{eq}}\left[\dot{W}_g^{pl}+\dot{E}_V-\left(\dot{E}_F+\Delta\dot{E}_F\right)\right] \tag{44}$$

The subscript "*g*" implies the general case, where required. $\chi_v=\chi$, χ_v^{eq} is value of χ in steady equilibrium when only vibration is applied. Considering that the presence of vibration changes the magnitude of the contact dissipation, $\dot{E}_F'$ is adopted. From Eqs. (41), (43), and (44), the evolution law of configurational temperature can be written as

$$C_0\dot{\chi}_v=\left(1-\frac{\chi_v}{\chi^{eq}}\right)\dot{W}_g^{pl}+\left(1-\eta\frac{\chi_v}{\chi_v^{eq}}\right)\left(\dot{E}_V-\dot{E}_F'\right) \tag{45}$$

with

$$\eta=\frac{\chi-l'\chi_v}{\chi-\left(\chi^{eq}/\chi_v^{eq}\right)l'\chi_v}>1,\quad l'=\frac{\dot{W}_g^{pl}}{\dot{W}_s^{pl}} \tag{46}$$

where $\dot{W}_g^{pl}$ is the rate of plastic strain energy in the presence of $\dot{E}_V$ and $\dot{E}_F$, and η >1. Because η varies in a small range around 1, a constant value can be adopted as a first-order approximation.

Conclusions

This study explored the thermodynamic basis of the granular STZ model and its application in understanding the mechanism of ViSRR in granular soils. The basic rules of thermodynamics were applied to an athermal granular soil system dominated by mechanical energy instead of thermal energy. The resulting energy equations during deformation include vibration energy, quasi-static work due to shear, and contact dissipation induced by the inelastic contact deformation of particles.

By utilizing the concept of "critical state" the evolution law of configurational temperature was directly derived from the energy equation. As a governing function, this evolution law provides a thermodynamic foundation for the micromechanics-based granular STZ model, which can replicate the process of ViSRR in granular soil under combined static loading and vibration. Furthermore, the roles of vibration energy and contact dissipation in a granular soil's shear resistance were discussed. The analysis reveals that:

(1) The occurrence of ViSRR requires both continuous vibration and restricted deformation rate of soils at the onset of vibration.

(2) The rate of contact dissipation due to inelastic contact deformation is proportional to the rate of plastic strain energy. The increase in contact dissipation helps offset

some of the vibration energy and thus increases the granular soil's shear resistance.

(3) Vibrations can reduce the shear resistance in granular soils if the deformation rate of soils under vibration is restricted. The relative reduction in shear resistance induced by vibration at the critical state increases with the vibration energy rate and is inversely proportional to the rate of plastic strain energy.

It should be noted that this paper is mainly based on the principles of thermodynamics and discusses the mechanism of ViSRR purely from the perspective of energy. It can only provide us with a general framework and lacks physical mechanisms, which requires further analysis from the perspective of microscopic mechanics using the discrete element method. Secondly, the regularities revealed in the paper need to be combined with experiments and subsequent theoretical analysis, e.g., the granular STZ model, which is exactly what we are currently doing.

Acknowledgments

Funding from the Natural Sciences and Engineering Research Council of Canada is greatly appreciated.

References

Asmaei, S., Shourijeh, P. T., Binesh, S. M., & Ghaedsharafi, M. H. (2018). An Experimental Parametric Study of Segregation in Cohesionless Soils of Embankment Dams. Geotechnical Testing Journal, 41(3), 473-493.

Barkan, D. D. (1962). Dynamics of bases and foundations, Trans. L. Drashevska, McGraw-Hill, New York, 207–210.

Bingham, C. M., Stone, D. A., Schofield, N., Howe, D., & Peel, D. (2000). Amplitude and frequency control of a vibratory pile driver. IEEE Transactions on Industrial Electronics, 47(3), 623-631.

Blekhman, I.I. (2000). Vibrational mechanics. World Scientific, Singapore. 509 p.

Bouchbinder, E., & Langer, J. S. (2009a). Nonequilibrium thermodynamics of driven amorphous materials. I. Internal degrees of freedom and volume deformation. Physical Review E, 80(3), 031131.

Bouchbinder, E., & Langer, J. S. (2009b). Nonequilibrium thermodynamics of driven amorphous materials. II. Effective-temperature theory. Physical Review E, 80(3),

031132.

Denies, N. (2010). Dynamic behavior of vibrated dry sand: sphere penetration experiments and discrete element modeling of vibrofluidization (Doctoral dissertation, UCL-Université Catholique de Louvain).

Denies, N., & Holeyman, A. (2017). Shear strength loss of vibrated dry sand. Soil Dynamics and Earthquake Engineering, 95, 106-117.

Edwards, S. F., & Oakeshott, R. B. S. (1989). Theory of powders. Physica A: Statistical Mechanics and its Applications, 157(3), 1080-1090.

Edwards, S. F., & Grinev, D. V. (1998). Statistical mechanics of vibration-induced compaction of powders. Physical Review E, 58(4), 4758.

Falk, M. L., & Langer, J. S. (1998). Dynamics of viscoplastic deformation in amorphous solids. Physical Review E, 57(6), 7192.

Ferdowsi, B., Griffa, M., Guyer, R. A., Johnson, P. A., Marone, C., & Carmeliet, J. (2014). Three-dimensional discrete element modeling of triggered slip in sheared granular media. Physical Review E, 89(4), 042204.

Ferdowsi, B., Griffa, M., Guyer, R. A., Johnson, P. A., Marone, C., & Carmeliet, J. (2015). Acoustically induced slip in sheared granular layers: Application to dynamic earthquake triggering. Geophysical Research Letters, 42(22), 9750-9757.

Fierro, A., Nicodemi, M., & Coniglio, A. (2002). Thermodynamics and statistical mechanics of frozen systems in inherent states. Physical Review E, 66(6), 061301.

Griffa, M., Ferdowsi, B., Guyer, R. A., Daub, E. G., Johnson, P. A., Marone, C., & Carmeliet, J. (2013). Influence of vibration amplitude on dynamic triggering of slip in sheared granular layers. Physical Review E, 87(1), 012205.

Haff, P. K. (1986). A physical picture of kinetic granular fluids. Journal of Rheology, 30(5), 931-948.

Heerema, E. P. (1978, January). Predicting pile driveability: Heather as an illustration of the "friction fatigue" theory. In SPE European Petroleum Conference. Society of Petroleum Engineers.

Hosoi, A. E., & Goldman, D. I. (2015). Beneath our feet: strategies for locomotion in granular media. Annual review of fluid mechanics, 47.

Hwang, J. H., Liang, N., & Chen, C. H. (2001). Ground response during pile driving. Journal of Geotechnical and Geoenvironmental Engineering, 127(11), 939-949.

Jaeger, H. M., Nagel, S. R., & Behringer, R. P. (1996). Granular solids, liquids, and gases. Reviews of modern physics, 68(4), 1259.

Kothari, K. R., & Elbanna, A. E. (2017). Localization and instability in sheared granular materials: Role of friction and vibration. Physical Review E, 95(2), 022901.The Journal of chemical physics, 4(4), 283-291.

Kremer, G. M. (2010). Entropy, entropy flux and entropy rate of granular materials. Physica A: Statistical Mechanics and its Applications, 389(19), 4018-4025.

Krey, H. (1932). Erddruck, Erdwiderstand und Tragfähigkeit des Baugrundes Berlin, Deutschland, Wilhelm Ernst ahd Sohn.

Lemaître, A. (2002). Rearrangements and dilatancy for sheared dense materials.

Physical Review Letters, 89(19), 195503.

Mehta, A., & Edwards, S. F. (1989). Statistical mechanics of powder mixtures. Physica A: Statistical Mechanics and its Applications, 157(3), 1091-1100.

Melosh, H. J. (1987). The mechanics of large rock avalanches: Geological Society of America Review in Engineering Geology, v. 7.

Melosh, H. J. (1996). Dynamical weakening of faults by acoustic fluidization. Nature, 379(6566), 601-606.

Moriyasu, S., Kobayashi, S. I., & Matsumoto, T. (2018). Experimental study on friction fatigue of vibratory driven piles by in situ model tests. Soils and foundations, 58(4), 853-865.

O'Neill, M. W., Vipulanadan, C., & Wong, D. O. (1990). Evaluation of bearing capacity of vibro-driven piles from laboratory experiments. Transportation Research Record, (1277).

Osinov, V. A. (2013). Application of a high-cycle accumulation model to the analysis of soil liquefaction around a vibrating pile toe. Acta Geotechnica, 8(6), 675-684.

Pechenik, L. (2005). Dynamics of shear-transformation zones in amorphous plasticity: Nonlinear theory at low temperatures. Physical Review E, 72(2), 021507.

Pestana, J. M., Hunt, C. E., & Bray, J. D. (2002). Soil deformation and excess pore pressure field around a closed-ended pile. Journal of geotechnical and geoenvironmental engineering, 128(1), 1-12.

Roscoe, K. H., Schofield, A., & Wroth, A. P. (1958). On the yielding of soils. Geotechnique, 8(1), 22-53. https://doi.org/10.1680/geot.1958.8.1.22

Schofield, A. N., & Wroth, P. (1968). Critical state soil mechanics (Vol. 310). Soil Use Manag. 25(3), 128–105. London: McGraw-hill. https://doi.org/10.1111/j.1475-2743.1987.tb00718.x

Sharpe, S. S., Kuckuk, R., & Goldman, D. I. (2015). Controlled preparation of wet granular media reveals limits to lizard burial ability. Physical biology, 12(4), 046009.

Taslagyan, K. A., Chan, D. H., & Morgenstern, N. R. (2015). Effect of vibration on the critical state of dry granular soils. Granular Matter, 17(6), 687-702.

Taslagyan, K. A., Chan, D. H., & Morgenstern, N. R. (2016). Vibrational fluidization of granular media. International Journal of Geomechanics, 16(3), 04015080

Urata, S., & Li, S. (2018). A multiscale shear-transformation-zone (STZ) model and simulation of plasticity in amorphous solids. Acta Materialia, 155, 153-165.

Uzuoka, R., Sento, N., Kazama, M., & Unno, T. (2005). Landslides during the earthquakes on May 26 and July 26, 2003 in Miyagi, Japan. Soils and Foundations, 45(4), 149-163.

Vanden Berghe, J. F., Holeyman, A., Juaristi, E., & Schmitt, A. (2001). Interlock friction in a sheet pile wall: laboratory tests. In International Conference on soil mechanics and geotechnical engineering (pp. 1273-1276).

Viking, K., & Bodare, A. (1999). Laboratory studies of dynamic shaft resistance response of a vibro-driven model pile in granular soil by varying the relative

density. In Proceedings of the 12th European Conference on Soil Mechanics and Geotechnical Engineering (pp. 863-869).

Viking, K. (2002). Vibro-driveability-a field study of vibratory driven sheet piles in non-cohesive soils (Doctoral dissertation, Byggvetenskap).

White, D. J., & Lehane, B. M. (2004). Friction fatigue on displacement piles in sand. Géotechnique, 54(10), 645-658.

Xie, T., & Guo, P. (2021). A Modified Triaxial Apparatus for Soils under High-Frequency, Low-Amplitude Vibrations. Geotechnical Testing Journal, 45(1).

Xie, T., Guo, P., & Stolle, D., (2022). Experimental investigation of vibration-induced shear resistance reduction in sheared granular soils. Canada Geotechnical Journal. https://doi.org/10.1139/cgj-2021-0662

Youd, T. L. (1967). The engineering properties of cohesionless materials during vibration. PhD dissertation, Iowa State University.

Zhao, C. F., Salami, Y., Hicher, P. Y., & Yin, Z. Y. (2019). Multiscale modeling of unsaturated granular materials based on thermodynamic principles. Continuum Mechanics and Thermodynamics, 31(1), 341-359.

Ringer, D. U., & Mujumdar, A. S. (1983). Analysis of aerodynamics and heat transfer in vibro-fluidized beds. Drying Technology, 2(4), 449-470.

Pestana, J. M., & Whittle, A. J. (1995). Compression model for cohesionless soils. Géotechnique, 45(4), 611-631.

Einav, I. (2007). Breakage mechanics—part I: theory. Journal of the Mechanics and Physics of Solids, 55(6), 1274-1297.

Forterre, Y., & Pouliquen, O. (2008). Flows of dense granular media. Annu. Rev. Fluid Mech., 40, 1-24.

Xie, T., Guo, P., & Stolle, D. (2022b). Development of extended STZ model for granular soils subjected to combined static loading and vibration. Géotechnique, 1-9. https://doi.org/10.1680/jgeot.22.00099

Xie, T., Guo, P., & Stolle, D. (2023). Experimental and modelling investigation of vibration‐induced fluidization in sheared granular soils. International Journal for Numerical and Analytical Methods in Geomechanics. https://doi.org/10.1002/nag.3520

Part Ⅲ: Mechanism & Modelling Analysis

Chapter 6 Mechanism and modelling simulations

(Paper 5)

Shear resistance relaxation of granular materials under vibration and restricted deforming conditions

Géotechnique, *1-13*

Tao Xie[1], Peijun Guo[1], Dieter Stolle[1]

[1]Department of Civil Engineering, McMaster University, 1280 Main St W, Hamilton, ON, L8S 4L7, Canada

Abstract: The phenomenon of vibration-induced shear resistance relaxation (ViSRR) refers to the loss of shear resistance in granular materials subjected to vibration, without an observable increase of excess pore pressure, under restricted deforming conditions. Essentially, ViSRR occurs when the total deformation of granular materials is unable to keep up with the plastic deformation induced by the vibration, given the restricted deforming conditions. In this study, we investigate ViSRR through a series of specially designed experiments together with theoretical simulation based on the extended shear-transformation-zone (STZ) model developed for granular materials. The results demonstrate that ViSRR takes place in granular materials under monotonic shearing when the vibration is superimposed, and the magnitude of shear resistance relaxation depends on the intensity of the vibration. The occurrence of ViSRR is subject to two fundamental prerequisites: superimposed vibration as the driving force for plastic deformation, and restricted total deformation that impedes a granular material's deformability to follow the development of plastic deformation. The simulation results obtained from the extended STZ model are in agreement with laboratory test results, indicating that the model is effective in describing the process of shear resistance relaxation and the accompanying volumetric strain during vibration.

Keywords: granular material; shear resistance relaxation; extended STZ model; restricted deforming condition

1. Introduction

Stress relaxation is generally referred to as the time-dependent decrease in stress experienced by a material subjected to a constant strain or deformation, due to plastic strain development within the material as a result of rheological behaviour. In essence, stress relaxation can be viewed as a consequence when the total deformation of a material does not "follow" the time-dependent change in the material's fabric or internal structure owing to plastic deformation. In other words, the plastic strain and fixed deformation cause the relaxation of the stress. This phenomenon has also been observed in various materials such as metals and alloys (Gupta & Li, 1970), polymers (Blonski et al., 1994; Dimitrakopoulos et al., 2001), metallic glasses (Qiao et al., 2006), concrete (Krishnan & Rajagopal, 2004), rock and soil (Tatsuoka, 2001; Augustesen et al., 2004).

In granular materials, a comparable phenomenon is vibration-induced volumetric compaction coupled with stress relaxation (Richard et al., 2005), or shear resistance relaxation (ViSRR). ViSRR refers to "a granular material in a restricted quasi-static deforming condition losing its shear resistance in response to plastic strains generated by vibrations". Herein the "restricted quasi-static deforming condition" implies that the rate of static deformation is restricted to a certain level rather than a completely fixed strain as in the classical stress relaxation tests, which results in an observed shear resistance reduction. Similar to stress relaxation, this kind of shear resistance reduction is termed "shear resistance relaxation". Essentially, the mechanisms of ViSRR are similar to those inducing stress relaxation, with vibration instead of rheology serving as the driving force of plastic strain development. Therefore, ViSRR is time-independent, not being related to the viscosity of a granular material.

In practice, ViSRR is a potential mechanism related to the shear strength reduction of granular materials under vibration, such as observed during landslides of dry soils on the moon & Mars (Melosh, 1987), or during earthquakes (Uzuoka et al., 2005), the triggering of avalanches, the weakening of granular "fault gauges" as a potential triggering mechanism of earthquakes (Melosh, 1996; Griffa et al., 2013). Moreover, the

decreased shear resistance due to vibration has multiple applications in nature and engineering. For instance, the head oscillation is utilized by Ocellated skinks to reduce the resistance when boring in granular soil (Sharpe et al., 2015). In geotechnical engineering, vibratory pile installation has been widely used, in which vibration reduces the penetration resistance and allows the pile to achieve a higher penetration speed than that when piles are jacked (Perzyna, 1963; Bingham et al., 2000; Viking, 2002).

Although the vibration-induced shear resistance reduction of granular materials has been observed in different scenarios and has many potential applications, there is still no constitutive model that properly accommodates this phenomenon. One of the challenges to develop such a constitutive model is how to handle the combined static and dynamic loadings that have different characteristic times. Stress-strain models based on continuum mechanics, such as elasticity models (linear or nonlinear), elasto-plasticity models (Roscoe et al., 1963; Roscoe & Burland, 1968; Duncan & Chang, 1970), as well as visco-elasticity and visco-plasticity models (Truesdell, 1955; Perzyna, 1963), are phenomenological models. These models, however, have limited capacity in considering the importance of a granular material's internal structure that is closely related to the connectivity and spatial arrangement of particles. In addition, these models cannot be adopted directly for problems involving slow and fast processes simultaneously.

Stress-strain models for granular materials have also been developed based on the micromechanics of granular materials. This category of models accounts for the interaction between particles on the particle scale. The discrete element method (DEM) has been used to help understand the behaviour of granular materials on the particle level (Cundall & Strack, 1979; Chang et al., 1992; Potyondy & Cundall, 2004; Zhou et al., 2020). The micromechanics of granular mechanics, on the other hand, provides various approaches to correlate the quantities on the particle level (e.g., contact forces, particle displacement and rotation, particle connectivity) with the macroscopic quantities such as stress tensor, strain tensor and fabric tensor. In specific, the

constitutive behaviour of granular materials in the micromechanics approach can be considered at three levels: particle level, a cluster of particles, and representative element volume (REV) level (Chang et al., 1992). The particle level analysis such as with DEM deals with the relative movement and contact force between particles at their contacts. The connectivity of particles as well as the distribution of contact forces are also of interest at the particle level. At the REV level, various measures adopted in continuum mechanics are applicable and used in the development of stress-strain models. The particle cluster level information provides additional information about the deformation modes of granular materials. Nevertheless, it is still challenging in the micromechanics approach to bridge different quantities across the scales. It should be noted that efforts have been made to apply DEM simulations to solving boundary-valued problems instead of using stress-strain models. Although significant progress has been achieved in this area with an obvious increase in computing power and improved algorithms, the number of particles that can be handled by computer simulation is still limited when compared with the huge number of particles that must be considered even for a handful of sand.

An increasing effort has been made to apply the fundamental principles of thermodynamics to solve problems involving different time and length scales (Cugliandolo et al., 1997; Edwards & Grinev, 1998; Falk & Langer, 1998; Bouchbinder & Langer, 2009a; Lieou et al., 2014b). For example, the shear-transformation-zone (STZ) theory is a framework that has been successfully used for modelling amorphous solids (Falk & Langer, 1998; Bouchbinder & Langer, 2009b; Manning et al., 2009) and granular fault gauges in geophysics (Daub & Carlson, 2008 & 2010; Lieou et al., 2014a). Instead of focusing on the contact forces and relative motion between particles as for micromechanics-based models, the emphasis of the STZ model is placed on the STZ motion that includes the creation, annihilation (or destruction), and flipping (or transition) of STZs in a system using the basic principles of statistical mechanics and thermodynamics. The plastic volumetric strain associated with the creation and

destruction of STZs makes it possible to apply the conventional STZ model to granular materials to address the shear- and vibration-induced plastic volume change; see the framework of the extended STZ model (Xie et al., 2022b). In general, as the main source of plastic deformation, the motion of STZs plays an essential role in determining the mechanical behaviour of the material. One of the keys to develop the extended STZ model is to correlate the motion of STZs (on the mesoscopic scale) with the macroscopic plastic strain. In the process of transformation, the driving power for the motion of STZs is the energy input in different forms, such as quasi-static shearing, vibration or temperature change.

The objective of this paper is twofold: the first is to address the mechanism of ViSRR and to demonstrate its existence via a series of laboratory tests using a modified triaxial apparatus (Xie & Guo, 2021) and theoretical analysis using the extended STZ model; and the second is to examine the performance of the extended STZ model in coping with combined quasi-static loading and vibration. The paper is organized as follows: (1) demonstration of ViSRR using the modified triaxial apparatus from laboratory tests with restricted deformation rate and superimposed vibration (i.e., vibration is superimposed on a specimen during a monotonic triaxial compression test at a constant axial strain rate); (2) an outline of the extended STZ model, followed by an intensive investigation of ViSRR using the extended STZ model; and (3) a comparison between the results obtained from the extended STZ model and laboratory tests to verify the suitability of the model.

2. Experimental investigations

2.1 Experimental setup

A modified triaxial apparatus was developed to investigate the loading and deformation conditions, under which ViSRR occurs (Xie & Guo, 2021). The modified apparatus is based on a conventional Bishop-type triaxial apparatus that uses the existing static loading and measurement modules. The major modification is an addition

of a low-inertia linear voice coil actuator mounted coaxially with the vertical loading rod, by which vertical vibration can be superimposed on the monotonic loading. During a test, the minor and intermediate principal stresses are kept constant as $\sigma_3 = \sigma_2 =$ 50 kPa, and the rate of axial displacement is fixed at 0.1%/min, as shown in Figure 1. It is worth noting that there may be a coupling effect between the background quasi-static monotonic shearing rate and the vibration frequency, particularly when the period of vibration is shorter than the characteristic time of local rearrangement of particles (STZ), as shown in previous studies (Lockner & Beeler, 1999; Beeler & Lockner, 2003; Savage & Marone, 2007). In this research, the superimposed vibration has relatively high frequencies (60~120 Hz), which are much higher than the frequencies where the coupling effect has been observed in previous studies (< 1 Hz). Therefore, we believe that the potential coupling effect between the background monotonic shearing rate and vibration frequency is negligible.

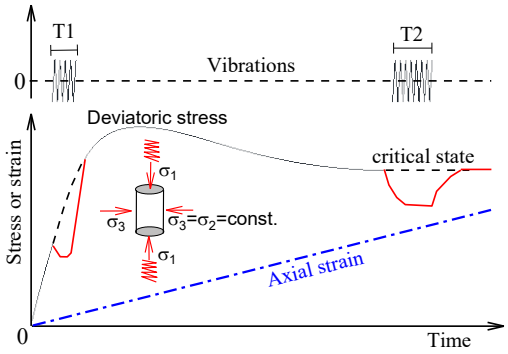

Figure 1. Loading scheme in laboratory tests using the modified triaxial apparatus

Uniform C-109 Standard Ottawa sand was used for the tests. It is fine sand composed of rounded to sub-rounded grains with a mean particle size of 0.375 mm. To measure the volumetric strain during testing, fully saturated cylindrical specimens of 50 mm diameter and 100 mm height were tested under drained conditions. The average initial void ratio of the specimens was 0.59 corresponding to a relative density of D_r = 70%.

2.2 Typical experimental results

Figure 2 illustrates the dynamic responses of a sand specimen under combined vibration and monotonic shearing. Seven sequential vibrations of 60 Hz with varying intensities (characterized by peak acceleration a) were superimposed to the same specimen at different strain levels. The duration of vibrations ranged from 10 to 35 seconds. Moreover, to better observe changes in shear resistance and volumetric strain induced by vibration, the results of a standard monotonic triaxial test under the same conditions were used as a reference. It should be noted that the normalized vertical peak acceleration a/g with g being gravitational acceleration is not the acceleration of the specimen. Instead, it is the acceleration measured by the accelerometer attached to the axial loading rod and thus can be regarded only as an indicator of vibration intensity that reflects the motion at the top of the specimen. The deviatoric stress $q = \sigma_1 - \sigma_3$ that is used as an indicator for the mobilized shear resistance of the specimen.

As shown in Figure 2, under monotonic shearing, the deviatoric stress q increases monotonically with axial strain before reaching the peak value. After the peak stress state, q decreases gradually until an apparent critical state is approached when the deviatoric stress and volumetric strain ε_v are both constant. A minor volumetric contraction is observed at the initial stage of monotonic shearing. As the monotonic shearing continues, the volumetric contraction is offset by the shear-induced dilation that dominates the volumetric change for the rest of the monotonic shearing.

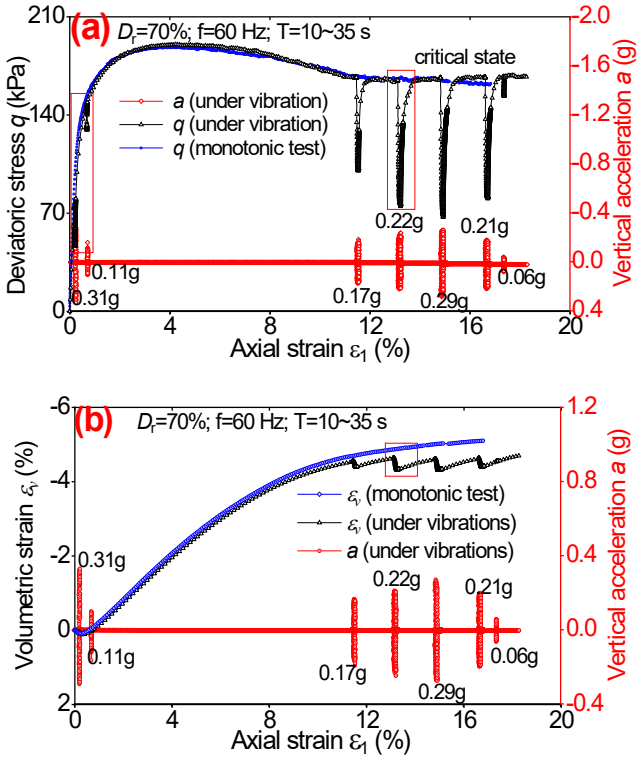

Figure 2. Experimental observation of ViSRR and volume change: (a) deviatoric stress; (b) volumetric strain

The application of vibration changes the trajectories of deviatoric stress q and volumetric strain ε_v, as observed in Figure 2 and Figure 3(a). An obvious decline in the deviatoric stress q takes place when the vibration is superimposed on the monotonic shearing. At the same time, the rate of q variation decreased until it approached a stable value, as shown in Figure 3(b). This phenomenon was detected regardless of whether the vibration was applied at the near-critical state or pre-peak state. This uncharacteristic behaviour confirms the existence of ViSRR in granular materials. Additional tests show that the higher the value of a/g, the greater the value of ViSRR, as observed in Figure 2(a). After the termination of vibration, q gradually recovered to the trajectory of monotonic shearing without vibration. In other words, ViSRR only occurred during the process of vibration.

To ensure that the shear resistance reduction after the application of vibration is not

caused by the development of excess pore pressure Δu, additional tests were performed in which drainage was allowed at the bottom of a specimen during vibration, while the drainage valve at the top of the specimen was closed to measure Δu. Figure 3(c) presents the development of Δu in two series of vibrations. A minor increase of excess pore pressure occurred when vibration was applied at near-critical state. On the other hand, vibration applied at the pre-peak state caused small negative excess pore pressure, possibly due to the tendency of dilation of the soil under vibration. Even when a/g reaches a high level of 0.29, Δu accounted for approximately 10% of the initial effective confining pressure, while the strength decreases by 60%. When drainage occurred at both ends of the specimen, the excess pore pressure in the mid-height of the specimen was expected to be much lower than that shown in Figure 3(c). Consequently, we conclude that the shear resistance reduction after the application of vibration is not induced by the generation of excess pore pressure Δu. As reported by Xie et al. (2022a), vibration-induced shear resistance reduction was also observed in tests on dry sand. Referring to Figure 2(b) and Figure 3(d), vibration also induced significant contraction in volumetric strain ε_v, especially when the vibration was imposed at near-critical state. Unlike the deviatoric stress q, the recovery of ε_v was not observed after vibration, implying that the vibration-induced volumetric compression was permanent. It should be noted that the measured volumetric strain ε_v induced by vibration could have been slightly underestimated due to the presence of minor excess pore pressure.

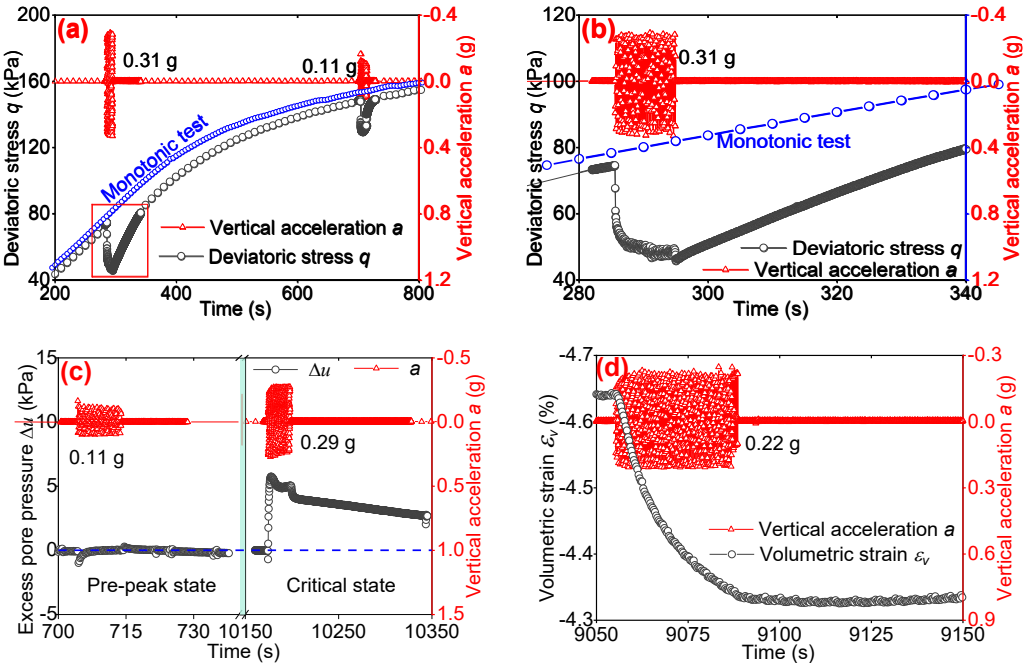

Figure 3. Time histories of deviatoric stress, excess pore pressure Δu, and volumetric strain: (a) ViSRR at pre-peak state; (b) vibration of a/g = 0.31 imposed at pre-peak state; (c) development of Δu when vibrations were imposed at pre-peak and near-critical states, respectively; (d) volumetric strain change when the vibration of a/g = 0.22 was imposed at near-critical state.

Finally, the continued monotonic shearing after vibration allowed the volumetric strain and the deviatoric stress q to return to the critical state, as shown in Figure 2. In other words, the superimposed vibrations did not prevent the soil from reaching critical state under monotonic shearing. This observation is consistent with the concept of critical state in soil mechanics. The critical state of soil (Roscoe et al., 1985; Schofield & Wroth, 1968) is unique, i.e., there is no further change in deviatoric stress and volumetric strain (or void ratio) during continuous shearing under drained conditions. When the internal structure is considered, the fabric measure of soil at critical state is also expected to be constant. It should be noted that only typical test results were presented in this section. Additional experimental results were given in Xie et al. (2022a), in which vibration frequency, dry specimens, and the initial density of specimen effect were also discussed.

3. Formulation of extended STZ model

This section outlines the extended STZ model that are used to further investigate the ViSRR. More details of the model derivation were presented in Xie et al. (2022b).

3.1 General formulation

In essence, a STZ is a "weak domain" composed of several or dozens of locally packed particles in the material. Referring to Xie et al. (2022b), STZs in the granular medium may have different forms, either as a weak "particle loop/cluster" with more than three particles or a group of particles with a large local void ratio. Subjected to external disturbances such as static shearing and low-intensity vibration, the STZ can transit from one equilibrium state to another by overcoming their neighbours' constraint, and at the same time generates plastic deformation, both shear strain volume change. Herein, the neighbours' constraints are characterized as an "energy barrier" and the transition process takes place as long as the energy input overcomes the "energy barrier".

As shown in Figure 4, a STZ can be created, destructed, and transited from one configuration to another, which are collectively called the "motion of STZs". To better describe the motion of STZs and their spatial distribution, a STZ tensor H_{ij} is introduced as

$$H_{ij} = \frac{1}{N_g}\sum_{\alpha=1}^{N} h_i^{\alpha} h_j^{\alpha} \tag{1}$$

with h_i^{α} being the unit orientation vector of the α^{th} STZ; N_g is the number of particles and N is the amount of STZs.

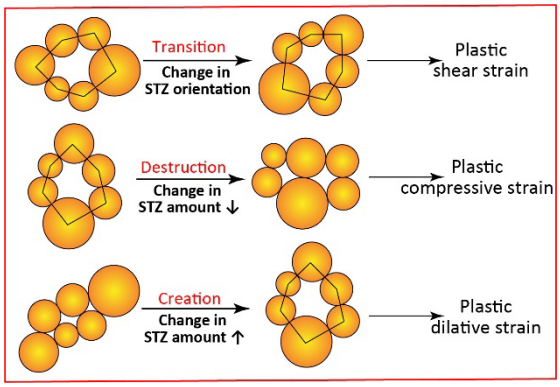

Figure 4. Basic assumptions of the extended STZ model (Xie et al., 2022b)

The core function of the extended STZ model is to transfer the motions of internal variables (i.e., STZs) into macroscopic plastic strains of a granular material. To be specific, the plastic strain ε_{ij}^{pl} of granular soil in the extended STZ model comes from three mechanisms: the plastic deviatoric strain generated by STZ transition, the plastic dilative strain generated by STZ creation, and the plastic compressive strain generated by STZ destruction, i.e.,

$$\dot{\varepsilon}_{ij}^{pl}=\omega_s \dot{H}_{ij}^{tra}-\omega_v\left(\dot{H}_{ij}^{cre}+\dot{H}_{ij}^{des}\right) \tag{2}$$

in which $\omega_v = v_v / v_g$ is the "elementary increment" of plastic strain associated with the STZ creation or destruction, and ω_s is the "elementary increment" of plastic strain owing to the STZ transition. Herein, $v_g = V/N_g$ is the occupied volume of a single particle, and V is the volume of the REV; The first and the second terms on the right side of Eq. (2) reflect the plastic strains induced by the change in the STZ orientation (transition) and the change in STZ density (creation & destruction), respectively; $\dot{H}_{ij}^{tra}$, $\dot{H}_{ij}^{cre}$, $\dot{H}_{ij}^{des}$ are rates of the STZ tensor variation induced by the transition, creation, and destruction of STZs, respectively. They are determined by

$$\tau_0 \dot{H}_{ij}^{tra} = \Lambda R_{ij} - R^* H_{ij} \tag{3}$$

$$\tau_0\left(\dot{H}_{ij}^{cre}+\dot{H}_{ij}^{des}\right)=\left(\frac{\Lambda^{eq}}{\Lambda}-1\right)\tilde{\Gamma}_{im}H_{mj} \tag{4}$$

where τ_0 is a time scale reflecting the activity of STZ motion. In traditional triaxial

compression tests, τ_0 is assumed to be inversely proportional to the loading rate $\dot{\varepsilon}_a$ (axial strain rate), *i.e.*, $\tau_0 = \kappa\dot{\varepsilon}_a^{-1}$; R_{ij} is the transition rate tensor and $R^* = R_{ii}$; $\Lambda = H_{ii}$ is STZ density; Λ^{eq} is the value of Λ in steady equilibrium (corresponds to the critical state in soil mechanics); $\tilde{\Gamma}_{ij}$ is the loading strength tensor defined by

$$\tilde{\Gamma}_{ij} = \Gamma\delta_{ij} + \lambda d_{ij} \tag{5}$$

in which d_{ij} is a unit-magnitude deviatoric tensor with the major principal orientation in the direction of vibration; Γ and λ denote the mechanical and vibrational noise strengths, respectively. Γ and λ are defined by

$$\Gamma = \frac{\xi_d s_{ij}}{\Lambda p_0}\left(\Lambda R_{ij} - R^* H_{ij}\right) - \frac{\xi_v p}{p_0}\left(\frac{\Lambda^{eq}}{\Lambda} - 1\right) \tag{6}$$

$$\dot{E}_V - \dot{E}_F = \lambda A_0 \tag{7}$$

where ξ_v, ξ_d, and A_0 are constant coefficients; p_0 is a reference pressure chosen as $p_0 = 1$ kPa; p and s_{ij} are the mean stress and the deviatoric stress tensor, respectively; $\dot{E}_V$ is the rate of vibrational energy input per unit volume. In this study, $\dot{E}_V$ is produced by the voice coil actuator in the modified triaxial apparatus. In engineering practice, $\dot{E}_V$ can be induced by different mechanisms, for example, the seismic wave during an earthquake or the vibration of machine foundations. The STZ model, based on the framework of thermodynamics, utilizes the concept of energy to address all external disturbances, including static and dynamic loadings. This allows us to analyze the behaviour of granular materials under different conditions. However, a limitation of the current STZ model is that it only captures steady-state changes in the soil behaviour under dynamic loading without characterizing instantaneous changes of material behaviour, e.g., stress path history during cyclic loading. $\dot{E}_F$, which is the "contact dissipation", is the rate of energy dissipation per unit volume as the result of inelastic contact deformation of particles when vibration is applied. The first term in Eq. (6) characterizes the plastic deformations induced by the deviatoric stress (shearing), while

the last term characterizes the plastic deformations induced by the mean stress.

Inserting Eqs. (3) and (4) into Eq. (2), the rate of plastic strain can be obtained as

$$\tau_0 \dot{\varepsilon}_{ij}^{pl} = \omega_s \left(\Lambda R_{ij} - R^* H_{ij} \right) - \omega_v \left(\frac{\Lambda^{eq}}{\Lambda} - 1 \right) \tilde{\Gamma}_{im} H_{mj} \tag{8}$$

The motion of STZ ($\dot{H}_{ij}$) is described by

$$\tau_0 \dot{H}_{ij} = \tau_0 \left(\dot{H}_{ij}^{tra} + \dot{H}_{ij}^{cre} + \dot{H}_{ij}^{des} \right) = \Lambda R_{ij} - R^* H_{ij} + \left(\frac{\Lambda^{eq}}{\Lambda} - 1 \right) \tilde{\Gamma}_{im} H_{mj} \tag{9}$$

Although we have defined the STZ tensor in Eq. (1) by linking STZs with weak particle loops, the identification for the orientation of particle loops of arbitrary shapes, and the connection of destruction/creation of particle loops with the evolution of $\dot{H}_{ij}$ still need to be further investigated with the help of the Discrete Element Method (DEM). Currently, we rely on Eq. (9) to describe the motion of STZs, which is one of the basic functions of the STZ model for granular materials.

According to Eq. (8), the plastic volumetric strain $\dot{\varepsilon}_v^{pl}$ only depends on the change in STZ density Λ, with

$$\dot{\varepsilon}_v^{pl} = \dot{\varepsilon}_{ii}^{pl} = -\omega_v \dot{\Lambda} = -\omega_v \left(\frac{\Lambda^{eq}}{\Lambda} - 1 \right) \tilde{\Gamma}_{im} H_{mi} \tag{10}$$

This relation implies the transition of STZ only yields deviatoric plastic strain, while the creation and destruction of STZs cause plastic volumetric strain. Λ^{eq} and R_{ij} in Eq. (9) are given as

$$\Lambda^{eq} = \begin{cases} \exp(-e_z / \chi^{eq}), & \lambda=0 \\ \exp\left[-e_z \cdot \chi^{eq} / (\chi \cdot \chi_v^{eq}) \right], & \lambda>0 \end{cases}, \quad R_{ij} = \frac{R_0}{3} \exp(\omega_s v_g s_{ij} / \chi) \tag{11}$$

where R_0 is a constant coefficient; e_z is the energy barrier or the formation energy of a STZ; χ is the configurational temperature that characterizes the internal state of the material; χ_v^{eq} and χ^{eq} are values of χ at the steady equilibrium state with and without vibrations, respectively. Because the magnitude of $\omega_s v_g s_{ij} / \chi$ is small, $R^* = R_{ii} \approx R_0$ holds.

Obviously, both Λ^{eq} and R_{ij} are a function of the configurational temperature χ. As an internal variable of granular systems, the configurational temperature χ changes during deformation in response to external driving energy, such as vibrations and static loadings, which promotes the motion STZs within the system. Consequently, the evolution law of χ is a key governing function that is given as

$$\tau_0 C_0 \dot{\chi} = \left[\omega_s s_{ij}\left(\Lambda R_{ij} - R_0 H_{ij}\right) - p\omega_v \tau_0 \dot{\Lambda}\right]\left(1 - \frac{\chi}{\chi^{eq}}\right) + \lambda A_0 \left(1 - \eta \frac{\chi}{\chi_v^{eq}}\right) \tag{12}$$

with C_0 denoting the energy capacity coefficient of the granular system, and η>1 is a constant.

In summary, the extended STZ model has three groups of governing equations: (a) the motion of STZ, including transition, creation, and destruction under external disturbance such as vibration and quasi-static loading, as shown in Eq. (9); (b) the relationship between the motion of STZ and the macroscopic plastic strain as indicated in Eq. (8); and (c) the evolution law of configurational temperature χ in Eq. (12) characterizing the internal states. By selecting a strain measure ε_a and considering $\tau_0 \mathrm{d}\_ / \mathrm{d}t = \tau_0 \dot{\varepsilon}_a \mathrm{d}\_ / \mathrm{d}\varepsilon_a = \kappa \mathrm{d}\_ / \mathrm{d}\varepsilon_a$, these governing equations can be rewritten as

$$\kappa \frac{\mathrm{d}\varepsilon_{ij}^{pl}}{\mathrm{d}\varepsilon_a} = \omega_s \left(\Lambda R_{ij} - R_0 H_{ij}\right) - \omega_v \left(\frac{\Lambda^{eq}}{\Lambda} - 1\right)\tilde{\Gamma}_{im} H_{mj} \tag{13}$$

$$\kappa \frac{\mathrm{d}H_{ij}}{\mathrm{d}\varepsilon_a} = \Lambda R_{ij} - R_0 H_{ij} + \left(\frac{\Lambda^{eq}}{\Lambda} - 1\right)\tilde{\Gamma}_{im} H_{mj}, \quad \kappa \frac{\mathrm{d}\Lambda}{\mathrm{d}\varepsilon_a} = \left(\frac{\Lambda^{eq}}{\Lambda} - 1\right)\tilde{\Gamma}_{im} H_{mi} \tag{14}$$

$$C_0 \kappa \frac{\mathrm{d}\chi}{\mathrm{d}\varepsilon_a} = \left[\omega_s s_{ij}\left(\Lambda R_{ij} - R_0 H_{ij}\right) - \omega_v p \kappa \frac{\mathrm{d}\Lambda}{\mathrm{d}\varepsilon_a}\right]\left(1 - \frac{\chi}{\chi^{eq}}\right) + \lambda A_0 \left(1 - \eta \frac{\chi}{\chi_v^{eq}}\right) \tag{15}$$

3.2 Formulation for triaxial stress conditions

For an initially isotropic granular soil subjected to triaxial shearing, H_{ij} is co-directional with the stress tensor and strain tensors since the principal directions of stresses and strains are fixed without rotation. Thus, the general formulation of the extended STZ model can be simplified for triaxial stress conditions by expressing the

model in the principal space of the involved tensors (H_{ij}, R_{ij}, s_{ij}, and ε_{ij}^{pl}). In other words, the tensors of the governing functions can be replaced by their principal values.

When vibration is superimposed in the vertical direction (ε_1), the governing functions Eqs. (13) ~ (15) are further simplified as

$$\kappa\frac{\mathrm{d}\varepsilon_1^{pl}}{\mathrm{d}\varepsilon_1}=\frac{\omega_s}{2}\Lambda R_0\left(m-T\right)-\omega_v\frac{\mathrm{d}\Lambda}{2\,\mathrm{d}\varepsilon_1}\left[1+\frac{\lambda\left(1-m\right)}{2\Gamma+\lambda\left(1-m\right)}\right],\quad \frac{\mathrm{d}\varepsilon_v^{pl}}{\mathrm{d}\varepsilon_1}=-\omega_v\frac{\mathrm{d}\Lambda}{\mathrm{d}\varepsilon_1} \tag{16}$$

$$\kappa\frac{\mathrm{d}\Lambda}{\mathrm{d}\varepsilon_1}=\left(\Gamma+\lambda\frac{1-m}{2}\right)\left(\Lambda^{eq}-\Lambda\right),\quad \kappa\frac{\mathrm{d}m}{\mathrm{d}\varepsilon_1}=-R_0\left(m-T\right)+\frac{\lambda m\left(1+m\right)}{2\Gamma+\lambda\left(1-m\right)}\frac{\kappa\mathrm{d}\Lambda}{\Lambda\,\mathrm{d}\varepsilon_1} \tag{17}$$

$$\kappa C_0\frac{\mathrm{d}\chi}{\mathrm{d}\varepsilon_1}=\left[\frac{q}{2}\omega_s\Lambda R_0\left(m-T\right)-p\omega_v\kappa\frac{\mathrm{d}\Lambda}{\mathrm{d}\varepsilon_1}\right]\left(1-\frac{\chi}{\chi^{eq}}\right)+\lambda A_0\left(1-\eta\frac{\chi}{\chi_v^{eq}}\right) \tag{18}$$

with

$$m=\frac{N_2+N_3-N_1}{N_1+N_2+N_3} \tag{19}$$

$$T=\frac{R_2+R_3-R_1}{R_1+R_2+R_3}=\frac{\exp(\omega_s v_g s_2/\chi)+\exp(\omega_s v_g s_3/\chi)-\exp(\omega_s v_g s_1/\chi)}{\exp(\omega_s v_g s_1/\chi)+\exp(\omega_s v_g s_2/\chi)+\exp(\omega_s v_g s_3/\chi)} \tag{20}$$

being the orientation bias and transition bias, respectively. Herein, N_1, N_2, and N_3 are the principal values of STZ tensor H_{ij}; R_1, R_2, and R_3 are principal values of R_{ij}; s_1, s_2, and s_3 are principal values of s_{ij}; ε_1^{pl} are the plastic component of axial strain ε_1. Given that $s_2=s_3=-q/3$ and $s_1=2q/3$ for triaxial stress states, Γ and T can be further simplified to

$$\Gamma=\frac{\xi_d R_0 q}{2p_0}\left(m-T\right)-\frac{\xi_v p}{p_0}\left(\frac{\Lambda^{eq}}{\Lambda}-1\right) \tag{21}$$

$$T=\frac{2-\exp(\omega_s v_g q/\chi)}{2+\exp(\omega_s v_g q/\chi)} \tag{22}$$

To complete the formulation of the stress-strain model, we assume a linear elastic relation, i.e.,

$$\dot{\sigma}_i=2G\left(\dot{\varepsilon}_i-\dot{\varepsilon}_i^{pl}\right)+\frac{2G\upsilon}{1-2\upsilon}\left(\dot{\varepsilon}_v-\dot{\varepsilon}_v^{pl}\right) \tag{23}$$

in which σ_i is the principal stress and ε_i is the principal stain with i =1, 2 or 3; G is

the shear modulus; and υ is the Poisson's ratio. Under drained conditions, we have $\sigma_2 = \sigma_3 = \sigma_c = const.$ and $\varepsilon_2 = \varepsilon_3$ with constant $\dot{\varepsilon}_1$; Then, the incremental stress-strain relation in Eq. (23) can be expressed as

$$\frac{\mathrm{d}q}{\mathrm{d}\varepsilon_1} = 3\frac{\mathrm{d}p}{\mathrm{d}\varepsilon_1} = 2\left(1+\upsilon\right)G\left(1-\frac{\mathrm{d}\varepsilon_1^{pl}}{\mathrm{d}\varepsilon_1}\right) \tag{24}$$

$$\frac{\mathrm{d}\varepsilon_v}{\mathrm{d}\varepsilon_1} = \left(1-2\upsilon\right)\left(1-\frac{\mathrm{d}\varepsilon_1^{pl}}{\mathrm{d}\varepsilon_1}\right)+\frac{\mathrm{d}\varepsilon_v^{pl}}{\mathrm{d}\varepsilon_1} \tag{25}$$

4. Modelling results

4.1 Model parameters and static responses

Given the novelty of the extended STZ model for soil mechanics, information on the model parameters is very limited and the methods to determine the corresponding parameters also need to be further explored. As such, this section only presents a parametric study using parameters of approximate order. A continuous in-depth investigation is required either by numerical simulations or by experimental study.

(1) *Model parameters*

Table 1 Parameters used in the extended STZ model

e_z (J)	χ^{eq} (J)	R_0	ω_s	κ	ξ_d	η
2.5*10^{-4}	2*10^{-4}	3	30	5	1	1.2
v_g (m^3)	χ_v^{eq} (J)	C_0	ω_v	A_0	ξ_v	υ
4*10^{-11}	1.9*10^{-4}	300	1.6	10^3	6	0.25

Table 1 summarizes the values of different parameters adopted in the parametric study. The occupied volume v_g of a particle is approximately the particle volume, which is considered a constant since the compressibility of the particles is assumed to be negligible. Physically, the "elementary increment" $\omega_v = v_v / v_g$ of the plastic strain associated with the creation or destruction of a single STZ can also be approximated as

constant. For an isotopic specimen consolidated under hydrostatic pressure σ_c = 50 kPa, the initial amount of STZ in the three principal directions are identical, which corresponds to m = 1/3 according to Eq. (19). Moreover, the initial value of Λ is determined by the initial value of configurational temperature as $\Lambda_0 = \exp(-e_z / \chi_0)$, in which χ_0 plays a role as the soil's initial void ratio (Chang et al.,1992). The other parameters are determined via numerical optimization to match the stress-strain response of two specimens with D_r = 70% and 35% tested under monotonic shearing. Figure 5 presents a comparison of the test results and model predictions with the parameters listed in Table 1.

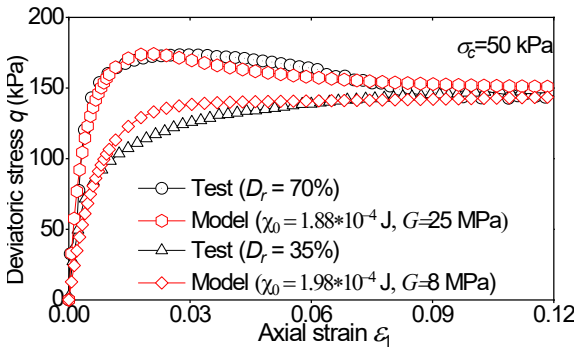

Figure 5. Stress-strain responses of monotonic triaxial tests to determine model parameters

It should be emphasized the vibrational noise strength λ is not a material parameter, Instead, it is an indicator of vibration intensity and λ = 0 implies the absence of vibration, as stated previously.

(2) *Static responses*

In particular, a denser specimen with a lower void ratio has a lower configurational temperature χ_0. At a low value of χ_0 = 1.85×10^{-4} J corresponding a dense soil, the stress-strain curve has an obvious peak followed by a gradual decrease of the deviatoric stress until it reaches a plateau, as shown in Figure 6(a). With an increase of χ_0 that

is associated with an increase in soil's void ratio, the peak strength gradually decreases until the strain-softening response completely vanishes. This tendency is accompanied by a transition in volumetric deformation from dilation to contraction, as observed from the volumetric strain responses presented in Figure 6(b).

The volume change of a specimen is the competition of STZ generation and destruction, as clearly shown in Eqs. (10), (14) and (17). In particular, volumetric contraction occurs when the destruction or collapse of STZ overmatches the generation of STZs. For densely compacted specimens with χ_0 = 1.85~1.95*10^{-4} J, there are two competing mechanisms controlling the generation and destruction of STZs and hence the volume change: mean stress induced compression and deviatoric stress (shearing) induced dilation. At the onset of loading, the destruction of STZ as the result of mean stress growth dominates the change of volumetric strain and thus a slight compression is found at the beginning of monotonic shearing. Then, as the shearing continues, this transitory compression is offset by shear-induced dilation (generation of STZ) that dominates the volume change of soil until a stable near-critical state is approached.

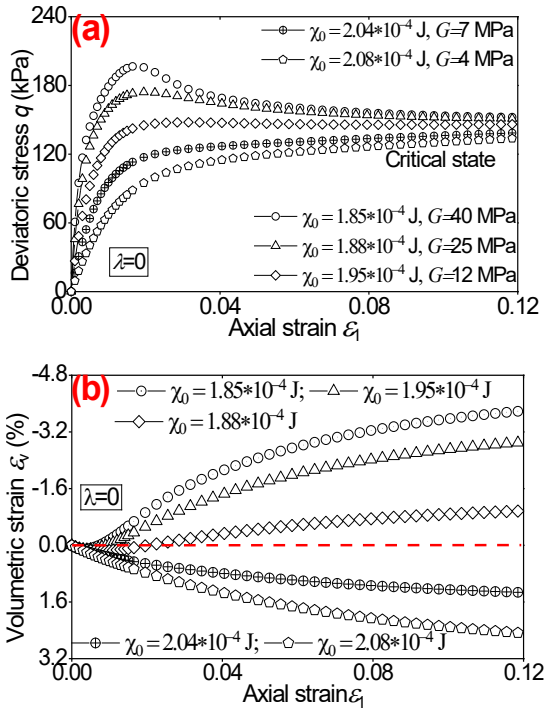

Figure 6. Influence of initial density on granular soil's behaviour under static loadings: (a) stress-strain relationship; (b) volumetric strain

Referring to Figure 6, the stress-strain curves and the volume change responses reveal that specimens with χ_0 = 2.04~2.08×10^{-4} J reflect the behaviour of loose sand that has shear-induced volumetric contraction and strain-hardening behaviour. When χ_0 = 1.85 ~ 1.95×10^{-4} J, the specimens have typical strain-softening stress-strain responses and significant dilation at large axial strains, which is typical for dense sand. The calculated stress-strain and volumetric strain responses suggest that the proposed extended STZ model can capture the stress-strain behaviour of granular materials for both loose and dense materials taking into account the influence of the void ratio. It should be pointed out that the shear modulus G depends on the void ratio and the mean effective stress. In this study, we only consider the dependency of G on the void ratio.

The appearance of the peak strength on the stress-strain curves is the result of shear-induced dilation that partially offsets the compressive plastic strain at the initial stage of loading, as illustrated in Figure 7(a). At the beginning of monotonic loading, at a given axial strain, the strain ratio $\mathrm{d}\varepsilon_1^{pl}/\mathrm{d}\varepsilon_1$ tends to decrease with an increase of χ_0. This decreasing trend accelerates the growth of deviatoric stress q, which is attributed to the fact that the creation of STZ is more active than the destruction of STZ and hence results in more dilative volumetric strain.

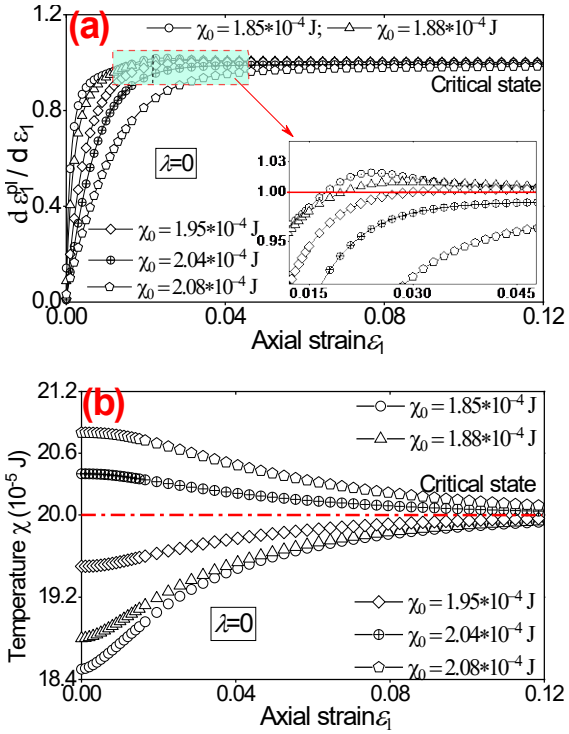

Figure 7. Influence of soil's initial density on configurational temperature and plastic axial strain rate: (a) plastic axial strain ratio; (b) configurational temperature

It is suggested in the literature that the strain-softening after the peak strength can be attributed to the rapid development of plastic strain that causes a larger free volume (corresponding to χ) in the granular soil, which in turn weakens the material (Johnson et al., 2002; Lemaître, 2002; Manning et al., 2007). As observed in Figure 7(b), this statement is true only for initially dense specimens in which the increasing plastic strain rate is accompanied by an increase of the configurational temperature χ. For loose sand with higher initial configurational temperature χ_0, the values of χ and $\mathrm{d}\varepsilon_1^{pl}/\mathrm{d}\varepsilon_1$ both increase with the axial strain continuously without strain-softening on the stress-strain curves. These observations confirm that the stress-strain responses depend on the motion of STZs and the configurational temperature χ rather than χ only. Moreover, as shown in Figure 7(b), the values of χ approach the same value of $\chi^{eq} = 2.0\times10^{-4}$ J at large axial strain. The value of χ^{eq} is independent of the initial configurational temperature χ_0, which confirms the existence of a critical void ratio at the critical state.

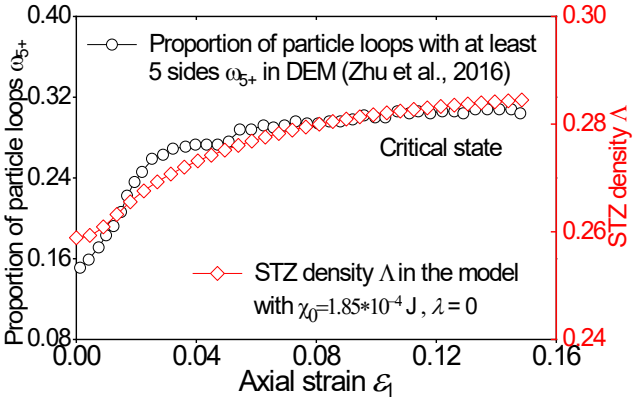

Figure 8. Comparison of weak particle loop evolution with at least 5 sides during biaxial loading in DEM simulation (Zhu et al., 2016) and STZ density evolution during triaxial monotonic shearing

To evaluate the performance of the extended STZ model for granular materials in describing the internal structural changes of granular materials during deformation, the evolution of STZ density (denoted as $\Lambda = H_{ii}$) resulting from STZ creation and destruction during monotonic triaxial shearing is compared with the evolution of weak particle loops with at least 5 sides (denoted as ω_{5+}) obtained from biaxial DEM simulations (Zhu et al., 2016); as shown in Figure 8. It is observed that both the proportion of weak particle loops ω_{5+} from the 2D DEM simulations and the STZ density Λ from the extended STZ model increase monotonically with the axial strain and eventually approach a plateau at the critical state. Despite the differences in the model used for the analysis, material properties and stress states, both quantities (Λ and ω_{5+}) have the same trend of evolution with respect to the axial strain. This suggests that the extended STZ model has the capability to capture the change of internal structure (or the evolution of particle loops) in granular materials during deformation. Nevertheless, further exploration is required for a more comprehensive investigation to improve the understanding of the determination and evolution of the configurational temperature, as well as the characterization of STZs in granular materials.

4.2 ViSRR at near-critical state

(1) *Dynamic responses*

To compare the results of theoretical modelling and laboratory tests, the loading scheme used in the simulation is identical to that adopted in triaxial compression tests illustrated in Figure 1. As shown in Figure 9(a), an obvious ViSRR is observed when the vibration is superimposed on the monotonic quasi-static loading at near-critical states. When vibration is applied, the deviatoric stress q undergoes an immediate drop. Thereafter, the rate of q reduction gradually decreases, and the value of q approaches a constant value as the vibration continues. When compared with the experimental results shown in Figure 2 and Figure 3, the vibration-induced shear resistance reduction predicted by the STZ model takes a longer time to stabilize than that observed in the laboratory tests. The most likely explanation is that the contribution of vibration in the activity of the STZ motion is out of consideration in this model. In other words, the time scales for the STZ motion are different under static and dynamic loadings. For simplicity, the same time scale τ_0 is adopted in simulation under static and dynamic loading conditions, which makes the motion of STZ during vibration much slower than in tests.

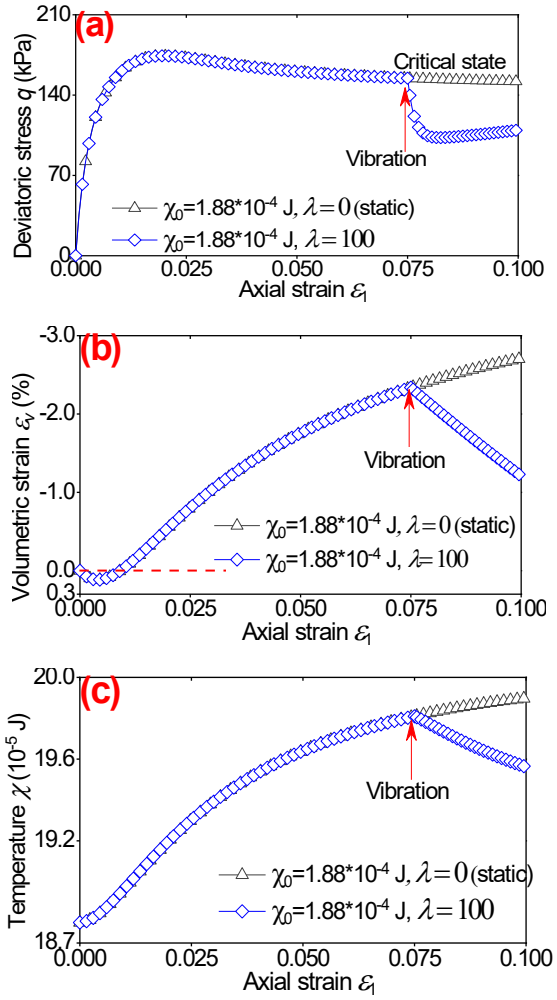

Figure 9. ViSRR as vibration superimposed at near-critical state: (a) shear resistance relaxation; (b) volumetric strain; (c) configuration temperature

Similar to the test results presented in Figure 2(b), vibration causes ViSRR and volumetric contraction simultaneously, as shown in Figure 9(b). This can be attributed to the change in STZ density induced by vibration, which is captured by the STZ model correctly. More specifically, the superimposed vibration causes a rise in STZ destruction and thus contractive plastic volumetric strain. Owing to the volumetric contraction induced by vibration, the configurational temperature decreases after superimposing vibration to the specimen; as shown in Figure 9(c).

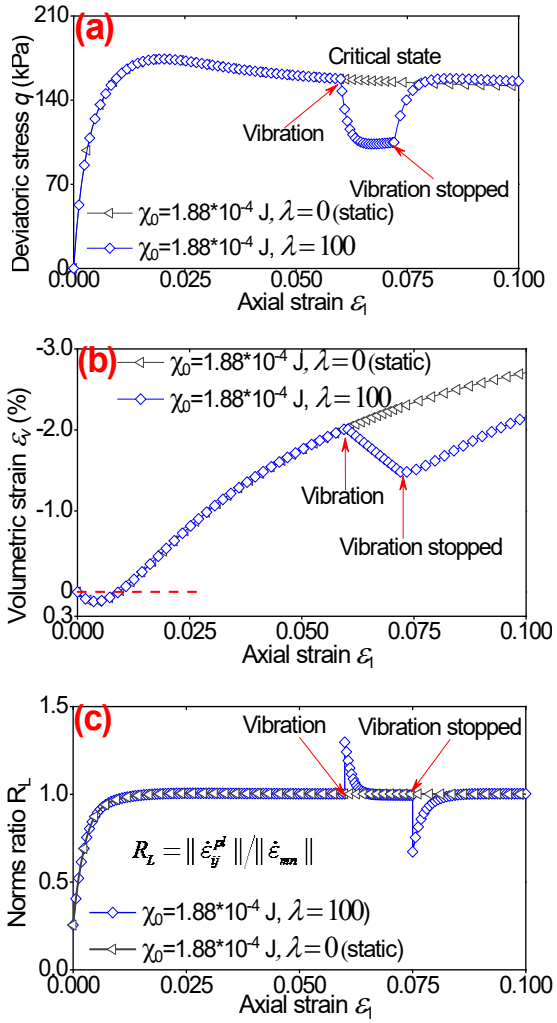

Figure 10. Shear resistance reduction and recovery during and after vibrations at near-critical state: (a) reduction and recovery of shear resistances; (b) volumetric strain; (c) ratio of the plastic strain rate tensor norm to the total strain rate tensor norm R_L

Recalling the test results in Figure 2(a), a full recovery of shear resistance occurs as the quasi-static shearing continues after the termination of vibration. This phenomenon is reproduced by the STZ model, as shown in Figure 10(a). Owing to the vibration-induced volumetric contraction, the deviatoric stress curve after vibration is slightly higher than that induced by monotonic shearing without vibration, which is the same as that observed from the experimental curve in Figure 2(a). During the application of vibration, the specimen has a remarkable contractive volumetric strain ε_v, which is permanent and irrecoverable if the laboratory testing is terminated after vibration. However, continuous monotonic shearing after the termination of vibration causes

volumetric dilation, as shown in Figure 10(b). Unlike the deviatoric stress q, the vibration-induced volumetric contraction recovers much slower as monotonic shearing continues but eventually goes back to the trajectory of the monotonic shearing without vibration. This is attributed to the void ratio at the critical state being unique and independent of the loading history (vibration). In the STZ model, the unique value of critical state configurational temperature χ^{eq} guarantees the uniqueness of the critical void ratio, as illustrated in Figure 7(b).

The occurrence of ViSRR can be explained by examining the differences in $\dot{\varepsilon}_1^{pl}$ over $\dot{\varepsilon}_1$ or more generally the variation of $R_L = \left\|\dot{\boldsymbol{\varepsilon}}^{pl}\right\| / \left\|\dot{\boldsymbol{\varepsilon}}\right\| = \sqrt{\left(\dot{\varepsilon}_{ij}^{pl}\dot{\varepsilon}_{ij}^{pl}\right) / \left(\dot{\varepsilon}_{mn}\dot{\varepsilon}_{mn}\right)}$. Figure 10(c) presents the variation of R_L during the deformation process corresponding to the stress-strain history presented in Figure 10(a) when the vibration is supervised at near-critical state. Under triaxial drained conditions with constant confining pressure, it is identified that R_L<1, =1 and >1 correspond to growth, no change, and a decline in the deviatoric stress q, respectively. At the onset of vibration, R_L increases from 1.0 to 1.3 suddenly, which corresponds to a decline in q (Figure 10(a)). If the rate of the total axial strain $\dot{\varepsilon}_1$ is not restricted and the specimen can deform freely such as that in a stress-control test, a surge in ε_1 is expected at the onset of vibration and thus R_L would still remain at a low level during vibrations. In this case, the ViSRR (*i.e.*, reduction of q) would not take place. Therefore, we conclude that the occurrence of ViSRR requires both (a) the superimposed vibration that can trigger additional plastic deformation and (b) a restricted deformation rate to ensure the total deformation of soil unable to "follow" the development of plastic deformation induced by vibration.

It should be pointed out that the constant rate of total deformation of the specimen is sufficient but not necessary for the occurrence of ViSRR, although the rate of axial

strain was fixed to a constant value in our experiments and simulations. More generally, ViSRR occurs under other stress paths besides triaxial stress, such as simple shearing and direct shear tests (e.g., Taslagyan et al., 2016), as long as the rate of total deformation is restricted to be lower than the rate of plastic deformation under vibration. In other words, ViSRR is a universal phenomenon for granular materials subjected to external vibrations and restricted deforming conditions.

(2) *Influence of vibration intensity*

As an indicator of vibration intensity, the vibrational noise strength λ is an increasing function of the rate of vibrational energy. Figure 11(a) illustrates the influence of λ on the ViSRR of granular soil. With an increase of λ, the ViSRR becomes more significant. For example, the deviatoric stress reduction Δq is about 40 kPa at λ = 100, when compared with $\Delta q \approx$ 100 kPa at λ = 300. Furthermore, the higher vibration intensity results in a more significant volumetric contraction and configurational temperature decrease, as shown in Figure 11(b) and Figure 11(c), respectively.

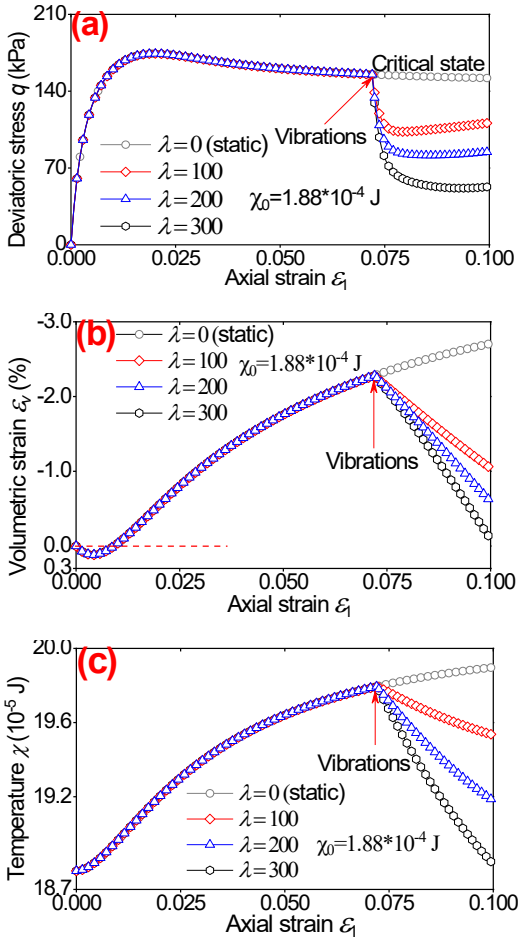

Figure 11. Influence of vibration intensity on soil responses as vibrations applied at near-critical state: (a) shear resistance relaxation; (b) volumetric strain; (c) configuration temperature

As shown in Figure 12, the ViSRR when normalized by q_0 increases linearly with the vibrational noise strength λ. Herein q_0 is the deviatoric stress when vibration is superimposed. Interestingly, the $\Delta q / q_0 \sim \lambda$ relation is independent of the initial configurational temperature χ_0 (or the initial void ratio of soil). This theoretical finding is consistent with experimental results presented in Figure 13 (Xie et al., 2022a) for the high-frequency vibration of f = 60~120 Hz. The laboratory test results show that the normalized shear resistance reduction $\Delta q/q_0$ increases linearly with the normalized vertical acceleration a/g, and is independent of a specimen's initial density. The

normalized vertical acceleration a/g can be considered as an indicator of intensity for high-frequency vibrations for the range f = 60~120 Hz used in the tests.

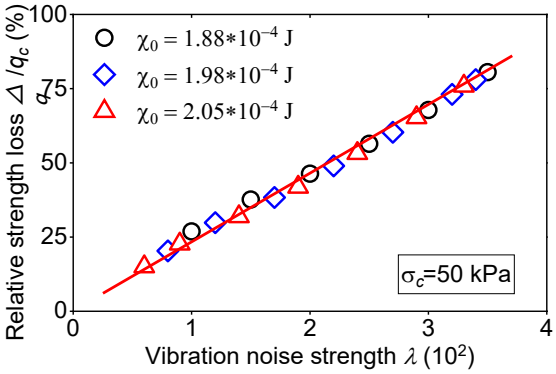

Figure 12. Influence of vibration intensity on ViSRR in the model

Given the linear $\Delta q/q_c \sim a/g$ relation obtained from the laboratory tests and the linear $\Delta q/q_c \sim \lambda$ relationship based on the STZ model for granular materials, the vibrational noise strength λ can be related to a/g via

$$\lambda = 1.15 \times 10^2 (a / g) \tag{26}$$

This relationship holds for the range f = 60~120 Hz with effective confining pressure σ_c = 50 kPa. Therefore, the relationship between $\Delta q/q_c$ and λ obtained from the proposed model can be transformed as the $\Delta q/q_c \sim a/g$ curves, as shown in Figure 13.

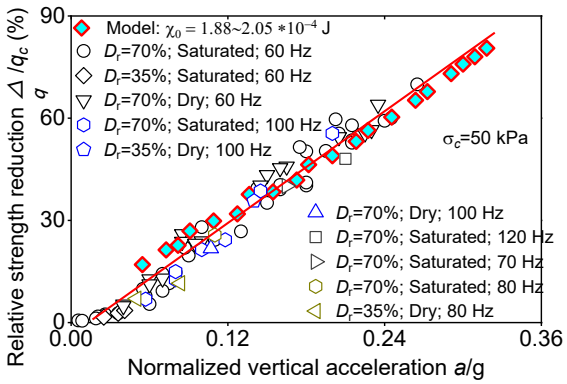

Figure 13. Comparison of ViSRR between experiment and extended STZ model at near-critical state

Since the STZ model for granular materials quantifies the external excitation via the vibrational noise strength λ, the vibration frequency is not explicitly incorporated. The influence of frequency mainly affects the vibration-induced contact dissipation E_F that is associated with the inelastic contact deformation of particles. The influence of frequency on E_F is comparable to the effect of frequency on the dynamic response of a structure. Resonance is expected to occur if the vibration energy is fully transferred to the kinetic energy of the structure when the vibration frequency is close to a structure's intrinsic frequency at minimized E_F. According to Eq. (7), the vibrational noise strength λ includes the magnitude of E_F. In other words, λ reflects the efficiency of the energy transformation from the vibration actuator to the soil's configuration. Moreover, there could be a cut-off frequency below which ViSRR may not occur, particularly during the pre-peak state. The rationale is that a low frequency vibration can only cause a low velocity of particle motion, which corresponds to a low plastic deformation rate. Consequently, the rate of plastic deformation may be unable to exceed the rate of total deformation, even under restricted deforming conditions, preventing the occurrence of ViSRR.

4.3 ViSRR at pre-peak state

(1) *Dynamic responses*

Figure 14 gives the ViSRR in granular soils when vibration is superimposed at different deviatoric stresses (q_0 = 50 and 100 kPa) prior to reaching the peak stress state of the stress-strain curve. Using the stress-strain curve obtained from the monotonic tests as a reference, an immediate drop in the deviatoric stress q is observed as the vibration is applied. The more intensive the vibration, the more significant the decrease in the deviatoric stress q. This process is analogous to the cases when vibrations are

imposed at the near-critical state. Once again, the predicted deviatoric stresses during vibration take a longer time to stabilize than that observed from the test results. Nevertheless, the soil's dynamic responses are generally in line with the experimental observations.

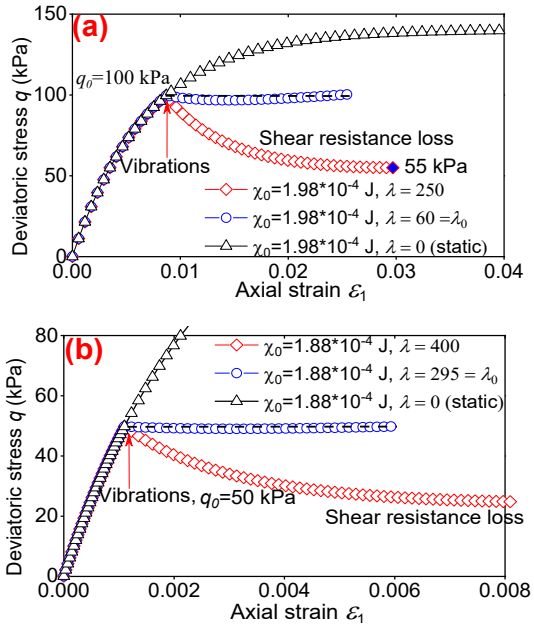

Figure 14. ViSRR of granular soils as vibration is superimposed at pre-peak state: (a) loose sample at q_0=100 kPa; (b) dense sample at q_0=50 kPa

Given that the rate of shear resistance reduction during vibration is much slower than it was during the tests, a growth of q induced by the monotonic loading during the vibration period is unavoidable and cannot be neglected in a simulation using the STZ model. It is necessary to use an initial vibration intensity λ_0 to offset this part growth in q. To exclude the deviatoric stress change induced by monotonic shearing during the period of vibration, a modified vibration intensity λ_m should be used for a given Δq, and $\lambda_m = \lambda - \lambda_0$. For example, λ_0 = 60 and λ_m = (250-60) when Δq = (100-55) kPa in Figure 14(a).

(2) *Influences of vibration intensity*

Figure 15 summarizes the influences of the modified vibration strength λ_m and the initial stress levels q_0 on the mobilized shear resistance reduction Δq. A linear relation, which is independent of the initial stress level q_0, is identified between λ_m and Δq. This implies that the vibration induced reduction of the mobilized shear resistance only depends on the modified intensity of vibration.

Moreover, the data presented in Figure 15 suggest that the initial density (or the configurational temperature χ_0) of the material seems to have a marginal influence on the $\Delta q \sim \lambda_m$ relationship when vibration is imposed at pre-peak state. In other words, for the same λ_m, specimens with different initial void ratios have the same magnitude of mobilized shear resistance reduction at any deviatoric stress level. Intuitively, this observation is inconsistent with the general understanding that dense granular soils usually have a stronger resistance to external vibration than loose ones. Indeed, from the definition $\lambda=(\dot{E}_V - \dot{E}_F) / \mathrm{A}_0$ we know that λ is not only involved in the vibrational energy E_V but also involved in contact dissipation E_F. There is usually a larger component of $\dot{E}_F$ in a dense specimen than in a loose specimen (Lobkovsky et al., 2009) due to the higher density of granular materials having more particle-to-particle contacts and interactions, which leads to a larger $\dot{E}_V$ being required to cause the same mobilized shear resistance reduction for dense specimens to allow $(\dot{E}_V - \dot{E}_F)$ to remain the same.

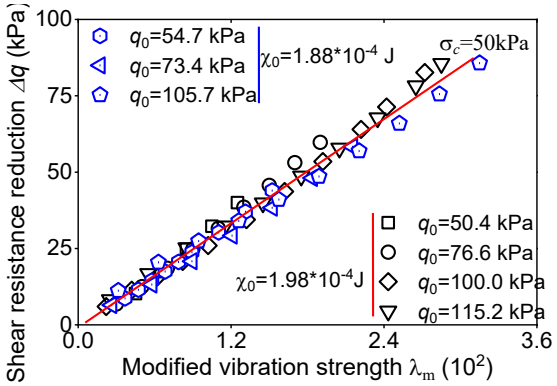

Figure 15. Influences of vibration strength and initial stress level on ViSRR at pre-peak state in the model

The linear relation between the mobilized shear resistance reduction and the vibration intensity prior to pre-peak was also observed from laboratory test results. According to Xie et al. (2022a), when vibrations of f=60 Hz were imposed at pre-peak state on the sand specimens, the normalized reduction of deviatoric stress $\Delta q/q_0$ increased linearly with the normalized acceleration a/g, as presented in Figure 16. Similar to that at near-critical state, a linear relationship can be established between a/g and the modified vibrational noise strength λ_m used in the extended STZ model:

$$\lambda_m = Kq_0(a/g) \tag{27}$$

in which K is a coefficient whose value is related to effective confining pressure and vibration frequency. More investigation is required to determine K under general conditions.

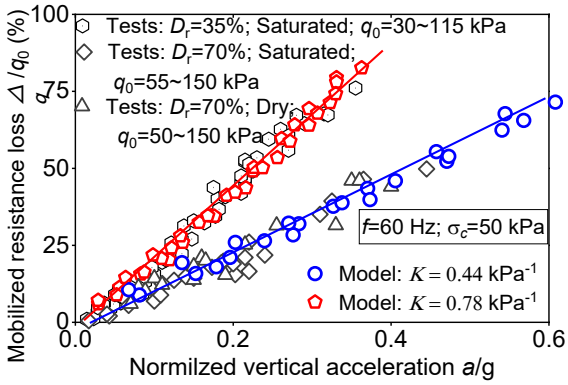

Figure 16. Comparison of ViSRR between experiment and extended STZ model at pre-peak state

As suggested in Figure 16, the values of K are 0.78 kPa^{-1} and 0.44 kPa^{-1} at the pre-peak state for D_r = 35% and 70%, respectively. Moreover, Eq. (27) is also valid for the vibration-induced shear resistance reduction at the near-critical state. In other words, the relationship revealed by Eq. (26) is a special case of Eq. (27). For example, Eq. (26) leads to K = 0.79 kPa^{-1} at near-critical state for f = 60~120 Hz with $\lambda_m = \lambda$, $q_0 = q_c$ ≈145 kPa.

Conclusions

This study reported the phenomenon of vibration-induced shear resistance relaxation (ViSRR) in granular materials based on both laboratory tests and theoretical simulation using the extended STZ model for granular material. The analyses demonstrated that the extended STZ model is capable of capturing the process of ViSRR in granular soils subjected to combined static shearing and vibration, taking into account the influences of a granular soil's initial density, stress level q_0 corresponding to the time at which vibration is imposed, and vibration intensity.

It was found that the vibration intensity, as measured by the normalized acceleration a/g in laboratory tests and the vibrational noise strength λ used in the STZ model, has a striking impact on the magnitude of ViSRR. Specifically, the magnitude of $\Delta q/q_0$ was found to be proportional to the vibration intensity when vibrations were superimposed at pre-peak state and near-critical state. This linear relationship was independent of the soil's initial density at near-critical state. By combining the model and experimental results, it was possible to develop a linear expression between the vibration strength λ and the normalized acceleration a/g. Thus, good agreement could be obtained between the model predictions and the ViSRR experiments.

Overall, our study provides new insights into the underlying mechanisms of ViSRR and highlights the potential of the extended STZ model in predicting and simulating this

phenomenon. These findings are expected to have important implications for the design and engineering of granular materials in a variety of applications.

Acknowledgments

The funding from the Natural Science and Engineering Research Council of Canada is sincerely appreciated.

References

Augustesen, A., Liingaard, M., & Lade, P. V. (2004). Evaluation of time-dependent behavior of soils. International Journal of Geomechanics, 4(3), 137-156.

Beeler, N. M., & Lockner, D. A. (2003). Why earthquakes correlate weakly with the solid Earth tides: Effects of periodic stress on the rate and probability of earthquake occurrence. Journal of Geophysical Research: Solid Earth, 108(B8).

Bingham, C. M., Stone, D. A., Schofield, N., Howe, D., & Peel, D. (2000). Amplitude and frequency control of a vibratory pile driver. IEEE Transactions on Industrial Electronics, 47(3), 623-631.

Blonski, S., Brostow, W., & Kuba, J. (1994). Molecular-dynamics simulations of stress relaxation in metals and polymers. Physical Review B, 49(10), 6494.

Bouchbinder, E., & Langer, J. S. (2009a). Nonequilibrium thermodynamics of driven amorphous materials. II. Effective-temperature theory. Physical Review E, 80(3), 031132.

Bouchbinder, E., & Langer, J. S. (2009b). Nonequilibrium thermodynamics of driven amorphous materials. III. Shear-transformation-zone plasticity. Physical Review E, 80(3), 031133.

Chang, C. S., Chang, Y., & Kabir, M. G. (1992). Micromechanics modeling for stress-strain behavior of granular soils. I: Theory. Journal of geotechnical engineering, 118(12), 1959-1974.

Cottrell, J. A., Hughes, T. J., & Bazilevs, Y. (2009). Isogeometric analysis: toward integration of CAD and FEA. John Wiley & Sons.

Cugliandolo, L. F., Kurchan, J., & Peliti, L. (1997). Energy flow, partial equilibration, and effective temperatures in systems with slow dynamics. Physical Review E, 55(4), 3898.

Cundall, P. A., & Strack, O. D. (1979). A discrete numerical model for granular assemblies. geotechnique, 29(1), 47-65.

Daub, E. G., & Carlson, J. M. (2008). A constitutive model for fault gouge deformation in dynamic rupture simulations. Journal of Geophysical Research: Solid Earth, 113(B12).

Daub, E. G., & Carlson, J. M. (2010). Friction, fracture, and earthquakes. Annu. Rev. Condens. Matter Phys., 1(1), 397-418.

Denies, N. (2010). Dynamic behavior of vibrated dry sand: sphere penetration experiments and discrete element modeling of vibrofluidization (Doctoral dissertation, UCL-Université Catholique de Louvain).

Dimitrakopoulos, P., Brady, J. F., & Wang, Z. G. (2001). Short-and intermediate-time behavior of the linear stress relaxation in semiflexible polymers. Physical Review E, 64(5), 050803.

Duncan, J. M., & Chang, C. Y. (1970). Nonlinear analysis of stress and strain in soils. Journal of Soil Mechanics & Foundations Div.

Edwards, S. F., & Grinev, D. V. (1998). Statistical mechanics of vibration-induced compaction of powders. Physical Review E, 58(4), 4758.

Falk, M. L., & Langer, J. S. (1998). Dynamics of viscoplastic deformation in amorphous solids. Physical Review E, 57(6), 7192.

Griffa, M., Ferdowsi, B., Guyer, R. A., Daub, E. G., Johnson, P. A., Marone, C., & Carmeliet, J. (2013). Influence of vibration amplitude on dynamic triggering of slip in sheared granular layers. Physical Review E, 87(1), 012205.

Gupta, I., & Li, J. C. M. (1970). Stress relaxation, internal stress, and work hardening in some bcc metals and alloys. Metallurgical Transactions, 1(8), 2323-2330.

Johnson, W. L., Lu, J., & Demetriou, M. D. (2002). Deformation and flow in bulk metallic glasses and deeply undercooled glass forming liquids—a self consistent dynamic free volume model. Intermetallics, 10(11-12), 1039-1046.

Krishnan, J. M., & Rajagopal, K. R. (2004). Triaxial testing and stress relaxation of asphalt concrete. Mechanics of Materials, 36(9), 849-864.

Lemaître, A. (2002). Rearrangements and dilatancy for sheared dense materials. Physical Review Letters, 89(19), 195503.

Lieou, C. K., Elbanna, A. E., & Carlson, J. M. (2014a). Grain fragmentation in sheared granular flow: Weakening effects, energy dissipation, and strain localization. Physical Review E, 89(2), 022203.

Lieou, C. K., Elbanna, A. E., Langer, J. S., & Carlson, J. M. (2014b). Shear flow of angular grains: acoustic effects and non-monotonic rate dependence of. arXiv preprint arXiv:1405.1371.

Lobkovsky, A. E., Reyes, F. V., & Urbach, J. S. (2009). The effects of forcing and dissipation on phase transitions in thin granular layers. The European Physical Journal Special Topics, 179(1), 113-122.

Lockner, D. A., & Beeler, N. M. (1999). Premonitory slip and tidal triggering of earthquakes. Journal of Geophysical Research: Solid Earth, 104(B9), 20133-20151.

Manning, M. L., Langer, J. S., & Carlson, J. M. (2007). Strain localization in a shear transformation zone model for amorphous solids. Physical review E, 76(5), 056106.

Manning, M. L., Daub, E. G., Langer, J. S., & Carlson, J. M. (2009). Rate-dependent shear bands in a shear-transformation-zone model of amorphous solids. Physical Review E, 79(1), 016110.

Melosh, H. J. (1987). The mechanics of large rock avalanches.

Melosh, H. J. (1996). Dynamical weakening of faults by acoustic fluidization. Nature, 379(6566), 601-606.

O'Neill, M. W., & Vipulanandan, C. (1989). Laboratory evaluation of piles installed with vibratory drivers (No. 316).

Perzyna, P. (1963). The constitutive equation for work-hardening and rate sensitive plastic

materials. In Proc. Vibrational Problems (Vol. 4, No. 3, pp. 281-290).

Potyondy, D. O., & Cundall, P. A. (2004). A bonded-particle model for rock. International journal of rock mechanics and mining sciences, 41(8), 1329-1364.

Qiao, J. C., Wang, Y. J., Zhao, L. Z., Dai, L. H., Crespo, D., Pelletier, J. M., ... & Yao, Y. (2016). Transition from stress-driven to thermally activated stress relaxation in metallic glasses. Physical Review B, 94(10), 104203.

Richard, P., Nicodemi, M., Delannay, R., Ribière, P., & Bideau, D. (2005). Slow relaxation and compaction of granular systems. Nature Materials, 4(2), 121–128. doi:10.1038/nmat1300

Roscoe, K. H., Schofield, A., & Wroth, A. P. (1958). On the yielding of soils. Geotechnique, 8(1), 22-53.

Roscoe, K. H., Schofield, A., & Thurairajah, A. (1963). Yielding of clays in states wetter than critical. Geotechnique, 13(3), 211-240.

Roscoe, K., & Burland, J. B. (1968). On the generalized stress-strain behaviour of wet clay.

Savage, H. M., & Marone, C. (2007). Effects of shear velocity oscillations on stick‐slip behavior in laboratory experiments. Journal of Geophysical Research: Solid Earth, 112(B2).

Schaeffer, D. G., Barker, T., Tsuji, D., Gremaud, P., Shearer, M., & Gray, J. M. N. T. (2019). Constitutive relations for compressible granular flow in the inertial regime. Journal of Fluid Mechanics, 874, 926-951.

Schofield, A. N., & Wroth, P. (1968). Critical state soil mechanics (Vol. 310). London: McGraw-hill.

Sharpe, S. S., Kuckuk, R., & Goldman, D. I. (2015). Controlled preparation of wet granular media reveals limits to lizard burial ability. Physical biology, 12(4), 046009.

Taslagyan, K. A., Chan, D. H., & Morgenstern, N. R. (2016). Vibrational fluidization of granular media. International Journal of Geomechanics, 16(3), 04015080.

Tatsuoka, F. (2001). Time-dependent deformation characteristics of stiff geomaterials in engineering practice. In Proc. 2nd Int. Conf. on Pre-failure Deformation Characteristics of Geomaterials, Torino, 1999 (Vol. 2, pp. 1161-1262). Balkema.

Truesdell, C. (1955). Hypo-elasticity. Journal of Rational Mechanics and Analysis, 4, 83-1020.

Uzuoka, R., Sento, N., Kazama, M., & Unno, T. (2005). Landslides during the earthquakes on May 26 and July 26, 2003 in Miyagi, Japan. Soils and Foundations, 45(4), 149-163.

Viking, K. (2002). Vibro-driveability-a field study of vibratory driven sheet piles in non-cohesive soils (Doctoral dissertation, Byggvetenskap).

Xie, T., & Guo, P. (2021). A Modified Triaxial Apparatus for Soils under High-Frequency, Low-Amplitude Vibrations. Geotechnical Testing Journal, 45(1).

Xie, T., Guo, P., & Stolle, D., (2022a). Experimental investigation of vibration-induced shear resistance reduction in sheared granular soils. Canada Geotechnical Journal. https://doi.org/10.1139/cgj-2021-0662

Xie, T., Guo, P., & Stolle, D. (2022b). Development of extended STZ model for granular soils subjected to combined static loading and vibration. Géotechnique, 1-9. https://doi.org/10.1680/jgeot.22.00099

Zhou, G. G., Du, J., Song, D., Choi, C. E., Hu, H. S., & Jiang, C. (2020). Numerical study of

granular debris flow run-up against slit dams by discrete element method. Landslides, 17(3), 585-595.

Zhu, H., Nicot, F., & Darve, F. (2016). Meso-structure evolution in a 2D granular material during biaxial loading. Granular Matter, 18(1), 3.

Chapter 7 Vibration-induced fluidization

(Paper 6)

Experimental and modelling investigation of vibration-induced fluidization in sheared granular soils

International Journal for Numerical and Analytical Methods in Geomechanics, *47(8)*, *1399-1415*

Tao Xie[1], Peijun Guo[1], Dieter Stolle[1]

[1]Department of Civil Engineering, McMaster University, 1280 Main St W, Hamilton, ON, L8S 4L7, Canada

Abstract: Vibration-induced fluidization (ViF) refers to that a granular medium under vibration completely loses shearing resistance and thus behaves like a fluid without invoking remarkable excess pore pressure. This paper was committed to investigating ViF via a series of modified triaxial experiments and the extended shear-transformation-zone (STZ) model which is a micromechanics-based model correlating the macroscopic plastic strain to the motion of internal mesoscopic weak spots (i.e., STZs) within the granular material. The test results revealed that the ViF takes place whether the vibration is applied at critical or non-critical states. Further investigation from the extended STZ model shown that the vibration intensity to cause fluidization grows linearly with the initial stress level at which vibration is imposed. The model results are generally in consistent with tests, indicating that the extended STZ model has a desirable performance in simulating fluidization of granular soil subjected to quasi-static shearing and vibration simultaneously.

Keywords: Fluidization; granular soil; modified triaxial experiments; extended STZ model

1. Introduction

Different from ordinary solids or liquids, a granular material usually exhibits multiple metastable configurations, and a transition from a solid-state to a liquid-state may happen under vibration (Jaeger et al., 1996; Umbanhowar & Van Hecke, 2005; Jia et al., 2011). This process is called "fluidization" in which a granular material completely loses shear resistance without invoking marked pore pressure and behaves like a fluid (Richards et al., 1990). Distinct from the liquefaction saturated of sand that is due to the decrease of effective stresses induced by excess pore pressure increase under undrained conditions, the fluidization usually takes place without remarkable effective stress loss, and the soil's deformation is finite and incremental. For a vertically vibrated granular medium, it is usually regarded that fluidization occurs only when the vertical acceleration of material is larger than the gravitational acceleration (Taguchi, 1993; Luding et al., 1994; Huan, 2008). However, increasing evidence both from numerical and experimental observations indicates that fluidization takes place even when acceleration is much less than the gravitational acceleration (Johnson & Jia, 2005; Janda et al., 2009; Lastakowski et al., 2015).

The fluidization involves a broad spectrum of natural (Hosoi & Goldman, 2015; Sharpe et al., 2015) and geophysical (Griffa et al., 2013; Ferdowsi et al., 2015) processes, mining and pharmaceutical industries (Ringer & Mujumdar, 1983; Rosato et al., 2002; Hsiau et al., 2011), engineering applications (O'Neill et al., 1990; Viking & Bodare, 1999; Bingham et al., 2000), and the disposal of hazardous waste (Mohabuth et al., 2007). It is believed as the primary reason for some long-runout landslides of dry soil on the moon and Mars (Melosh, 1987). Melosh (Melosh, 1979 & 1983; Sornette & Sornette, 2000) also attributed the fact that dry rock debris behaves like a fluid in some earthquakes to fluidization. In geophysics, more and more observations indicated that the weakening of granular "fault gauges" is one of the potential triggering mechanisms of earthquakes (Van Der Elst & Brodsky, 2010; Marsan & Lengline, 2008). The fault gouges accumulate energy from seismic waves and are finally transferred from the

'stick' phase to the 'slip' phase (Brace & Byerlee, 1966; Johnson et al., 1973 & 2008). In civil engineering, the application of vibration-induced fluidization is also common, e.g., vibratory-driven piles. The local fluidization of granular soils around the pile accelerates the penetration rate of vibratory-driven piles, which makes them move faster than jacked piles (O'Neill et al., 1990; Viking & Bodare, 1999; Bingham et al., 2000). In some cases, the vibration even allows the pile to be driven into soils under its weight.

To explore fluidization, different experimental apparatuses have been adopted according to the objective of the research. In the early stage, the vibrational platform was widely used such as the experimental works by Krey (1932), Barkan (1962), Mogami and Kubo (1953), as well as Youd (1967). They usually directly put the testing device, e.g., a direct shear box, on the vibrational platform. Based on test results, a consensus is reached that the vibration intensity has a salient impact on fluidization. Recently, a modified direct shear apparatus was used by Taslagyan et al. (Taslagyan et al., 2015 & 2016), by which the vibration can be superimposed horizontally by an actuator connecting with the loading rod. Test results revealed that the shear resistance of granular material declines significantly with the increase of vibrational acceleration, and a transition from a solid-like state to a fluid-like state is expected under an intensive enough vibration. Moreover, some conceptual tests such as "sphere penetration test" and "intruder penetration test" (Denies et al., 2010; Darbois Texier et al., 2017; Omidvar et al., 2019) were also frequently exploited to study fluidization, which involves in pushing a sphere or intruder into a granular media by vibration. The aforementioned tests deepen our understanding of fluidization. However, they are not enough for developing a constitutive model owing to the unexplicit stress, unclear loading conditions, and non-uniform deformation within the specimens.

Regarding the mechanism behind fluidization, we have very limited knowledge although several hypotheses have been proposed. Barkan (1962) thought it is the vanishment of "dry friction" under vibration that should be responsible for fluidization. During fluidization, the "dry friction" of granular media at solid-state is gradually

converted into the velocity-dependent "viscous friction". However, there is no evidence supporting the existence of "viscous friction", although Blekhman (Blekhman, 2000) proposed the concept of "vibrational force" as the nature of "viscous friction". In addition to that, L'Hermite and Tournon (2017) further created the concept of "shaking pressure" to explain fluidization in vibrated dry sand. Nevertheless, the source of "shaking pressure" and how to quantify it are still in debate. Except for the aforementioned explanations, other hypotheses such as local liquefaction for saturated sand (Hwang et al., 2001; Pestana et al., 2002; Osinov, 2013), the formation of horizontal soil arches surrounding the vibratory driven pile (White & Lehane, 2004; Moriyasu et al., 2018), as well as a decrease in contact force and contact lifetime in a vibrated granular soil (Denies, 2010) were also frequently mentioned. The challenge is how to quantify these changes and correlate them with the shear resistance reduction during fluidization algebraically. Recently, a new mechanism "vibration-induced shear resistance relaxation (ViSRR)" has been proposed (Xie et al., 2022b), which is defined as that the granular material under a restricted deformation condition partially or completely loses its shear resistance in response to the plastic deformation yield by vibrations. The logic behind ViSRR is that the total deformation rate of the granular material under vibration is restricted to be lower than the development of plastic deformation and consequently results in an observed "shear resistance relaxation", which is similar to stress relaxation but with the vibration instead of the time-dependent rheology serving as the source of plastic deformation. Hence, the occurrence of ViSRR must satisfy two basic requirements: a continuous vibration to allow the material has a tendency of compression and a restricted total deformation rate to ensure the material is unable to "follow" the vibration-induced compression. Considering the complexity of the loading and boundary conditions, there may be multiple potential mechanisms for fluidization. In this paper, to distinguish from other mechanisms, the fluidization we investigated is a special case of ViSRR.

On the model side, the conventional constitutive model in soil mechanics is either

based on continuum mechanics, e.g., elastoplastic models (Roscoe et al., 1963; Roscoe & Burland, 1968), or based on granular mechanics such as the "Discrete Element Method (DEM)" (Cundall & Strack, 1979; Potyondy & Cundall, 2004; Zhou et al., 2020) and micromechanics models (Chang et al., 1992). Essentially, the models based on continuum mechanics are phenomenological without considering the internal interaction of particles. The DEM copes with granular material responses at a particle level, whereas the biggest limitation at present is the small population of particles that can be simulated by computer. Micromechanics models also handle the granular material's behavior at the mesoscale level. The challenge is to correlate the mesoscale interaction of particles with the macroscale strain and stress. Unlike other micromechanics-based models focusing on the contact force of particles, the "shear-transformation-zone (STZ)" model (Falk & Langer, 1998; Daub & Carlson, 2008; Manning et al., 2009; Lieou et al., 2014) emphasizes the flipping of STZ (or called transition of STZ in granular soils), i.e., change in STZ orientation, as the main source of plastic shear deformation. Explicitly, as the "weak spot" in a granular medium, a STZ is a local group of particles that is more susceptible than their neighbours to shearing transformation in a certain direction. The transition of STZ is restricted by its neighbour particles and this constraint is characterized by the concept of "energy barrier". Besides, considering the non-uniform energy distribution of particles within a system, the basic principles of thermodynamics are adopted to describe the energy distribution and its evolution within a system. The conventional STZ model is originally used in the amorphous solids (Falk & Langer, 1998; Manning et al., 2009) under pure shear stress conditions in two dimensions (2D) to handle the influence of vibration on material's responses at a steady state. Furthermore, the emphasis of the conventional STZ model is placed on plastic shear deformation which makes it unable to consider the plastic volumetric deformation of granular materials, such as the shear-induced dilation, spherical stress- or vibration-induced compressions. Recently, by correlating the creation and destruction of STZ, i.e., change in STZ amount, with the plastic volumetric

strain, the STZ model was further extended to soil mechanics to investigate granular soil's responses subjected to vibration and static loading simultaneously (Xie et al., 2022a).

This paper is devoted to exploring the ViF experimentally and theoretically based on a modified triaxial apparatus and the extended STZ model (Xie et al., 2022a), respectively. First, to reproduce the process of fluidization in the laboratory, a specially designed testing apparatus based on the conventional triaxial shear apparatus is established, by which the vibration and static shearing can be imposed synchronously. Then, further investigations about the influence of vibration intensity, the stress level at which vibration is applied, and the initial density of granular material are undertaken based on the extended STZ model.

2. Experiments

2.1 Testing equipment and design

(1) *Testing equipment*

To investigate the ViF in the laboratory, a modified triaxial shear apparatus (Xie & Guo, 2021) was established based on the conventional triaxial shear equipment to utilize its existing measurement and static loading modules. Two independent loading modules were used: one is the dynamic loading module with a low-inertia linear voice coil actuator (VCA) mounted coaxially with the loading rod, as shown in Figure 1, and another is the static loading module from the conventional triaxial apparatus. During tests, a vibration can be superimposed to the monotonic shearing (the static loading module) vertically via the dynamic loading module. Moreover, an accelerometer was attached to the loading rod to measure the vertical acceleration of vibrations, considering the acceleration is an indicator of vibration intensity more significant than cyclic stress at high frequency.

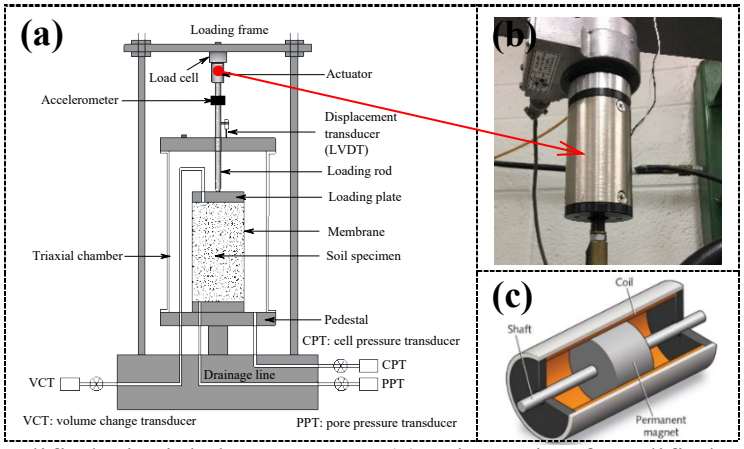

Figure 1. Modified triaxial shear system: (a) schematic of modified triaxial shear apparatus; (b) picture of voice coil actuator (VCA); (c) internal structure of VCA

(2) *Loading scheme*

The loading scheme adopted in tests is illustrated in Figure 2. Firstly, a monotonic static loading is applied with a constant axial strain of 0.1% per minute. During this process, the effective confining pressure is fixed at σ_c = 50kPa under drained conditions. Then, a vibration with constant intensity (the energy input level of VCA) and frequency is superimposed to the monotonic shearing at a designed stress level q_0 which could be at near-critical or pre-peak states. The required vibration intensity to generate fluidization is depended on the stress level q_0 at which vibration is imposed. During vibration, the monotonic shearing continues and thr rate of axial strain keeps constant to make sure a restricted deformation rate in the direction of vibration. In other words, in the process of ViF the soil specimen is subjected to vibration and monotonic shearing at the same time. The reason for superimposing the vibrations near the critical state is that the deviatoric stress q is more stable and thus the influence of monotonic shearing on q is minimum.

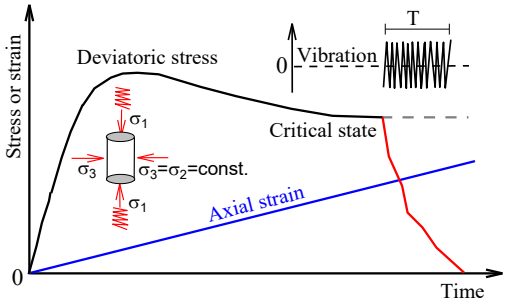

Figure 2. Loading scheme in tests

It should be noted that the duration of fluidization process is very sensitive to the imposed vibration intensity. If the vibration intensity is slightly larger than expected, the soil specimen may collapse suddenly so that the whole process of fluidization cannot be recorded by the testing system, while a slightly smaller vibration is not sufficient to cause fluidization. Hence, to observe the details of ViF, which requires the ViF process to last at least several seconds, several trial tests with different vibration intensities may be conducted in order to obtain a desirable experimental test.

(3) *Material properties*

The material used in the tests is Standard Ottawa sand C-109 which is uniform quartz sand of sub-rounded particles. The mean grain size is 0.375 mm with a uniformity coefficient of1.80 and a curvature coefficient of 1.20. The minimum and maximum void ratios are 0.503 and 0.811 based on ASTM test methods D4253-00 and D4254-00, respectively. The cylinder specimen is 50 mm in diameter and around 100 mm in height. Both air-dry and fully saturated specimens with relative density D_r = 70% and 35% were used in the tests. More details of the test matrix are given in Table 1. The selection of fully saturated specimens is to record the volume change in the process of ViF, whereas the air-dry specimens are mainly used to exclude the influence of possible excess pore pressure.

Table 1 Test matrix

Factors	Range
Vibration frequency (f)	20~100 Hz
Stress level at which vibration is imposed (q_0)	75 ~ 155 kPa at Pre-peak state or near critical state
Effective confining pressure (σ_c)	50 kPa
Relative density (D_r)	35%, 75%
Moisture	Air-dried, fully saturated

2.2 Fluidization in experiment

(1) *Fluidization at near-critical state*

Figure 3 presents the dynamic responses of granular soil with D_r = 70% under vibrations. The specimen is fully saturated in order to record the volumetric strain during vibration. Furthermore, a pore pressure transducer is used to measure the possible excess pore pressure induced by vibrations. This is achieved by allowing the drainage valve at the top of the specimen to open while measuring the pore pressure at the bottom of the specimen. Three sequential vibrations of 20 Hz with different intensities are superimposed to the monotonic loading when the specimen is approaching the critical state. It can be seen that the first two vibrations are not intensive enough to generate fluidization, as indicated in Figure 3 and Figure 4(a). The deviatoric stresses q undergoes a certain degree of decrease until approaches a stable level when vibration is applied, and this is followed by a full recovery to its original level when vibration is stopped. Fluidization takes place under the third vibration where the deviatoric stress q immediately drops to zero and the granular behaves like a fluid with a huge volumetric compressive deformation.

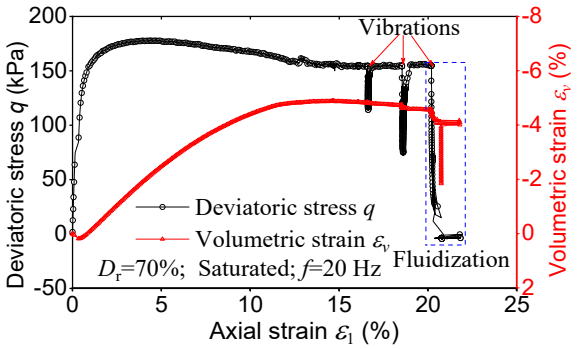

Figure 3. ViF of saturated dense specimen at the critical state: deviatoric stress and volumetric strain

The details of the ViF history are depicted in Figure 4(b) and Figure 4(c). Based on the evolution of the normalized vertical acceleration A/g with A being peak acceleration g being the gravitational acceleration, the whole fluidization process can be divided into two stages. There is a continuous growth in A/g at stage I with a gradual decrease of about 80% in q being observed. It is noted that the acceleration given in the figure is the additional acceleration induced by the VCA with the acceleration of gravity being excluded, which can be regarded as an indicator of vibration intensity instead of the acceleration of the specimen. Moreover, because the water could not be immediately expelled out under the high-frequency vibration, a slight decline in effective confining stress σ_c as a result of excess pore pressure Δu is also found, as shown in Figure 4(b). Although Δu induced by the vibration may accelerate the process of fluidization, it is not the main reason for fluidization. It can be seen at the end of stage I that the deviatoric stress has lost 80% while the decrease in σ_c is only about 30%. Indeed, to eliminate the influence of Δu on fluidization, tests with dry specimens were also conducted, demonstrating that the ViF also occurs in the absence of excess pore pressure. That will be discussed in the next section where dry specimens at the pre-peak state were fluidized under vibration. Once getting stage II as shown in Figure 4(b) and Figure 4(c), an abrupt surge both in the volumetric strain and pore pressure happens immediately, and the soil

completely loses its shear resistance. In the whole fluidization process as presented in Figure 4(c), the amplitude of oscillation σ_d experienced a stable growth due to the declining shearing resistance, although the intensity of vibration (energy input level of VCA) is constant.

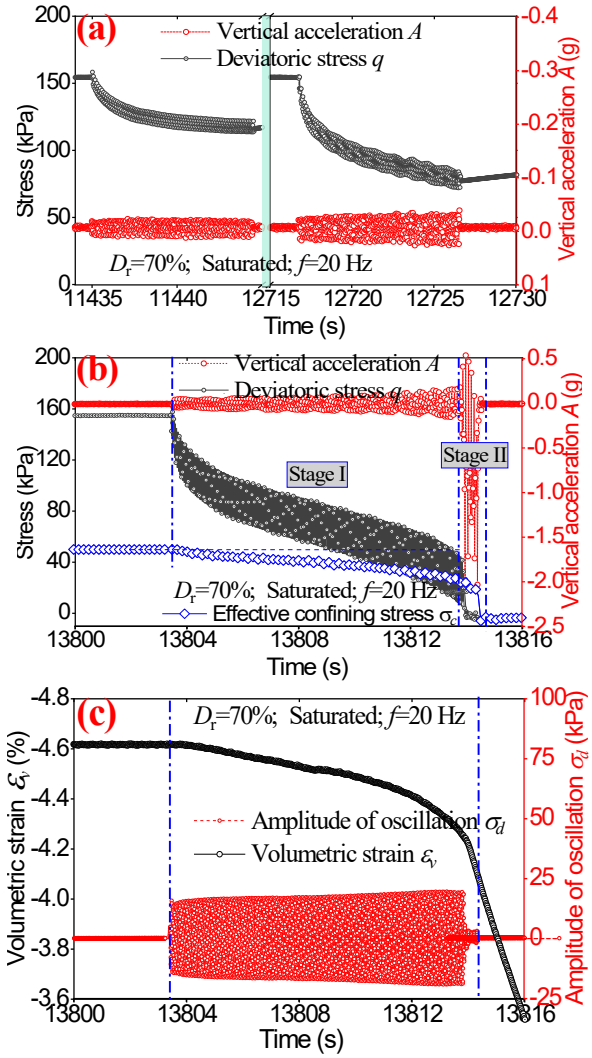

Figure 4. History of ViF in the test: (a) history of deviatoric stress when the first two vibrations are not strong enough to generate fluidization (b) history of deviatoric stress and effective confining pressure during fluidization; (c) volumetric strain and amplitude of oscillation during fluidization

(2) *Fluidization at the pre-peak state*

An example of a dry loose specimen of D_r = 35% fluidized at the pre-peak state is presented in Figure 5. The vibration of f = 60 Hz is superimposed on the specimen when

q grows to 100 kPa. According to the developments of q and normalized vertical acceleration A/g, the whole process can be also classified into two stages. Generally, the developments in q and A/g at stage I are relatively stable compared with stage II. The whole process is similar to those discussed above.

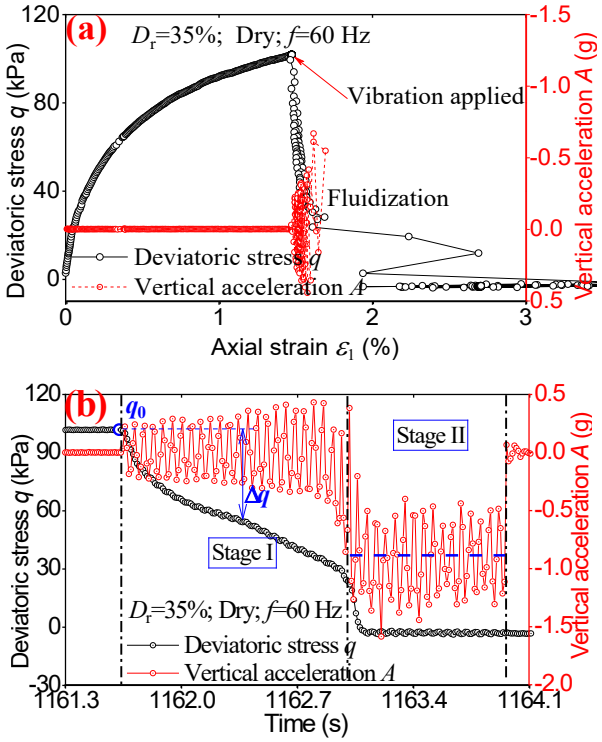

Figure 5. ViF of dry specimen at the pre-peak state: (a) stress-strain relationship; (b) history of deviatoric stress

(3) *Shear resistance reduction $\Delta q/q_0$ versus axial strain increment* $\Delta\varepsilon_1$

Figure 6 summarizes the relationship between $\Delta q/q_0$ and axial strain increment $\Delta\varepsilon_1$ induced by vibration during fluidizations, in which the fluidizations of dry and saturated specimens are presented. Vibrations of f = 20~100 Hz are applied at the critical state and pre-peak state, with q_0 ranging from 75 to 155 kPa. It can be seen from Figure 6 that the development of $\Delta q/q_0$ with $\Delta\varepsilon_1$ experienced two stages. A growth of $\Delta q/q_0$ with a decreasing rate of $\Delta\varepsilon_1$ is observed at stage I and almost 80% of shear resistance

has been lost in this stage. Then, an abrupt increase in $\Delta\varepsilon_1$ is followed once reaching stage II until complete fluidization. Interestingly, the $\Delta q/q_0 \sim \Delta\varepsilon_1$ curves under different conditions seem to follow the same trajectory that can be described by a hyperbolic curve, which is independent of q_0 both at the near-critical state and pre-peak state, as evidenced in Figure 6.

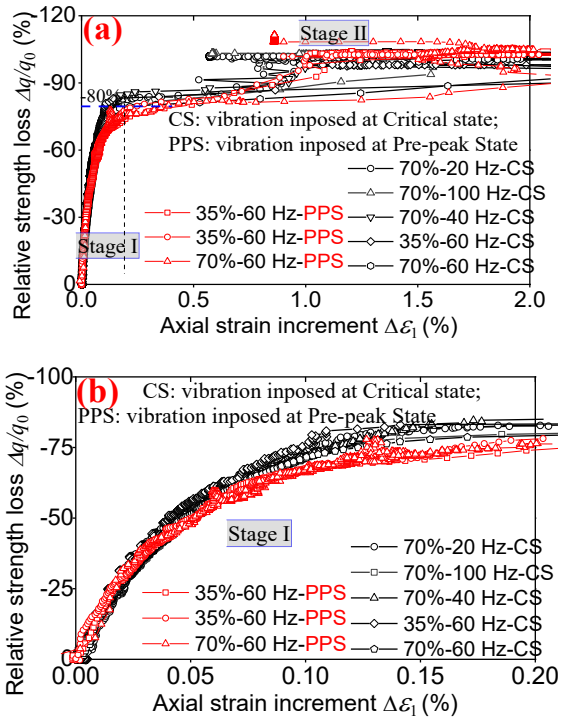

Figure 6. Relationship of $\Delta q/q_0$ and $\Delta\varepsilon_1$ during ViFs: (a) in the whole process; (b) at stage I

3. Extended STZ model

3.1 Formulation

(1) *General conditions*

The extended STZ model is model which can consider the static loading and vibration simultaneously. In granular materials, a STZ (weak spot) can be visualized as a weak particle loop with at least four grains as shown in Figure 7. The transition of an STZ, which corresponds to the change in STZ orientation, generates plastic deviatoric (shear)

strain, whereas the creation and destruction of STZs, which corresponds to the change in STZ amount (or density), are the sources of plastic volumetric strain. The processes of transition, creation, and destruction are collectively called the motion of STZ, which is driven by the evolution of internal energy in the granular system. Hence, the extended STZ model has three groups of governing functions: (1) the motion of STZ, (2) the evolution law for the configurational temperature χ as an indicator of internal energy and the driving power associated with the motion of STZ, and (3) the relationship between the motion of STZ and the corresponding plastic strains.

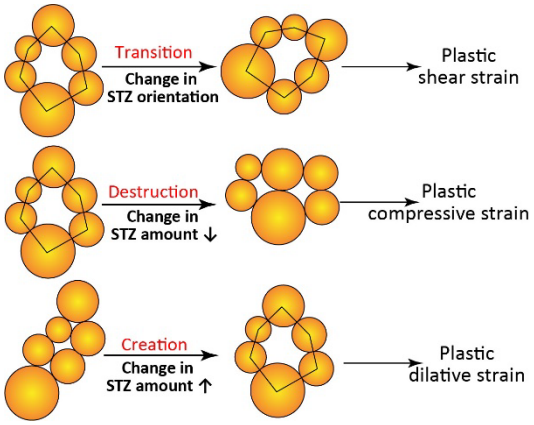

Figure 7. Motion of STZs and the corresponding plastic strains in the extended STZ model

First, the motion of STZ can be described by

$$\tau_0 \dot{H}_{ij} = \Lambda R_{ij} - R^* H_{ij} + \left(\frac{\Lambda^{eq}}{\Lambda} - 1 \right) \tilde{\Gamma}_{im} H_{mj} \tag{1}$$

with

$$H_{ij} = \frac{1}{N_g} \sum_{\alpha=1}^{N} h_i^\alpha h_j^\alpha, \quad \tilde{\Gamma}_{ij} = \Gamma \delta_{ij} + \lambda d_{ij} \tag{2}$$

In which H_{ij} is STZ tensor used to illustrate the spatial distribution of STZ with h_i^α being the unit orientation vector of the α^{th} STZ; N and N_g are the total number of STZ and the total number of particles in a REV, respectively; τ_0 is a time scale and is assumed to be inversely proportional to the loading rate $\dot{\varepsilon}_1$ (axial strain rate in

traditional triaxial compression tests), i.e., $\tau_0 = \kappa\dot{\varepsilon}_1^{-1}$; R_{ij} is transition rate tensor with $R^* = R_{ii}$; $\tilde{\Gamma}_{ij}$ is loading strength tensor reflecting the effect of external disturbance such as static shearing and vibration on the creation and destruction of STZs; Γ and λ respectively refers to mechanical and vibrational noise strengths; d_{ij} is a unit-magnitude deviatoric tensor with major principal direction in the direction of vibration; $\Lambda = H_{ii}$ is STZ density, and Λ^{eq} is the value of Λ in steady equilibrium (critical state). It is noted that the first and second terms on the right side of Eq. (1) describe the transition of STZ, i.e., change in STZ orientation; and the last term describes the creation and destruction of STZ, i.e., change in STZ density.

Second, the relationship between the motion of STZ and the resulting plastic strains is given as

$$\tau_0\dot{\varepsilon}_{ij}^{pl} = \omega_s\left(\Lambda R_{ij} - R^* H_{ij}\right) - \omega_v\left(\frac{\Lambda^{eq}}{\Lambda} - 1\right)\tilde{\Gamma}_{im}H_{mj} \tag{3}$$

with ω_s and ω_v being the elementary increments of plastic strain during STZ transition and STZ creation/destruction, respectively. It can be derived from Eq. (3) that the rate of plastic volumetric strain $\dot{\varepsilon}_v^{pl}$ is

$$\dot{\varepsilon}_v^{pl} = \dot{\varepsilon}_{ii}^{pl} = -\omega_v\left(\frac{\Lambda^{eq}}{\Lambda} - 1\right)\tilde{\Gamma}_{im}H_{mi} = -\omega_v\dot{\Lambda} \tag{4}$$

That indicates rate of plastic volumetric strain is proportional to the rate of STZ density, and the creation and destruction of STZs are the only sources of plastic volumetric strain.

Finally, the evolution law of configurational temperature χ is determined by

$$\tau_0 C_0\dot{\chi} = \left[\omega_s s_{ij}\left(\Lambda R_{ij} - R^* H_{ij}\right) - p\omega_v\tau_0\dot{\Lambda}\right]\left(1 - \frac{\chi}{\chi^{eq}}\right) + \lambda A_0\left(1 - \eta\frac{\chi}{\chi_v^{eq}}\right) \tag{5}$$

where s_{ij} is deviatoric stress tensor; p is mean stress; C_0 is an energy capacity coefficient; η is a constant parameter and η>1; χ^{eq} and χ_v^{eq} denote the values of χ in steady equilibrium in the absence and presence of vibrations, respectively; and A_0 is a

coefficient related to vibrational noise strength and rates of vibrational energy density $\dot{E}_V$, see

$$\dot{E}_V - \dot{E}_F = \lambda A_0 \tag{6}$$

Herein, $\dot{E}_F$ stands for the rate of energy dissipation per unit volume generated by inelastic contact deformations and collisions of particles, which has no contribution to the plastic deformation of granular soils.

Other involved parameters are given as follows

$$R_{ij} = \frac{R_0}{3}\exp(\omega_s v_g s_{ij} / \chi) \tag{7}$$

$$\Gamma = \frac{\xi_d s_{ij}}{\Lambda p_0}\left(\Lambda R_{ij} - R^* H_{ij}\right) - \frac{\xi_v p}{p_0}\left(\frac{\Lambda^{eq}}{\Lambda} - 1\right) \tag{8}$$

$$\Lambda^{eq} = \begin{cases} \exp(-e_z / \chi^{eq}), & \lambda=0 \\ \exp\left[-e_z \cdot \chi^{eq} / (\chi \cdot \chi_v^{eq})\right], & \lambda>0 \end{cases} \tag{9}$$

In the above, p_0 is unit pressure; e_z is energy barrier; ξ_d and ξ_v represent energy coefficients; R_0 is a constant coefficient, and $R^* = R_{ii} \approx R_0$ holds owing to $\omega_s v_g s_{ij} / \chi \to \mathbf{0}$ with v_g being occupied volume of the particle. Hence, R^* can be replaced by R_0 in involved expressions. Taking $\tau_0 \mathrm{d}\square/\mathrm{d}t = \tau_0 \dot{\varepsilon}_1 \mathrm{d}\square/\mathrm{d}\varepsilon_1 = \kappa \mathrm{d}\square/\mathrm{d}\varepsilon_1$ into the above three governing functions Eqs. (1), (3), and (5) yields

$$\kappa \frac{\mathrm{d}\varepsilon_{ij}^{pl}}{\mathrm{d}\varepsilon_1} = \omega_s\left(\Lambda R_{ij} - R_0 H_{ij}\right) - \omega_v\left(\frac{\Lambda^{eq}}{\Lambda} - 1\right)\tilde{\Gamma}_{im} H_{mj} \tag{10}$$

$$\kappa \frac{\mathrm{d}H_{ij}}{\mathrm{d}\varepsilon_1} = \Lambda R_{ij} - R_0 H_{ij} + \left(\frac{\Lambda^{eq}}{\Lambda} - 1\right)\tilde{\Gamma}_{im} H_{mj} \tag{11}$$

$$C_0 \kappa \frac{\mathrm{d}\chi}{\mathrm{d}\varepsilon_1} = \left[\omega_s s_{ij}\left(\Lambda R_{ij} - R_0 H_{ij}\right) - \omega_v p \kappa \frac{\mathrm{d}\Lambda}{\mathrm{d}\varepsilon_1}\right]\left(1 - \frac{\chi}{\chi^{eq}}\right) + \lambda A_0\left(1 - \eta \frac{\chi}{\chi_v^{eq}}\right) \tag{12}$$

(2) *Triaxial stress conditions*

For initially isotropic soils subjected to combined vertical vibration and triaxial monotonic loading, as shown in Figure 2, we have $\sigma_2 = \sigma_3 = \sigma_c$, $\varepsilon_1 = \varepsilon_2$, as well as

constant $\dot{\varepsilon}_1 = \dot{\varepsilon}_a$ and effective confining pressure σ_c. Herein, σ_k and ε_k (k = 1, 2, or 3) represent principal stress and principal strain, respectively. The tensors in the governing functions Eqs. (10) ~ (12) can be further simplified using principal values, *i.e.*,

$$\kappa \frac{\mathrm{d}\varepsilon_1^{pl}}{\mathrm{d}\,\varepsilon_1} = \frac{\omega_s}{2}\Lambda R_0\left(m-T\right) - \omega_v \frac{\mathrm{d}\Lambda}{2\,\mathrm{d}\,\varepsilon_1}\left[1+\frac{\lambda\left(1-m\right)}{2\Gamma+\lambda\left(1-m\right)}\right], \quad \text{and} \quad \frac{\mathrm{d}\varepsilon_v^{pl}}{\mathrm{d}\,\varepsilon_1} = -\omega_v \frac{\mathrm{d}\Lambda}{\mathrm{d}\,\varepsilon_1} \tag{13}$$

$$\kappa \frac{\mathrm{d}\Lambda}{\mathrm{d}\,\varepsilon_1} = \left(\Gamma+\lambda\frac{1-m}{2}\right)\left(\Lambda^{eq}-\Lambda\right), \quad \kappa \frac{\mathrm{d}m}{\mathrm{d}\,\varepsilon_1} = -R_0\left(m-T\right) + \frac{\lambda\left(1+m\right)m}{2\Gamma+\lambda\left(1-m\right)}\frac{\kappa \mathrm{d}\Lambda}{\Lambda\,\mathrm{d}\,\varepsilon_1} \tag{14}$$

$$\kappa C_0 \frac{\mathrm{d}\chi}{\mathrm{d}\,\varepsilon_1} = \left[\frac{q}{2}\omega_s \Lambda R_0\left(m-T\right) - p\omega_v \kappa \frac{\mathrm{d}\Lambda}{\mathrm{d}\,\varepsilon_1}\right]\left(1-\frac{\chi}{\chi^{eq}}\right) + \lambda A_0\left(1-\eta\frac{\chi}{\chi_v^{eq}}\right) \tag{15}$$

with

$$m = \frac{N_2+N_3-N_1}{N_1+N_2+N_3}, \quad T = \frac{R_2+R_3-R_1}{R_1+R_2+R_3} = \frac{2-\exp(\omega_s v_g q/\chi)}{2+\exp(\omega_s v_g q/\chi)} \tag{16}$$

$$\Gamma = \frac{\xi_d R_0 q}{2p_0}\left(m_1 - T_1\right) - \frac{\xi_v p}{p_0}\left(\frac{\Lambda^{eq}}{\Lambda}-1\right) \tag{17}$$

In which N_k and R_k (k = 1, 2, or 3) are principal values of H_{ij} and R_{ij}, respectively; m and T are respectively called orientation bias and transition bias.

Moreover, a linear stiffness relationship is adopted in the model as

$$\frac{\mathrm{d}q}{\mathrm{d}\varepsilon_1} = 3\frac{\mathrm{d}p}{\mathrm{d}\varepsilon_1} = 2\left(1+\nu\right)G\left(1-\frac{\mathrm{d}\varepsilon_1^{pl}}{\mathrm{d}\varepsilon_1}\right) \tag{18}$$

$$\frac{\mathrm{d}\varepsilon_v}{\mathrm{d}\varepsilon_1} = \left(1-2\nu\right)\left(1-\frac{\mathrm{d}\varepsilon_1^{pl}}{\mathrm{d}\varepsilon_1}\right) + \frac{\mathrm{d}\varepsilon_v^{pl}}{\mathrm{d}\varepsilon_1} \tag{19}$$

where G and ν are the shear modulus and Poisson's ratio, respectively.

3.2 Model results

Two compressive triaxial tests of Standard Ottawa Sand under drained conditions are first used to determine the parameters of the extended STZ model, as shown in Figure 8. Due to the absence of vibration, the vibrational noise strength λ as an indicator of vibration intensity is set to zero. Other parameters are given in Table 2. It should be noted that the initial value of STZ density $\Lambda_0 = \exp(-e_z/\chi_0)$ with χ_0 being the

initial temperature and the initial value of m is 1/3 for isotopically consolidated soils (σ_c = 50 kPa). The occupied volume (v_g) of the particle roughly equals particle volume.

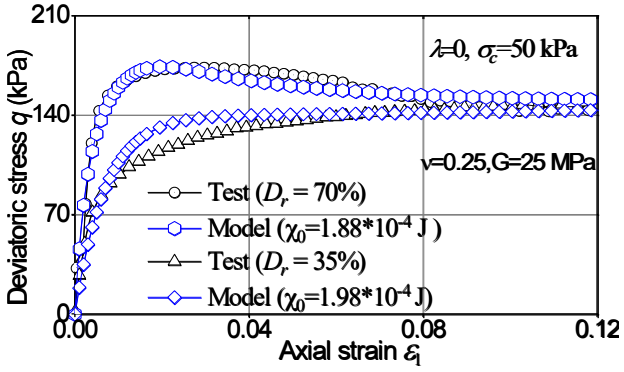

Figure 8. Triaxial monotonic tests for determining model parameters.

Table 2 Parameters for the extended STZ model

e_z (J)	χ^{eq} (J)	χ_v^{eq} (J)	v_g (m^3)	κ	η	R_0	ω_v	ω_s	C_0	ξ_v	ξ_d	A_0
2.5*10^{-4}	2*10^{-4}	1.9*10^{-4}	4*10^{-11}	5	1.2	3	1.6	30	300	6	1	10^3

The configurational temperature χ, as a function of the compactivity of granular materials, is a volume-controlled parameter and plays a role in the soil's void ratio. Hence, the initial configurational temperature χ_0 corresponds to the soil's initial void ratio and its influence on the soil's static responses is illustrated in Figure 8. For a high initial configurational temperature χ_0 = 1.98*10^{-4} J (corresponding to loose soil), the deviatoric stress q increases at a declining rate with the development of axial strain ε_1 until reaching a plateau at near-critical state; For dense sand with χ_0 = 1.88*10^{-4} J, q firstly undergoes an obvious increase to a peak value. After that, q starts to decline because of the strain-softening and then reaches the same plateau as the loose sand. Interestingly, the same deviatoric stresses q is achieved at critical state with different χ_0, implying that the soil's shear strength at critical state is independent of its initial void ratio. This observation is in accord with the concepts of soil mechanics.

Incidentally, the determined parameters in Table 2 and Figure 8 are also used in the simulation of granular soil's fluidization.

(1) *Fluidization at near-critical state*

Figure 9 illustrates the fluidization of granular soil subjected to vibration at the near-critical state. To compare the model results with tests, the same loading scheme is adopted in the model as in experiments, as given in Figure 2. The granular soil undergoes a significant increase in deviatoric stress q before gradually declining to a stable value, as shown in Figure 9(a). Then, as the vibration is superimposed on the specimen, an immediate decrease in q is witnessed. The rate of decrease in q is declining during vibration until the soil completely loses shear strength. This process is accompanied by a continuous compression in volumetric strain, as shown in Figure 9(b). It is seen that there is a slight compression at the beginning of monotonic shearing. Then, this initial compression is offset by the followed dilation which dominates the change of volumetric strain in the followed monotonic shearing phase. At near-critical state, the rate of volumetric strain is close to zero and the volumetric strain is approaching a table value. However, the superimposed vibration changes the trajectory of the volumetric strain and an obvious compression is accompanied by the vibration until the soil is completely fluidized. The whole process is like the observations in the tests. Here, the vibrational noise strength λ is an increasing function of the vibration energy rate $\dot{E}_V$ as defined in Eq. (6). Therefore, λ can be regarded as an indicator of vibration intensity in the extended STZ model.

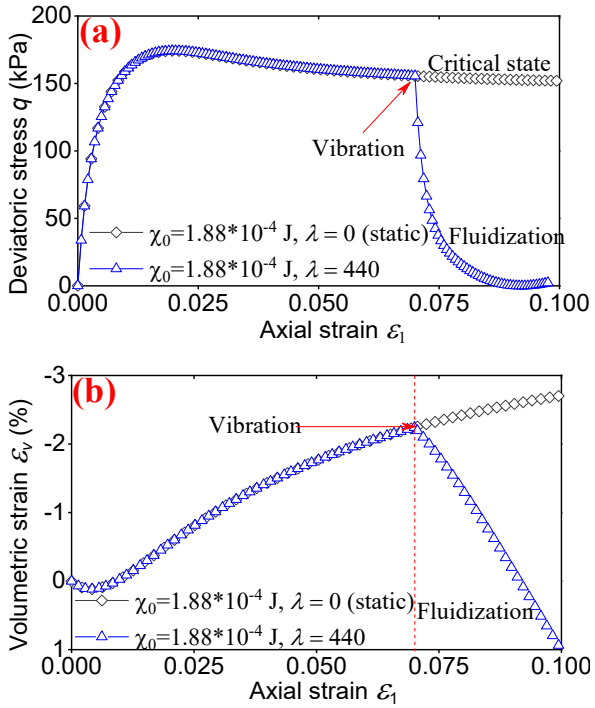

Figure 9. ViF of dense granular soil as vibration applied at near-critical state: (a) deviatoric stress; (b) volumetric strain

The evolution of configurational temperature χ is given in Figure 10(a). Prior to vibration, the χ experiences an outstanding growth at the beginning of monotonic shearing and then tends to a stable value at the critical state which corresponds to the critical void ratio. Under vibration, a dramatic decrease in χ is also accompanied by the fluidization process which implies a decline in the soil's void ratio. The details of the strain ratio $\mathrm{d}\varepsilon_1^{pl}/\mathrm{d}\varepsilon_1$ during fluidization are given in Figure 10(b), Here, $\mathrm{d}\varepsilon_1^{pl}/\mathrm{d}\varepsilon_1$ <1 means the increment of plastic strain $\mathrm{d}\varepsilon_1^{pl}$ is smaller than the increment of total axial strain $\mathrm{d}\varepsilon_1$ and hence results in a growth in q. Oppositely, $\mathrm{d}\varepsilon_1^{pl}/\mathrm{d}\varepsilon_1$ >1 indicates a decline in q, and $\mathrm{d}\varepsilon_1^{pl}/\mathrm{d}\varepsilon_1 = 1$ indicates no change in q. It can be seen the evolution of $\mathrm{d}\varepsilon_1^{pl}/\mathrm{d}\varepsilon_1$ during monotonic shearing is similar to that of χ. Near the critical state, $\mathrm{d}\varepsilon_1^{pl}/\mathrm{d}\varepsilon_1 \approx 1$ and that implies an approximately constant q.

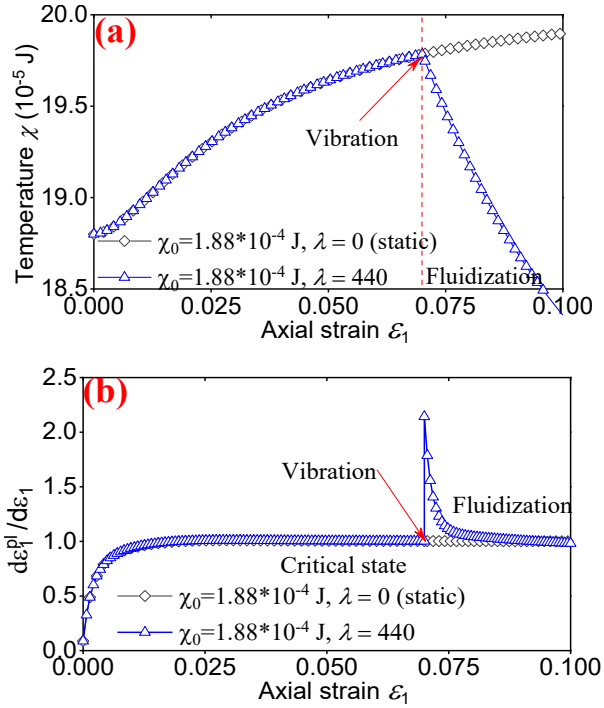

Figure 10. ViF in dense sand when vibration is applied at near-critical state: (a) configuration temperature; (b) plastic axial strain rate

The evolution of $\mathrm{d}\varepsilon_1^{pl}/\mathrm{d}\varepsilon_1$ can be used to explain the mechanism of ViF phenomenally. At the onset of vibration, an abrupt surge followed by a gradual recovery in $\mathrm{d}\varepsilon_1^{pl}/\mathrm{d}\varepsilon_1$ takes place as long as the vibration is applied. This is because the superimposed vibration promotes the development of plastic strain, i.e., an increase in $\mathrm{d}\varepsilon_1^{pl}/\mathrm{d}t$. At the same time, the total deformation rate of axial strain is fixed to constant ($\mathrm{d}\varepsilon_1/\mathrm{d}t = const.$), which makes the soil in a "restricted" deformation condition unable to "follow" the development of plastic strain induced by vibration ($\mathrm{d}\varepsilon_1^{pl}/\mathrm{d}\varepsilon_1$>1), and hence causes a relaxation in shear resistance q. From the perspective of STZ motion driven by external energies, the superimposed vibration accelerates the destruction of STZ and thus leads to a rise in $\mathrm{d}\varepsilon_1^{pl}/\mathrm{d}\varepsilon_1$. The mechanical noise strength Γ and vibrational strength λ determine the intensity of STZ destruction. At near-critical state, the magnitude of Γ is approaching stable and $\lambda = 0$ before vibration. The superimposed vibration ($\lambda > 0$) promotes the destruction of STZ, as indicated in the

evolution of STZ density Λ in Figure 11(a). The STZ density Λ undergoes a slight rise at the beginning of monotonic loading. Then, due to the shear-induced dilation, the rate of Λ change experiences an increase at first and then a decline with the development of axial strain. A stable Λ is expected at critical state if without vibration. However, the superimposed vibration changes the trajectory of STZ density Λ. Under vibration, a continuous decline in STZ density is observed during the fluidization process.

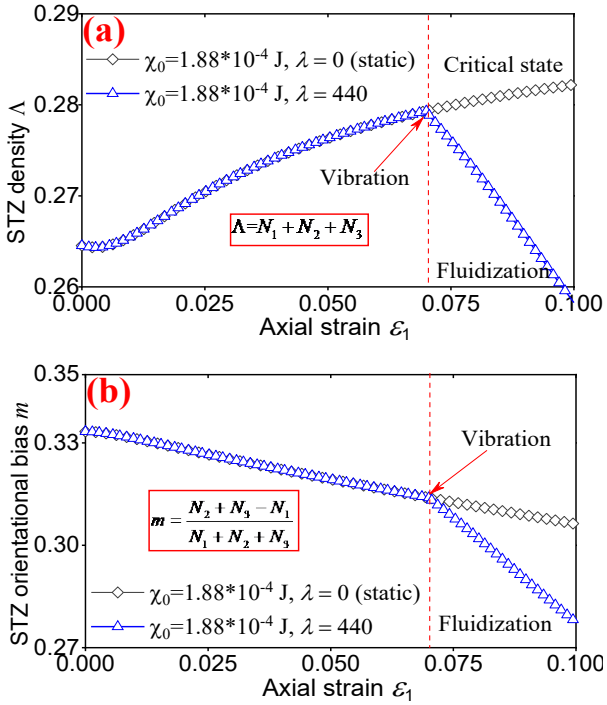

Figure 11. Motion of STZ before and during fluidization: (a) STZ density; (b) orientational bias of STZ

The orientational bias of STZ m is an indicator of STZ transition which has no influence on the STZ density but can change the STZ orientation. As indicated in Figure 11(b), the initial value of m is 1/3 because all principal values of STZ tensor are the same for isotopically consolidated specimens, i.e., $N_1 = N_2 = N_3$. With the increase of axial strain ε_1, a continuous decline is found in the orientational bias m, suggesting that the amount of STZs transit from the axial direction to the horizontal plane is more than

the amount of STZ transit back to the axial direction from the horizontal plane. Because the application of vibration accelerates this process, a steep decline in m takes place during fluidization, as depicted in Figure 11(b).

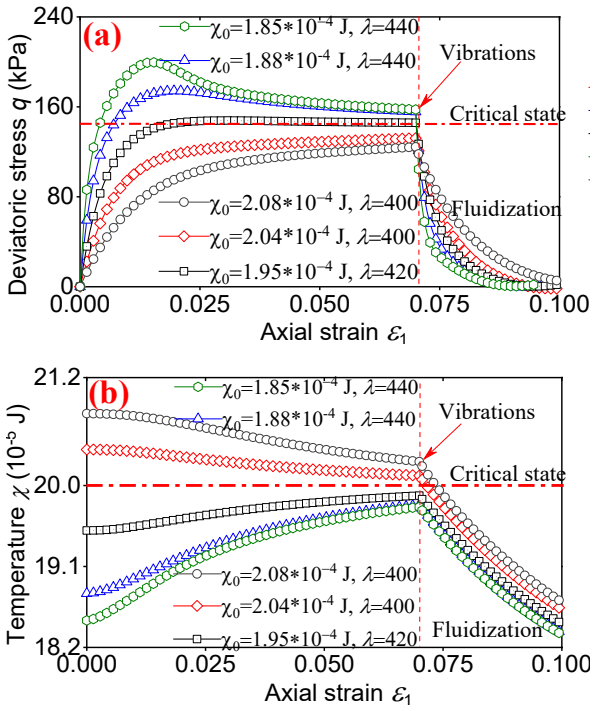

Figure 12. Influence of soil's initial density on fluidization at near critical state: (a) deviatoric stress; (b) configurational temperature

Figure 12 summarizes the influence of initial density (χ_0) on the vibration intensity λ^{flu} at fluidization. As the indicator of soil's initial void ratio, a higher χ_0 corresponds to a looser initial density. It is seen from Figure 12(a) that a significant strain-softening with obvious peak strength occurs in dense soils at small values of χ_0. This effect gradually phases out and completely disappears with the increase in χ_0. Moreover, the deviatoric stress of soil at different initial densities tends to approach the same value at near-critical state, which indicates an identical shear strength. It can be attributed to the same void ratio at critical state (critical void ratio) which is independent of the soil's initial density, as shown in Figure 12(b) where the same χ would be expected for soils at different χ_0 if without vibration. However, the superimposed

vibrations changed the trajectories of deviatoric stress and configurational temperature χ. A steep decrease is observed both in q and χ with the application of vibration, implying that compression is always accompanied by vibration. More interestingly, the vibration intensity λ^{flu} for granular soils at different initial densities is close ($\lambda = \lambda^{flu}$ = 400~440) at fluidization, as evidenced in Figure 12(a). The small fluctuation of λ^{flu} is only due to the tiny difference in initial deviatoric stress when vibration is applied.

It is noted that the fluidization in the STZ model is much slower than observations in experiments. In the other words, the reduction in deviatoric stress during fluidization observed in tests is much faster than in the extended model. The possible reason is that the vibration of particles accelerates the motion of STZ and hence further promotes fluidization whereas this effect is excluded in the model. Excepting this problem, this model is generally in line with the experimental findings.

(2) *Fluidization at pre-peak state*

The process of fluidization, when vibrations are superimposed at different initial stress levels q_0 at the pre-peak state, is given in Figure 13. With the application of vibration, a sharp decrease in q at a declining rate is witnessed until the soil completely loses its shear resistance. The granular soil is transferred from a solid-state to a liquid-state and the ViF takes place.

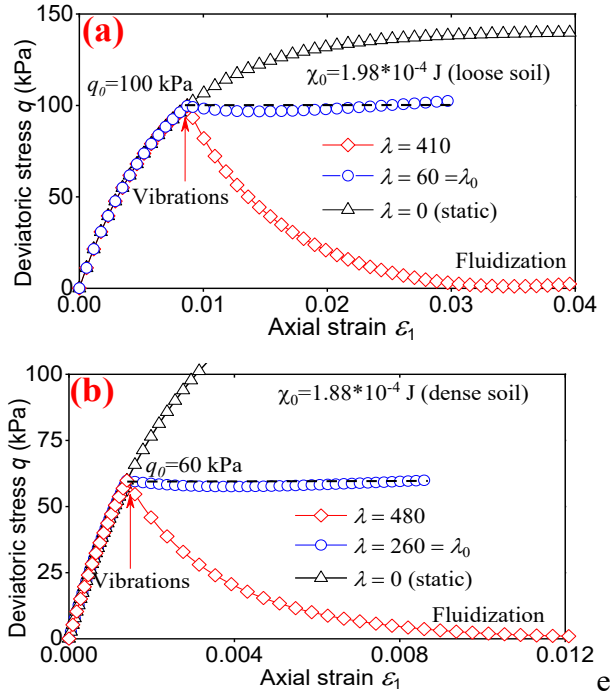

Figure 13. Vibration-induced fluidization of loose sand as vibration applied at pre-peak states: (a) loose soil, q_0 = 100 kPa; (b) dense soil, q_0 = 60 kPa

Notably, due to the problem that the rate of fluidization in the model is much slower than in the test, as mentioned above, the growth in q induced by the monotonic shearing is unavoidable during the period of vibration. This growth is negligible in tests because the fluidization only lasts for several seconds. To offset this part growth of q in the model, it is required to set an initial vibration intensity λ_0 for keeping a constant q during vibration, as sketched in Figure 13. The actual vibration intensity λ^{flu} required to fluidize the granular soil is the difference between λ and λ_0. For instance, the vibration intensity for fluidization λ^{flu} = (410 - 60) at q_0 = 100 kPa in Figure 13(a) and λ^{flu} = (480-260) at q_0 = 60 kPa in Figure 13(b), suggesting that the larger the q_0, the greater the vibration intensity is needed to fluidize a granular soil.

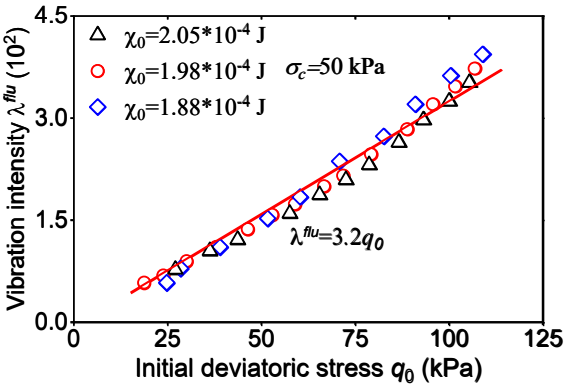

Figure 14. Influence of stress level q_0 on vibration intensity λ^{flu} required for fluidization at pre-peak state

Figure 14 summarizes the effects of stress level q_0 on the required vibration intensity λ^{flu} at fluidization. Interestingly, a roughly linear relationship between q_0 and λ^{flu} is observed for a given χ_0 (initial density). That means the λ^{flu} is proportional to the initial stress level q_0 at which vibration is applied. Moreover, the $q_0 \sim \lambda^{flu}$ curve is independent of the initial configurational temperature χ_0. At the same initial stress level q_0, the same λ^{flu} is required for dense granular soils with smaller χ_0 and loose ones. Intuitively, this discipline seems to violate and defy the common sense of soil mechanics where dense soils usually have stronger resistance to vibration than loose soils. In fact, the same λ^{flu} for dense soils does not mean the same vibration energy input is required to cause fluidization, because the vibration-induced energy dissipation E_F is also included in λ from the definition in Eq. (6). Usually, the proportion of $\dot{E}_F / \dot{E}_V$ is higher for a dense soil than a loose one. This part of dissipation energy $\dot{E}_F$ partially offsets the effect of $\dot{E}_V$. To be exact, the value of λ^{flu} can be regarded as the "effective vibration strength".

The above discussion proved that the STZ model is a desirable tool for ViSRR. Incidentally, the influence of vibration frequency is not explicitly incorporated in the

model. It is mainly reflected in the magnitude of energy dissipation $\dot{E}_F$ and thus on λ in this model. Specifically, the frequency mostly affects the efficiency of energy transferred from vibration into the soil. In essence, $\dot{E}_V - \dot{E}_F$ is the portion of vibration energy that effectively acts on the soil's configuration and thus causes fluidization.

Conclusions

This paper studied the ViF in granular soils under vibration both from the modified triaxial tests and the extended STZ model. The major works and the corresponding conclusions are summarized as follows:

First, to reproduce fluidization in the laboratory, a range of specially designed tests were performed under drained conditions via a modified triaxial shear apparatus. Both dry and saturated specimens with D_r=35% and 70% were performed. The experimental results have shown: (1) the ViF takes place in both dry and saturated specimens, while the presence of water does accelerate the fluidization of soil; (2) the $\Delta q/q_0$ increases with a declining rate with axial strain increment $\Delta\varepsilon_1$ during the fluidization. The $\Delta q/q_0$~ $\Delta\varepsilon_1$ relationship follows a hyperbolic function and is independent of initial stress level q_0 no matter whether vibrations are applied at near-critical or pre-peak states.

Second, the extended STZ model is a constitutive model committed to converting the motion of mesoscopic STZ as the weak spot in a granular material, into the macroscopic plastic strain of granular materials subjected to combined vibration and static loading. The analyses from the extended STZ model suggested that: (1) the vibration intensity λ^{flu} for fluidization is approximately proportional to q_0, indicating an increase in q_0 is contributable to resisting the vibration-induced fluidization in the field; (2) As an indicator of soil's initial void ratio, the initial configurational temperature χ_0 has no impact on the λ^{flu} when vibration is imposed at near-critical state.

Acknowledgments

This research was supported by funding from the Natural Science and Engineering Research Council of Canada.

References

Barkan, D. D. (1962). Dynamics of bases and foundations, Trans. L. Drashevska, McGraw-Hill, New York, 207–210.

Bingham, C. M., Stone, D. A., Schofield, N., Howe, D., & Peel, D. (2000). Amplitude and frequency control of a vibratory pile driver. IEEE Transactions on Industrial Electronics, 47(3), 623-631.

Blekhman, I.I. (2000). Vibrational mechanics. World Scientific, Singapore. 509 p.

Brace, W. F., & Byerlee, J. D. (1966). Stick-slip as a mechanism for earthquakes. Science, 153(3739), 990-992.

Chang, C. S., Chang, Y., & Kabir, M. G. (1992). Micromechanics modeling for stress-strain behavior of granular soils. I: Theory. Journal of geotechnical engineering, 118(12), 1959-1974.

Cundall, P. A., & Strack, O. D. (1979). A discrete numerical model for granular assemblies. geotechnique, 29(1), 47-65.

Darbois Texier, B., Ibarra, A., & Melo, F. (2017). Low-resistive vibratory penetration in granular media. PloS one, 12(4), e0175412.

Daub, E. G., & Carlson, J. M. (2008). A constitutive model for fault gouge deformation in dynamic rupture simulations. Journal of Geophysical Research: Solid Earth, 113(B12).

Denies, N., Canou, J., Roux, J. N., & Holeyman, A. (2010). Sphere penetration experiments in vertically vibrated sand.

Denies, N. (2010). Dynamic behavior of vibrated dry sand: sphere penetration experiments and discrete element modeling of vibrofluidization (Doctoral dissertation, UCL-Université Catholique de Louvain).

Denies, N., & Holeyman, A. (2017). Shear strength loss of vibrated dry sand. Soil Dynamics and Earthquake Engineering, 95, 106-117.

Falk, M. L., & Langer, J. S. (1998). Dynamics of viscoplastic deformation in amorphous solids. Physical Review E, 57(6), 7192.

Ferdowsi, B., Griffa, M., Guyer, R. A., Johnson, P. A., Marone, C., & Carmeliet, J. (2015). Acoustically induced slip in sheared granular layers: Application to dynamic earthquake triggering. Geophysical Research Letters, 42(22), 9750-9757.

Griffa, M., Ferdowsi, B., Guyer, R. A., Daub, E. G., Johnson, P. A., Marone, C., & Carmeliet, J. (2013). Influence of vibration amplitude on dynamic triggering of slip in sheared granular layers. Physical Review E, 87(1), 012205.

Hosoi, A. E., & Goldman, D. I. (2015). Beneath our feet: strategies for locomotion in granular media. Annual review of fluid mechanics, 47.

Hsiau, S. S., Liao, C. C., Sheng, P. Y., & Tai, S. C. (2011). Experimental study on the influence of bed height on convection cell formation. Experiments in fluids, 51(3), 795.

Huan, C. (2008). NMR experiments on vibrofluidized and gas fluidized granular systems. University of Massachusetts Amherst.

Hwang, J. H., Liang, N., & Chen, C. H. (2001). Ground response during pile driving. Journal of Geotechnical and Geoenvironmental Engineering, 127(11), 939-949.

Jaeger, H. M., Nagel, S. R., & Behringer, R. P. (1996). Granular solids, liquids, and gases. Reviews of modern physics, 68(4), 1259.

Janda, A., Maza, D., Garcimartín, A., Kolb, E., Lanuza, J., & Clément, E. (2009). Unjamming a granular hopper by vibration. EPL (Europhysics Letters), 87(2), 24002.

Jia, X., Brunet, T., & Laurent, J. (2011). Elastic weakening of a dense granular pack by acoustic fluidization: Slipping, compaction, and aging. Physical Review E, 84(2), 020301.

Johnson, T., Wu, F. T., & Scholz, C. H. (1973). Source parameters for stick-slip and for earthquakes. Science, 179(4070), 278-280.

Johnson, P. A., & Jia, X. (2005). Nonlinear dynamics, granular media and dynamic earthquake triggering. Nature, 437(7060), 871-874.

Johnson, P. A., Savage, H., Knuth, M., Gomberg, J., & Marone, C. (2008). Effects of acoustic waves on stick–slip in granular media and implications for earthquakes. Nature, 451(7174), 57-60.

Krey, H. (1932). Erddruck, Erdwiderstand und Tragfähigkeit des Baugrundes Berlin, Deutschland, Wilhelm Ernst ahd Sohn.

Lastakowski, H., Géminard, J. C., & Vidal, V. (2015). Granular friction: Triggering large events with small vibrations. Scientific reports, 5(1), 1-5.

Lieou, C. K., Elbanna, A. E., & Carlson, J. M. (2014). Grain fragmentation in sheared granular flow: Weakening effects, energy dissipation, and strain localization. Physical Review E, 89(2), 022203.

Luding, S., Herrmann, H. J., & Blumen, A. (1994). Simulations of two-dimensional arrays of beads under external vibrations: Scaling behavior. Physical Review E, 50(4), 3100.

Manning, M. L., Daub, E. G., Langer, J. S., & Carlson, J. M. (2009). Rate-dependent shear bands in a shear-transformation-zone model of amorphous solids. Physical Review E, 79(1), 016110.

Marsan, D., & Lengline, O. (2008). Extending earthquakes' reach through cascading. Science, 319(5866), 1076-1079.

Melosh, H. J. (1979). Acoustic fluidization: A new geologic process?. Journal of Geophysical Research: Solid Earth, 84(B13), 7513-7520.

Melosh, H. J. (1983). Acoustic fluidization: can sound waves explain why dry rock debris appears to flow like a fluid in some energetic geologic events?. American Scientist, 71(2), 158-165.

Melosh, H. J. (1987). The mechanics of large rock avalanches: Geological Society of America Review in Engineering Geology, v. 7.

Mogami, T. and Kubo, K. (1953). The behavior of soil during vibration. Proc. 3rd Int. Conf. on Soil Mech. and Found. Eng., Switzerland, Vol. 1, 152-155.

Mohabuth, N., Hall, P., & Miles, N. (2007). Investigating the use of vertical vibration to recover metal from electrical and electronic waste. Minerals engineering, 20(9), 926-932.

Moriyasu, S., Kobayashi, S. I., & Matsumoto, T. (2018). Experimental study on friction fatigue of vibratory driven piles by in situ model tests. Soils and foundations, 58(4), 853-865.

O'Neill, M. W., Vipulanadan, C., & Wong, D. O. (1990). Evaluation of bearing capacity of vibro-driven piles from laboratory experiments. Transportation Research Record, (1277).

Omidvar, M., Bless, S., & Iskander, M. (2019). Recent insights into penetration of sand and similar granular materials. In Shock Phenomena in Granular and Porous Materials (pp. 137-163). Springer, Cham.

Osinov, V. A. (2013). Application of a high-cycle accumulation model to the analysis of soil liquefaction around a vibrating pile toe. Acta Geotechnica, 8(6), 675-684.

Pestana, J. M., Hunt, C. E., & Bray, J. D. (2002). Soil deformation and excess pore pressure field around a closed-ended pile. Journal of geotechnical and geoenvironmental engineering, 128(1), 1-12.

Potyondy, D. O., & Cundall, P. A. (2004). A bonded-particle model for rock. International journal of rock mechanics and mining sciences, 41(8), 1329-1364.

Richards Jr, R., Elms, D. G., & Budhu, M. (1990). Dynamic fluidization of soils. Journal of Geotechnical Engineering, 116(5), 740-759.

Ringer, D. U., & Mujumdar, A. S. (1983). Analysis of aerodynamics and heat transfer in vibro-fluidized beds. Drying Technology, 2(4), 449-470.

Rosato, A. D., Blackmore, D. L., Zhang, N., & Lan, Y. (2002). A perspective on vibration-induced size segregation of granular materials. Chemical Engineering Science, 57(2), 265-275.

Roscoe, K., & Burland, J. B. (1968). On the generalized stress-strain behaviour of wet clay.

Roscoe, K. H., Schofield, A., & Thurairajah, A. (1963). Yielding of clays in states wetter than critical. Geotechnique, 13(3), 211-240.

Sharpe, S. S., Kuckuk, R., & Goldman, D. I. (2015). Controlled preparation of wet granular media reveals limits to lizard burial ability. Physical biology, 12(4), 046009.

Sornette, D., & Sornette, A. (2000). Acoustic fluidization for earthquakes?. Bulletin of the Seismological Society of America, 90(3), 781-785.

Taguchi, Y. H. (1993). k-5/3 Power Spectrum in Powder–Turbulent Flow in a Vibrated Bed: Numerical Results. EPL (Europhysics Letters), 24(3), 203.

Taslagyan, K. A., Chan, D. H., & Morgenstern, N. R. (2015). Effect of vibration on the

critical state of dry granular soils. Granular Matter, 17(6), 687-702.

Taslagyan, K. A., Chan, D. H., & Morgenstern, N. R. (2016). Vibrational fluidization of granular media. International Journal of Geomechanics, 16(3), 04015080.

Umbanhowar, P., & Van Hecke, M. (2005). Force dynamics in weakly vibrated granular packings. Physical Review E, 72(3), 030301.

Van Der Elst, N. J., & Brodsky, E. E. (2010). Connecting near‐field and far‐field earthquake triggering to dynamic strain. Journal of Geophysical Research: Solid Earth, 115(B7).

Viking, K., & Bodare, A. (1999). Laboratory studies of dynamic shaft resistance response of a vibro-driven model pile in granular soil by varying the relative density. In Proceedings of the 12th European Conference on Soil Mechanics and Geotechnical Engineering (pp. 863-869).

White, D. J., & Lehane, B. M. (2004). Friction fatigue on displacement piles in sand. Géotechnique, 54(10), 645-658.

Xie, T., & Guo, P. (2021). A Modified Triaxial Apparatus for Soils under High-Frequency, Low-Amplitude Vibrations. Geotechnical Testing Journal, 45(1).

Xie, T., Guo, P., & Stolle, D., (2022a). Development of extended STZ model for granular soils subjected to combined static loading and vibration. Geotechnique. https://doi.org/10.1680/jgeot.22.00099

Xie, T., Guo, P., & Stolle, D., (2022b). Vibration-induced shear resistance relaxation in granular materials: experiment and model. Geotechnique. (under review)

Youd, T. L. (1967). The engineering properties of cohesionless materials during vibration. PhD dissertation, Iowa State University.

Zhou, G. G., Du, J., Song, D., Choi, C. E., Hu, H. S., & Jiang, C. (2020). Numerical study of granular debris flow run-up against slit dams by discrete element method. Landslides, 17(3), 585-595.

Chapter 8 Conclusions and Recommendations

8.1 Main contributions

The main contributions of this research can be summarized according to three components: (1) obtaining the basic features of ViSRR through a series of laboratory tests; (2) developing a thermodynamics-based model, i.e., the extended STZ model, to simulate ViSRR, in which macroscopic plastic strains are correlated to the transition, creation, and destruction of mesoscopic STZs (weak particle groups); and (3) proposing the concept of "vibration-induced shear resistance relaxation" to explain the mechanism behind ViSRR. Based on this research, the following conclusions can be drawn:

- Laboratory tests revealed that a significant reduction in shear resistance, accompanied by volume change, occurred in the tested granular soils that were subjected to monotonic shearing with superimposed high-frequency vibrations (60-120 Hz). The reduction in shear resistance increased linearly with vertical acceleration. The shear resistance can be recovered in monotonic shearing after vibration. Tests on dry specimens confirmed that the shear resistance reduction was not caused by excess pore pressure.
- The extended STZ model could capture the coupling effects of vibration and quasi-static loadings on granular soils during ViSRR. The model incorporates three groups of governing functions: the motion of STZs (transition, creation, and destruction of STZs); the relation between the motion of STZs and plastic strain; and the evolution law of the "configurational temperature" that reflects the internal energy driving the motion of STZs.
- Given the experimental results and the extended STZ model analyses, the concept of "shear resistance relaxation" (SRR) of granular soil under vibration was proposed, which could be used to explain the mechanism of ViSRR. The SRR refers to the phenomenon where a granular material, under restricted deformation,

loses shear resistance in response to the plastic strains generated by vibrations. This was found to require vibration to allow the compression of the material, coupled with a restricted total deformation rate to prevent it from "following" the vibration-induced compression. The extended STZ model demonstrated a good agreement with laboratory test results, indicating its effectiveness in simulating the process of ViSRR.

8.2 Recommendations for future work

The extended STZ model developed in this study, which correlated the evolution of internal structure (STZ) of geomaterials at the particle group scale with the macroscopic plastic strain at the representative element volume (REV) scale, represented a significant step towards my long-term research goal. This goal is to develop a comprehensive multiscale model for granular materials subjected to coupled dynamic and static loadings, integrating the force chain at the particle scale, the weak domain (STZ) at the particle group scale, and the macroscopic strain at the REV scale within the same framework. Recommendations for future work include:

- Extensive experimental study on ViSRR: To understand the behavior of ViSRR more, it is recommended that testing should be completed with different granular materials, such as glass beads, to explore the impact of a granular assembly's structure. Furthermore, further investigations should be conducted to examine the influence of effective confining pressure and duration of vibration on the vibration-induced volume change.
- Further refinement of the extended STZ model: The framework of the extended STZ model has been established in this research and applied primarily to triaxial stress conditions. In the future, the model should be further refined to incorporate more complex stress and loading conditions.
- Discrete Element Method (DEM) study: The DEM should be carried out to provide additional insight in the transition, creation, and destruction of STZ captured by the

extended STZ model. DEM allows for detailed tracking of granular media at the contact level, including changes in internal structure and evolution of internal energies during vibration.